İSTANBUL TECHNICAL UNIVERSITY ★ INSTITUTE OF SCIENCE AND TECHNOLOGY

SWELLING, ELASTICITY AND INHOMOGENEITY OF POLY(N,N-DIMETHYLACRYLAMIDE) HYDROGELS

Ph.D. Thesis by
Nermin ORAKDÖĞEN, M.Sc.

Department : **Polymer Science and Technology**

Programme : **Polymer Science and Technology**

NOVEMBER 2006

İSTANBUL TECHNICAL UNIVERSITY ★ INSTITUTE OF SCIENCE AND TECHNOLOGY

SWELLING, ELASTICITY AND INHOMOGENEITY OF POLY(N,N-DIMETHYLACRYLAMIDE) HYDROGELS

Ph.D. Thesis by

Nermin ORAKDÖĞEN, M.Sc.

(515012001)

Date of submission : 15 September 2006

Date of defence examination: 10 November 2006

Supervisor (Chairman): Prof. Dr. Oğuz OKAY

Members of the Examining Committee Prof.Dr. Yusuf YAĞCI (İ.T.Ü.)

Prof.Dr. Önder PEKCAN (I.Ü.)

Prof.Dr. Yıldırım ERBİL (G.Y.T.E.)

Prof.Dr. Ferdane YILMAZ (Y.T.Ü.)

NOVEMBER 2006

İSTANBUL TEKNİK ÜNİVERSİTESİ ★ FEN BİLİMLERİ ENSTİTÜSÜ

POLİ(N,N-DİMETİLAKRİLAMİD) HİDROJELLERİNİN ŞİŞME, ELASTİSİTE VE İNHOMOJENİTE ÖZELLİKLERİ

DOKTORA TEZİ

Y. Kimyager Nermin ORAKDÖĞEN
(515012001)

Tezin Enstitüye Verildiği Tarih : 15 Eylül 2006
Tezin Savunulduğu Tarih : 10 Kasım 2006

Tez Danışmanı :	**Prof. Dr. Oğuz OKAY**
Diğer Jüri Üyeleri	**Prof.Dr. Yusuf YAĞCI (İ.T.Ü.)**
	Prof.Dr. Önder PEKCAN (I.Ü.)
	Prof.Dr. Yıldırım ERBİL (G.Y.T.E.)
	Prof.Dr. Ferdane YILMAZ (Y.T.Ü.)

KASIM 2006

ACKNOWLEDGEMENTS

I am most grateful to my supervisor, Prof. Dr. Oğuz OKAY, who introduced me into the wonderful world of gels. He tried his best to give me constructive advice and help me on many aspects. His original ideas and his critical discussions benefit me the most. I would like to thank him for the opportunity to learn and grow as a researcher in the Polymeric Gels and Networks Laboratory. His professional approach towards the scientific research and his tireless working attitude in solving scientific problems has always inspired me, both in laboratory and in real world.

I also would like to express my thanks to the members of the committee, Prof. Dr. Yusuf YAĞCI, Prof. Dr. Önder PEKCAN, Prof. Dr. Yıldırım ERBİL and Prof. Dr. Ferdane YILMAZ for their patience and precious time to read my thesis.

It would be impossible to thank everyone, but I would like to acknowledge the many members and staff of the Department of Chemistry and Polymer Science and Technology Program that have helped and supported me as I earned my PhD.

I would like to thank the former and current members in Polymeric Gels and Networks Lab., Mine YENER KIZILAY, Selda SEZGİNGİL, M. Murat ÖZMEN, Volkan CAN, Deniz CEYLAN and Maria Valentina DİNU for their help during my studying in the laboratory. Special thanks to my friends and colleagues who have discussed my work with me. As I will go on the next step into my career, I will keep with me their teachings, friendship and support.

And I would like to offer the most gratitude to my parents, my parents-in-law, my brothers and their wifes for their understanding, patience and support both in my university studies and every stage in my life. I am deeply indepted to everyone of them for making this possible for me.

My greatest appreciation goes to my husband Associate Prof. Dr. Engin ORAKDÖĞEN, who has always been with me during my Ph.D. study. His love, support, help, and encouragement have always provided a shelter for me to overcome the difficulties during the study. Special thanks to my lovely daughter Nihan ORAKDÖĞEN. They made everything possible. This thesis is dedicated with great appreciation and love to them.

Finally, but perhaps most importantly, I would like to thank to the founder of the Turkish Republic and its first President, Mustafa Kemal Atatürk for many reforms to give Turkish women equal rights and opportunities.

November, 2006 Nermin ORAKDÖĞEN

TABLE OF CONTENTS

LIST OF ABBREVIATIONS

DMAAm : N,N-dimethylacrylamide
AAm : Acrylamide
PDMAAm : Poly(N,N-dimethylacrylamide)
PAAm : Poly(acrylamide)
BAAm : N,N'-methylenebisacrylamide
AMPS : 2-acrylamido-2-methylpropane sulfonic acid
APS : Ammonium persulfate
SPS : Sodium metabisulfite
TEMED : N,N,N',N'-tetramethylethylenediamine
IPA : Isopropylalcohol
DMSO : Dimethylsulfoxide
THF : Tetrahydrofuran
CTA : Chain Transfer Agent

LIST OF TABLES

LIST OF FIGURES

LIST OF SYMBOLS

A_2, A_3	: Second and third osmotic virial coefficients
c	: Concentration
c^*	: Overlap concentration
$\tilde{c}$	: Speed of light
C_0	: Initial molar concentration of the monomer
C_{ion}^{gel}, C_{ion}^{sol}	: Mobile ion concentration in the gel and the solution phases
D, D_0	: Diameter of gels after equilibrium swelling and after preparation
E	: Strength of the electric field
E_0	: Maximum amplitude of the field
E_s	: Magnitude of the scattered electric field for the scattered light
f	: Stress
f	: Effective charge density
G	: Elastic modulus of swollen gels
G_0	: Elastic modulus of gels after preparation
G_r	: Reduced modulus
G_1, G_2, G_{12}	: Free energy of the solvent, polymer and polymer solution
H	: Strength of the magnetic field
I_s	: Intensity of thescattered light
I_0	: Intensity of the incident light
$I(q)$	: Intensity of the scattered light at q
$I(0)$	: Intensity of the scattered light at q=0
k	: Boltzmann constant
K	: Optical constant
l	: Bond length
m_{dry}	: Weight of gels in the dry state
$m_{swollen}$	: Weights of gels in the swollen state
$\bar{M}_w$	: Molecular weight of the network chains
N	: Number of segments between two successive crosslinks
N	: Total number of lattice positions present
N_A	: Avogadro's number
N_p	: Number of particles per unit volume
n	: Refractive index
n_1, n_2	: Number of moles of the solvent and the polymer
p	: Oscillating dipole
P	: Number of possible ways of arranging the mixture
$P(\theta)$	: Particle scattering function
q	: Scattering vector
q_F	: Dilution degree after the gel synthesis
q_v	: Equilibrium volume swelling ratio
q_w	: Equilibrium weight swelling ratio
r	: Distance of the detector from the center of the scattering volume
r	: End-to-end distance

$\langle r^2 \rangle$: Mean square end-to-end distance

$\langle r^2 \rangle_0$: Mean square length of the polymer chains in the undeformed state

R_g : Radius of gyration of polymer chains

R_θ : Rayleigh ratio

$R_{ex}(q)$: Excess scattering from polymer gel

$R_{gel}(q)$: Scattering intensity from gels

$R_{sol}(q)$: Scattering intensity from a semi-dilute polymer solution

S : Entropy of the polymer chain

S_0 : Entropy of the polymer chain in the undeformed state

T : Absolute temperature

$\bar{V}_1$: Molar volume of the solvent

V_{eq} : Equilibrium swelling ratio of the hydrogel

V_P , V_1 : Volumes of the polymer network and the segment

$\bar{V}_r$: Molar volume of the polymer repeat unit

W : Work

$W(x, y, z)$: Probability density

$W(r)$: Radial distribution function

w_{11}, w_{22}, w_{12} : Interactions for solvent-solvent (1-1), the polymer-polymer (2-2), and polymer-solvent (1-2) contact

x : Chain segments

X : Crosslinker ratio

z : Coordination number

ΔA : Change in the Helmholz free energy

ΔE_1 , ΔE_2 : Energies of vaporization of components 1 and 2

ΔE_{el} : Change of internal energy on elastic deformation

$\Delta G_{swelling}$: Change in the Gibbs free energy during the swelling process

ΔG_{mix} : Changes in the free energy of mixing

ΔG_{el} : Changes in the free energy of elastic deformation

ΔG_{ionic} : Change in Gibbs free energy due to the ionic nature of polymer network

ΔG_{int} : Free energy of volume interactions

ΔH_{mix} : Enthalpy of mixing

ΔS_{mix} : Entropy of mixing

ΔV_{el} : Volume change on elastic deformation

α : Polarizability

$\langle \alpha \rangle$: Average polarizability

α : Linear deformation ratio

β : Isothermal compressibility

χ_{12} : Interaction between polymer and solvent

δ : Solubility

ε_0 : Dielectric coefficient at vacuum.

ϕ : Functionality of the crosslinks

$\gamma(r)$: Correlation function of the fluctuation

$\langle \eta^2 \rangle$: Mean square fluctuation of the refractive index

φ : Organic solvent partition parameter

λ_x : Entension ratio in the *x* direction

μ : Number of junctions

μ_1 : Chemical potential of solvent

μ_1° : Solvent chemical potential at a reference state

$\Delta\mu_1$: Excess chemical potential of solvent

$\Delta\mu_{\mathbf{mix}}$: Changes of the chemical potential due to mixing

$\Delta\mu_{\mathbf{el}}$: Changes of the chemical potential due to elastic forces

$\Delta\mu_{\mathbf{ion}}$: Change of the chemical potential due to ionic character of polymer gel

v_e : Effective crosslink density

π : Osmotic pressure of the solution

θ : Scattering angle

θ_1 : Angle between the direction of polarization and the direction of scattering

ρ : Polymer density

ν : Number of polymer network chains per unit volume

$\bar{\nu}$: Number of moles of polymer chains of polymer network per unit volume

ν_1, ν_2 : Volume fractions of the solvent and the polymer, respectively

ν' : Concentrations in the external solution

ν_2^0 : Volume fractions of the polymer network after gel preparation

ν_2 : Volume fractions of the polymer network at equilibrium swelling

ξ : Correlation length

ξ : Cycle rank

Ξ : Mean size of the static concentration fluctuations

SWELLING , ELASTICITY AND INHOMOGENEITY OF POLY(N,N-DIMETHYLACRYLAMIDE) HYDROGELS

SUMMARY

The swelling behavior and the elastic properties of the hydrogels have been powerfully and widely investigated to understand their macroscopic properties. In recent years, research conducted on the microscopic structure of gels indicates an inhomogeneous crosslink density distribution, known as spatial gel inhomogeneity. The study of the gel inhomogeneity becomes an attractive research problem to clarify the formation process during gelation and the structure of the resulting gels.

The aim of this study is to investigate the swelling, elasticity and inhomogeneity of poly(N,N-dimethylacrylamide) (PDMAAm) hydrogels by static light scattering technique. Since the major experimental technique used in the work of this thesis is the static light scattering, the time-resolved light scattering technique was also used to present the scattering intensity profile of hydrogels during the formation process. A significant amount of both theoretical and experimental data was collected during this thesis. The theoretical predictions have been presented before the experimental results. Any formulae or models needed to explain the data is also presented in the results and discussion section as needed.

In the experimental work of this thesis, non-ionic and ionic PDMAAm hydrogels were prepared by free-radical crosslinking copolymerization reactions of N,N-dimethylacrylamide (DMAAm) monomer and N,N'-methylenebis(acrylamide) (BAAm) crosslinker. Sodium salt of 2-acrylamido-2-methylpropane sulfonic acid (AMPS) was used as the ionic comonomer for the preparation of ionic hydrogels. In order to make a comparison poly(acrylamide) PAAm hydrogels were also prepared under the same experimental condition. The extent of the spatial inhomogeneity in the hydrogels was investigated by the light scattering technique depending on the gel synthesis parameters; the initial monomer concentration, the ionic comonomer concentration and the type of the redox-initiator systems used to initiate the gelation reactions. The effect of the gel inhomogeneity on the macroscopic gel properties was also examined by the elasticity and swelling measurements. These studies would reveal the relations between the microscopic properties of gels and their macroscopic behavior.

The effect of the initial monomer concentration ν_2^0 on the equilibrium swelling degree and the modulus of elasticity of non-ionic PDMAAm hydrogels were investigated. It was found that the linear swelling ratio of the gels is not a monotonic function of ν_2^0, it first decreases with increasing ν_2^0, but then increases continuously. By using the Flory-Rehner theory, a scaling relation between the monomer

concentration ν_2^0 and the network chain length N was derived to generalize the monomer concentration dependence of the swelling ratio.

The effective crosslink density of non-ionic PDMAAm hydrogels were investigated as a function the monomer concentration ν_2^0. It was found that the effective crosslink density of the hydrogels ν_e is not a monotonic function of the monomer concentration ν_2^0. The experimental results showed three different gel regimes depending on the value of ν_2^0.

The effect of the initial monomer concentration ν_2^0 on the spatial inhomogeneity in non-ionic PDMAAm hydrogels was also investigated. The results showed that non-ionic PDMAAm hydrogels exhibit a maximum scattering at a critical polymer concentration. This phenomena was explained by the competition of two opposite effects: the crosslink density effect and the concentration effect. Below the critical polymer concentration, the crosslink density effect dominates over the concentration effect so that the gel inhomogeneity increases. After the critical value, the concentration effect is more dominant than the crosslink density effect so that the gel inhomogeneity decreases.

The swelling behavior of non-ionic PDMAAm hydrogels was also investigated in aqueous organic solvent mixtures. The hydrogels exhibit reentrant conformation transition with increasing volume fraction ϕ of acetone, tetrahydrofuran, or 1,4-dioxane in the aqueous solution. During this transition, the hydrogels first deswell in the range of ϕ between 0.4 and 0.9, and then rapidly reswells if the solvent composition is monotonically increased. The theoretical calculations were performed to predict the swelling behavior of non-ionic PDMAAm hydrogels in aqueous organic solvent mixtures by using Flory-Rehner theory. The interaction parameters in the gel system as well as the partition parameter of the organic solvent between the gel and the solution phases were calculated.

The swelling behavior of ionic PDMAAm hydrogels was investigated in water. The equilibrium degree of the hydrogels increases with increasing ionic group content x_i. The swelling of the hydrogels was also investigated in aqueous NaCl solutions. The swelling ratio of hydrogels decreases with increasing NaCl concentration in the external solution. The swelling behavior of ionic hydrogels was studied in acetone–water mixtures. It was found that the hydrogels exhibit reentrant transition at low charge densities. The reentrant transition gradually disappears and becomes a deswelling transition at high charge densities.

The elasticity measurements of ionic PDMAAm hydrogels showed that the elastic modulus of the hydrogels after their preparation G_0 first increases with ionic comonomer concentration then decreases continuously. The results were indicated two opposite effects of charged groups on the elastic modulus of the ionic hydrogels: Formation of multiplets acting as additional crosslinks in the hydrogel increases the elastic modulus, whereas the effect of the electrostatic interactions of the charged groups on elastic free energy decreases the modulus.

The effect of the ionic comonomer concentration on the spatial inhomogeneity in ionic PDMAAm hydrogels was also investigated. The results show that the degree of spatial inhomogeneity in PDMAAm hydrogels decreases drastically with increasing AMPS content of the network chains. At 30 mol% AMPS, the scattered light intensity from gels becomes equal to that from solutions, i.e., gels behave like a solution at this AMPS concentration.

The scattering intensity profiles and the appearance of nano-scale, highly crosslinked regions during the formation process of PDMAAm and PAAm hydrogels were also investigated by using the light scattering technique. In order to investigate the effect of the initiator system used in the gel preparation on the spatial inhomogeneity, two different redox initiator system were used to prepare hydrogels; ammonium persulfate (APS)- N,N,N',N'-tetramethylenediamine (TEMED) and APS-sodium metabisulfite (SPS). The results showed that for APS-TEMED redox pair, the variation of the scattered light intensity during gelation of PDMAAm gels differs from that observed in PAAm gels. The reaction time dependence of the scattered light intensity for PAAm gels exhibits only a maximum at a critical reaction time. However, PDMAAm gels exhibits both a maximum and a minimum, corresponding to the overlap threshold and the gel point, respectively. Moreover, the scattered light intensity from PDMAAm gels is much smaller than that from PAAm gels, which indicates that PDMAAm gels are relatively homogeneous compared to PAAm hydrogels. This is due to late gelation in DMAAm polymerization, which produces a relatively homogeneous distribution of crosslinks.

It was also found that replacing TEMED with SPS as the accelerator significantly affects the degree of inhomogeneity in both PDMAAm and PAAm hydrogels. Compared to the APS-TEMED redox pair, no significant scattered light intensity rise was observed during the crosslinking polymerization reactions initiated by the APS-SPS system. It was also shown that, both gels are much more homogeneous when APS-SPS redox pair was used as the initiator. The results were explained with the formation of shorter primary chains as well as the delay of the gel point in APS-SPS initiated gel formation reactions.

Furthermore, a correlation was found between the macroscopic elastic behavior of PAAm hydrogels and the microscopic gel structure. The elasticity and light scattering measurements carried out on PAAm hydrogels showed that the concentration fluctuations in PAAm hydrogels strongly reduce as the crosslinker is consumed more effectively during the polymerization reactions, i.e., by suppression the extent of side reactions such as cyclization and multiple crosslinking with increasing monomer concentration during the hydrogel preparation.

POLİ(N,N-DİMETİLAKRİLAMİD) HİDROJELLERİNİN ŞİŞME, ELASTİSİTE VE İNHOMOJENİTE ÖZELLİKLERİ

ÖZET

Hidrojellerin makroskopik davranışlarını anlayabilmek için şişme davranışları ve elastik özellikleri yaygın olarak incelenmektedir. Son yıllarda ışık saçınım teknikleri ile jellerin mikroskopik yapılarını inceleyen araştırmalar gerçekleştirilmiş, jellerin çapraz bağ yoğunluklarının homojen olarak dağılmadığı ve sonuçta inhomojen yapıya sahip oldukları ortaya çıkmıştır. Dolayısıyla, jellerin oluşumunu ve yapılarını açıklayabilmek için jellerin inhomojenliği üzerine yapılan çalışmalar ilginç araştırma konuları arasına girmiştir.

Bu çalışmanın amacı poli(N,N-dimetilakrilamid) (PDMAAm) hidrojellerinin şişme ve elastik özelliklerinin ve sentez sonrasındaki inhomojenitenin statik ışık saçınımı tekniği ile incelenmesidir. Deneysel çalışmalarda kullanılan ana yöntem statik ışık saçınımı yöntemi olduğundan hidrojellerin oluşum reaksiyonları ve inhomojenitenin reaksiyon sırasında ortaya çıkışı gerçek-zamanlı ışık saçınım tekniği ile incelenmiştir. Çalışma kapsamında elde edilen teorik sonuçlar deneysel sonuçların anlaşılabilirliğini kolaylaştıracak şekilde verilmiştir.

Bu çalışmada iyonik grup içeren ve içermeyen PDMAAm hidrojelleri N,N-dimetilakrilamid (DMAAm) monomeri ile N,N'-metilenbis(akrilamid) (BAAm) çapraz bağlayıcısının serbest radikal mekanizma ile kopolimerizasyonu sonucunda elde edilmiştir. 2-akrilamido-2-metilpropan sülfonik asit sodyum tuzu (AMPS) iyonik komonomer olarak kullanılmıştır. Sonuçların karşılaştırılması için aynı koşullarda poli(akrilamid) (PAAm) hidrojelleri de sentezlenmiştir. Sentezlenen hidrojellerin inhomojenite derecesi; başlangıç monomer konsantrasyonu, iyonik komonomer konsantrasyonu ve kullanılan redox başlatıcı sisteminin tipi gibi değişik reaksiyon şartlarına bağlı olarak incelenmiştir. Jellerdeki inhomojenitenin, onların makroskopik özelliklerine etkisini araştırmak için elastik modül ve şişme ölçümleri yapılmıştır. Bu çalışmalar ile jellerin mikroskopik özellikleri ile makroskopik davranışları arasında bağıntılar ortaya çıkartılmıştır.

Sentez sırasında kullanılan başlangıç monomer konsantrasyonunun iyonik olmayan PDMAAm hidrojellerinin şişme ve elastik özelliklerine etkisi incelenmiştir. Jellerin şişme oranı ile kullanılan başlangıç monomer konsantrasyonu arasında lineer bağıntı olmadığı görülmüştür. Monomer konsantrasyonu arttıkça şişme oranı önce azalmakta ve belli bir değerden sonra tekrar artmaktadır. Flory-Rehner teorisi kullanılarak şişme oranının polimer ağ yapıdaki zincir uzunluğuna bağlılığını veren genel bir bağıntı türetilmiştir.

İyonik olmayan PDMAAm hidrojellerinin etkin çapraz bağ yoğunluğunun sentez sırasında kullanılan başlangıç monomer konsantrasyonuna göre değişimi incelendiğinde yine lineer bir bağıntının olmadığı ve üç farklı bölgenin olduğu görülmüştür.

Statik ışık saçınım tekniği ile sentez sırasında kullanılan başlangıç monomer konsantrasyonunun iyonik olmayan PDMAAm hidrojellerinin inhomojenliğine etkisi incelenmiştir. Yapılan çalışmalar sonucunda jellerdeki inhomojenite derecesinin kritik bir polimer konsantrasyonunda maksimum bir değere ulaştığı görülmüştür. Bu sonuç, çapraz bağ yoğunluğu ve konsantrasyon etkisi ile açıklanmıştır. Kritik polimer konsantrasyonundan önce çapraz bağ yoğunluğu arttıkça inhomojenite artarken, kritik değerden sonra konsantrasyon etkisinden dolayı azalmaktadır.

İyonik olmayan PDMAAm hidrojellerinin çeşitli çözücü karışımlarındaki şişme davranışlarının incelendiği çalışmada, jellerin Aseton, tetrahidrofuran ve 1,4-dioksan' ın sulu çözeltilerinde reentrant konformasyonel geçişler gösterdiği bulunmuştur. Karışımdaki çözücünün mol fraksiyonu 0.4 ile 0.9 arasındayken jellerin büzüldüğü sonra yeniden hızlıca şiştiği görülmüştür. Deneysel sonuçlar şişme teorisi kullanılarak teorik olarak desteklenmiştir. Jel sistemindeki etkileşim parametreleri ile jel ve çözelti fazındaki dağılım parametreleri teorik olarak hesaplanmıştır.

AMPS iyonik komonomeri kullanılarak hazırlanan PDMAAm hidrojellerinin saf su, aseton-su karışımı ve tuz çözeltilerindeki sişme davranışları incelenmiştir. Su içindeki şişme ölçümleri sonucunda; hidrojellerin şişme oranının jel içindeki AMPS mol kesri x_i ile arttığı görülmüştür. İyonik hidrojellerin tuz çözeltilerindeki şişme davranışları incelendiğinde çözeltinin tuz konsantrasyonu arttıkça jellerin şişme oranının azaldığı gözlenmiştir. Aseton-su karışımlarına atılan jellerden düşük yük yoğunluğuna sahip olanların reentrant geçiş gösterdiği, yük yoğunluğu arttıkça reentrant geçişin kaybolduğu ve jellerin sürekli olarak büzüldüğü gözlenmiştir.

İyonik hidrojellerin elastik özelliklerinin araştırıldığı çalışmalar jellerin sentez sonrası elastik modüllerinin iyonik komonomer konsantrasyonu ile önce arttığını daha sonrada azaldığını göstermiştir. Bu sonuç yüklü grupların hidrojelin elastik modülüne iki zıt etkisi olduğunu göstermektedir: çok katlı çapraz bağlanmalar jel içinde ek çapraz bağlar gibi davranarak jelin modülünü arttırırken, yüklü gruplar elastik serbest enerji ile birbirleri ile etkileşerek elastik modülü azaltmaktadırlar. Jellerdeki yük yoğunlunun jellerin yapısal inhomojenitesine etkisi de araştırılmıştır. Yapılan ölçümler sonucunda PDMAAm jellerinin inhomojenliğinin iyonik komonomer AMPS miktarı ile azaldığı saptanmıştır. % 30 mol AMPS içeren jellerin ve polimer çözeltilerinin saçınma intensitelerinin birbirine eşit olduğu bulunmuştur. Bu sonuç belirtilen miktarda AMPS içeren jellerin çözelti gibi davrandığını göstermektedir.

Statik ışık saçınımı tekniği kullanılarak PDMAAm ve PAAm hidrojellerinin oluşum reaksiyonları ve reaksiyon sırasında mikrofaz ayırımı süreci ve jel içerisinde nano boyutlarda yüksek çapraz bağlı bölgelerin ortaya çıkışı incelenmiştir. Hidrojellerin sentezinde kullanılan başlatıcı-hızlandırıcı sisteminin, jellerin inhomojenliğine etkisi incelenmiştir. Bu amaçla iki farklı redoks başlatıcı sistemi seçilmiştir; amonyum persulfat (APS) - N,N,N',N'-tetrametiletilendiamin (TEMED) ve APS - sodyum metabisülfit (SPS). Hızlandırıcı olarak TEMED kullanılarak sentezlenen PDMAAm

hidrojellerinden saçınan ışık intensitesi gerçek zamanlı olarak izlenmiş ve PAAm hidrojellerinden çok farklı olduğu gözlenmiştir. PAAm jellerinin intensitesi bir maksimum değere ulaşıp sonra azalarak sabit kalırken, PDMAAm hidrojelleri bir maksimum ve bir minimum gösterdikten sonra tekrar atmakta ve daha sonra sabit kalmaktadır. Bu maksimum nokta kritik örtüşme konsantrasyonu olarak, minimum nokta ise jel noktası olarak açıklanmıştır. Ayrıca PDMAAm jellerinden saçınan ışık intensitesinin PAAm jellerine göre çok daha az olduğu gözlenmiştir ki bu sonuç PDMAAm hidrojellerinin daha homojen yapıda olduklarını göstermektedir. PDMAAm hidrojellerinde jelleşmenin daha geç meydana gelmesi, jel örneği boyunca çapraz bağ yoğunluğunun daha homojen olarak dağılmasını sağlamakta ve sonuç olarak jel inhomojenitesi azalmaktadır. Diğer taraftan, sentezlerde hızlandırıcı olarak TEMED yerine SPS kullanımının hidrojellerin inhomojenlik derecesini belirgin bir şekilde azalttığı ve dolayısıyla çok daha homojen jellerin elde edildiğini göstermiştir. Bu sonuç reaksiyon sırasında daha kısa zincirlerin oluşması ve APS-SPS sisteminde jelleşmenin daha geç gerçekleşmesi ile açıklanmıştır.

PAAm hidrojellerin mikroskopik özellikleri ile makroskopik davranışları arasındaki ilişkiyi açıklayabilmek için yapılan elastisite ve ışık saçınımı ölçümlerinin sonucunda; polimerizasyon reaksiyonu sırasında çapraz bağlayıcının daha etkin olarak kullanılmasının, jellerdeki konsantrasyon dalgalanmalarını belirgin şekilde azalttığı anlaşılmıştır. Başlangıç monomer konsantrasyonu artırıldığında, halka ve çok katlı çapraz bağlanmaların oluşumunun azaldığı, çapraz bağlayıcının etkin olarak kullanıldığı ve dolayısıyla yan reaksiyonlarda harcanmadığı anlaşılmıştır.

1. INTRODUCTION

The term ‘gel’ is easier to recognize than to define. A commonly accepted topological definition is that a polymer gel is a multi-component system consisting of a polymer network and a solvent as a swelling agent[1]. Thus, the properties of a gel depend strongly on the interactions of its two components; the polymer network and the solvent. The major component of the gel is a liquid; in some cases the gel can be as much as 90 % liquid or more. Furthermore, the polymer network serves as a matrix to hold the liquid together; the liquid prevents the polymer network from collapsing into a compact mass. Another aspect of the gels is that the gel is a “single polymer molecule”. It means that all the monomer units in the gel are connected to each other and form one big molecule on macroscopic scale.

What can be agreed upon is that the gel is a state that is neither completely “liquid” nor completely “solid”. Since the gels have properties of both solid and liquid phase, they are also called “solid liquids”. These half liquid-like and half solid-like properties cause many interesting relaxation behaviors that are not found in either a pure solid or a pure liquid. The mechanical or phenomenological definition of a gel always includes the criteria of “having solid-like behavior”[2]. The exact meaning of “solid-like behavior” depends on the characterization techniques used. For instance, take a small amount of gelatin polymer, mix it with water, and then cool it below 30 °C, the gelatin-water solution, which had flowed like any other fluid, turns into a solid-like mass in which a small fraction of gelatin molecules hold the water hostage not letting it flow. Thus, the essential characteristic of the gel is its solid-like behavior.

Hydrogels are a unique class of the polymer gels which are three-dimensional macromolecular networks made of hydrophilic polymer chains weakly crosslinked together by covalent bonds and can absorb a significant amount of water (> 20 % of their dry mass) within their structure, do not dissolve and are soft and pliable[3,4]. Some hydrogels can reversibly swell or shrink up to 1000 times in volume based in

response to a variety of external stimuli. Their ability to absorb and store much water and water solutions make hydrogels unique materials for a variety of applications.

The most important structural feature distinguishing the hydrogel or polymer gel from the linear polymer is its network structure. The polymer networks consist of long and linear polymer chains that are crosslinked to form three-dimensional mesh-like structures. If the linkages which connect the hydrogel structure erode, large changes in the properties of the hydrogel are expected. A network chain (a chain between two junction points) forms the basis of the elementary molecular theory of amorphous polymer networks.

In general, the network chains exhibit a distribution of molecular weights about an average, which serves as a representative reference quantity in describing network structure. The molecular weight between crosslinks is the average weight of the chain between two adjacent chemical crooslinks (denoted M_c). Other than the chemical crosslinks, there are physical entanglements which act as effective crosslinks under certain circumstances as shown in Figure1.1.

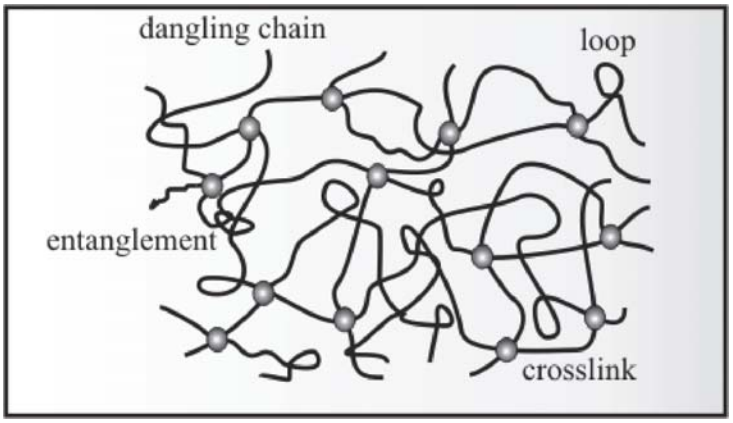

Figure 1.1: Schematic representation of a part of a typical polymer network containing loops, dangling chains, entanglements and crosslinks which are represented by the filled particles.

The number of chains meeting at each junction is called the functionality ϕ of that junction. A chain connected to a junction of the network at one end only is called a dangling chain, and one having both its ends attached to the same junction is called a loop. A network with no dangling chains or loops and in which all junctions have a functionality greater than 2 is called a perfect network.

The topological structure of the perfect network may be described by the following parameters;

1- The average molecular weight between junctions M_c,

2- The average functionality ϕ,

3- The number of network chains ν,

4- The number of junctions μ,

5- The cycle rank ξ, which denotes the number of chains that have to be cut in order to reduce the network to a tree with no closed cycles.

These parameters are not independent and are related by the following equations;

$$\mu = 2\nu/\phi \tag{1.1}$$

which states that to get ν chains in the perfect tetrafunctional network, only $\mu/2$ junctions are required. The cycle rank also equals to;

$$\xi = (1-2/\phi)\nu \tag{1.2}$$

There are different kinds of gels but they all have the common feature of being a continuous polymer network. Some classification of gels follows:

i. Polymer gels can be classified as neutral or ionic gels depending on the type of the repeating units and the nature of the side groups on the polymer backbone. The neutral gels, for example, poly(vinyl alcohol), do not have the ionizable groups on the polymer backbone or the side chain. Thus, the swelling of these gels is independent of pH or ionic strength. On the other hand, the ionic gels contain the ionizable functional groups. Therefore, they can be further classified as, anionic and cationic gels depending on the nature of the ionizable groups on their backbones. The anionic gels usually contain acid groups which form –COO- and swell at high pH and collapse at low pH values. In the unionized state, the hydrogen of the carboxylic group might be donated to a nearby electron-rich group to form hydrogen bonding which leads to the formation of polymer complexes. Poly(acrylic acid) and poly(methacrylic acid) are typical examples of the anionic gels. The cationic gels usually contain amino groups which form $-NH_3^+$ and swell at low pH and collapse at

high pH. Dimethylaminoethyl methacrylate (DMAEM) and Diethylaminoethyl methacrylate (DEAEM) are the typical cationic monomers.

ii. They can be homopolymer or copolymer networks based on the method of preparation.

iii. According to their mechanical and structural characteristics, they can be classified as affine or phantom networks.

iv. Polymer gels are random networks of flexible polymer chains and usually prepared by bulk, solution, emulsion or suspension polymerization of monomers in the presence of a crosslinking agent. According to the nature of the crosslinks between the monomers the gels are divided into two classes;

1- Chemical gels (where crosslinking is strong): These gels are created when the monomers form permanent covalent bonds. The gel network is permanent once formed and are stable against changes in thermodynamic parameters such as temperature.
2- Physical gels (where the bonds are weak): These gels are formed when the bonds between the units which make up the gel are due to some other physical mechanism. Since the bond are not chemical bonds, they can break or rebond by changes in thermodynamic parameters.

Considering the technological importance and scientific richness, the unique properties of gels allow them to be useful in various applications. Low molecular weight, hydrophilic polymers are soluble in water at room temperature and form a free flowing low viscosity liquid; upon warming or crosslinking, the solution may transform into a strong elastic gel. Figure 1.2 shows photographs taken from a gel sample and a polymer solution. The transition between liquid and gel occurs rapidly. With this combination of properties, the polymeric gels are mostly used in pharmaceutical industries as drug controlled-release media, cavity fillers, cell encapsulating membranes, biadhesives and enteric dosage forms. They are also used to fabricate soft contact lenses, artifical lenses, artifical vitreous, and materials for plastic surgeries. Gel sheets have been developed that tightly wrap fresh fish and meats for efficient transportation and storage. They play a vital role in the fields of medicine, artificial muscles, actuators, mass separation, sensors, chemical memories, foods, toys, chemical, agricultural and other industries[5-7].

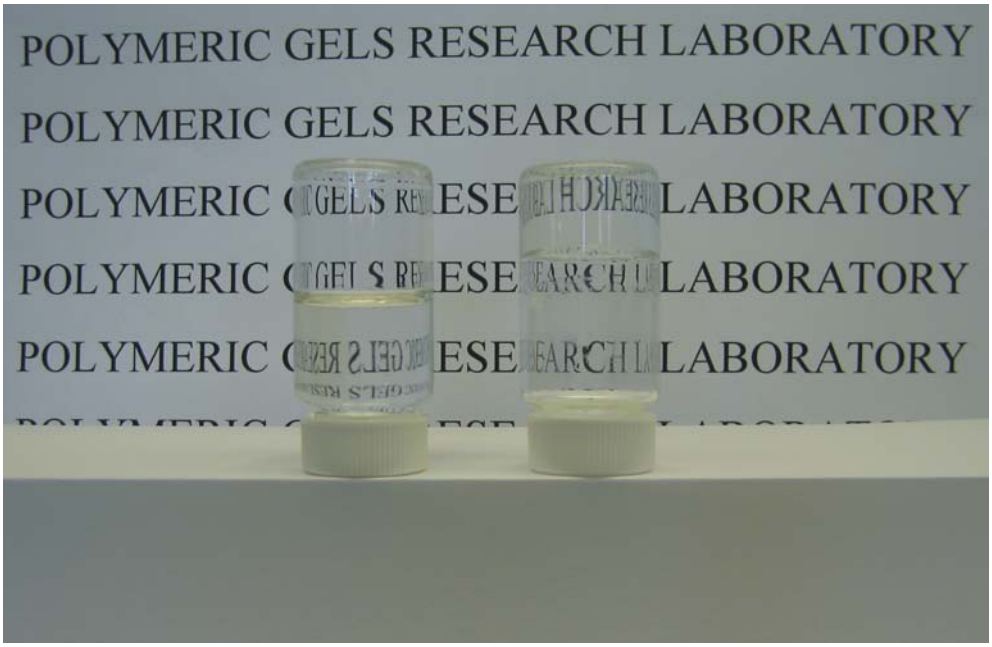

Figure 1.2: Photographs of the polymer solution (left) and the gel sample (right).

The swelling behavior of gels has been studied for more than four decades for its significance in fundamental science and application. In recent years, particular interest has been devoted to the swelling and collapsed phenomena of polymer gels that are observed when a polymer gel is brought into contact with a solvent[5]. The possibility of a first-order volume phase transition in hydrogels has been predicted theoretically and proved experimentally on (alkyl)acrylamide-based hydrogels swollen in solvents. In such a first-order phase transition, a change in an external variable like pH, solvent composition, ionic strength or temperature can induce a discontinuous change in the volume of the swollen gel[8,9].

Reentrant phase transitions were observed in poly(N-isopropylacrylamide) (PNIPA) hydrogels in aqueous solutions of dimethylsulfoxide (DMSO)[11], methanol[12], ethanol[12], as well as in aqueous solutions of poly(ethylene glycol)s of various molecular weights[12–14]. It was shown that poly(N,N-dimethylacrylamide) gels (PDMAAm) exhibit reentrant transitions in water–acetone and water–dioxane mixtures [15]. Liu and Tong predicted the essential roles of charged groups attached to the network in this transition. They have found that DMAAm hydrogels containing the ionic monomer 2-Acrylamido-2-methylpropane sulfonic acid (AMPS) undergo volume phase transition in a water/acetone mixture as the acetone concentration is increased[16]. Moreover, the hydrogels based on

N-t-butylacrylamide (TBA) and acrylamide (AAm) monomers with 40–60% TBA by mole exhibit reentrant transitions in water–DMSO and water–ethanol mixtures [17,18]. Since the reentrant phenomenon is not observable in polyacrylamide (PAAm) hydrogels or in hydrogels containing less than 40% TBA, it was suggested that the hydrophobic interactions are mainly responsible for the reentrant transition behavior of the hydrogels.

Since the hydrophobically modified hydrogels in solvent mixtures form a simple model system to understand the origin of hydrophobic interactions, the scientific and practical interest for PDMAAm hydrogels has been continuously increasing. Thus, several applications of PDMAAm-based products have been proposed ranging from hydrogels for drug-delivery purposes to polymer supports for protein synthesis[19]. Hydrogels derived from biocompatible copolymers of DMAAm have received considerable attention for use in drug delivery system, processing of agricultural products and sensors. More recently, macroporous hdyrogels of PDMAAm, also called hydrogel sponges, have been developed in tissue engineering[20].

For these reasons, N,N-dimethylacrylamide (DMAAm) was chosen as a principle monomer in the work of this thesis. Since either acrylamide or N-isopropylacrylamide are solids at the usual polymerization temperature, these monomers can not be polymerized without the use of a solvent. However, DMAAm is a liquid at room temperature and is extremely water soluble. Aqueous solutions of PDMAAm have only two methyl groups and no hydrogen-bonding ability and do not present any LCST behavior in water within the full temperature range of water (0-100°C). Thus, PDMAAm hydrogels can be prepared in aqueous solutions at monomer concentrations from a few percent up to 100 % (without the use of a solvent). In this way, it is possible to investigate the hydrogel properties over the whole range of the polymer concentration.

It is the purpose of this research to prepare a series of PDMAAm hydrogels and investigate the swelling, elasticity and spatial inhomogeneity of the hydrogels. The hydrogels were prepared by free radical crosslinking copolymerization of DMAAm monomer and N,N’-methylenebisacrylamide (BAAm) crosslinker in aqueous solutions. For, comparison poly(acrylamide) (PAAm) hydrogels were also prepared under the same experimental condition. AMPS was used as the ionic comonomer for the preparation of ionic hydrogels. To initiate the gelation reactions two different

redox-initiator systems, namely, ammonium persulfate (APS) – N,N,N',N'-tetramethylethylenediamine (TEMED) and APS – sodium metabisulfite (SPS) were used. The hydrogels were characterized by the swelling and elasticity tests as well as by the static light scattering technique.

The non-ionic PDMAAm hydrogels were prepared in aqueous solutions over the entire range of the initial monomer concentration and the swelling behavior of the hydrogels was first investigated in water. Then the reentrant conformation transition of the hydrogels was investigated in solvent mixtures both experimentally and theoretically. The swelling behavior of ionic PDMAAm hydrogels was also studied both in water and in aqueous salt solutions. In order to make a relation between the macroscopic elastic behavior of the hydrogels and their microscopic properties, the hydrogels were also subjected to the mechanical tests. The elastic behavior of both non-ionic and ionic PDMAAm hydrogels was investigated both after preparation and after equilibrium swelling. The results were used to calculate the elastic modulus as well as the effective crosslink density and the molecular weight of the network chains.

The formation processes of PDMAAm and PAAm hydrogels were also investigated by using the static light scattering technique. The dilatometric technique was used to monitor the polymerization reactions. The appearance of nano-scale, highly crosslinked regions during the formation process of the hydrogels were monitored by use of the on-line light scattering measurements. It was found that PDMAAm hydrogels exhibits different light scattering intensity profiles than PAAm hydrogels. During the formation of PDMAAm hydrogels, both a maximum and a minimum were detected corresponding to the overlap threshold and the gel point, respectively. It was demonstrated that PDMAAm hydrogel is much more homogeneous than the conventional PAAm hydrogel of the same effective crosslink density. It was shown that the spatial gel inhomogeneity can be controlled by varying the gel point with respect to the critical overlap concentration during the preparation of the hydrogels by free-radical mechanism.

The spatial inhomogeneities and the variation of the sizes of the nanoregions in both PDMAAm and PAAm hydrogels were also investigated as a function of the initial monomer concentration, the ionic comonomer concentration and the type of the redox initiator system. The results were explained in terms of the inhomogeneity

parameters of the Debye-Bueche theory, i.e., the mean square fluctuations of the refractive index $\langle \eta^2 \rangle$ and the correlation length of the scatterers ξ. The results of the light scattering and elasticity measurements on hydrogels are discussed together to make a correlation between the crosslinking efficiency and the extent of the spatial inhomogeneity in the hydrogels.

2. SWELLING BEHAVIOR OF POLYMER NETWORKS

If a dried gel is placed in a solvent, the gel absorbs the solvent and its volume increases sometimes up to several thousand times. This phenomenon is called the gel swelling. The swelling of polymer gels is a complex phenomenon resulting from the interplay of molecular architecture of the network and the specific polymer-solvent interactions.

The driving force behind the gel swelling is the free energy of mixing of the polymer and solvent. If the polymer molecules making up the gel were not joined together, they would dissolve in the solvent to decrease the free energy of mixing, and eventually would be distributed. However, the polymers in a gel are connected, and so if the gel absorbs enough solvent it can attain an equilibrium state since there are two competing factors that determine its volume. One factor is the free energy of mixing of the gel and the solvent, which tries to increase the gel volume. The other factor is the change in elastic energy of the gel when the volume is varied, which acts to hinder the volume expansion.

2.1. Swelling Process and Swelling Ratio

The degree of swelling is one of the essential parameters to characterize the gels. Since the gel can be regarded as a container of solvent made of a three dimensional mesh, one can investigate the molecular interaction between the polymer network and the solvent by simply measuring the degree of swelling[21]. In a dried state, the gel is a solid material. However, the gel can take several hours to days to swell until it reaches the swelling equilibrium when the solvent is added.

Figure 2.1 represents the swelling and drying process of polymer gel with characteristic parameters, such as; the diameter, weight and volume which are denoted by D, m and V, respectively. The two types of swelling ratio of the hydrogels can be described as:

1) The equilibrium volume swelling ratio (q_v):

$$q_v = \frac{\text{volume of swollen gel}}{\text{volume of dry gel}} = \frac{V_{swollen}}{V_{dry}} \tag{2.1}$$

2) The equilibrium weight swelling ratio (q_w) :

$$q_w = \frac{\text{weight of swollen gel}}{\text{weight of dry gel}} = \frac{m_{swollen}}{m_{dry}} \tag{2.2}$$

where $V_{swollen}$, V_{dry} and $m_{swollen}$, m_{dry} are the volumes and the weights of the gels in the swollen state and the dry state, respectively. For the determination of both swelling ratios q_v and q_w, the volumetric and gravimetric techniques are used as will be described in Section 5.6.2.

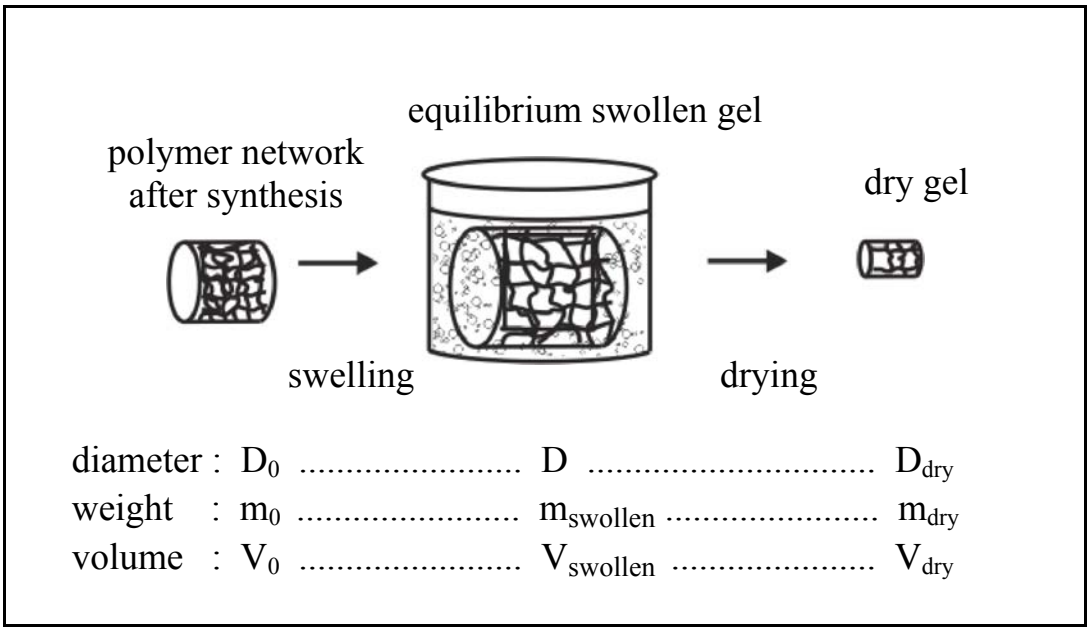

Figure 2.1: A schematic representation of swelling process of polymer network in a solvent until the equilibrium swelling and drying process of polymer gel

Figure 2.2 shows schematically the differences of two characteristic synthesis parameters, namely, ν_2 and ν_2^0. ν_2 is the volume fraction of the network in the swollen gel and can be defined as the ratio of volume of dry polymer in the swollen gel to the total volume of the swollen gel by:

$$\nu_2 = \frac{\text{volume of dry gel}}{\text{volume of the equilibrium swollen gel}} = \frac{V_{\text{dry}}}{V_{\text{swollen}}} \tag{2.3}$$

On the other hand, ν_2^0 is the volume fraction of the network after the gel synthesis and corresponds to the ratio of the volume of dry polymer to the volume of the gel after synthesis as follows:

$$\nu_2^0 = \frac{\text{volume of dry gel}}{\text{volume of the gel after synthesis}} = \frac{V_{\text{dry}}}{V_0} \tag{2.4}$$

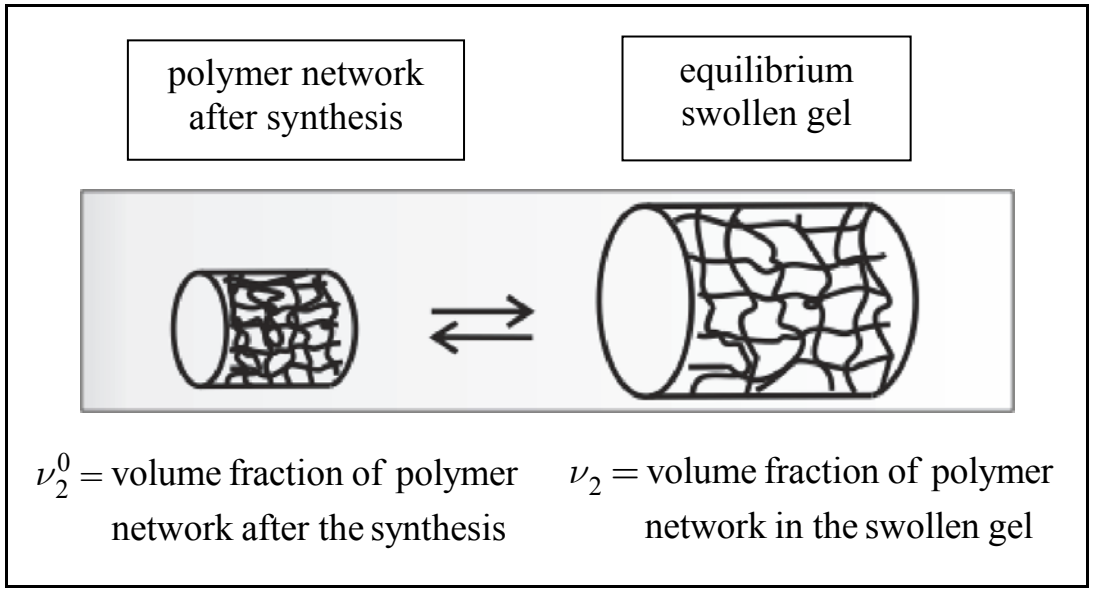

Figure 2.2: The volume fractions of the network after equilibrium swelling and after gel synthesis which is denoted by ν_2 and ν_2^0, respectively.

Equation (2.1) can be rewritten by using the definition of ν_2 in Equation (2.3) as follows:

$$q_{\text{v}} = \frac{V_{\text{swollen}}}{V_{\text{dry}}} = \frac{1}{\nu_2} \tag{2.5}$$

One of the difficulties of the determination of the swelling ratio, q_v is the measurement of the volume of dry gel due to the deformation of the shape of the gel. The gels are usually dried in vacuum and transferred from a rubbery to the glassy

state. During this process, the cylindrical shape of the gel sometimes undergoes deformation and the volume determination of dry gel becomes difficult. However, the volume of the swollen gel can be determined easily by measuring the diameter of the swollen gel sample by a calibrated digital compass. In this case, it is more convenient to write the equilibrium volume swelling ratio of the gels in terms of the volume of the gel after synthesis, i.e.,

$$q_v = \left(\frac{\text{volume of the equilibrium swollen gel}}{\text{volume of the gel after synthesis}} \right) \left(\frac{\text{volume of the gel after synthesis}}{\text{volume of dry gel}} \right) \tag{2.6a}$$

$$q_{\mathrm{v}} = \frac{V_{\mathrm{swollen}}}{V_0} \frac{V_0}{V_{\mathrm{dry}}} = \frac{V_{\mathrm{swollen}}}{V_{\mathrm{dry}}} \tag{2.6b}$$

Thus, Equation (2.6b) can be rewritten in terms of the volume fractions ν_2 and ν_2^0, by combining Equation (2.4) and (2.5) as follows:

$$q_{\mathrm{v}} = \frac{1}{\nu_2} = \frac{V_{\mathrm{swollen}} / V_0}{\nu_2^0} \tag{2.7}$$

According to Equation (2.7), the volume fractions of the network after equilibrium swelling and after gel synthesis ν_2 and ν_2^0, respectively, relate to the volume swelling ratio by:

$$\nu_2 = \nu_2^0 \left(\frac{V_{\mathrm{swollen}}}{V_0} \right)^{-1} \tag{2.8}$$

Moreover, the equilibrium swelling ratio of gels $V_{swollen}/V_0$, can be calculated as:

$$\frac{V_{\mathrm{swollen}}}{V_0} = \left(\frac{D}{D_0} \right)^3 \tag{2.9}$$

where D and D_0 are the diameter of the gels after equilibrium swelling and after preparation, respectively. Hence, by combining Equation (2.7) and (2.9), the

equilibrium volume swelling ratio of the gels can be written in terms of the synthesis parameters, ν_2 and ν_2^0, and the diameter of the gels:

$$q_{\mathrm{v}} = \frac{1}{\nu_2} = \frac{V_{\mathrm{swollen}}/V_0}{\nu_2^0} = \frac{\left(D/D_0\right)^3}{\nu_2^0} \tag{2.10}$$

Assuming additivity of volumes within the swollen gel, the interrelation between q_{v} and q_{w} is given by:

$$q_{\mathrm{v}} = 1 + \frac{\left(q_{\mathrm{w}} - 1\right)\rho}{d_1} \tag{2.11}$$

where d_1 is the density of the swelling agent. If it is assumed that the monomer conversion is complete after the crosslinking copolymerization, then the volume fraction of the polymer network after the synthesis ν_2^0, can be written in terms of the amount of the monomer used in the synthesis m_{mon}:

$$\nu_2^0 = \frac{V_{poly}}{V_{tot}} = \frac{V_{mon}}{V_{tot}} = \frac{m_{mon}/\rho_{poly}}{V_{tot}} \tag{2.12}$$

where V_{tot} is the total volume of the pre-gel solution and ρ_{poly} is the density of the polymer. The volume fraction of the polymer network after synthesis ν_2^0 can be written in terms of the initial molar concentration of the monomer, C_0 (mol/L):

$$\nu_2^0 = \frac{m_{mon}/\rho_{poly}}{V_{tot}} = \frac{n_{mon}M_{w,mon}/\rho_{poly}}{V_{tot}} = C_0\frac{M_{w,mon}}{V_{tot}} = C_0\bar{V}_r \tag{2.13}$$

where n_{mon} the mole number of the monomer used in the synthesis, $M_{w,mon}$ is its molecular weight and $\bar{V}_{\mathrm{r}}$ is the molar volume of the polymer repeat units (in ml/mol). By using Equation (2.13), the theoretical value of ν_2^0 can be calculated from the initial monomer concentration used in the gel preparation. The volume

fraction of the polymer network after synthesis ν_2^0 can be calculated experimentally by using the equation:

$$\nu_2^0 = \left[1 + \frac{(q_F - 1)\rho}{d}\right]^{-1} \tag{2.14}$$

where q_F is the dilution degree after the gel synthesis which can be defined as:

$$q_F = \frac{\text{weight of gel after synthesis}}{\text{weight of dry gel}} = \frac{m_0}{m_{dry}} \tag{2.15}$$

2.2. Factors Affecting Swelling Behavior of Polymer Networks

The interaction between the solvent and the polymer network strongly affects the swelling properties of the gel. The gel swells to a large extent in a good solvent, whereas it shrinks to a compact form in a poor solvent. The swelling is accompanied by diffusion of the polymer network in the solvent rather than the solvent diffusion into the polymer network, therefore both the gel elasticity and the friction between the polymer network and the solvent determine the gel swelling.

i. The initial molar concentration of the monomer, C_0 (mol/L): The swelling behavior of the gels sensitively depend on the degree of dilution at which they are formed. The degree of dilution of the polymer networks after their preparation is denoted by ν_2^0, the volume fraction of the network after synthesis. Equation (2.13) shows that ν_2^0 is proportional to the initial molar concentration of the monomer, C_0. This means that, the higher the initial concentration of the monomer, C_0 , the higher the value of ν_2^0. On the other hand, according to Equation (2.7), ν_2^0 is inversely proportional to the equilibrium volume swelling ratio q_v. Hence, the equilibrium swelling ratio of the gels with constant crosslink density decreases with increasing monomer concentration. The higher the initial monomer concentration, the larger the effective crosslink density of the hydrogels and the smaller their swelling capacity.

ii. The crosslinker concentration, i.e. the crosslinker ratio, *X*: The equilibrium volume swelling ratio of the gels decreases with increasing crosslinker ratio. The crosslinker ratio can be defined as the number of crosslinks per unit volume of the polymer network and written as the mole ratio of crosslinker to the monomer:

$$X = \frac{[\text{crosslinker}]}{[\text{total monomer}]} = \frac{1}{2N} \tag{2.16}$$

where *N* is the number of segments between two successive crosslinks. Increasing monomer concentration also increases the effective crosslink density ν_e of the gels due to the more efficient consumption of the crosslinker in concentrated monomer solutions. Increasing crosslink density will decrease the swelling of gels due to decreasing number of segments *N* and the molecular weight of network chain $\bar{M}_c$ between two successive crosslinks which are also shown schematically in Figure 2.3.

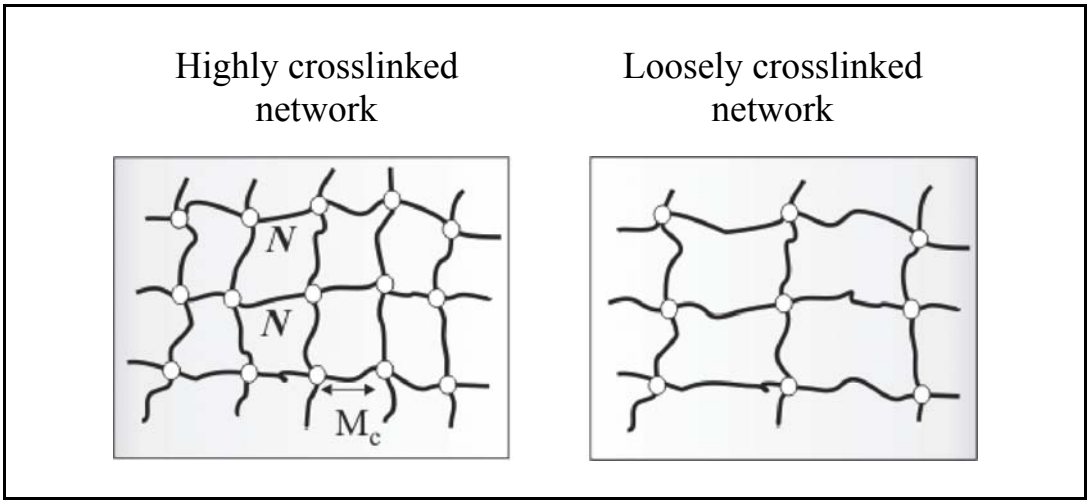

Figure 2.3: A schematic representation of highly and loosely crosslinked polymer networks. The number of segments *N* and the molecular weight of the network chain $\bar{M}_c$ between two successive crosslinks are also indicated in the figure.

It was also found that the dependence of the swelling rate on the crosslinker content shows two different regimes. Below a critical crosslinker concentration, increasing the crosslinker concentration decreases the rate of swelling of the networks. Because, rising the crosslinker content in the gel brings about a decrease in the mesh size of the gel network and the diffusion of the solvent molecules into the gel networks

becomes difficult. Thus the gel with a high amount of crosslinker absorbs less amount of solvent in the equilibrium swelling state.

The higher the crosslinker (BAAm) content, the lower the swelling capacity of the gels. However, above the critical crosslinker concentration, although the swelling capacity of the network continue to decrease, the rate of swelling rapidly increases with increasing crosslinker content, which is opposite to what observed below the critical value. This point can be explained with the formation of heterogeneous structures in the polymer network. Below the critical crosslinker concentration, the network consist of aggregates of spherical domains which are called as microspheres. After passing the critical crosslinker concentration, the network structure changes from homogeneous to heterogeneous ones. Further increase of the crosslinker content increases both the rate of swelling and the porosity of the network[22].

iii. The solvent quality and the interactions between polymer and solvent: The degree of swelling of the gels also depends on the compatibility of the solvent with the polymer network. The quality of the solvent may be expressed by the parameter χ or χ_{12} (in which the subscripts 1 and 2 denote the solvent and polymer, respectively). The interaction parameter is used to indicate whether a solvent is good or poor for the polymer. A good solvent has a low value of χ_{12} while a poor solvent has a high value of χ_{12}. In good solvents, the polymer network chains are in the extended conformation due to the strong molecular interaction between the polymer segment and the solvent. Thus, the degree of swelling at equilibrium in a good solvent increases with decreasing crosslinking. On the other hand, in poor solvents, the molecular interaction between the polymer segment and the solvent molecules is not favored and the polymer-polymer contacts are preferred. The polymer segments reduce their resistance against each other and an attractive force developed between them. Thus, the polymer chains tend to shrink. The relation between the interaction parameter and the solubility parameter of the solvent and the polymer can be given through the equation as:

$$\chi = V_{\mathrm{m}} \frac{\left(\delta_{\mathrm{solvent}} - \delta_{\mathrm{polymer}}\right)^2}{RT} \tag{2.17}$$

where V_m is the molar volume of the polymer solution and δ denotes the solubility parameter of the solvent and the polymer.

As shown in Figure 2.4, a positive χ denotes that the polymer-solvent contacts are less favored compared with the polymer-polymer and the solvent-solvent contacts. A negative χ means that the polymer-solvent contacts are preferred, promoting solvation of the polymer.

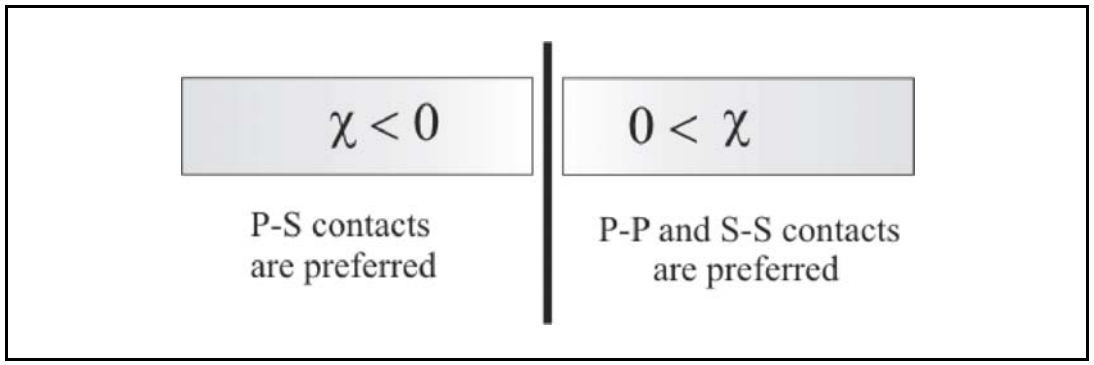

Figure 2.4: Negative χ promotes mixing of polymer with the solvent, whereas positive χ prefers polymer-polymer and solvent-solvent contacts to polymer-solvent contacts.

iv. The ionic group concentration: The swelling behavior is also dependent on the presence of the ionic groups in the network chains. If the network chains of the gel carry ionic groups also called charged units, the gel swells much more than the corresponding uncharged gel. The reason of this excess swelling is the existence of mobile counterions in the gel and the additional swelling forces due to the electrostatic repulsion between like charges on the polymer chains.

As the ionic group concentration increases, the counterions concentration inside the gel also increases to maintain the electroneutrality condition. As a result, the difference between the counterion concentration inside and outside the gel increases with increasing the ionic group concentration, which creates an additional osmotic pressure that expands the gel.

v. External factors: Some of the external parameters affecting the swelling of hydrogels include pH, ionic strength, temperature, solvent composition and electromagnetic radiation [23-25].

2.3. Phase Transition of Polymer Gels

Analogous to a single chain that exhibits a coil-globule transition, the hydrogels sometimes undergo reversible discontinuous or continuous volume change when it is stimulated by chemical or physical factors. The volume phase transition means a dramatic volume change of the gel between its swollen and collapsed states induced by a tiny environmental change. In a sense, the volume phase transition of gels is a macroscopic manifestation of a coil-globule transition of polymer chains. The microscopic and macroscopic views of volume phase transition are shown in Figure 2.5.

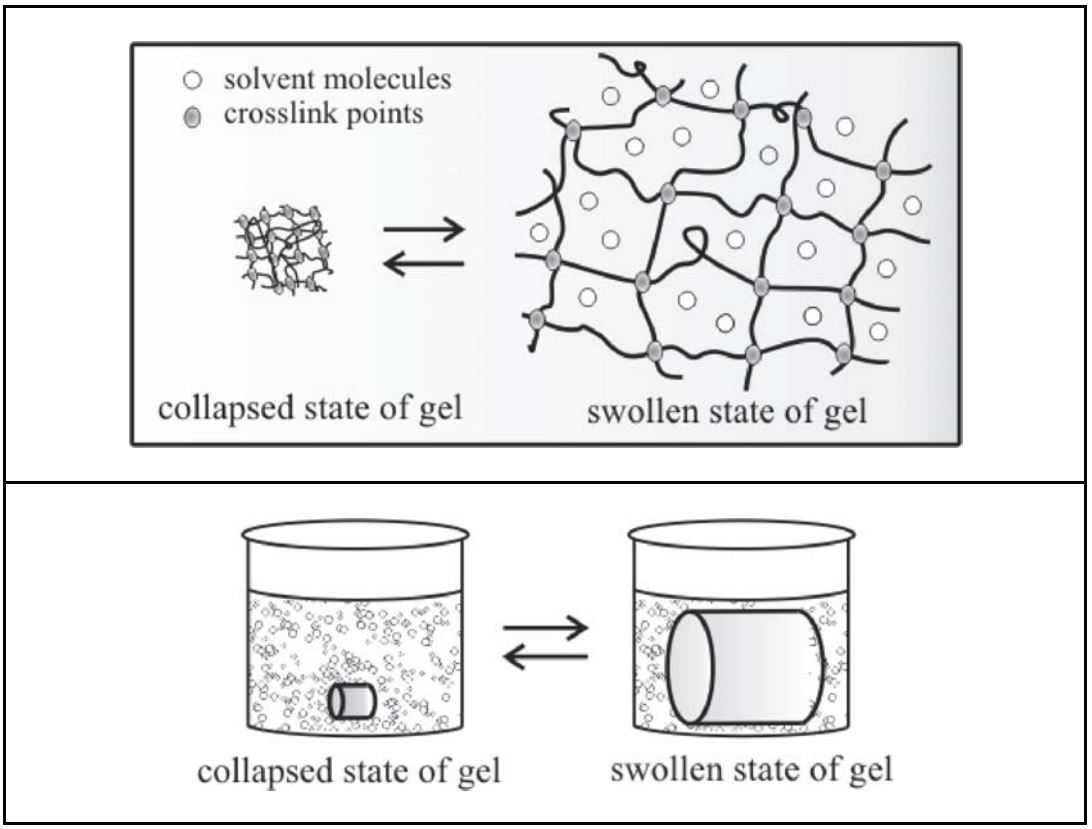

Figure 2.5: The microscopic view of phase transition of polymeric gel-unfolding and folding of polymer network (upper). The macroscopic view of reversible phase transition of polymeric gel (lower).

The phase transition in polymer gels has been studied for about two decades since its theoretical prediction by Dusek and Patterson as early as 1968 [9]. They suggested that when the external forces are applied to the gels, the gel volume might undergo discontinuous change. The experimental verification was first made by Tanaka in 1978 using hydrolysed poly(acrylamide) gels swollen in water/acetone[8]. The gels

of various degree of hydrolysis were placed in acetone-water mixtures with different concentrations of acetone at room temperature. After one day, it was found that half of the gels is in a swollen state and half of the gels is in a collapsed state. Thus, the volume phase transition of the gels was discovered and opened a new aera of the study of the polymer gels.

The volume phase transition of polymer gel is a result of a competitive balance between repulsive forces that act to expand the polymer network and attractive forces that act to shrink the polymer network. The attractive forces include van der Waals[25], hydrophobic interaction[26,27], and hydrogen bonding[28,29]. The repulsive forces include the electrostatic interaction between the polymer charges of the same kind and the osmotic pressure by the counter ions[30]. The fundamental molecular interactions, which control the interactions between the polymer backbone and the small molecules inside the polymer are illustrated in Figure 2.6.

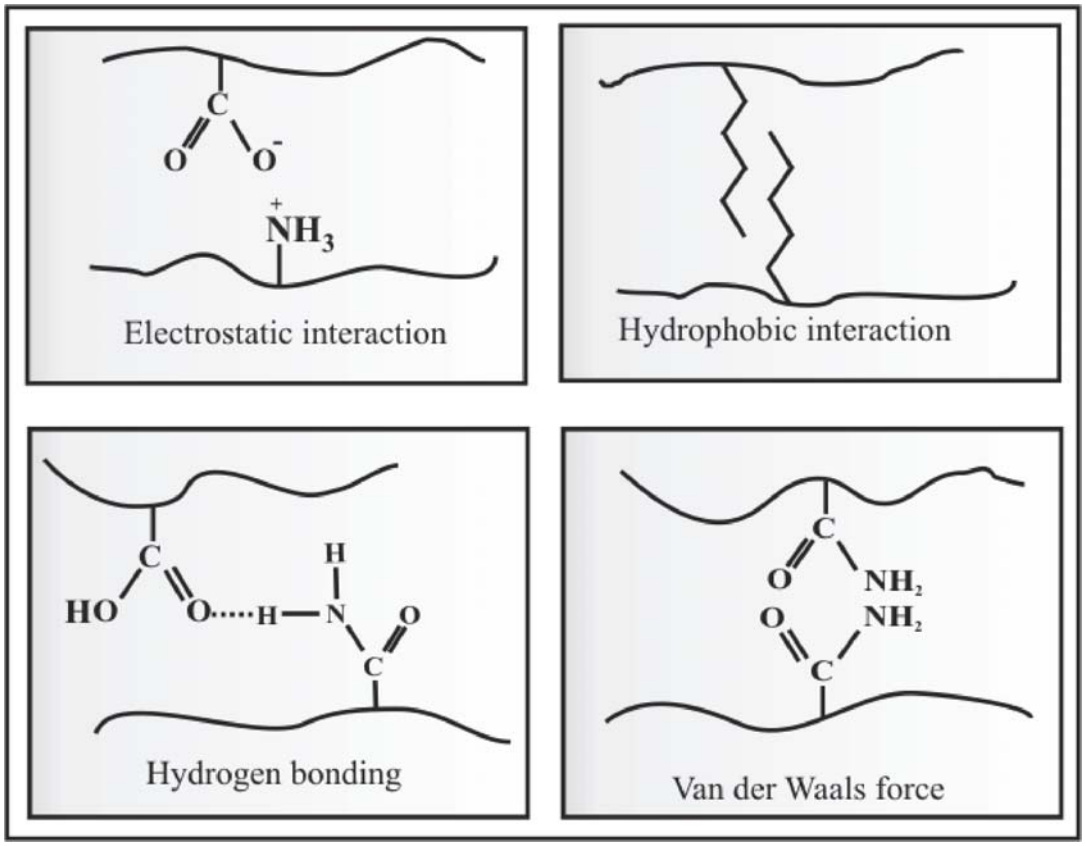

Figure 2.6: Fundamental interactions for phase transition of a gel[31].

The major attraction force between the polymer chains is the van der Waals force. The volume phase transition of the partially hydrolyzed poly(acrylamide) gel is

believed to be due to the van der Waals interaction. A poor nonpolar solvent must be added to a good solvent in order to increase this interaction large enough to induce the volume phase transition of the gel[25].

2.4. Thermodynamics of Gel Swelling and Flory-Rehner Theory

The classical gel swelling theory was developed in the mid 1940's. Since then the theoretical and experimental efforts have been done in order to better understand the swelling phenomenon in the polymer gels. A large portion of this work was developed by Paul J. Flory whose concepts and basic approach are still largely used to improve the swelling of gels.[32] In the following paraghraphs, the swelling process of the polymer gel immersed in a solvent will be described at first and then the theory of the equilibrium swelling will be discussed.

During the swelling process, the network chains are forced to attain more elongated, less probable configurations. The absorption of the solvent by the gel causes the network to expand and its chains to stretch. As a result, the chains making up the network is assumed in a stretched conformation as the network swells. Hence, like pulling a spring from both ends, a decrease in chain configurational entropy is produced by swelling. Opposing this, an increase in entropy of mixing of solvent with polymer accompanies the swelling. In addition, the enthalpy of mixing also controls the extent of swelling. Accordingly, mainly three forces arise from different sources during the process of swelling:

1. The entropy change caused by mixing polymer and solvent: The entropy change from this source is positive and favors swelling.

2. The entropy change caused by reduction in the number of possible chain conformations as the polymer network swells: The entropy change from this source is negative and opposes swelling.

3. The heat of mixing of polymer and solvent, which may be positive, negative, or zero. Usually, it is slightly positive and opposing mixing.

The combination of thermodynamic and elasticity theories states that the crosslinked polymer gel which is immersed in the solvent and allowed to reach equilibrium with its surroundings is subject only to two opposing forces; one is the swelling force which is the interaction between the polymer and the solvent. The other is the elastic

force which depends on the degree of crosslinking. A state of equilibrium swelling is reached when these two forces are equal.

The ability to absorb good solvents arises from the spontaneity of the mixing processes, while their resistance to dissolution arises from crosslinks between the network chains. As the network is swollen by absorption of solvent, the chains between network junctions are required to assume elongated configurations and an elastic retractive force consequently develops in opposition to the swelling process. As the mixing of the solvent and the polymer proceeds, the driving force for mixing decreases and the elastic retractive forces increase until the process reaches a state of equilibrium swelling in which these two forces are in balance[32].

The Flory-Rehner phenomenological theory has been most widely used to explain the swelling process of gels that do not contain ionic moieties[33]. A basic element of the Flory-Rehner theory is the so-called "additivity assumptions", which states that the change in the Gibbs free energy ($\Delta G_{\text{swelling}}$) during the swelling process could be expressed as the sum of the individual free energy terms, i.e., the changes in the free energy of mixing ΔG_{mix}, in the free energy of elastic deformation ΔG_{el} [32,33,39]:

$$\Delta G_{\text{swelling}} = \Delta G_{\text{mix}} + \Delta G_{\text{el}} \tag{2.18}$$

where ΔG_{mix} is the free energy change of mixing of the solvent molecules and the polymer chains. This term is a measure of the compatibility of the polymer with the solvent molecules and ΔG_{el} is the elastic free energy change due to the configurational rearranging and stretching of the crosslinked network chains during the swelling process.

In the Flory-Rehner approach, the polymer-solvent mixing free energy term is obtained from the Flory-Huggins theory, and the elastic free energy term is obtained from the affine network theory for rubber elasticity. The theories used to describe these contributions will be discussed in the following sections.

2.4.1. Thermodynamic Relations and Flory-Huggins Theory

2.4.1.1. Thermodynamics of Polymer Solutions

The interaction between the polymer and the solvent molecule can be defined in terms of the thermodynamic properties of the polymer solution. When an amorphous polymer is mixed with a suitable solvent, it disperses in the solvent. In a good solvent the energetic interaction between the polymer and the solvent is favorable and the coil size is expanded beyond its unperturbed dimension, whereas in a poor solvent the interaction is not as favorable, and the coil size is much nearer the unperturbed dimension. This energetic interaction can be defined in terms of the Gibbs free energy of mixing, ΔG_{mix} :

$$\Delta G_{\text{mix}} = G_{12} - (G_1 + G_2) = \Delta H_{\text{mix}} - T\Delta S_{\text{mix}} \tag{2.19}$$

where, G_1 is the free energy of the solvent, G_2 is the free energy of the polymer, G_{12} is the free energy of the polymer solution, ΔH_{mix} the enthalpy of mixing, and ΔS_{mix} the entropy of mixing. If $\Delta G_{\text{mix}} < 0$ then the polymer will dissolve in the solvent and form a solution.

The theory of polymer solutions started from the Flory-Huggins lattice model, which is the simplest state theory of polymer solutions and is based on the concept developed by Hildebrand theory for solutions of small molecules. The difference between the Hildebrand and Flory-Huggins theory is that it considered the effect of different molecular sizes on the entropy contribution to the free energy change, which accompanies the mixing of two kinds of molecules with different sizes. In the following, thermodynamics of regular solutions will be discussed and then an overview of the Flory-Huggins Lattice theory for polymer solutions including basic assumptions will be given[34,35].

The idea of regular solution was introduced independantly by Hildebrant and Wood [34]. The molecules are placed in a regular lattice and the mixing enthalpy (always positive) is calculated from nearest-neighbour interaction. The volume of the regular solution is equal to the sum of the volume of its components, i.e. there is no change in the volume on mixing the components. It is convenient to think about regular

solution in terms of a regular lattice with positions that can be occupied by either of the components. It being assumed that each molecule occupies only one lattice position, as shown in Figure 2.7(left).

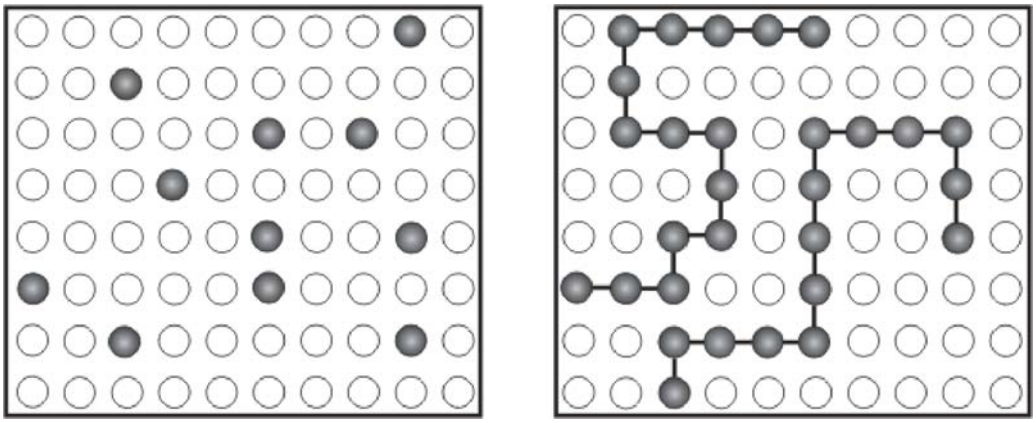

Figure 2.7: Illustration of two types of molecules on the lattice structure for a binary solution of small molecules (left) and for a polymer dissolved in a low molar mass of solvent (right). The gray sites are occupied by solute, and the white sites are occupied by solvent molecules.

The mixing entropy is determined by the number of possible ways (P) of arranging the mixture of two low molar mass components, denoted 1 and 2. P is given by:

$$P = \frac{N!}{N_1!N_2!} \tag{2.20}$$

where N is the total number of lattice positions present, N_1 is the number of molecules of type 1 and N_2 is the number of molecules of type 2. The Boltzmann's entropy law ($S = k\ln P$) may then be applied to obtain the mixing entropy:

$$\Delta S_{\text{mix}} = k \ln P = k\left(\ln N! - \ln N_1! - \ln N_2!\right) \tag{2.21}$$

and using Stirling's approximation ($\ln x! \approx x \ln x - x$), the following equation is obtained:

$$\Delta S_{\text{mix}} = k\left(\ln N - N - N_1 \ln_1 + N_1 - N_2 \ln N_2 + N_2\right) \tag{2.22}$$

which can be simplified, since $N = N_1 + N_2$:

$$\Delta S_{\text{mix}} = -k\left(N_1 \ln x_1 + N_2 \ln x_2\right) \tag{2.23}$$

where x_1 and x_2 are the mole fractions of component 1 and 2, respectively. Equation (2.23) can be rewritten using quantities in molar terms:

$$\Delta S_{\text{mix}} = -R\left(n_1 \ln x_1 + n_2 \ln x_2\right) \tag{2.24}$$

in which n_1 and n_2 are the number of moles of component 1 and 2, respectively. The enthalpy of mixing $\left(\Delta H_{\text{mix}}\right)$ can be calculated from the interaction energies of the contacting atoms (1-1, 2-2, and 1-2 contacts) as:

$$\Delta H_{\text{mix}} = \left(\sqrt{\Delta E_1} - \sqrt{\Delta E_2}\right)^2 x_1 x_2 = B x_1 x_2 \tag{2.25}$$

where ΔE_1 and ΔE_2 are the energies of vaporization of components 1 and 2. Equation (2.25) is strictly valid only for the solutions consisting of components of equal sizes in the absence of specific interactions such as the hydrogen bonding. The free energy of mixing $\left(\Delta G_{\text{mix}}\right)$ for the regular solution is obtained by inserting the entropic and the enthalpic components into the Equation (2.19) as follows:

$$\Delta G_{\text{mix}} = B x_1 x_2 + RT\left(n_1 \ln x_1 + n_2 \ln x_2\right) \tag{2.26}$$

2.4.1.2. A General View of Flory-Huggins Theory

The theory of the regular solution is valid only for solutions possessing molecules of the same size. For the polymer solution where the solute and the solvent molecules significantly differ in their size, Flory and Huggins put forward independently a statistical theory to take into account the contribution of the entropy of mixing. Both models are based on the idea of a lattice in which the components of the mixture are placed. Both models assume that the volume is unchanged during mixing. The mixing entropy is strongly influenced by the chain connectivity of the polymer component. The mixing entalpy should for polymer-small molecule mixtures have a form similar to that for regular solutions. The mixing entropy and enthalpy are first

calculated separately in the Flory-Huggins treatment and then brought together in the free energy of mixing as in the case of the regular solution model[35,36].

i. Entropy of mixing for polymer solutions

In order to calculate the entropy of mixing, the polymer molecules are divided into *x* chain segments, each of which is in equal in size to a solvent molecule. Figure 2.7(right) shows schematically the lattice model used in the calculations. Each segment occupies one position in the lattice and so does each solvent molecule. The *N* lattice position are partitioned between N_1 solvent molecules and N_2 polymer solute molecule. Each polymer molecule occupies *x* lattice positions so that *N* equals to $N_1 + xN_2$. The situation at which the analysis starts is when *i* polymer molecules have already been placed in the lattice.

The number of vacant positions is then $N - xi,$ which is equal to the number of different ways of placing the first segment of the $(i+1)$th molecule. The number of different ways of arranging the next segment is equal to the product of the coordination number (*z*) of the lattice and the fraction of remaining vacant position $(1-f_i)$, so that $z(1-f_i)$. The third segment have one adjacent position occupied by the 'previous' segment, hence they can take any of $(z-1)(1-f_i)$ positions. The number of different ways of arranging the $(i+1)$th molecule becomes:

$$\nu_{i+1} = (N - xi)\, z\,(z-1)^{x-2}\,(1-f_i)^{x-1} \tag{2.27}$$

The number of different ways to arrange all the polymer molecule is:

$$P_2 = \frac{\nu_1 \nu_2 \nu_3 \nu_4 \ldots \nu_{N_2}}{N_2!} \tag{2.28}$$

The reason for introducing the divisor $N_2!$ is that the different polymer molecules cannot be distiguished. Since the fraction of the vacant positions $1-f_i$ equals to $(N-xi)/N$. Equation (2.27) can be rewritten as follows:

$$v_{i+1} = \left(N - xi\right)^{x} \left(\frac{z-1}{N}\right)^{x-1} \tag{2.29}$$

Only diluted solutions are considered in the theory, so that $N >> x$. Under these conditions, Equation (2.29) can be expressed approximately as:

$$v_{i+1} = \frac{\left(N - xi\right)^{x}}{\left[N - x\left(i+1\right)\right]!} \left(\frac{z-1}{N}\right)^{x-1} \tag{2.30}$$

Insertion of Equation (2.30) into Equation (2.28) gives:

$$P_2 = \frac{1}{N_2!} \frac{\left(N-x\right)!}{\left(N-\left(N_2+1\right)x\right)!} \left(\frac{z-1}{N}\right)^{N_2\left(x-1\right)} \approx \frac{N!}{\left(N-N_2x\right)!N_2!} \left(\frac{z-1}{N}\right)^{N_2\left(x-1\right)} \tag{2.31}$$

The entropy of the solution is calculated from the Boltzmann equation $\left(S = k \ln P_2\right)$:

$$S = k \ln P_2 = k\left\{\ln N! - \ln\left(N - xN_2\right)! - \ln N_2! + N_2\left(x-1\right)\ln\left(z-1\right) - N_2\left(x-1\right)\ln N\right\} \tag{2.32}$$

which after inserting Stirling's approximation becomes:

$$S = k\left\{N \ln N - \left(N - xN_2\right)\ln\left(N - xN_2\right) - N_2 \ln N_2 - N_2\left(x-1\right) + N_2\left(x-1\right)\ln\left(z-1\right)\right. \tag{2.33}$$

$$\left. - N_2\left(x-1\right)\ln N \right\}$$

Equation (2.33) can be simplified by considering that $N = N_1 + xN_2$:

$$S = k\left\{-N_1 \ln\left(\frac{N_1}{N_1 + N_2x}\right) - N_2 \ln\left(\frac{N_2}{N_1 + N_2x}\right) + N_2\left(x-1\right)\ln\left(\frac{z-1}{e}\right)\right\} \tag{2.34}$$

As shown in Figure 2.8, the formation of the polymer solution takes places in two steps:

(a) Disorientation of the polymer molecules.

(b) The mixing of the polymers and the solvent.

The entropy of disorientation state prior to mixing the polymer with the solvent is calculated by inserting $N_1 = 0$ into Equation (2.34), which gives:

$$S_{\text{disorientation}} = kN_2\left[\ln x + (x-1)\ln\left(\frac{z-1}{e}\right)\right] \tag{2.35}$$

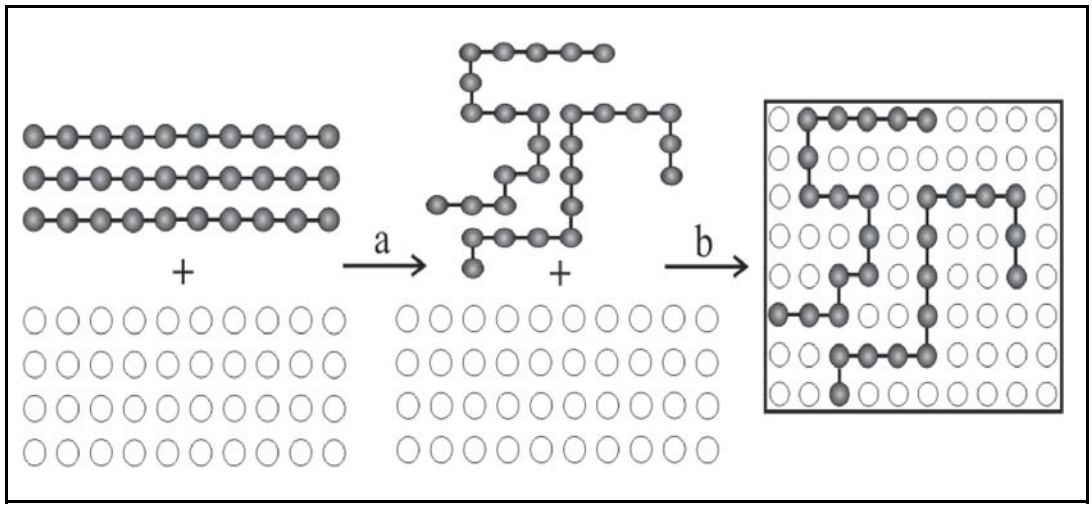

Figure 2.8: Schematic representation of steps (a) and (b) in the disordering and mixing of the polymer and the solvent.

The entropy increase obtained when the molecules are disorientated according to step (a) is subtracted from the total entropy increase (Equation (2.34)) to obtain the entropy of mixing (step (b)). Equation (2.35) is then subtracted from Equation (2.34) to obtain ΔS_{mix} :

$$\Delta S_{\text{mix}} = -k\left\{N_1 \ln\left(\frac{N_1}{N_1 + xN_2}\right) N_2 \ln\left(\frac{xN_2}{N_1 + xN_2}\right)\right\} \tag{2.36}$$

which, after considering that,

$$\nu_1 = \frac{N_1}{N_1 + xN_2} \qquad \text{and} \qquad \nu_2 = \frac{xN_2}{N_1 + xN_2} \tag{2.37}$$

where ν_1 and ν_2 are the volume fractions of the solvent and the polymer respectively, becomes:

$$\Delta S_{\text{mix}} = -k(N_1 \ln \nu_1 + N_2 \ln \nu_2) \tag{2.38}$$

which in molar terms converts to:

$$\Delta S_{\text{mix}} = -R(n_1 \ln \nu_1 + n_2 \ln \nu_2) \tag{2.39}$$

where n_1 and n_2 are the number of moles of the solvent and the polymer, respectively.

ii. Heat of mixing for polymer solutions

For an ideal solution $\Delta H_{\text{mix}} = 0$. This assumption is not valid for the polymer solutions. There is a finite enthalpy change which accompanies the polymer dissolution due to the replacement of the polymer-polymer and the solvent-solvent contacts with the polymer-solvent contacts. Again using the lattice model and taking only the interactions between nearest neighbors in the solution, the mixing enthalpy can be calculated by considering the interaction energies between the solvent molecules and the polymer segments.

In Figure 2.9, the interactions between the solvent and the polymer molecules are shown schematically. The interactions for the solvent-solvent (1-1) contact, the polymer-polymer (2-2) contact, and the polymer-solvent (1-2) contact is denoted by w_{11}, w_{22}, and w_{12}, respectively. Consider that a polymer segment surrounded by $\nu_1 z$ neighbors of solvent molecules and $\nu_2 z$ neighbors of polymer segments (Figure 2.9; left-hand side). The interaction energy is $\nu_1 z w_{12} + \nu_2 z w_{22}$. The lattice consists of $n\nu_2$ polymer segments each interacting in this manner. The total interaction energy (H_2) is thus,

$$H_2 = \frac{1}{2} N \nu_2 (\nu_1 z w_{12} + \nu_2 z w_{22}) \tag{2.40}$$

The factor ½ enters this expression because each pair of interacting species is counted twice by this procedure.

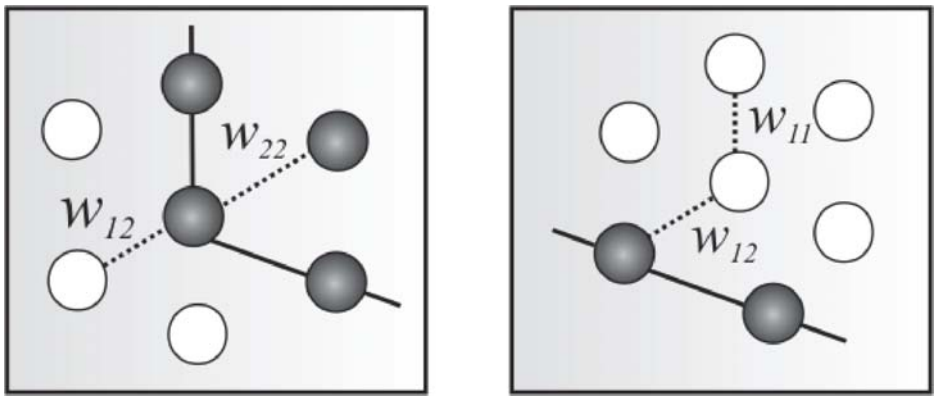

Figure 2.9: Schematic illustration of the interactions between the solvent (open) and polymer (filled) molecules.

In the same way (Figure 2.9; right-hand side), the interaction energy (H_1) for the solvent molecules is obtained as follows:

$$H_1 = \frac{1}{2} N\nu_1(\nu_1 z w_{11} + \nu_2 z w_{12}) \tag{2.41}$$

The (1-1) and (2-2) interaction energies characteristic of the pure states, denoted H_{01} and H_{02}, are thus:

$$H_{01} = \frac{1}{2} N\nu_{11} z w_{11} \qquad \text{and} \qquad H_{02} = \frac{1}{2} N\nu_2 z w_{22} \tag{2.42}$$

Equations (4.40)-(4.42) are then combined to obtain the enthalpy of mixing (ΔH_{mix}):

$$\Delta H_{\text{mix}} = (H_1 + H_2) - (H_{01} + H_{02}) = \frac{1}{2} N z \nu_1 \nu_2 (2w_{12} - w_{11} - w_{22}) \tag{2.43}$$

Mixing the solvent and the polymer changes the overall interaction energy through rearrangement of contacts. Figure 2.10 illustrates the change in the two-dimensional rendering of the lattice. Before mixing, there are four (2-2) contacts and four (1-1) contacts between a total of eight sites. Mixing replaces two (2-2) contacts and two (1-1) contacts with four (1-2) contacts. The interaction energy on these eight bonds changes from ($4w_{11} + 4w_{22}$) to ($4w_{12} + 2w_{11} + 2w_{22}$).

The difference is $(4w_{12} - 2(w_{11} + w_{22}))$. Per newly created (1-2) contact, the change in the energies Δw_{12} is:

$$\Delta w_{12} = w_{12} - \frac{1}{2}(w_{11} + w_{22}) \tag{2.44}$$

and which is inserted into Equation (2.43) to give:

$$\Delta H_{\text{mix}} = Nz\nu_1\nu_2\Delta w_{12} = N_1 z\nu_2\Delta w_{12} \tag{2.45}$$

i. If the (1-2) attractions are stronger than the (1-1) and (2-2) attractions, both Δw_{12} and ΔH_{mix} are negative, and the mixing process is exothermal.

ii. If the (1-1) and (2-2) attractions are stronger than the (1-2) interaction, Δw_{12} and ΔH_{mix} are positive and the mixing is endothermal.

iii. The intermediate case, when Δw_{12} and ΔH_{mix} are zero, is called athermal mixing.

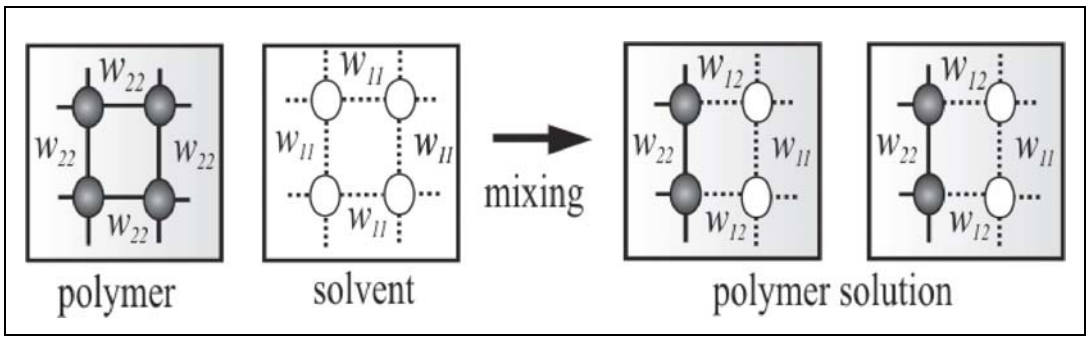

Figure 2.10: Change in the contacts between nearest neighbors when the polymer chain mixes with the solvent molecules.

The χ_{12} parameter, also called Flory-Huggins parameter, is defined as the product of the lattice coordinate *z* and the energy change reduced by kT :

$$\chi_{12} = z\left[w_{12} - (w_{11} + w_{22})/2\right]/kT \tag{2.46}$$

By using molar notation, Equation (2.45) can be written in the following form:

$$\Delta H_{\text{mix}} = kT\chi_{12}N_1\nu_2 = RT\chi_{12}n_1\nu_2 \tag{2.47}$$

Using the above expression for the heat of mixing and assuming that the entropy of mixing is adequately represented by Equation (2.39), the total free energy change due to mixing can be calculated as follows:

$$\Delta G_{\text{mix}} = RT\left[n_1 \ln \nu_1 + n_2 \ln \nu_2 + \chi_{12} n_1 \nu_2\right] \tag{2.48}$$

Equation (2.48) along with one for the elastic behavior of the crosslinked systems can be used to describe the swelling process. The following chapter describes the rubber elasticity theory in which the elastic free energy of the polymer network is given by the Equation (3.37). Substitution of the Equations given for ΔG_{el} and ΔG_{mix} into the Equation (2.18) gives the free energy equation of swelling for non-ionic polymer networks as follows:

$$\Delta G_{\text{swelling}} = RT\left[n_1 \ln \nu_1 + n_2 \ln \nu_2 + \chi_{12} n_1 \nu_2 + \frac{3}{2}\overline{\nu}\left\{\left(\frac{\nu_2^0}{\nu_2}\right)^{2/3} - 1 - \ln\left(\frac{\nu_2^0}{\nu_2}\right)^{1/3}\right\}\right] \tag{2.49}$$

2.4.2. Swelling Behavior of Polymer Network in Single Solvent

The theory for the thermodynamics of gels provides a qualitative understanding of the swelling behavior of these systems. Figure 2.11 illustrates schematically the equilibrium swelling state of the polymer network.

When the crosslinked polymer network is placed in the solvent, it absorbs the solvent and swells. It is necessary to understand the factors influencing the equilibrium degree of swelling. Therefore, the thermodynamics of gel swelling will be reviewed throughly in order to provide a sufficient background. According to the definition of equilibrium, the free energy change during swelling would pass through a minimum as shown in Figure 2.12. The gel will swell until the chemical potential of solvent, μ_1, inside the gel is equal to that of in the solution, subject to the condition of minimum total free energy at equilibrium.

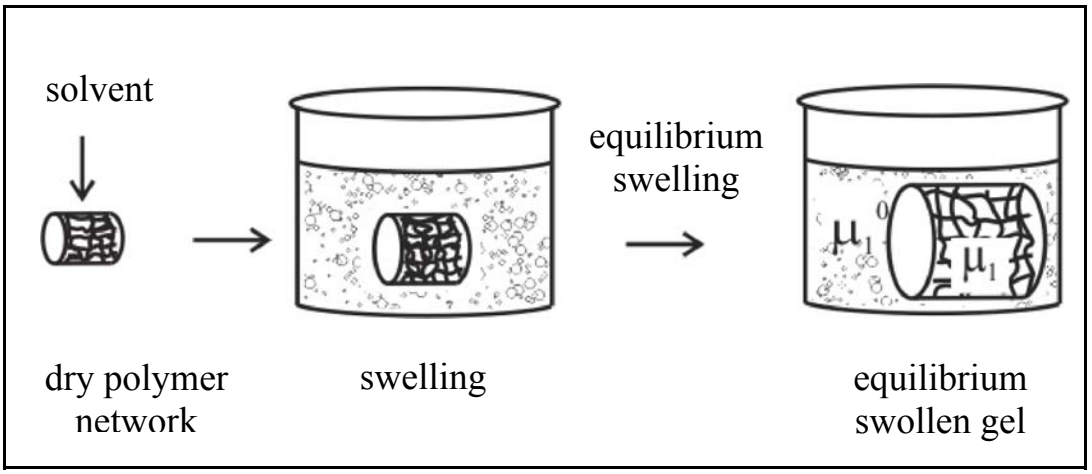

Figure 2.11: Schematic representation of the swelling of the polymer network until the equilibrium swelling state.

Thus, at equilibrium, the difference between the chemical potentials of the solvent outside and inside the gel must be zero. This may be written as follows:

$$\left(\mu_1 - \mu_1^{\,o}\right)^{\text{gel}} = \left(\mu_1 - \mu_1^{\,o}\right)^{\text{solution}} \qquad \text{and} \qquad \Delta\mu_1^{\,\text{gel}} = \Delta\mu_1^{\,\text{solution}} \tag{2.50}$$

where $\mu_1^{\,o}$ represents the solvent chemical potential at a reference state and $\Delta\mu_1$ is the excess chemical potential of solvent.

In terms of the osmotic pressure, the total osmotic pressure, π, becomes equal to zero at the swelling equilibrium. Osmotic pressure of a gel determines whether the gel tends to expand or to shrink.

When non-zero, π provides a driving force for the gel volume change. The solvent moves into or out of the gel until π is zero, i.e. until forces acting on the gel are balanced. The chemical potential may be converted to the osmotic swelling pressure as:

$$\pi = \frac{-\left(\mu_1^{\text{gel}} - \mu_1^{\text{sol}}\right)}{V_1} = \frac{-\Delta\mu_1}{V_1} = 0 \tag{2.51}$$

where V_1 is the molar volume of the solvent.

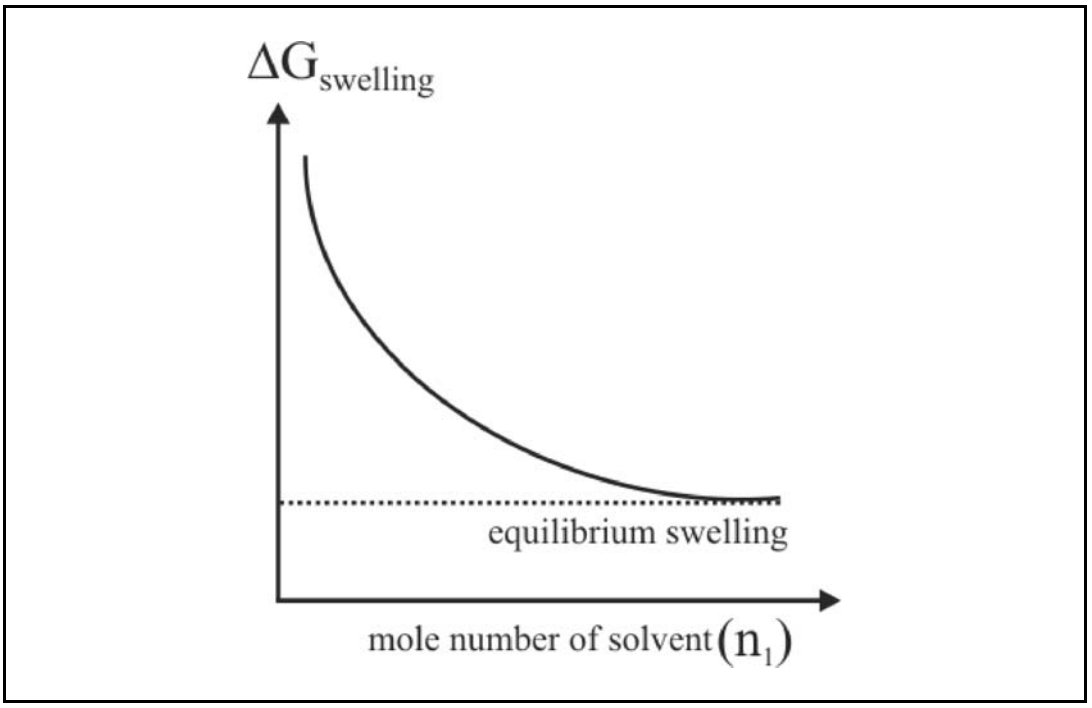

Figure 2.12: The variation of the total free energy of the gel-solvent system ΔG with the number of moles n_1 of the solvent molecules during the swelling of the polymer gel.

Since the chemical potential of a given component is defined as the partial derivative of the free energy with respect to the number of moles of that component, the excess chemical potential of solvent can be calculated by differentiation of the total free energy of swelling $\Delta G_{\text{swelling}}$ with respect to the number of moles n_1 of the solvent molecules as:

$$\left(\frac{\partial \Delta G_{\text{swelling}}}{\partial n_1}\right)_{\text{T,P}} = \Delta\mu_1 \tag{2.52}$$

Differentiation of the total free energy of swelling $\Delta G_{\text{swelling}}$ given by Equation (2.49) with respect to the number of moles of the solvent molecules while keeping the temperature and the pressure constant, result in the following equations for affine and phantom networks, respectively:

$$\Delta\mu_1 = RT\left[\ln(1-\nu_2)+\nu_2\left(1-\frac{1}{x}\right)+\chi_{12}\nu_2^2+\frac{\bar{\nu}}{xn_2}\left(\nu_2^{1/3}\left(\nu_2^0\right)^{2/3}-\nu_2/2\right)\right] \tag{2.53}$$

$$\Delta\mu_1 = RT\left[\ln\left(1-\nu_2\right)+\nu_2\left(1-\frac{1}{x}\right)+\chi_{12}\nu_2^2+\frac{\xi}{xn_2}\nu_2^{1/3}\left(\nu_2^0\right)^{2/3}\right] \tag{2.54}$$

Due to the large value of x, $1/x << 1$, so that it can be neglected, and Equation (2.53) becomes:

$$\Delta\mu_1 = RT\left[\ln\left(1-\nu_2\right)+\nu_2+\chi_{12}\nu_2^2+\frac{\overline{\nu}}{xn_2}\left(\nu_2^{1/3}\left(\nu_2^0\right)^{2/3}-\nu_2/2\right)\right] \tag{2.55}$$

If the term $\overline{\nu}/xn_2$ is divided by $\overline{V}_1$, one obtains the term $\overline{\nu}/xn_2\overline{V}_1$, in which, the denominator corresponds to the total volume of the polymer in the gel. Hence, the term $\overline{\nu}/xn_2\overline{V}_1$ corresponds to the number of the network chains per unit volume of the polymer (v_e) called the chain concentration. v_e can be also defined in terms of the other characteristic network parameters. If the average molecular weight of the network chains is $\overline{M}_c$, there will be $1/\overline{M}_c$ moles of network chains in 1 gram of polymer. On the other hand, if ρ is the polymer network density, there will be $\rho/\overline{M}_c$ moles of network chains per ml of polymer, so that the relation between v_e and $\overline{M}_c$ can be written as:

$$v_e = \frac{\overline{\nu}}{xn_2\overline{V}_1} = \frac{\rho}{\overline{M}_c} \tag{2.56}$$

If N is defined as the number of the segments in one polymer chain between successive crosslinks, then the volume of one network chain will be $N\overline{V}_1$, so that there will be $1/N\overline{V}_1$ network chains per ml of polymer. Thus, the chain concentration v_e is related to the the number of segments between the successive crosslinks N by:

$$\nu_e = \frac{\overline{\nu}}{xn_2\overline{V}_1} = \frac{\rho}{\overline{M}_c} = \frac{1}{N\overline{V}_1} \tag{2.57}$$

which may be inserted into Equation (2.53) for an affine network to give:

$$\Delta\mu_1 = RT\left[\ln\left(1-\nu_2\right)+\nu_2+\chi_{12}\nu_2^2+\frac{1}{N}\left(\nu_2^{1/3}\left(\nu_2^0\right)^{2/3}-\nu_2/2\right)\right] \tag{2.58}$$

The state of equilibrium swelling is obtained when this equation is equal to zero:

$$\ln\left(1-\nu_2\right)+\nu_2+\chi_{12}\nu_2^2+\frac{1}{N}\left(\nu_2^{1/3}\left(\nu_2^0\right)^{2/3}-\frac{\nu_2}{2}\right)=0 \tag{2.59}$$

This equation is called Flory-Rehner Equation for non-ionic gels and gives a quantitative relation between the swelling degree and the network properties such as $N, \bar{M}_c$ and ν_2^0. The Equation (2.59) can be rewritten by expanding the term $\ln\left(1-\nu_2\right)$ in a Taylor expansion form (for $\nu_2 << 1$, i.e., for highly swollen gels). Moreover, since $\nu_2/2 << \nu_2^{1/3}$ for highly swollen gels, the swelling equilibrium equation becomes:

$$\nu_2 = \frac{\left(\nu_2^0\right)^{2/5}}{\left(0.5-\chi\right)^{3/5}}\left(\frac{1}{N}\right)^{3/5} \tag{2.60}$$

2.4.3. Swelling Behavior of Ionic Polymer Network

Polymer gels consisting of chains with charged groups are called the polyelectrolyte gels. The presence of charged units in the network chains can significantly affect their swelling behavior. If the polymer chains of the network contain the ionizable functional groups, the swelling forces may be greatly increased due to the electrostatic repulsion between like charges on the polymer chains. Thus, the degree of swelling of an ionic polymer network is much higher than that of a nonionic polymer network. The exchange of the ions and the solvent between the external solution and the swollen ionic gel in which the fixed ion is taken to be a cation is schematically represented in Figure 2.13.

It is apparent that the equilibrium between the swollen ionic gel and its surrounding closely resembles Donnan membrane equilibria. The polmer acts as its own membrane preventing the charged substituents, which are distributed essentially at random through the gel from diffusing into the outer solution.

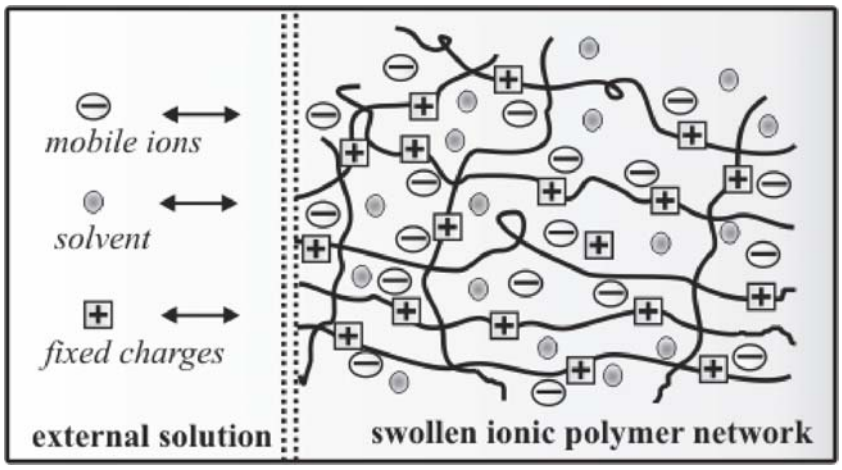

Figure 2.13: The diagram of the swollen ionic gel in equilibrium with the external solution. The fixed ion is taken to be a cation.

The swelling force resulting from the presence of these fixed charges may be identified with the swelling pressure or the osmotic pressure. Because of the attracting power of the fixed charges, the concentration of the mobile ions inside the gel will always be greater than outside. Consequently, the osmotic pressure of the solution inside will exceed that of the external solution.

The theory of the swelling of ionic polymer networks was also developed by Flory. The presence of ionic groups in polymer networks makes the theoretical treatment of swelling much more complex. In addition to the ΔG_{mix} and ΔG_{el} in the Equation (2.18), there is an additional contribution to the total change in Gibbs free energy due to the ionic nature of the polymer network, ΔG_{ionic} :

$$\Delta G = \Delta G_{\text{mix}} + \Delta G_{\text{el}} + \Delta G_{\text{ionic}} \tag{2.61}$$

The expression for the ionic contribution to the total Gibbs free energy change exhibit strong dependencies on the ionic strength of the surrounding media and on the nature of the ions present in the solvent[37].

Upon differentiating Equation (2.61) with respect to the number of moles of the solvent molecules keeping T and P constant, the expression for the excess chemical potential can be derived:

$$\Delta \mu_1 = \Delta \mu_{1,\text{non-ion}} + \Delta \mu_{1,\text{ion}} \tag{2.62}$$

Here, $\Delta\mu_{1,\text{non-ion}}$ is the excess chemical potential for the non-ionic gels and is equal to $\Delta\mu_1$ given by Equation (2.53) or (2.54) and $\Delta\mu_{\text{ion}}$ is the change of the chemical potential due to the ionic character of the polymer gel.

In the following paragraphs, the expression for the ionic contribution to the chemical potential will be derived. When the gel is immersed in water, the counterions ions cannot escape outside the gel due to the condition of electroneutrality. As a result, the concentration difference between the gel and the outer solution (water) creates an additional osmotic pressure, which is given by the following equation:

$$\pi_{\text{ion}} = RT\left(C_{\text{ion}}^{\text{gel}} - C_{\text{ion}}^{\text{sol}}\right) \tag{2.63}$$

where C_{ion} is the mobile ion concentration and the superscripts denote the gel and the solution phases, respectively. The counterion concentration in the solution phase should be equal to zero, due to the fact that the counterions cannot escape outside the gel phase; $C_{\text{ion}}^{\text{sol}} = 0$. In this case, Equation (2.63), can be rewritten as:

$$\pi_{\text{ion}} = RTC_{\text{ion}}^{\text{gel}} \tag{2.64}$$

where $C_{\text{ion}}^{\text{gel}}$ is the concentration of the fixed charges in the swollen gel. If f is defined as the effective charge density, i.e. the mole fraction of the charged units in the network chains that are effective in the gel swelling, and $\overline{V}_1$ is the molar volume of the solvent, there will be $f/\overline{V}_1$ ionic segment in 1 ml of dry polymer network.

On the other hand, since ν_2 ml of dry polymer exists in 1 ml of swollen gel, the concentration of the fixed charges in 1 ml of swollen gel can be written as:

$$C_{\text{ion}}^{\text{gel}} = \frac{f}{\overline{V}_1}\nu_2 \tag{2.65}$$

Substitution of Equation (2.65) into Equation (2.64) gives the osmotic pressure due to the non-uniform distribution of the mobile counterions between the gel and the solution phases:

$$\pi_{\text{ion}} = RT\frac{f}{\bar{V}_1}\nu_2 \tag{2.66}$$

By using the relation between the chemical potential and the osmotic pressure given by Equation (2.51), the excess chemical potential due to the ionic contribution $\Delta\mu_{\text{ion}}$ can be calculated as:

$$\Delta\mu_{\text{ion}} = -RTf\nu_2 \tag{2.67}$$

In the case of ionic gels, Equation (2.67) must be added to Equation (2.58) to calculate their excess chemical potential:

$$\Delta\mu_1 = RT\left[\ln(1-\nu_2)+\nu_2+\chi_{12}\nu_2^2+\frac{1}{N}\left(\nu_2^{1/3}\left(\nu_2^0\right)^{2/3}-\nu_2/2\right)\right]-f\nu_2 \tag{2.68}$$

Thus, the swelling of ionic gels can be described by the following equation:

$$\ln(1-\nu_2)+\nu_2+\chi_{12}\nu_2^2+\frac{1}{N}\left(\nu_2^{1/3}\left(\nu_2^0\right)^{2/3}-\frac{\nu_2}{2}\right)-f\nu_2 = 0 \tag{2.69}$$

This equation is called Flory-Rehner Equation for ionic gels. According to the Equation (2.69), the higher the ionic group content of the hydrogels, i.e. the higher *f*, the lower the polymer volume fraction ν_2.

Thus, highly swollen gels ($\nu_2 << 1$) can be obtained if a large fraction of an ionic comonomer is used in the gel preparation. In Equation (2.69), the first two term can be neglected, because they are too small and in a good solvent χ is equal to zero, and the third term is also neglected, hence the polymer volume fraction ν_2 is obtained as:

$$\nu_2 = \frac{\nu_2^0}{f^{3/2}}\left(\frac{1}{N}\right)^{3/2} \tag{2.70}$$

2.4.4. Swelling Behavior of Polymer Network in Solvent Mixtures

In the following paragraphs, the equilibrium swelling theory of hydrogels in solvent mixtures will be presented and the interaction parameters as well as the partition of the solvent components between the gel and the solution phases will be derived. Here, the swelling theory is applied to a gel system consisting of three components *i*; two liquid components (i = 1 for water, and i = 3 for the solvent) and a polymer segment (i = 2). The number of segments on the component *i* is denoted by x_i. The interactions between the components *i* and *j* are represented by the interaction parameter χ_{ij} ($i \neq j, \chi_{ij} = \chi_{ji}\, x_i/x_j$). Each of the network chains is assumed to have *N* segments. It is assumed that the gel is immersed into an infinite volume of liquid mixture so that the composition of the liquid mixture outside the gel is fixed.

When a non-ionic polymer network is immersed in a solvent mixture, similar to Equation (2.49), the free energy change ΔG during swelling process can be written as a sum of two free energy terms [34]:

$$\Delta G = RT\left(\sum_{i=1}^{3} n_i \ln \nu_i + \sum_{i=1}^{3} n_i \nu_j \chi_{ij} + \frac{3}{2}\frac{V_P}{NV_1}\left(\alpha^2 - 1 - \ln\alpha\right)\right) \tag{2.71}$$

where n_i is the moles of the species i, ν_i, its volume fraction, V_P and V_1 are the volumes of the polymer network and the segment, respectively, and α is the linear swelling ratio with respect to the after synthesis-stage of the gel, i.e., $\alpha = \left(\nu_2^0/\nu_2\right)^{1/3}$. Differentiating Equation (2.71) with respect to the number of moles of the components *i* yield the following equation for the excess chemical potential of the component *i* in the gel phase ($\Delta\mu_i^{gel}$):

$$\frac{\Delta\mu_i^{gel}}{x_i RT} = x_i^{-1}\ln\nu_i + x_i^{-1}(1-\nu_i) - \sum_{j=1}^{3}\nu_j/x_i + x_i^{-1}\sum_{j=1}^{3}\chi_{ij}\nu_j\sum_{j=1}^{3}\nu_j \tag{2.72}$$

$$-x_j^{-1}\chi_{ij}\nu_j\nu_k + \left(\frac{\partial\Delta G_{el}}{\partial n_i}\right)_{T,P,n_j}$$

(i, j, k = 1, 2, and 3; j, k ≠ i; j < k)

The chemical potential of the components *i* in the solution ($\Delta\mu_i^{sol}$) can be obtained from Equation (2.72) as:

$$\frac{\Delta\mu_i^{sol}}{x_i RT} = x_i^{-1}\ln\nu_i' + x_i^{-1}\left(1-\nu_i'\right) + x_i^{-1}\chi_{ij}\left(1-\nu_i'\right)^2 \tag{2.73}$$

(i,j = 1 and 3; j ≠ i)

where the symbols with a prime denote the concentrations in the external solution ($\nu_1' + \nu_3' = 1$). Note that, since it is assumed that the gel is in contact with an infinite volume of liquid mixture ν_3' and thus ν_1' are constant. In the following, ν_3' is defined as ϕ. The state of equilibrium swelling of the hydrogel in the solvent mixture is obtained when each of the solvent components are in thermodynamic equilibrium with those outside. This equilibrium state is described by the equality of the chemical potential of the components in both phases. Thus, at the swelling equilibrium:

$$\Delta\mu_i^{gel} = \Delta\mu_i^{sol} \qquad (i = 1 \text{ and } 3) \tag{2.74}$$

Combining Eqs (2.71) - (2.73) and setting $x_2 = \infty$ for the polymer network give the following two equations describing the thermodynamic equilibrium condition of the non-ionic gel immersed in the solvent mixture:

$$\ln\left(\frac{1-\nu_2-\nu_3}{1-\phi}\right) + \left(\nu_2+\nu_3-\phi\right) - \left(\nu_3-\phi\right)/y + \chi_{12}\nu_2^2 + \chi_{13}\left(\nu_3^2-\phi^2\right) \tag{2.75}$$

$$+\left(\chi_{12}+\chi_{13}-\chi_{23}\right)\nu_2\nu_3 + \frac{1}{N}\nu_2\left(\alpha^2-1/2\right) = 0$$

$$-\ln\left(\frac{1-\nu_2-\nu_3}{1-\phi}\right) + (1/y)\ln\left(\nu_3/\phi\right) - 2\chi_{13}\left(\nu_3-\phi\right) + \left(\chi_{23}-\chi_{12}-\chi_{13}\right)\nu_2 = 0 \tag{2.76}$$

where *y* is the ratio of the molar volumes of the liquid components, $y = x_3 / x_1$. The equilibrium concentrations (ν_2 and ν_3) in the gel phase can be obtained by solving

Eqs. (2.75) and (2.76) for a given composition ϕ of the external liquid mixture. The calculation results of ν_3 are presented in terms of the organic solvent partition parameter φ,

$$\varphi = \frac{\nu_3}{\phi\left(1-\nu_2\right)} \tag{2.77}$$

which is the ratio of the organic solvent concentration inside the gel to that in the external solution. Thus, $\varphi = 1$ means that the organic solvent concentration in the gel is equal to that in the solution, while $\varphi = 0$ means total exclusion of the organic solvent molecules from the polymer network.

2.4.5. Scaling Relation Between α and ν_2^0

In the following paragraphs, a scaling relation between the linear swelling ratio α and ν_2^0 will be derived to discuss the monomer concentration dependence of the linear swelling ratio α and demonstrate that α is not a monotonic function of ν_2^0. In the Flory-Rehner theory, the swelling equilibrium is determined by a competition between the volume interactions of segments and the gel rubber-like elasticity[33]. According to the theory of rubber elasticity of Gaussian chains, the free energy of elastic deformation ΔG_{el} scales with the second power of the deformation ratio as given in Equation (3.37)[39]:

$$\Delta G_{el} \approx N^{-1}\alpha^2 \tag{2.78}$$

where N is the number of segments between two successive crosslinks, i.e., the network chain length. On the other hand, the free energy of volume interactions ΔG_{int} scales with α as[32,40,41]:

$$\Delta G_{\text{int}} \approx B\nu_2^0/\alpha^3 + 2C\left(\nu_2^0/\alpha^3\right)^2 \tag{2.79}$$

where B and C are the second and third virial coefficients, respectively.

Balancing the two opposite free energy contributions represented by ΔG_{el} and ΔG_{int} by minimizing their sum with respect to α, one obtains[41]:

$$\alpha^5 = B\nu_2^0 N + 2C\left(\nu_2^0\right)^2 N \Big/ \alpha^3 \tag{2.80}$$

For highly swollen gels in a good solvent, since α >>1, $B > 0$, and $C \cong 0$, Equation (2.80) becomes:

$$\alpha \approx \left(\nu_2^0 N\right)^{1/5} \tag{2.81}$$

which indicates, for a fixed value of ν_2^0, a scaling parameter of 0.2 between the linear deformation ratio of gels and the network chain length N. Under θ-conditions where the second virial coefficient vanishes, Equation (2.80) reduces to Eq. (2.82) and the scaling parameter becomes 0.125:

$$\alpha \approx \left(\nu_2^0\right)^{1/4} N^{1/8} \tag{2.82}$$

Differentiating Equation (2.82) with respect to ν_2^0 gives the monomer concentration dependence of the swelling ratio α as:

$$\frac{d\ln\alpha}{d\ln\nu_2^0} \approx \frac{1}{5} + \frac{1}{5}\frac{d\ln N}{d\nu_2^0} \tag{2.83}$$

Since $N \approx \left(\nu_2^0\right)^{-2}$ at low polymer concentrations, then

$$\alpha \approx \left(\nu_2^0\right)^{-1/5} \qquad (\text{for } \nu_2^0 < 0.1) \tag{2.84}$$

while at high polymer concentrations, since N is nearly ν_2^0 independent, one obtains:

$$\alpha \approx \left(\nu_2^0\right)^{1/5} \qquad (\text{for } \nu_2^0 > 0.1) \tag{2.85}$$

3. MECHANICAL BEHAVIOR OF POLYMER NETWORKS

3.1. General Considerations on Polymer Network Elasticity

The elasticity of polymer networks has been the subject of numerous experimental studies to make a relation between the elastic modulus and the molecular structure. The understanding of the polymer network elasticity began in the early 1930s. The forms of the stress-strain relationships were developed beginning in 1942 with Wall[42], Treloar[39], Flory-Rehner[33], and James-Guth[43]. The first molecular theory of rubber elasticity provided the first absolute prediction of mechanical modulus from network structure with the following assumptions:

i. The polymer network contains ν chains per unit volume.

ii. The mean square end-to-end distance for the chains consisting of N segments with each bond having a length l equals to $\left\langle r^2 \right\rangle = Nl^2$.

iii. There is no change of the volume on deformation.

iv. The junction points between the chains move on deformation as if they were embedded in an elastic continuum. As a result the components of lenght of each chain change in the same ratio as the corresponding dimensions.

v. The entropy of the network is the sum of the entropies of the individual chains.

Rubber resembles a solid, but behaves as a liquid in that the volume stays essentially constant as it undergoes isothermal deformation. Thus, the rubber is a good example of a polymer network. It can be described as a giant network molecule made by a crosslinking reaction between the polymers. The rubberlike elasticity of the polymer networks refers to two aspects: very high deformability and essentially complete recoverability. The crosslinked materials can undergo large deformations under tension without rupturing. When the deforming force is removed, they spontaneously recover their original dimensions[44]. Three molecular requirements are needed to exhibit this type of elasticity:

i. the material must consist of polymeric chains,

ii. the chains must have a high degree of flexibility and mobility,
iii. the chains must be joined into a network structure.

The first requirement is associated with the very high deformability. It arises from the fact that the molecules in an elastomeric material must be able to alter their arrangements and the extensions in space dramatically in response to an applied stress.

The second characteristic required for the rubberlike elasticity indicates that the chains be flexible and mobile and thus the different spatial arrangements of the chains be accessible.

The last requirement cited is required in order to obtain the recoverability part of the definition. The flexibility of the polymer chains in the networks allows these materials to have very large deformability with strain, and the crosslinked network structure allows them to have essentially complete recoverability[39].

3.2. Theory of Rubber Elasticity

Theories on rubber elasticity can be mainly divided into two categories; one based on statistical mechanics (classical and modern molecular based theories) and the other based on continuum mechanics.

i. The classical molecular based theories describe rubber elasticity of networks in simple and idealized ways and include the affine network theory and the phantom network theory. The modern molecular based theories consider the contribution of entanglements of polymer chains to the rubber elasticity and include the constrained junction model, the slip-link model and the tube model[43-49].

ii. Continuum mechanics based theories are built on the mathematical arguments regarding strain matrix invariant of a rubber under deformation, which include the Mooney- Rivlin Equation [50].

The network models used in this dissertation to describe the elasticity of the polymer networks correspond essentially to the affine and phantom network model. In the following section, these theories will be described and a comparison will be done between two network models.

3.2.1. Affine and Phantom Network Theories

Two elementary network models which relate the molecular structure and the macroscopic strain-stress are the affine and phantom network theories. The both models are based on mean-field approaches in which the anology between the elastic properties of an ideal, gaussian chain and a classical elastic spring is used to calculate the network free energy. These models share some common premises in idealizing a real polymer network:

1- The intermolecular interactions between network chains are independent of the configurations of these chains.
2- The chains are Gaussian, freely joined and volumeless.
3- The total number of configurations of an isotropic network is the product of the number of configurations of the individual chains.

The main assumption of the affine network theory is that the crosslink junction points move affinely with macroscopic deformation. In an affine network, diffusion of the junctions about their mean positions is restricted by the neighboring chains sharing the same region of space. With this assumption, the fluctuation of the crosslink junctions in the networks is suppressed. The other simple assumption is that the chain segments of the network deform independently and on a microscopic scale in the same way as the whole sample. The crosslinks are assumed to be fixed in space at positions exactly defined by the specimen deformation ratio[33,39,42].

The phantom network theory is different from the affine network theory in that, the junctions of the network chains can move freely and the chains can pass through each other like phantoms. Also, the junction points are assumed to fluctuate around their mean positions due to Brownian motion. They fluctuate over time without being hindered by the presence of the neighboring chains and their fluctuations around these positions are Gaussian. The junctions of the phantom network undergo displacements that are affected only by their connections to the network and not at all by their immediate surroundings[43,45].

The phantom network theory shows that the fluctuation of the junctions are substantial. The mean squared magnitude of the fluctuation (Δr) of the chain vector length (r) and the mean position of the junctions $\left(\overline{r}\right)^2$ are found as follows:

$$\left\langle (\bar{r})^2 \right\rangle = \left(1 - \frac{2}{\phi}\right) \left\langle (r)^2 \right\rangle_0 \tag{3.1}$$

where ϕ is the functionality representing the number of chains meeting at each junction. Figure 3.1 shows schematically the difference between the affine and phantom network models. In the affine network model, the crosslink points are embedded in the network have a specified fixed position. However, the junction points of the phantom network are allowed to fluctuate about their mean values (shown in Figure 3.1 by the points marked with an A)[46,47].

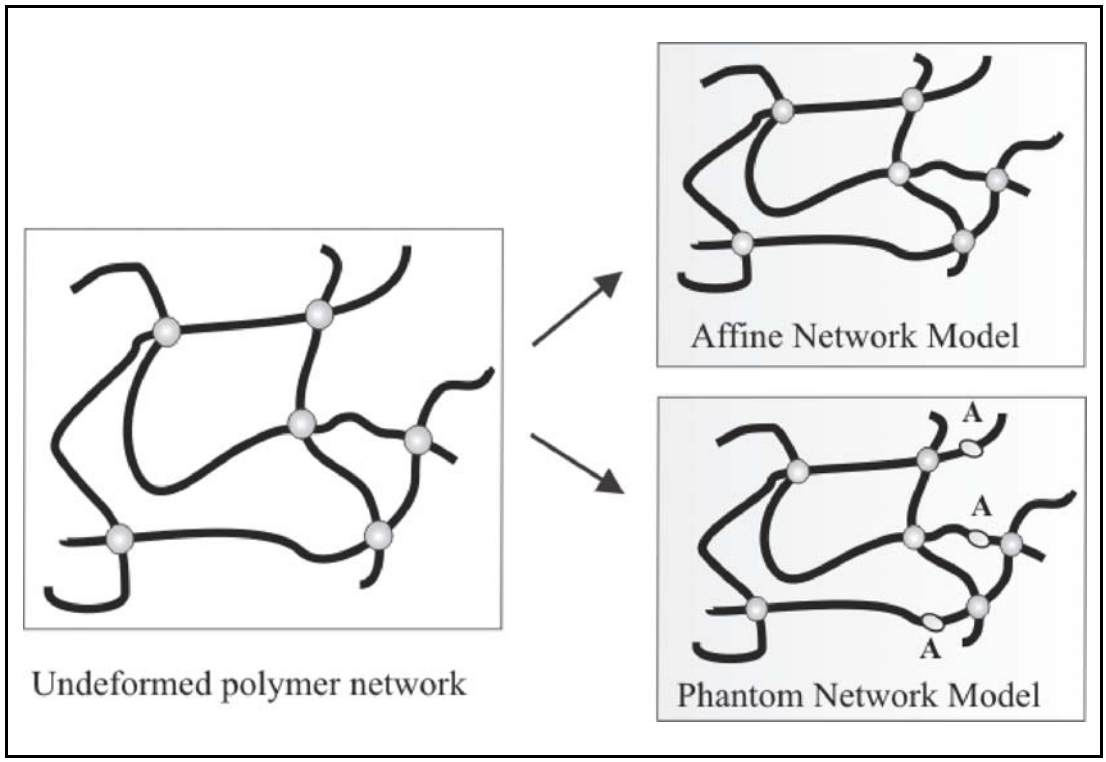

Figure 3.1: Schematical representation of the deformation of a network according to the affine network model and the phantom network model.

The expressions for the elastic free energy ΔG_{el} for an affine network and phantom network are given in Section 3.4 by Equations (3.32) and (3.33), respectively. The stress-strain relationships for both network models are also derived in Section 3.5. Comparing the stress-strain expressions obtained from these two theories, it was found that the only difference is the front factor for the deformation term, $(\alpha-\alpha^{-2})$. According to Equation (1.2), ξ equals to $(1/2)\nu$, for a perfectly tetrafunctional network, $\phi = 4$, which implies the theoretical modulus of the phantom network is

half that of the affine network. This is due to their varying assumptions regarding the positions of crosslink junction points in the network.

3.2.2. Statistical Mechanics of Real Networks

The affine and phantom networks are two idealized limits of the real polymer network. As discussed above, in the affine network theory, the junction movement is completely restricted while in the phantom network theory, no restriction exists on the junction movement. The stress-strain measurements revealed that the behavior of the real network was between these limits. In the case of uniaxial compression, the behavior of the network is approximately affine and the junction position is quite restricted for small deformations. In large deformations, the response of the network is more phantom-like and the junction positions are less restricted. When the network is swollen, the junction is less constrained, and hence, behavior of the swollen network deformation is closer to the phantom network theory.

One of the reasons for the difference in deformation behavior between the real polymer networks and the affine and phantom network models is the presence of entanglements between the polymer chains in the network. Since the phantom network model allows the crosslink junction to move freely, the modern molecular rubber elasticity theories are generally based on the phantom network model and the elastic free energy is the sum of the phantom network free energy and that which comes from entanglements[47,48]. A semiempirical equation known as the Mooney-Rivlin equation used to determine the elastic modulus can be given as[50]:

$$f/\left(\alpha-\alpha^{-2}\right)=2C_1+2C_2/\alpha \tag{3.2}$$

where f is the stress, and α is the extension ratio. By plotting the reduced force $f/\left(\alpha-\alpha^{-2}\right)$ which can be denoted by f^* against 1/ α, constants $2C_1$ and $2C_2$ can be obtained. $2C_1$ is the equilibrium modulus while $2C_2$ reflects the deviation from simple affine or phantom network behavior.

The statistical theory of rubber elasticity predicts that the reduced force should be constant and independent of strain throughout the full range of the uniaxial deformation for both of the affine and phantom network model, which is not the case for the Mooney-Rivlin equation. The force for simple elongation of a phantom

network is also smaller, although the form of the stress-strain relation is the same as given by the affine network theory. They differ only by a numerical factor, also called "structure factor", which depend on the functionality of the network. The real networks exhibit behavior between these two extremes. A schematic comparison of stress-strain isotherms between the network models is shown in Figure 3.2.

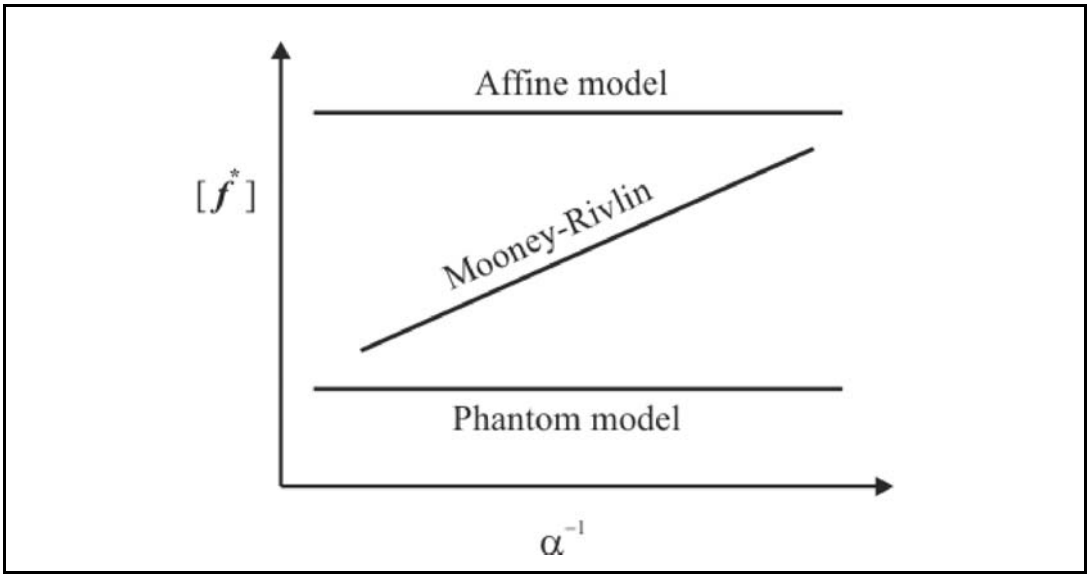

Figure 3.2: Reduced stress as a function of the reciprocal strain. The upper and lower horizontal lines represent result from affine and phantom network models, respectively.

3.3. Statistics and Elasticity of a Polymer Chain

The understanding of the macro-elasticity of a polymer network requires a microscopic study of single chain elasticity. Therefore, the elastic behavior of single polymer chains plays an important role in the mechanical properties of polymer networks. In this section, the statistics and the elasticity of a single polymer chain is discussed at first and followed by the elementary theory of elasticity of a polymer network.

i. Statistics of a single polymer chain

The first step in the molecular theory of rubberlike elasticity is the derivation of the statistical properties of a single chain. It is necessary to know the free energy of the molecule as a function of its end-to-end distance r and a quantitative relation between this distance and the force necessary to maintain it. The second step consists of the free energy of the network as a function of the macroscopic parameters which

characterize the deformation. Since the polymer network is formed by connecting single polymeric chains through the cross-links, the derivation ought to start from the expression for the free energy of a single polymer chain.

In the theory of rubberlike elasticity, the individual chains are approximated by the freely-jointed chain which consists of N bonds of length l with a contour length, therefore, of Nl. The contour length is the size of a fully extended jointed chain, and is thus the chain's maximum size. However, the macromolecule will not favor such an entropically constrained conformation in solution, and will usually adopt a much more coiled structure. This can be characterized by the displacement length, r, which is the end to end distance of the polymer.

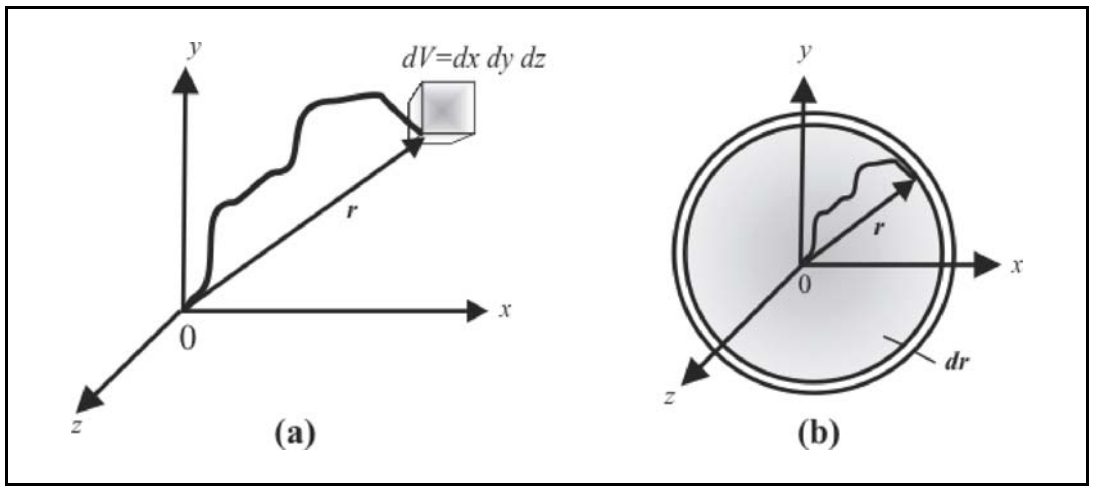

Figure 3.3: (a) The chain terminus is located at a specific location r between (x, y, z) and $(x+ dx, y+dy, z + dz)$, if the chain originates at (0, 0, 0). (b) The chain terminates in a spherical shell at a distance r (inner surface) and $r + dr$ (outer surface) from the origin.

Assume that the polymer chain has N segments and r represents the vector from the origin, where the chain begins, to (x, y, z), where the chain ends (Figure 3.3). The vector r joining the two ends of the polymer chain takes different values resulting from rotations about the individual bonds. This is a statistical variable, and if it is assumed that the distribution of the displacement length is Gaussian, then the probability density of finding the chain end in a small volume element between (x, y, z) and $(x + dx, y + dy, z + dz)$, with the other end fixed at the origin of a Cartesian coordinate system is the product of independent factors:

$$\mathrm{W}(x,y,z)\,dxdydz = W(x)W(y)W(z)\,dxdydz \tag{3.3}$$

$$= \left(3/2\pi\left\langle r^2\right\rangle_0\right)^{3/2} \exp\left(-3\left(x^2+y^2+z^2\right)/2\left\langle r^2\right\rangle_0\right) dxdydz$$

This result implies that, all directions of the end-to-end vector are equally probable in Figure 3.3. Here $\left\langle r^2\right\rangle_0$ represents the average of the squared end-to-end vectors, and the subscript zero indicates that the chain is in the so-called theta state (θ), where it is unperturbed by excluded volume effects. In terms of the end-to-end vector *r*, Equation (3.3) becomes:

$$W(r) = \left(3/2\pi\left\langle r^2\right\rangle_0\right)^{3/2} \exp\left(-3r^2/2\left\langle r^2\right\rangle_0\right) \tag{3.4}$$

in which the length of the end-to-end vector is *r*, $r^2 = x^2 + y^2 + z^2$. This equation is of fundamental importance in the theory of rubber elasticity and this form is only approximate, since its derivation involves the assumtion that the distance *r* between the ends of the chain is not comparable with the maximum or fully extended length *Nl* of the chain($r << Nl$). Experimentally it is the root mean square displacement length and can be calculated easily from the above distribution, and is defined as:

$$\overline{\left\langle r^2\right\rangle}^{1/2} = \sqrt{\int_0^x r^2 W(r)dr} = N^{1/2}l \tag{3.5}$$

The radial distribution function *W(r)* is obtained by multiplying *W(x, y, z)* with the area of the surface of the sphere with radius *r*. Hence, the probability of finding the chain end at some radius *r* in a spherical shell of thickness *dr* is:

$$W(r)\,dr = 4\pi r^2 W(x,y,z)\,dr \quad = 4\pi r^2 \left(3/2\pi\left\langle r^2\right\rangle_0\right)^{3/2} \exp\left(-3r^2/2\left\langle r^2\right\rangle_0\right) dr \tag{3.6}$$

In Figure 3.4, the shape of the distribution functions are shown. *W(x, y, z)* decreases monotonically with increasing *r* in Figure 3.4(a). Furthermore, the probability density *W(x, y, z)* is maximum when *r* = 0, that is when the two ends of the polymer

chain are coincident, and falls continuously as *r* increases. This means that if one end of the chain is fixed at the origin, the most probable position of the other end is at the same point.

The quantity of the radial distribution function *W(r)* is also shown as a function of *r* in Figure 3.4(b). The function *W(r)* is of an entirely different from the probability density function *W(x, y, z)*. *W(r)* is zero at $r = 0$ and reaches a maximum at a finite value of *r*.

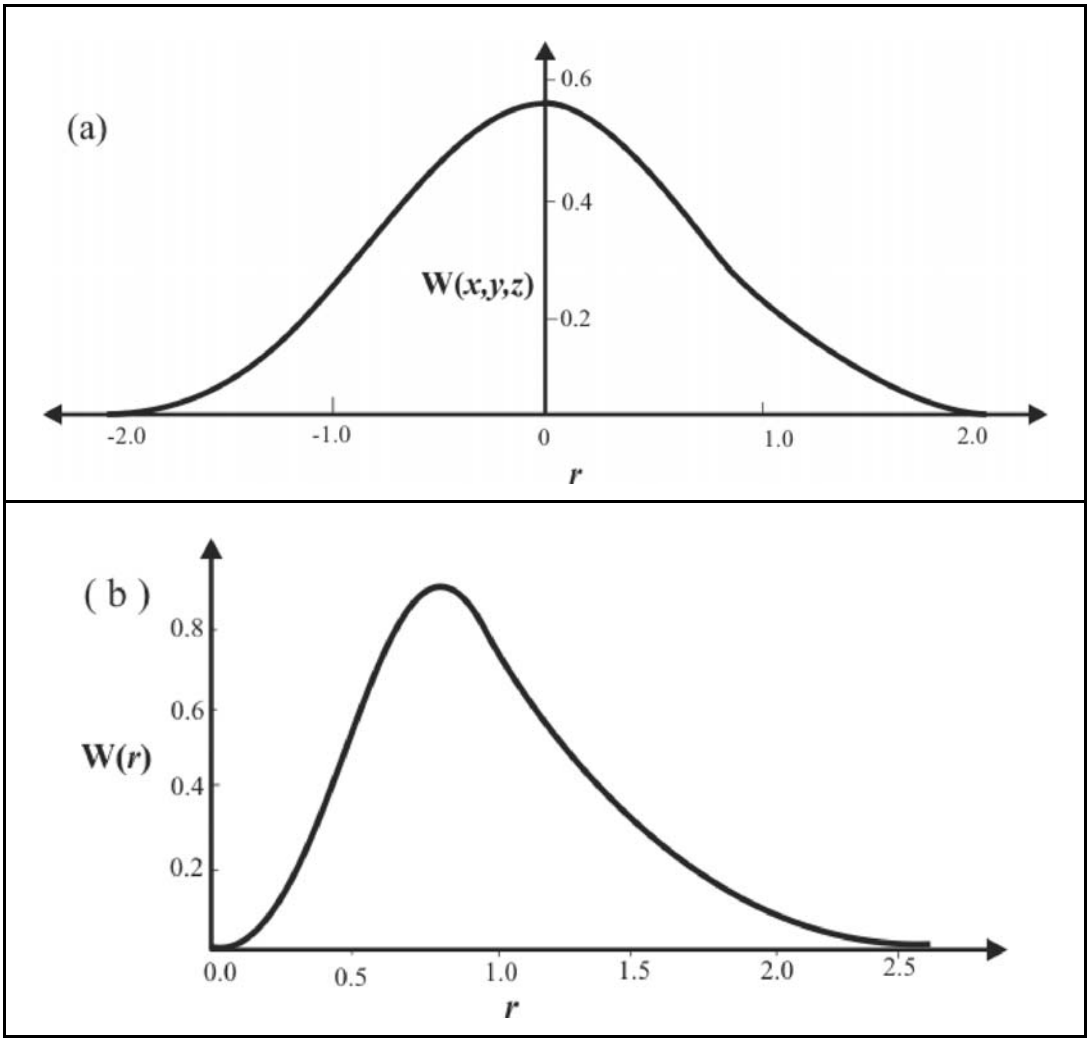

Figure 3.4: Schematic representation of distribution functions of *W(x, y, z)* and *W(r)* as a function of *r*.

ii. Elasticity of a single polymer chain

According to the general principles of the statistical thermodynamics developed by Boltzmann, the entropy will be proportional to the logarithm of the number of configurations available to the system. If one end of the polymer chain is fixed at the

origin in Figure 3.3(a) while the other end is confined to a small volume element *dV* at a distance *r* from the origin. In the presence of this restriction, the number of configurations available to the polymer chain is proportional to the probability density (Equation (3.4)) multiplied by the size of the volume element *dV*.

The entropy of the polymer chain is therefore given by Boltzmann's entropy relationship:

$$S = k \ln W\left(x, y, z\right) dxdydz \tag{3.7}$$

Subtitution of the expression Eq.(3.3) for *W(x,y,z)* into Eq.(3.7) thus yields:

$$S = k\left[\frac{3}{2}\ln\left(\frac{3}{2\pi\left\langle r^2\right\rangle_0}\right) - \frac{3\left(x^2 + y^2 + z^2\right)}{2\left\langle r^2\right\rangle_0} + \ln\left(dxdydz\right)\right] \tag{3.8}$$

by replacing the length of the end-to-end vector $x^2 + y^2 + z^2 = r^2$, the Equation (3.8) becomes,

$$S = k\left[\frac{3}{2}\ln\left(\frac{3}{2\pi.\left\langle r^2\right\rangle_0}\right) + \ln\left(dxdydz\right)\right] - k\frac{3r^2}{2\left\langle r^2\right\rangle_0} \tag{3.9}$$

Since the volume element *dV* is assumed constant and after simplification becomes,

$$S = C - k\frac{3r^2}{2\left\langle r^2\right\rangle_0} \tag{3.10}$$

where *C* is a constant. This equation shows the entropy to have its maximum value when the two ends of the chain are coincident ($r = 0$) and to decrease continuously with increasing distance between the ends as shown in Figure 3.5.

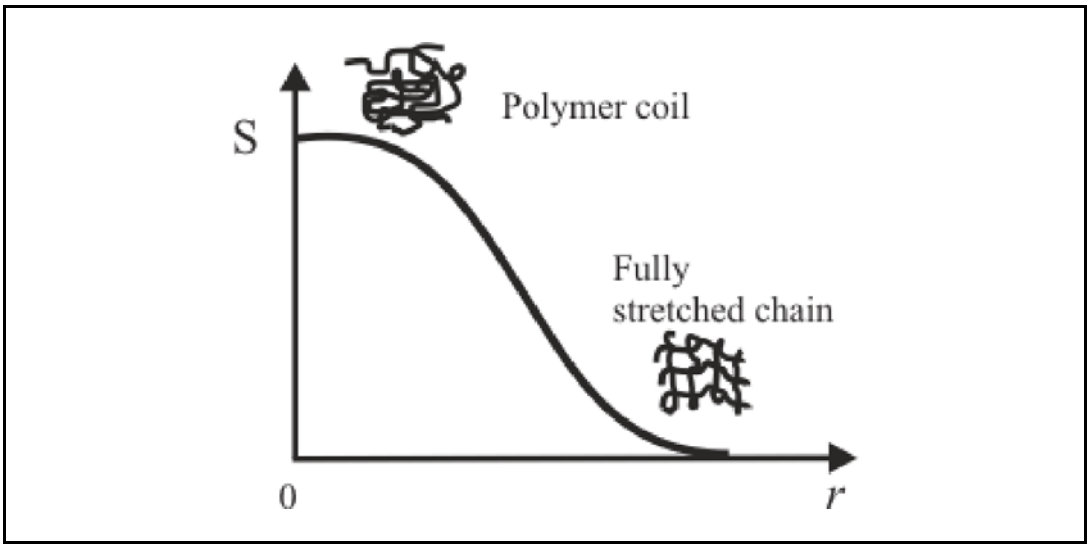

Figure 3.5: A schematic illustration of relation between the entropy and the distance between the two ends of the polymer chain.

iii. Thermodynamics of deformation of polymer chain

The most typical form of the polymer chains is coiled one. Due to great freedom of the segments motion in the rubbery state, the polymer chains under stress can obtain the straightened shape only, i.e. become uncoiled and great deformations occur. After the stress removal polymer chains obtain the initial shape, and the sample contracts. This unusual deformation mechanism leads to a series of anomalies in the mechanical behavior of the polymeric materials. One of these anomalies consists of heating up of polymeric materials existing in the rubbery state at stretching. The second anomaly is displayed in increasing rubbery modulus with temperature, but not decreasing as for usual elastic materials. Both these anomalies can be explained, if thermodynamics of rubbery deformation is discussed.

The element *dw* of work required to move one end of the polmer chain from a distance *r* to a distance (*r* + *dr*) is given by:

$$dA = dw = fdr \tag{3.11}$$

The quantity *dw* is also equal to the change in the Helmholtz free energy *dA*. Yielding from Eq. (3.11), it should be written as the following:

$$f = \left(\frac{\partial A}{\partial r}\right)_{T,V} = \left(\frac{\partial w}{\partial r}\right)_{T,V} \tag{3.12}$$

This equation is general and shows that under conditions T= const and V=const. The thermodynamic expression relating the free energy A_{el} of a polymer chain having an end-to-end vector r, to the distribution function $W(r)$ is given as:

$$A_{el} = -\mathrm{kT}\ln W(r) + \mathrm{C} \tag{3.13}$$

where C is the constant and k is the Boltzmann constant. Substituting Eq.(3.4) into Eq.(3.13) leads to the free energy of a polymer chain at a fixed r in the network as:

$$A_{el} = \left(\frac{3kT}{2\left\langle r^2 \right\rangle_0} \right) r^2 + C \tag{3.14}$$

Since the elastic free energy is the "work" function, the force - deformation relationship can be developed by differentiating the Helmholtz free energy with respect to the elongation of the network upon deformation. Therefore, the stress on the polymer chain ends is given by:

$$f = \left(\frac{\partial A_{el}}{\partial r} \right)_{T,V} = \frac{3kT}{\left\langle r^2 \right\rangle_0} r \tag{3.15}$$

Equation (3.15) means that the polymer chain behaves as a spring with spring constant $k = 3kT \Big/ \left\langle r^2 \right\rangle_0$. Figure 3.6 shows a schematic illustration of a gaussian chain of N segments realized by a spring-bead model consisting of N independent springs of a spring constant k. Thus, the polymeric materials can be stretched to many times their undeformed size. In its undeformed state, its average size is given by Eq.(3.5), so the polymer chain can be stretched by nearly a factor of $\sqrt{N}$.

If the ends of the polymer chain are pulled, the number of allowable configurations that the polymer chain can take is reduced. If the polymer chain is completely straightened as shown in Figure 3.7, it can display the only one completely straightened conformation. The probability of the existence of such conformation is extremely low. However, for a coiled polymer chain, a set of conformations will correspond to the same distance between the ends of it, that is, a state with higher entropy.

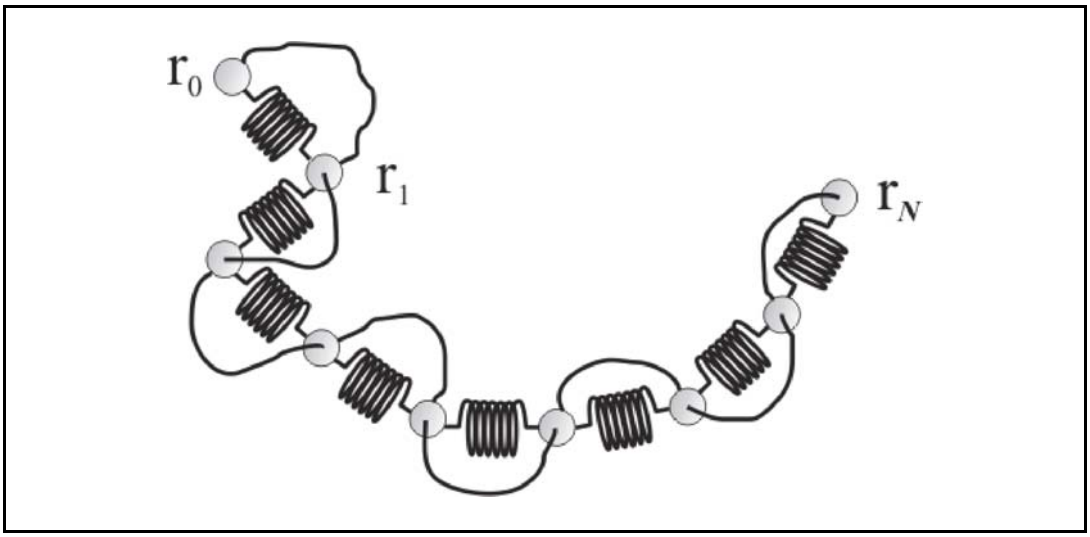

Figure 3.6: Gaussian chain of *N* segments is realized by a bead-spring model in which *N* springs are connected in series.

Analogies can be found between the rubbers and the gases. The thermodynamic behavior of the rubber shows a close anology with that of an ideal gas, the entropy of which decreases during compression. The pressure of the gas is predominantly entropically driven and so is the stress in the rubber. Therefore, the elastic equation of state for a rubber is similar to the molecular form of the equation of state for an ideal gas. The stress replaces the pressure and the number of network chains replaces the number of the gas molecules. The differences in the origins of the elasticity for a rubber and a gas are shown in Figure 3.7.

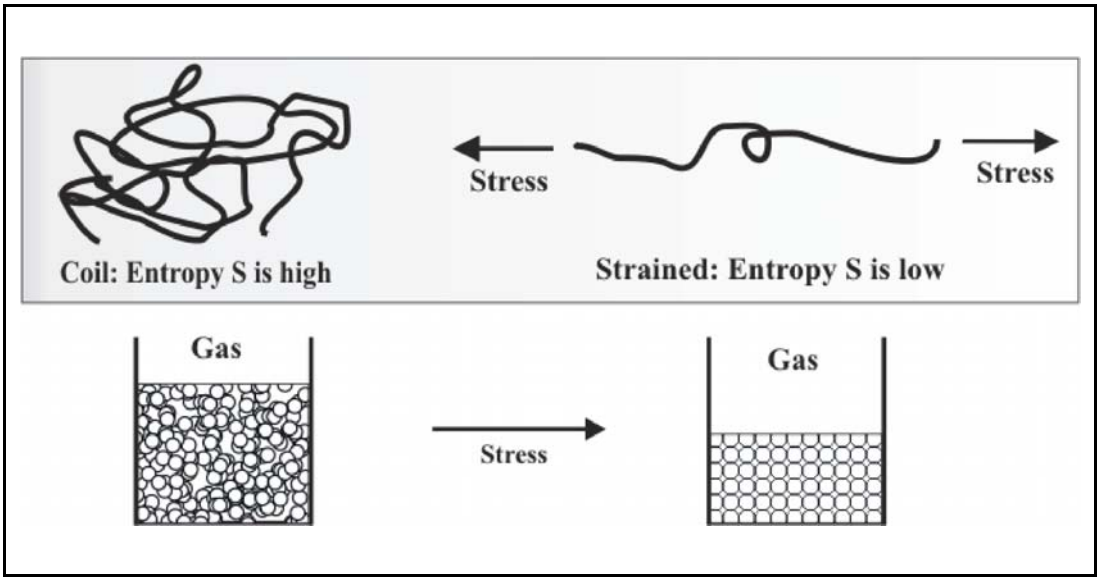

Figure 3.7: Sketches explaining the differences between the polymer chain and gas in terms of the entropy.

3.4. Elasticity of Polymer Networks

The basic postulate underlying the elasticity of the polymer networks is that the elastic free energy of the polymer network is equal to the sum of the elastic free energies of the individual chains. To calculate the elastic free energy of the polymer network due to the deformation, it is also necessary to calculate the change in the entropy of the polymer network. Since the polymer network consists of the polymer chains, the change in the entropy for the polymer network can be calculated starting from the expression for the entropy of the polymer chain between two junction points.

Assume that the polymer network undergoes a deformation in which the chain vectors transform proportionally with macroscopic deformation. In Figure 3.8, deformation of the polymer chain from undeformed state r_0 to deformed state r is shown in a Cartesian coordinate system. The polymer chain has an end-to-end distance represented by the vector r_0, with components (x_0, y_0, z_0) in the undeformed state, while after deformation, the components of the end-to-end vector length of the same chain will be (x, y, z), through the deformation matrix $\left(\alpha_x, \alpha_y, \alpha_z\right)$.

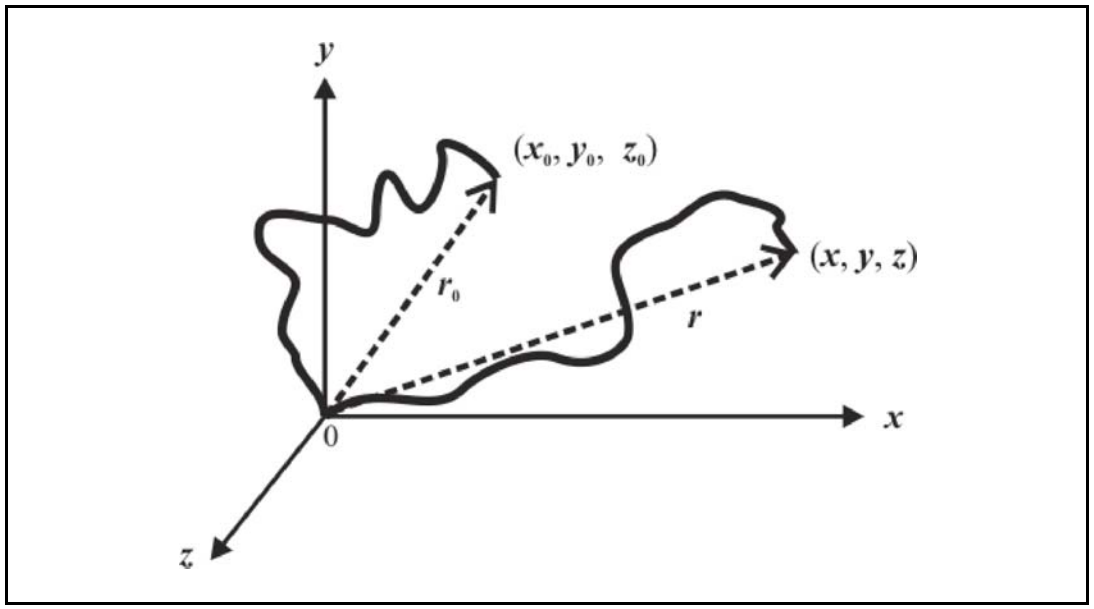

Figure 3.8: Schematic representation of deformation of the polymer chain from undeformed state r_0 to deformed state r in a Cartesian coordinate system.

If the polymer chain is deformed by a factor α_x in the *x*-direction, α_y in the *y*-direction, and α_z in the *z*-direction as seen in Figure 3.9, the chain end is moved to (*x*, *y*, *z*).

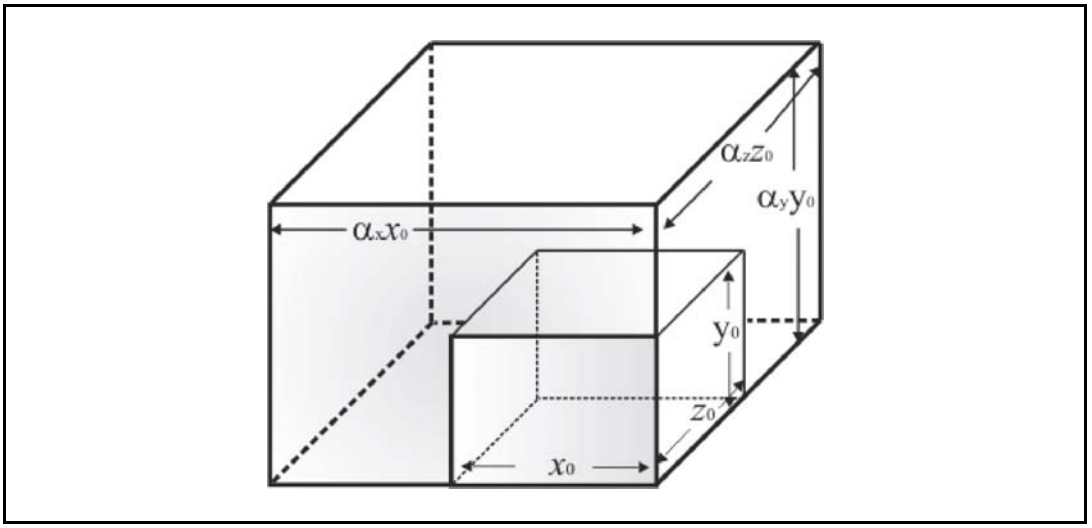

Figure 3.9: The deformation of a material from dimensions (x_0, y_0, z_0) to ($\alpha_x x_0$, $\alpha_y y_0$, $\alpha_z z_0$).

According to Affine deformation assumption:

$$x = \alpha_x x_0 , \quad y = \alpha_y y_0 , \quad z = \alpha_z z_0 \tag{3.16}$$

where the axes of coordinates being chosen to coincide with principal axes of strain. For the undeformed polymer chain, the end of the chain at (x_0, y_0, z_0) is given by:

$$r_0^2 = x_0^2 + y_0^2 + z_0^2 \tag{3.17}$$

Substituting Equation (3.17) into Equation (3.10) gives the entropy of the polymer chains in the undeformed state:

$$S_0 = C - k\left[\frac{3\left(x_0^2 + y_0^2 + z_0^2\right)}{2\left\langle r^2 \right\rangle_0}\right] \tag{3.18}$$

After the stress have been applied, the chain end at (*x*, *y*, *z*) is

$$r^2 = x^2 + y^2 + z^2 = \alpha_x^2 x_0^2 + \alpha_y^2 y_0^2 + \alpha_z^2 z_0^2 \tag{3.19}$$

The entropy of the same chain in the deformed state is obtained by substituting Eq.(3.19) into the Eq.(3.10) as:

$$S = C - k\left[\frac{3\left(\alpha_x^2.x_0^2 + \alpha_y^2.y_0^2 + \alpha_z^2.z_0^2\right)}{2\left\langle r^2\right\rangle_0}\right] \tag{3.20}$$

and the difference in the entropy between the two states is:

$$\Delta S = S - S_0 = -3k\left[\frac{\left(\alpha_x^2 - 1\right)x_0^2 + \left(\alpha_y^2 - 1\right)y_0^2 + \left(\alpha_z^2 - 1\right)z_0^2}{2\left\langle r^2\right\rangle_0}\right] \tag{3.21}$$

The change in the entropy for the polymer network is the sum of the contributions of all the ν polymer chains of the polymer network. It is assumed that the deformation is affine and so that the deformation matrix (α_i) is the same for all polymer chains;

$$\Delta S_{el} = \sum_1^{\nu} \Delta S = -3k\left[\frac{\left(\alpha_x^2 - 1\right)\sum_1^{\nu} x_0^2 + \left(\alpha_y^2 - 1\right)\sum_1^{\nu} y_0^2 + \left(\alpha_z^2 - 1\right)\sum_1^{\nu} z_0^2}{2\left\langle r^2\right\rangle_0}\right] \tag{3.22}$$

It is also assumed that the undeformed polymer chains are isotropic (all the directions are equivalent), then;

$$\sum_1^{\nu} x_0^2 = \sum_1^{\nu} y_0^2 = \sum_1^{\nu} z_0^2 \tag{3.23}$$

In this expression $\sum_1^{\nu} x_0^2$ is the sum of the squares of the x_0-components, in the undeformed state of the polymer network, for the assembly of ν chains. Since the direction of the chain vectors r_0 in the undeformed state are entirely random, there will be no preference for the *x*, *y*, or *z* directions and hence,

$$\sum_{1}^{\nu} x_0^2 + \sum_{1}^{\nu} y_0^2 + \sum_{1}^{\nu} z_0^2 = \sum_{1}^{\nu} r_0^2 \tag{3.24}$$

Then it can be written that;

$$\sum_{1}^{\nu} x_0^2 = \sum_{1}^{\nu} y_0^2 = \sum_{1}^{\nu} z_0^2 = \frac{1}{3}\sum_{1}^{\nu} r_0^2 = \frac{\nu\left\langle r^2\right\rangle_0}{3} \tag{3.25}$$

where $\left\langle r^2\right\rangle_0$ is the mean square length of the polymer chains in the undeformed state. Insertion of Eq.(3.25) into Eq.(3.22) gives:

$$\Delta S_{el} = \frac{-k\nu\left\langle r^2\right\rangle_0\left(\alpha_x^2 + \alpha_y^2 + \alpha_z^2 - 3\right)}{2\left\langle r^2\right\rangle_0} \tag{3.26}$$

and after simplification Eq.(3.26) becomes;

$$\Delta S_{el} = -\frac{1}{2}k\nu\left(\alpha_x^2 + \alpha_y^2 + \alpha_z^2 - 3\right) \tag{3.27}$$

This equation is basic to the molecular theories of rubberlike elasticity and can be used to obtain the elastic contribution to the free energy of the polymer network$\left(\Delta G_{el}\right)$:

$$\Delta G_{el} = \Delta H_{el} - T.\Delta S_{el} \tag{3.28}$$

Assuming, in accordance with the basic principles of the kinetic theory, that there is no change of internal energy on deformation and so, ΔE_{el}=0. Since it is assumed that there is no volume change on deformation and hence, $\Delta V_{el} = 0$.

Also, the interactions do not much change upon deformation ($\Delta H_{el} = \Delta E_{el} + p.\Delta V_{el}$) and $\Delta H_{el} = 0$. Substituting this result for ΔH_{el} and Eq.(3.27) for ΔS_{el} in the Eq.(3.28) gives the elastic contribution to the free energy of the polymer network$\left(\Delta G_{el}\right)$:

$$\Delta G_{el} = -T.\Delta S_{el} = \frac{1}{2}\nu kT\left[\alpha_x^2 + \alpha_y^2 + \alpha_z^2 - 3\right] \tag{3.29}$$

If the Eq.(3.29) is multiplied by the Avogadro's number N_A, and then divided by the same number;

$$\Delta G_{el} = \frac{1}{2}\frac{\nu}{N_A}kTN_A\left[\alpha_x^2 + \alpha_y^2 + \alpha_z^2 - 3\right] \tag{3.30}$$

Since $R = k.N_A$, Equation (3.30) becomes;

$$\Delta G_{el} = \frac{1}{2}\bar{\nu}RT\left[\alpha_x^2 + \alpha_y^2 + \alpha_z^2 - 3\right] \tag{3.31}$$

where R is the gas constant and $\bar{\nu}$ is the number of moles of polymer chains of the polymer network per unit volume. According to Flory, the elastic free energy expression should contain an additional logarithmic term that is a gaslike contribution resulting from the distribution of the cross-links over the sample volume. Thus the correct expression for the elastic free energy of the affine network model is[51];

$$\Delta G_{el,affine} = \frac{1}{2}\bar{\nu}RT\left[\alpha_x^2 + \alpha_y^2 + \alpha_z^2 - 3 - \ln\left(\alpha_x\alpha_y\alpha_z\right)\right] \tag{3.32}$$

The elastic free energy of the phantom network model is[43];

$$\Delta G_{el,phantom} = \frac{1}{2}\xi RT\left(\alpha_x{}^2 + \alpha_y{}^2 + \alpha_z{}^2 - 3\right) \tag{3.33}$$

where ξ is the cycle rank which was described before.

During the swelling process of a polymer network, deformation (elongation) of the network chains occur due to the diffusion of the solvent molecules inside the gel phase. In this case, the deformation is the same for all polymer chain and it is isotropic. Therefore, the deformation ratios $\alpha_x, \alpha_y,$ and α_z are related each other by:

$$\alpha_x = \alpha_y = \alpha_z = \alpha \tag{3.34}$$

Substitution of Eq. (3.34) in Eq.(3.32) yields;

$$\Delta G_{el,affine} = \frac{3}{2}\bar{\nu}RT\left[\alpha^2 - 1 - \ln\alpha\right] \tag{3.35}$$

in which the linear deformation ratio α is related to the equilibrium swelling by:

$$\alpha = \left(\frac{\nu_2^0}{\nu_2}\right)^{1/3} \tag{3.36}$$

where ν_2 and ν_2^0 represents the volume fractions of the polymer network at equilibrium swelling and after gel preparation, respectively. Substituting of Eq.(3.36) for α in Eq.(3.35) gives;

$$\Delta G_{el} = \frac{3}{2}\bar{\nu}RT\left[\left(\frac{\nu_2^0}{\nu_2}\right)^{2/3} - 1 - \ln\left(\frac{\nu_2^0}{\nu_2}\right)^{1/3}\right] \tag{3.37}$$

3.5. Mechanical Testing of Polymer Networks

In addition to the chemical analysis and the swelling measurements, analysis of the deformation of the polymer network resulting from application of a stress is one of the important ways to characterize the polymer networks. The results are generally expressed in terms of the stress *f* and the strain α, so as to be independent of sample geometry. Stress is the force acting per unit original cross-sectional area and its unit is Newtons per square meter (Nm^{-2}). Strain is the deformation per unit original dimension and is therefore dimensionless. The ratio of stress to strain is called the modulus, and a material is said to be 'Hookean' when its modulus is independent of strain which is typical of a metal spring or wire. The polymeric materials are Hookean only in the range of very small deformations. Additional deviations from the theory occur at high deformations, specifically increases of stress with elongation.

The most important result of the molecular or the statistical theories of rubber elasticity is the prediction of the relationship between the stress and strain for a deformed polymer network at constant temperature[32,52]. The experimental studies are generally based on the measurement of uniaxial deformation, particularly on the measurements of simple compression or elongation.

Equation (3.31) is general and can be used to obtain the stress-strain relationship for any type of the deformation. Its application is best illustrated in the case of elongation, which is the type of deformation used in the great majority of the experimental studies. In this dissertation, the compression test was used to characterize the mechanical properties of the gels.

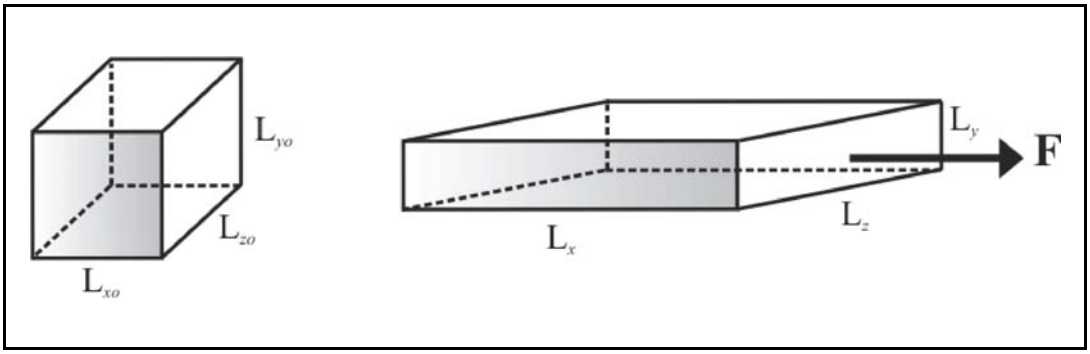

Figure 3.10: The uniaxial deformation of polymer network.

In the polymer network, applying a force in one direction can cause deformations in other directions. Consider that a cubic polymer network sample is subjected to a constant uniaxial stress to derive a stress-strain equation. As shown in Figure 3.10, under such a stress, the cubic polymer network is transformed into a rectangular parallelepiped having three edge length. The deformation ratios α_x, α_y, and α_z which are obtained directly from the dimensions of the polymer network in the strained state and in the (initial) unstrained state, equal to $\left(L/L_0\right)_i$, where $i = x, y,$ or z. These extension ratios may be either greater than 1, corresponding to a stretch, or less than 1, corresponding to a compression. This deformation occurs at essentially constant volume which can be formulated as follows:

$$\frac{V}{V_0} = \frac{L_x L_y L_z}{L_{xo} L_{yo} L_{zo}} = 1 \tag{3.38}$$

and hence $\alpha_x\alpha_y\alpha_z = 1$. Thus, the polymer network stretched by the amount $\alpha_x = \alpha > 1$ would have its perpendicular dimensions compressed by the amounts $\alpha_y = \alpha_z = 1/\sqrt{\alpha} < 1$. Then Equation (3.31) becomes:

$$\Delta G_{el} = \frac{1}{2}\bar{\nu}RT\left[\alpha^2 + \frac{2}{\alpha} - 3\right] \tag{3.39}$$

The change in the Helmholz free energy due to elastic deformation or work of deformation is obtainable directly from Eq.(3.39) and hence:

$$W = \Delta A_{el} \cong \Delta G_{el} = \frac{1}{2}\bar{\nu}RT\left[\alpha^2 + \frac{2}{\alpha} - 3\right] \tag{3.40}$$

in which *W* represents the work of deformation or elastically stored free energy per unit volume of the polymer network. According to Eq. (3.12), the force-deformation relationship is developed by differentiation of *W* or Helmholtz free energy with respect to the elongation of the polymer network upon deformation, α:

$$f = \left(\frac{\partial W}{\partial \alpha}\right)_{T,V} = \frac{1}{2}\bar{\nu}RT\left(2\alpha - \frac{2}{\alpha^2}\right) = \bar{\nu}RT\left(\alpha - \frac{1}{\alpha^2}\right) \tag{3.41}$$

Equation (3.41) contains a system-size-dependent quantity, $\bar{\nu}$ is the number of moles of polymer chains in a unit volume of the dry polymer network and is removed by considering that,

$$\frac{\bar{\nu}}{V_0} = \left(\frac{\bar{\nu}\bar{M}_c}{V_0}\right)\left(\frac{1}{\bar{M}_c}\right) = \left(\frac{m_0}{V_0}\right)\left(\frac{1}{\bar{M}_c}\right) = \frac{\rho}{\bar{M}_c} \tag{3.42}$$

in which V_0 is the volume of the polymer network, $\bar{M}_c$ is the number average molar mass of the gaussian chains and ρ is the polymer density. It is more convenient to write Eq.(3.41) in the form:

$$f = \frac{\rho RT}{\bar{M}_c}\left(\alpha - \frac{1}{\alpha^2}\right) \tag{3.42}$$

The effective crosslink density v_e is defined as the concentration of the elastically active chains. The number of segments between two successive crosslinks N and $\bar{M}_c$ are related to the cross-link density v_e through the equation:

$$v_e = \frac{\rho}{\bar{M}_c} = \frac{1}{N\bar{V}_1} \tag{3.43}$$

where $\bar{V}_1$ is the molar volume of a segment, which is generally taken as the molar volume of the solvent (i.e., for water, 18×10^{-6} m^3/mol).

In terms of the effective crosslink density, Equation (3.42) may also be written:

$$f = v_e RT\left(\alpha - \frac{1}{\alpha^2}\right) \tag{3.44}$$

According to the Gaussian statistical theory of rubber elasticity, the stress-strain relation for polymer network in simple elongation can be represented by the Equation (3.44).

This equation involves a single physical parameter $v_e RT$, which is called the elastic modulus of the gel in the dried state;

$$G_{dry} = v_e RT = \frac{\rho}{\bar{M}_c} RT \tag{3.45}$$

Equation (3.45) shows that, the elastic modulus increases in a linear manner with increasing temperature.

The other important aspect of Equation (3.45) is that the modulus is inversely proportional to $\bar{M}_c$. Hence, the polymer networks with a high crosslink density, i.e. low $\bar{M}_c$, behave stiffy.

3.6. Elastic Behavior of Swollen Polymer Networks

The polymer gel can be also defined as a polymeric network that contains solvent. To define the elastic behavior of the swollen networks, the swelling process can be considered as a result of two thermodynamic phenomena:

i. An increase of entropy of the network-solvent system by introduction of small molecules as diluent.

ii. A decrase of entropy of the polymer chains by the isotropic dilution.

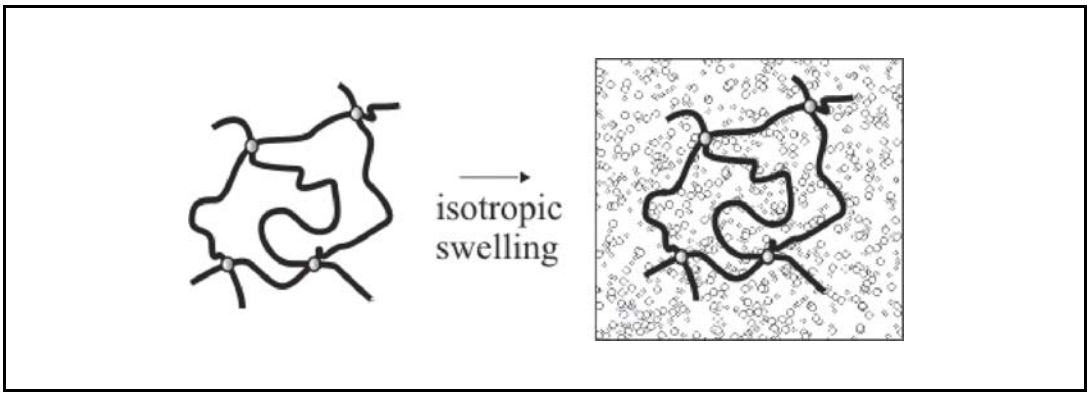

Figure 3.11: Isotropic swelling of a polymer network.

As shown in Figure 3.11, the swelling process itself corresponds to an isotropic expansion of the polymer network, and will therefore be accompanied by a reduction in the network entropy. On the application of a stress to the swollen gel there will be a further reduction of the entropy due to the deformation of the already swollen network.

The total reduction of the entropy involved in the transformation from the initial unstrained-after preparation state to the final strained-swollen state will thus be the sum of two terms: one associated purely with the swelling and the other with the subsequent strain.

Equation (3.27) for the entropy of deformation can be used to calculate the change of entropy ΔS_{12} associated with the initial isotropic swelling (process 1 to 2 in Figure 3.12), corresponding to the linear extension ratio α_0. The deformation matrix becomes:

$$\alpha_x \alpha_y \alpha_z = \frac{V}{V_0} \quad \text{and} \quad \alpha_x = \alpha_y = \alpha_z = \alpha_0 \tag{3.46}$$

Substituting Eq. (3.46) into Eq. (3.27) gives the change of entropy ΔS_{12} in passing from the initial unstrained-after preparation state to the unstrained-swollen state:

$$\Delta S_{12} = -\frac{1}{2}\nu k\left(3\alpha_0^2 - 3\right) \tag{3.47}$$

The state of the deformation passing from the initial unstrained-after preparation state to the final strained-swollen state may be defined in terms of three principal entension ratios λ_x, λ_y, and λ_z.

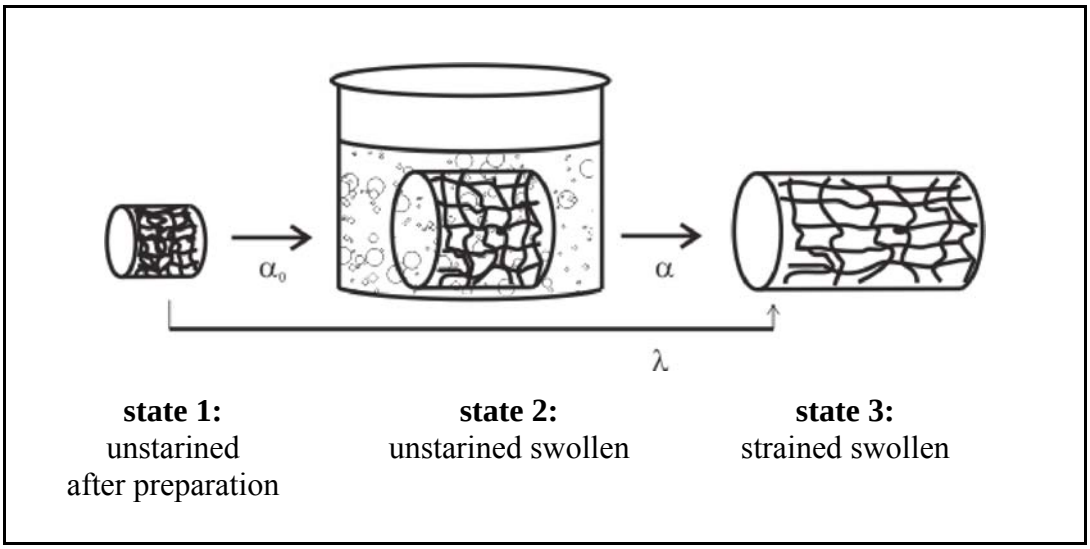

Figure 3.12: Schematic illustration of deformation of gels from the initial unstrained after preparation state to unstrained swollen state and the final strained swollen state.

The total entropy change ΔS_{13} in passing from the initial unstrained-after preparation state to the final strained-wollen state may be written in the form:

$$\Delta S_{13} = -\frac{1}{2}\nu k\left(\lambda_x^2 + \lambda_y^2 + \lambda_z^2 - 3\right) \tag{3.48}$$

The entropy of deformation ΔS_{23} of the swollen network is the difference between Eq. (3.48) and Eq. (3.47):

$$\Delta S_{23} = \Delta S_{13} - \Delta S_{12} = -\frac{1}{2}\nu k\left(\lambda_x^2 + \lambda_y^2 + \lambda_z^2 - 3\alpha_0^2\right) \tag{3.49}$$

The degree of swelling in terms of the volume fraction ν_2 of the polymer in the swollen gel and the equilibrium volume swelling ratio q_v referred to the dry state was defined through the Equation (2.5).

The corresponding isotropic strain or the linear dimensions of the swollen gel (linear extension ratio) can be related to the volume changes associated with swelling as:

$$\alpha_0^{\,3} = \frac{V}{V_0} = q_v = \frac{1}{\nu_2} \quad \text{and} \quad \alpha_0 = \frac{1}{\nu_2^{\,1/3}} \tag{3.50}$$

If the solvent is used during the synthesis, the linear swelling ratio with respect to the after preparation stage of the gel will be:

$$\alpha_0 = \left(\frac{V}{V_0}\right)^{1/3} = \left(\frac{\nu_2^0}{\nu_2}\right)^{1/3} \tag{3.51}$$

where ν_2^0 is the volume fraction of the crosslinked polymer after the gel preparation. Now, the extension ratios λ_x, λ_y, and λ_z should be defined with reference to the unstrained swollen state, so that:

$$\lambda = \frac{\mathrm{L}_{\text{deformation}}}{\mathrm{L}_{\text{after preparation}}} = \frac{\mathrm{L}_{\text{deformation}}}{\mathrm{L}_{\text{swollen}}} \cdot \frac{\mathrm{L}_{\text{swollen}}}{\mathrm{L}_{\text{after preparation}}} = \alpha\left(\frac{\nu_2^{\,0}}{\nu_2}\right)^{1/3} = \alpha.\alpha_0 \tag{3.52}$$

and substituting Eq.(3.52) into Eq.(3.49) gives:

$$\Delta S_{23} = -\frac{1}{2}\nu k\left(\alpha_x^2 + \alpha_y^2 + \alpha_z^2 - 3\right)\alpha_0^2 \tag{3.53}$$

Substitution of the Equation (3.51) for the corresponding linear swelling ratio yields:

$$\Delta S_{23} = -\frac{1}{2}\nu k\left(\alpha_x^2 + \alpha_y^2 + \alpha_z^2 - 3\right)\left(\frac{\nu_2^0}{\nu_2}\right)^{2/3} \tag{3.54}$$

This is the entropy of deformation per unit volume of the original unswollen polymer network. The entropy of deformation ΔS per unit volume of swollen gel is given by:

$$\Delta S = \frac{\nu_2}{\nu_2^0}\Delta S_{23} = -\frac{1}{2}\nu k\left(\alpha_x^2 + \alpha_y^2 + \alpha_z^2 - 3\right)\left(\frac{\nu_2^0}{\nu_2}\right)^{2/3} \tag{3.55}$$

and Equation (3.55) becomes after simplification :

$$\Delta S = -\frac{1}{2}\nu k\left(\alpha_x^2 + \alpha_y^2 + \alpha_z^2 - 3\right)\nu_2^{1/3}\left(\nu_2^0\right)^{1/3} \tag{3.56}$$

in which, ν is the number of polymer chains in a unit volume of the dry polymer network and after by introducing the term $\nu = v_e\nu_2^0$ and $R = k.N_A$, Equation (3.56) becomes:

$$\Delta S = -\frac{1}{2}v_e R\left(\alpha_x^2 + \alpha_y^2 + \alpha_z^2 - 3\right)\nu_2^{1/3}\left(\nu_2^0\right)^{2/3} \tag{3.57}$$

Substituting Eq.(3.29) into Eq.(3.40) gives the corresponding strain-energy function for the swollen gel:

$$W = -T\Delta S = \frac{1}{2}v_e RT\nu_2^{1/3}\left(\nu_2^0\right)^{2/3}\left(\alpha_x^2 + \alpha_y^2 + \alpha_z^2 - 3\right) \tag{3.58}$$

Equation (3.58) represents the properties of the swollen gel in terms of the extension ratios and the volume fraction of the polymer in the swollen gel ν_2. According to Equation (3.41), performing the differentiation, $f = \left(\partial W/\partial\alpha\right)_{T,V}$, leads to the expression for the uniaxial stress for affine networks as:

$$f = \nu_e RT \nu_2^{1/3} \left(\nu_2^0\right)^{2/3} \left(\alpha - \frac{1}{\alpha^2}\right) \tag{3.59}$$

According to this equation the elastic modulus of the swollen gels is defined as:

$$G = A\nu_e RT \nu_2^{1/3} \left(\nu_2^0\right)^{2/3} \tag{3.60}$$

where the front factor A equals 1 for an affine network and 1 - 2/ϕ for a phantom network, where ϕ is the functionality of the crosslinks. Since $\nu_2^0 = \nu_2$ for the hydrogels just after preparation, the modulus G_0 after preparation becomes:

$$G_0 = A\nu_e RT \nu_2^0 \tag{3.61}$$

The reduced modulus G_r defined as the ratio of the elastic modulus of the gel at a given degree of swelling to that of the same gel after its preparation is given for a network of Gaussian chains can be calculated from Eq.(3.60) and Eq.(3.61) as:

$$G_r = \frac{G}{G_0} = \left(\frac{\nu_2}{\nu_2^0}\right)^{-1/3} = \left(\frac{V}{V_0}\right)^{-1/3} = V_r^{-1/3} \tag{3.62}$$

Making use of Eq.(3.43), the elastic modulus of swollen gels may be defined in terms of the characteristic parameters such as, the number of segments between two successive cross-links N, and the molecular weight of the network chains $\bar{M}_c$ by:

$$G = \nu_e RT \left(\nu_2^0\right)^{2/3} \nu_2^{1/3} = \frac{\rho}{\bar{M}_c} RT \left(\nu_2^0\right)^{2/3} \nu_2^{1/3} = \frac{1}{N\bar{V}_1} RT \left(\nu_2^0\right)^{2/3} \nu_2^{1/3} \tag{3.63}$$

and by considering that for gels just after preparation $\nu_2^0 = \nu_2$, the elastic modulus of gels after preparation G_0 becomes:

$$G_0 = \nu_e RT \nu_2^0 = \frac{\rho}{\bar{M}_c} RT \nu_2^0 = \frac{1}{N\bar{V}_1} RT \nu_2^0 \tag{3.64}$$

3.7. Factors Affecting Elastic Modulus of Polymer Networks

When the polymer chains are chemically linked together to form a three-dimensional polymer network, the resulting material exhibits a unique set of elastic properties. If this polymer network is subjected to an external force, it undergoes elastic deformation which is dependent on its chemical composition and topology. The influence of the network structure on the elastic behavior is reflected principally through the macroscopic elastic modulus. In the next paragraphs, the elastic behavior of the polymer network is summarized in terms of the several factors.

i. Network structure: The stiffness of the polymer backbone of the gels affect the elastic modulus. A gel consist of stiff network chains due to the bulky side groups is expected to have higher elastic modulus than a flexible polymer[53]. Moroever, according to Equations (3.60) and (3.61), for usual tetrafunctional polymer networks, the elastic modulus of an affine network is twice as larger as the one for a corresponding phantom network with the same crosslink density and prepared under similar conditions.

ii. The initial monomer concentration: As the monomer concentration is increased, the effective crosslink density ν_e of the hydrogels also increases due to the more efficient consumption of BAAm in concentrated monomer solutions, so that the elastic modulus of gels becomes larger. In order to quantify the dependence of the effective crosslink density of gels on the monomer concentration ν_2^0, a statistical model was proposed by Bromberg et al. In this model, the gel growth process during polymerization was considered as a set of random walks of the growing radicals[54]. In Figure 3.13, the process of the gel growth is schematically illustrated. The random walk of the propagating radical, shown in the Figure by the solid curve, occurs between two successive hits of the radical center with the other kinetic chains, i.e., between A and B, B and C, etc. Each random walk is succession of g steps, during which the radical adds the monomer, the crosslinker and involves cyclization reactions with the pendant vinyl groups located on the same chain. Since in a random walk the end-to-end distance of a chain after g steps is $g^{1/2}$, the polymer segments concentration ν_2^0 during the crosslinking copolymerization scales with

$$g/g^{3/2} = g^{-1/2} \qquad \text{or} \qquad g \approx \left(\nu_2^0\right)^{-2} \tag{3.65}$$

After g steps, the growing chain will hit another chains. The model assumes that the probability p that the growing chain will meet a crosslinker unit on another chain is equal to the number fraction of the crosslinker molecules in the reaction system, i.e.,

$$p = X/(1+X) \cong X \qquad (\text{for X} << 1) \tag{3.66}$$

where X is the crosslinker ratio. Thus, after *1/p* hits, the growing chain will succeed to form an effective crosslink, for example at point C in Figure 3.13. The network chain length N will then be equal to;

$$N = \frac{g}{p} = \left(\nu_2^0\right)^{-2} X^{-1} \tag{3.67}$$

The network chain length N relates with the effective crosslink density according to Equation (3.43). Since $N \approx \nu_e^{-1}$, Equation (3.67) leads to:

$$\nu_e \approx (\nu_2^0)^2 \tag{3.68}$$

indicating that, at a fixed crosslinker ratio, the effective crosslink density of hydrogels scales with the second power of the monomer concentration ν_2^0.

iii. The crosslinker concentration, i.e. the crosslinker ratio X: The elastic modulus of gels sensitively depends on the crosslinker concentration. The modulus of gels increases with increasing BAAm concentration due to decreasing chain length between successive crosslinks. Furthermore, it was found that the dependence of the elastic modulus of the gels on the crosslinker content shows three different regimes: (1) At crosslinker contents much below the critical crosslinker concentration: G_0 increases, (2) Close to the critical crosslinker concentration: G_0 decreases and (3) Above the critical crosslinker concentration: G_0 first remains constant but then increases with increasing crosslinker content[22].

iv. Ionic group concentration: The elastic modulus of gels after their preparation first increases with increasing charge density but then decreases continuously. The results

indicate two opposite effects of charged groups: Formation of multiplets in the gel increases the elastic modulus of ionic hydrogels, whereas the effect of the electrostatic interaction of charged groups on elastic free energy decreases the modulus[55,56].

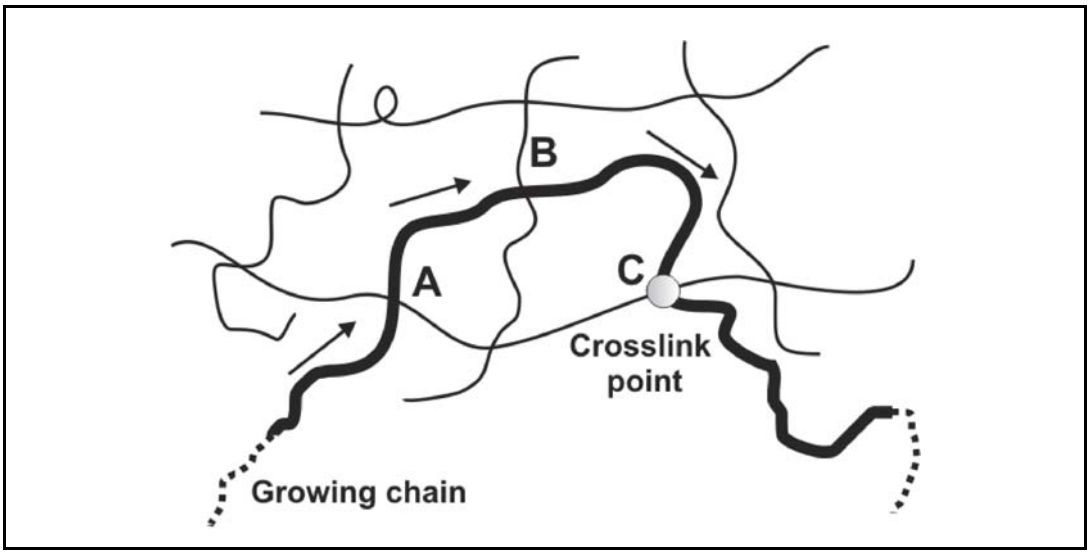

Figure 3.13: Gel growth during free-radical crosslinking copolymerization. The random walk of a propagating radical is shown by the solid curve. The growing chain hits another chains at A, B, and C. The dot represents a crosslink point.

v. Swelling: The modulus of gels decreases with increasing degree of swelling. The swelling process reduces the polymer network concentration, i.e. for swollen hydrogels $\nu_2 < \nu_2^0$. According to Equation (3.60), the elastic modulus after equilibrium swelling G is usually lower than that of after preparation G_0[57].

vi. Entanglements: The constrained junction theory as well as the slip-link model have been predicted that the modulus may increase due to the presence of entanglements. The decrease of the modulus with elongation can be interpreted as a result of relaxation of entanglement constraints due to the deformation[48,49].

vii. Structural heterogeneities: The elastic modulus of gels also depends on the sample location, at which the mechanical measurements are carried out. It was shown that G_0 increases continuously with increasing distance from the bottom of the gel rod, indicating that the effective crosslink density of the network chains increases along the same direction within the gel. It was also shown that the modulus decreases as the degree of the structural heterogeneity increaes[58].

4. SCATTERING PROPERTIES OF POLYMER NETWORKS

Light scattering is a process which covers a wide range of interactions of electromagnetic radiation with an atomic particle. Therefore, the analysis of the scattered radiation arising from these interactions is an important physical method.

The theory of light scattering was first developed to explain the color and the polarization of the sky light. In 1706, Newton suggested that there is a region in the atmosphere with a suspension of water droplets and the blue color of the sky is due to the interference of the rays reflected from the front and rear surfaces of the droplets[59]. Tyndall made the first experimental investigation of the light scattering and observed the scattering of natural light when it passed through a colloid dispersion. The scattered light showed a light bluish color if the incident light was polarized[60]. In 1881, based on Maxwell theory of electromagnetic field, Lord Rayleigh derived that the intensity of the scattered light by small particles is reversely proportional to the fourth power of the incident wavelength[61,62]. In 1944, Debye extended this theory to large particles and measured the molecular weight of the macromolecules from dilute solution using the light scattering method and derived the form factor of a flexible Gaussian chain in absence of excluded volume interaction[63]. The so-called Rayleigh-Debye theory was extended by Zimm, who calculated the scattering intensity of a dilute polymer solution in good solvent conditions and the famous Zimm plot was proposed in 1948[64]. Since then, the light scattering technique has widely used to study a whole range of materials including gases, pure liquids, and polymer solutions.

In this chapter, the fundamental principles and uses of static light scattering is presented. The static light scattering technique is a major technique in the work of this thesis to investigate the properties of the polymer solutions, gels as well as the sol-gel transitions. A detailed theoretical treatment in this chapter involves the interaction of the light with gas particles and gradually progress to the polymer solutions and gels. The scattering of

light from a gas is described at first and then the theory is applied to liquids and small polymer molecules with dimensions less than five percent of the wavelength of the incident light. Next, the polymer solutions of larger size are examined. The focus of this chapter is Section 4.5, where the light scattering and the spatial inhomogeneity in the polymer gels is discussed. Debye-Bueche theory, which includes suitable parameters for characterizing the gel inhomogeneity is also discussed in details.

4.1. Static Light Scattering

In the static light scattering technique, the total scattered intensity is measured which yields information on the properties such as the weight average molecular weight, the second osmotic virial coefficient, and z-average of the mean-square radius of gyration. In dynamic light scattering, the time dependence of the fluctuations in scattered intensity is analyzed, which provides information on the hydrodynamic properties of the polymer solution, such as the translational diffusion coefficient.

The light scattering intensity can be monitored either in the microsecond or in the second time range domain. This is the basic difference between the dynamic light scattering and the static light scattering. The fluctuations in the intensity of the light scattered by a small volume of a solution in the microsecond time range are directly related to the Brownian motion of the solute. Averaging the intensity over the second time range interval will cause a loss of the solute dynamic properties information; that is why light scattering is named either static or dynamic. The static light scattering refers to an experiment in which an intensity $I(\theta)$ is determined at a scattering angle θ by averaging the fluctuating intensity of the light scattered from a material over a time long compared with the time scale of the fluctuations.

In Figure 4.1, the geometry of a sample during the light scattering measurements is shown. A cylindrical light scattering vial containing a clear polymer solution or polymer gel is immersed in a flow cell and a vertically polarized laser beam enters into the vial. Nearly all of the incoming photons travel straight through the polymer solution or gel, forming a strong, unscattered (or forward-scattered) beam. The molecules in the beam path scatter a tiny fraction of the photons in all directions. The intensity of the scattered

beam is detected by a photodetector placed horizantally at a scattering angle θ from the forward-scattering direction. To prevent streak scattering at the air-glass interface, the flow cell has a planar cut at each side of the path of the direct beam.

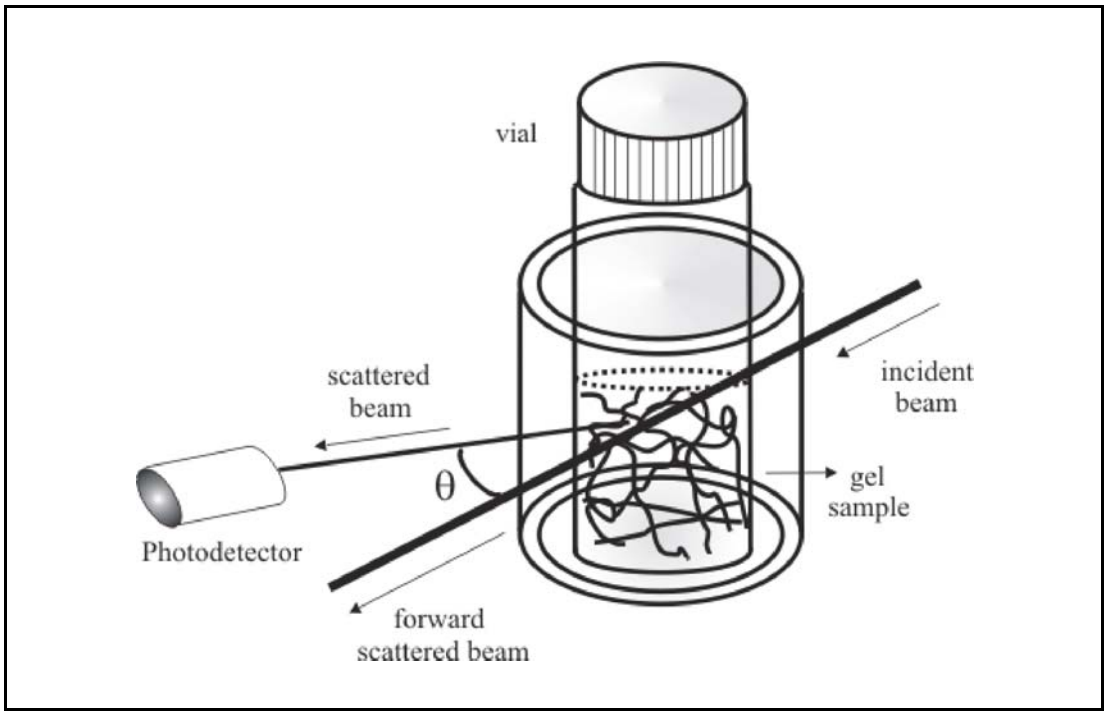

Figure 4.1: Schematic of the geometry around a sample cell in a light-scattering measurement system.

Figure 4.2 is a top view of the sample geometry. The incident beam has a wave vector k_i. The wave vector is parallel to the propagation direction of the beam and has a magnitude of $2\pi / (\lambda / n)$, where λ / n is the wavelength of light in the solvent of refractive index n. The wave vector k_s of the scattered beam has nearly the same magnitude as that of k_i. In static light scattering in which the molecules are assumed to be motionless, the two magnitudes are exactly equal; $|k_i| \approx |k_s|$.

The change in the wave vector upon scattering is called the scattering vector q which is defined as:

$$q \equiv k_i - k_s = 2\, k_s \sin(\theta/2) = 4\pi n/\lambda \sin(\theta/2) \qquad (4.1)$$

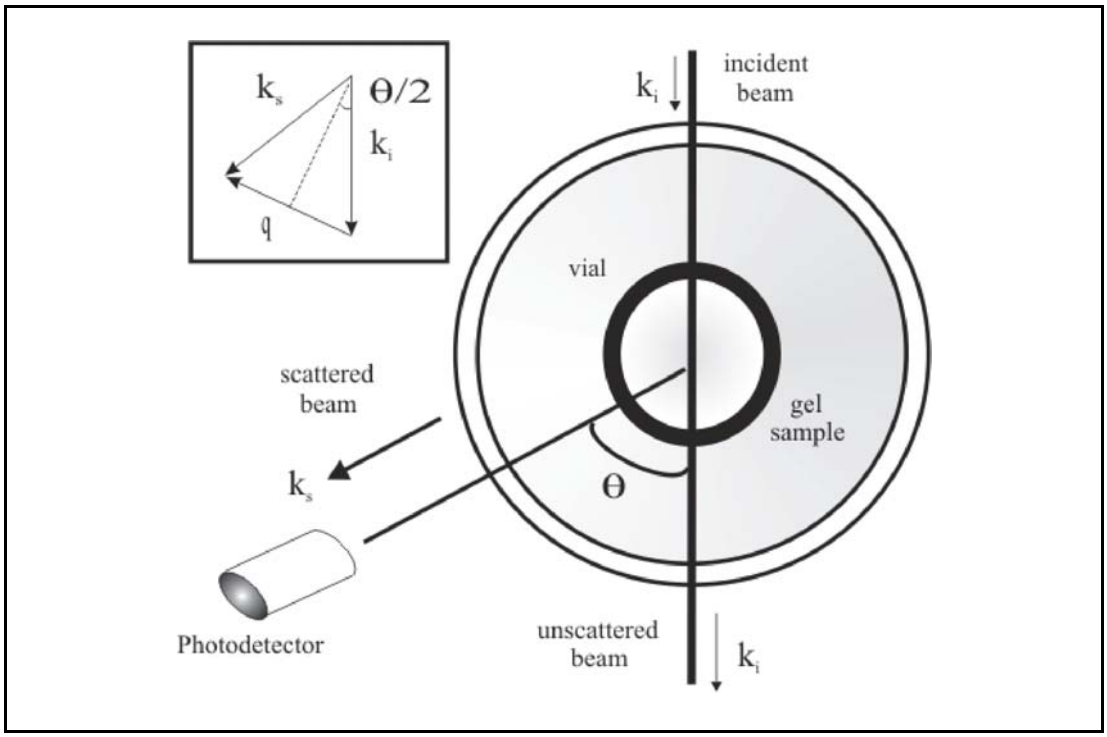

Figure 4.2: Top view of the geometry around the sample cell. The wave vector k_i of the incident beam changes to k_s when scattered. Two slits specify the scattering angle θ. The inset defines the scattering wave vector q.

4.2. Light Scattering by Dilute Gases

In order to understand the basic phenomena of the light scattering by polymer solutions, one must start by considering the scattering of light by a gas. A theoretical treatment of the scattering of light by the molecules of a gas was first given by Lord Rayleigh[62]. The light is defined as an electromagnetic field which propagates in time and space. A plane-polarized beam of light is composed of two main quantities the electric field E and the magnetic field H, perpendicular to each other and to the direction of propagation, each at a given point varying sinusoidally with time. As shown in Figure 4.3, if the light wave travels in the *x*-direction, then the electric and magnetic vectors would vibrate in *y* and *z* directions, respectively. There are three main factors involved in light scattering: the incident light, the particle and the scattered light. Taking this into consideration, Rayleigh started with the electric field of the incident light in the direction *x* which can be expressed as[62]:

$$E = E_0 \cos\left[2\pi\left(\upsilon t - x/\lambda\right)\right] \tag{4.2}$$

where E is the strength of the electric field, E_0 is the maximum amplitude of the field, υ is the frequency, t is the time and *x* is a position along the line of propagation. The wavelength of the incident light is denoted by λ.

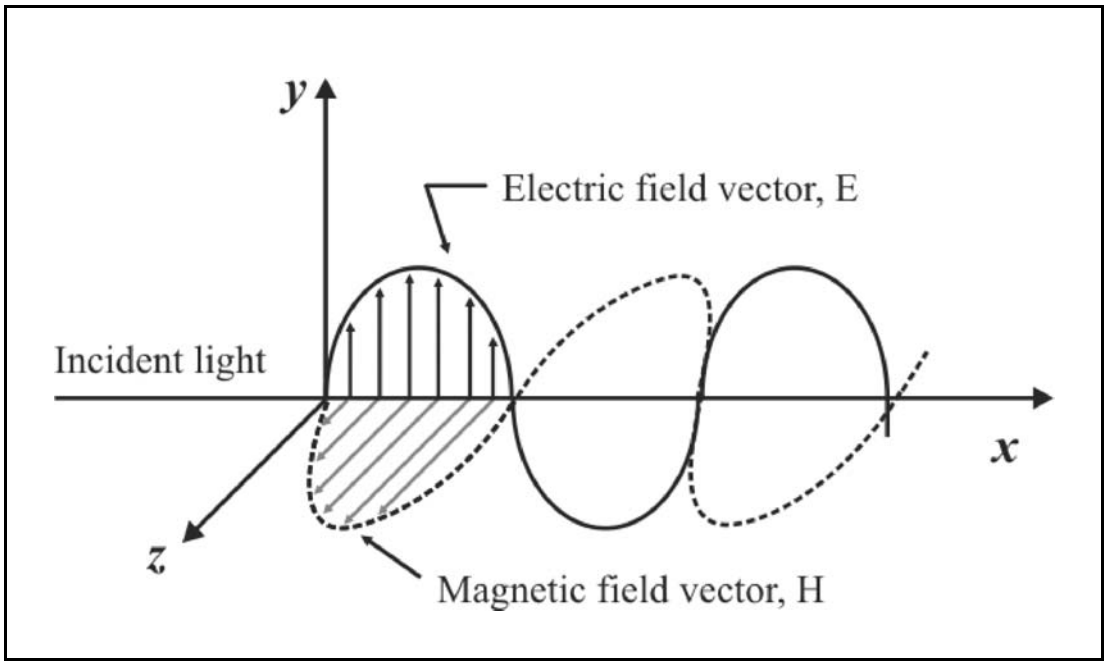

Figure 4.3: The relationship between the electric and magnetic fields of light.

According to the electromagnetic theory, the incident light hits the particle and this disturbs the electron distribution resulting in a polarization of the particle. The electrons are subsequently aligned in the direction of the field and the corresponding nuclei align in a direction opposite of the field. This polarization of the particle acts as an oscillating dipole (P) in which the electrons of the molecules oscillate at the frequency of the incident light. In terms of the electric field, the oscillating dipole is given by:

$$P = \alpha E = \alpha E_0 \cos\left[2\pi\left(\upsilon t - x/\lambda\right)\right] \tag{4.3}$$

where α is denoted as the polarizability. This oscillating dipole now becomes a secondary source of the radiation.

The magnitude of the scattered electric field is related to the second derivative of P with respect to time, d^2P/dt^2 as:

$$\frac{d^2P}{dt^2} = 4\pi^2\alpha\upsilon^2 E_0 \cos\left[2\pi\left(\upsilon t - x/\lambda\right)\right] \tag{4.4}$$

When the incident light is linearly polarized, the magnitude of the scattered electric field for the scattered light is:

$$E_s = \frac{\left(d^2P/dt^2\right)\sin\theta_1}{\tilde{c}^2 r} \tag{4.5}$$

where θ_1 is the angle between the direction of polarization and the direction of scattering, r is distance of the detector from the center of the scattering volume, and $\tilde{c}$ is the speed of light and the square of the speed of light has been used for dimensional reasons. Combining the relationships for d^2P/dt^2 and the above equation for E_s, the following is obtained:

$$E_s = \frac{4\pi^2\upsilon^2\alpha E_0 \sin\theta_1}{\tilde{c}^2 r}\cos 2\pi\left(\upsilon t - x/\lambda\right) \tag{4.6}$$

Three major comments are necessary concerning Equation (4.6). First, the scattered electric field has the same frequency as the incident field (Equation 4.2). Second, the strength of the scattered fields is inversely dependent on the distance between the scattering origin and the detector. Finally, the strength of the field depends on the angle of observation, θ_1. According to Poynting's theorem, the intensity is proportional to the electric field strength squared as[65]:

$$I = \varepsilon_o \tilde{c}\left\langle E^2\right\rangle \tag{4.7}$$

where ε_0 is the dielectric coefficient at vacuum.

Averaging Equations (4.2) and (4.5), and taking the ratio of the intensity of scattered light I_s to the intensity of the incident light I_0:

$$\frac{I_s}{I_0} = \frac{E_S^2}{E^2} = \frac{\left\{4\pi^2\upsilon^2\alpha E_0 \cos\left[2\pi\left(\upsilon t - x/\lambda\right)\right]\right\}^2 . \frac{\sin^2\theta_1}{\tilde{c}^4 r^4}}{\left\{E_0 \cos\left[2\pi\left(\upsilon t - x/\lambda\right)\right]\right\}^2} \tag{4.8}$$

where the quantity $\tilde{c}/\upsilon$ has been replaced by λ and λ_o is the wavelength in a vacuum and hence:

$$\frac{I_s}{I_0} = \frac{16\pi^4\alpha^2 \sin^2\theta_1}{\lambda_0^4 r^2} \tag{4.9}$$

Equation (4.9) is known as the Rayleigh ratio for vertically polarized light scattered by a single molecule and is commonly seen in the following form:

$$R_\theta = \frac{I_s r^2}{I_0 \sin^2\theta_1} = \frac{16\pi^4\alpha^2}{\lambda_0^4} \tag{4.10}$$

The Rayleigh ratio is measured in cm^{-1}. As a consequence of the relationship between the scattered intensity and the wavelength to the fourth power, the blue daytime and the red evening skies can be explained. The blue light is scattered more strongly than red due to this relationship[66]. For the case of dilute gases, the polarizability α is related to the dielectric constant, ε as follows:

$$\varepsilon = 1 + 4\pi\alpha N_p \tag{4.11}$$

where N_p is the number of particles per unit volume. Additionally, Maxwell's relationship for ε can be expressed as $\varepsilon = \tilde{n}^2$, where $\tilde{n}$ is the refractive index[61]. Thus, Equation (4.11) becomes:

$$\tilde{n}^2 - 1 = 4\pi\alpha N_p \tag{4.12}$$

An assumption is made here that the refractive index can be expanded in a Taylor series. This amounts to restricting the concentration of gas particles to be very low;

$$\tilde{n} = 1 + (d\tilde{n}/dc)c + \ldots \qquad \text{or} \qquad \tilde{n}^2 = 1 + 2(d\tilde{n}/dc)c + \ldots \tag{4.13}$$

In both equations, c is the concentration of the particles. Substitution of the latter expression into Equation (4.12), followed by rearranging, yields:

$$\alpha = \frac{c(d\tilde{n}/dc)}{2\pi N_p} = \frac{M(d\tilde{n}/dc)}{2\pi N_A} \tag{4.14}$$

where M is the molecular weight, N_A is Avogadro's number and $M/N_A = c/N_p$. Substituting into Equation (4.9), gives the Rayleigh equation for a single particle:

$$\frac{I_s}{I_0} = \frac{4\pi^2 M^2 (d\tilde{n}/dc)^2 \sin^2\theta_1}{N_A{}^2 \lambda^4 r^2} \tag{4.15}$$

To obtain the scattered intensity per unit volume, the above expression can be multiplied by the number of scatterers per unit volume ($N_A c/M$) and hence,

$$\frac{I_s}{I_0} = \frac{4\pi^2 Mc (d\tilde{n}/dc)^2 \sin^2\theta_1}{N_A \lambda^4 r^2} \tag{4.16}$$

The angular term $\sin^2\theta_1$ depends on the type of incident radiation. A vertically polarized beam will cause the oscillating dipole to vibrate in the vertical plane. Observation in the horizontal plane will be at 90˚ to the oscillating dipole. Consequently, the term $\sin^2\theta_1$ becomes unity and the scattered intensity is independent of observation angle. Generally, the light scattering is performed with an unpolarized incident beam. Here, the radiation is composed of two plane polarized beams which are of different phase but their planes of the polarization are perpendicular to each other. Therefore two different oscillating dipoles, one in the vertical plane and one in the horizontal plane are

observed. By using the superposition of two perpendicular plane polarized beams of equal intensity and contributing half to the total scattering intensity:

$$\frac{I_s}{I_0} = \frac{1}{2}\frac{4\pi^2 Mc\left(d\tilde{n}/dc\right)^2}{N_A\lambda^4 r^2}\left(\sin^2\theta_1 + \sin^2\theta_2\right) \tag{4.17}$$

It is convenient to relate the angles in this equation to the more conventional laboratory coordinate system, particularly to θ which is the angle formed between the incident beam and the observed scattered beam in this direction. In this case, the angular term can be written as $\sin^2\theta_1 + \sin^2\theta_2 = 1 + \cos^2\theta$ and Equation (4.17) becomes:

$$\frac{I_s}{I_0} = \frac{2\pi^2 Mc\left(d\tilde{n}/dc\right)^2}{N_A\lambda^4 r^2}\left(1 + \cos^2\theta\right) \tag{4.18}$$

4.3. Light Scattering From a Liquid

The thermodynamic treatment of the light scattering from liquids was developed by Einstein[67] and later adapted by Debye[68,69] for polymer solutions. In the case of the liquids and the polymer solutions, a more rigorous approach to the problem must be employed due to their non-ideality. The intensity scattered by a liquid can be obtained as if each particle of gas was replaced by an elemental volume δV, small enough to be considered as a point when compared to the wavelenght of the radiation. Each elemental volume will have a polarizability α that will fluctuate by a certain amount of $\Delta\alpha$ about the average polarizability of the system $\langle\alpha\rangle$. Expansion of the fluctuating term $\left(\langle\alpha\rangle + \Delta\alpha\right)^2$ followed by consideration of the various terms yields:

$$\alpha^2 = \left(\langle\alpha\rangle + \Delta\alpha\right)^2 = \langle\alpha\rangle^2 + 2\langle\alpha\rangle\Delta\alpha + \Delta\alpha^2 \tag{4.19}$$

Considering the intensity scattered by *N* elemental volumes within a unit volume, the value $\langle\alpha\rangle$ is the same for each volume element. Therefore, terms in $\langle\alpha\rangle$ will cancel for

the reason that the scattered light in an ordered system is zero. Also the average value of $2\langle\alpha\rangle\Delta\alpha$ will be zero, because $\Delta\alpha$ will take equivalent positive and negative values. Due to the size of the volume elements is much smaller than the wavelength of the incident light such that each volume element behaves as a Rayleigh scatterer. Consequently, via equation (4.10), the time average Rayleigh ratio for the scattering per unit volume containing $N_p = 1/\delta V$ volume elements becomes:

$$R_\theta = \frac{16\pi^4 \langle \Delta\alpha^2 \rangle}{\lambda_0{}^4 \delta V} \tag{4.20}$$

Taking into account the relation between the polarizability and the dielectric constant, the polarizability fluctuation can be expressed as:

$$\Delta\alpha = \frac{\delta V \Delta\varepsilon}{4\pi} \tag{4.21}$$

and substituting into Equation (4.20) yields:

$$R_\theta = \frac{\pi^2 \delta V \langle \Delta\varepsilon^2 \rangle}{\lambda_0{}^4} \tag{4.22}$$

In a pure liquid, the fluctuations in the local value of the dielectric constant are due to the fluctuations in both temperature and density, but in general the fluctuations in temperature are negligible and so,

$$\langle \Delta\varepsilon^2 \rangle = \left(\frac{\partial\varepsilon}{\partial\rho} \right)^2 \langle \Delta\rho^2 \rangle \tag{4.23}$$

According to the theory of fluctuation and thermodynamic arguments, Equation (4.22) becomes;

$$R_\theta = \frac{\pi^2 k T \rho^2 \beta}{\lambda_0^{\,4}} \left(\frac{\partial \varepsilon}{\partial c} \right)_T^2 \tag{4.24}$$

where k is the Boltzmann constant, T is the absolute temperature and β is the isothermal compressibility.

4.4. Light Scattering From Polymer Solutions

The polymer solutions can be divided into three different groups according to their concentration: the dilute, the semi-dilute and the concentrated solutions. A schematic description of the state of polymer molecules in the solutions with different polymer concentrations is given in Figure 4.4[70].

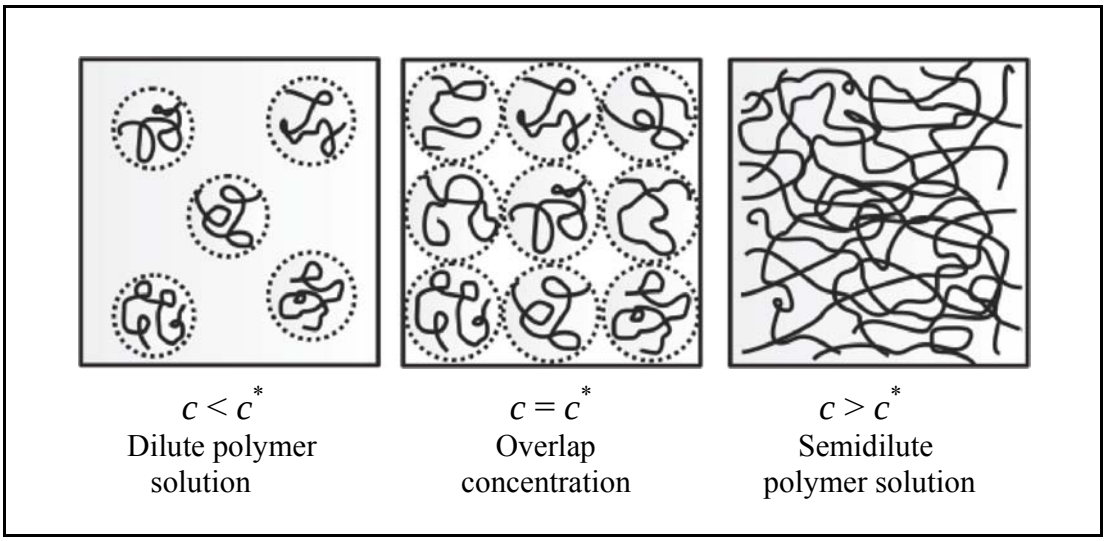

Figure 4.4: Schematics of (a) dilute, (b) chain overlapping threshold, and (c) semi-dilute regimes of polymer solutions.

The Brownian motion of the polymer molecules in solutions dominates the time dependent phenomena in polymer solutions such as the diffusion, the viscoelasticity and the dynamic light scattering. In polymer solutions, the solvent molecules and the polymer chains vigorously move inside and the chain conformation constantly varies. Although the thermodynamic and dynamic properties of the individual isolated polymer chains in dilute solutions are fairly understood, the dynamics of the polymer chains in

the semidilute and concentrated solutions still remains an open question[71]. In the following section, the behavior of polymer chains in dilute solutions will be discussed and then, the dynamics of semidilute and concentrated solutions will be presented.

4.4.1. Dilute Polymer Solutions and Single Chain Dynamics

The dilute solution behavior depends only on the polymer-solvent interactions and the interactions between different segments on a single polymer chain. In dilute solutions, the polymer molecules are well separated and independent from each other as schematically shown in Figure 4.4. Hence, the short ranged intermolecular interactions (chain-chain interactions) can be ignored as they are far away from each other and the polymer chains interact primarily with the solvent molecules. The dynamics in this regime is essentially single chain dynamics concerning only intramolecular and monomer-solvent interactions.

4.4.2. Dynamics of Many Chain Systems in Semidilute Solutions

The semidilute regime begins when there are significant interactions between polymer chains and so, they are entangled with each other and their mobility is greatly reduced in comparison with those in dilute solutions, schematically shown in Figure 4.4. If the concentration c is defined as the number of chains per unit volume or the number of monomers per unit volume, then the concentration at which the polymer chains in the solution start to overlap with each other is defined as the overlap concentration c^*. The situation becomes quite different when polymer concentration c is higher than the overlap concentration (c^*). The solutions in this regime are called semidilute solutions. It corresponds to the situation where the polymer coils would begin to touch one another throughout the solution and make a dilute physical network in the solvent.

When the concentration of polymer chains in a solution increases such that chains significantly overlap each other, the chain-chain interactions enters the problem and dynamics becomes much more complicated. If the concentration becomes sufficiently large, that is, if $c >> c^*$, the polymer chains are relative homogeneously distributed and the fluctuations become small. Such a solution is called concentrated solution. The properties of semidilute solutions are drastically different from those of dilute solutions.

The overall chain motion is much slower in semidilute solutions because they are entangled. Semidilute solutions with long chains can barely flow and sometimes behave like an elastic rubber. Dilute solutions involve only a minimum degree of interaction (overlap) between different polymer molecules. The semidilute case involves overlapping polymer molecules but still with a considerable separation of the segments of different molecules. Therefore, c^* defines a threshold beyond which the solution is semi-dilute. The condition for chains to overlap can be thought of as many spheres of radius R_g closely packed in the solution. Under this spatial arrangement, c^* can be calculated as[70]:

$$c^* = \frac{\overline{M}_w / N_A}{\left(\frac{4}{3}\pi \left\langle R_g^{\,2} \right\rangle^{3/2}\right)} 10^2 \tag{4.25}$$

where $\overline{M}_w$ and $\left\langle R_g^{\,2} \right\rangle^{1/2}$ are the weight-average molecular weight and the radius of gyration of the polymer chains, respectively. According to Equation (4.25), the lower limit of a semidilute regime depends on the physical property of polymers. As for the upper concentration limit, it is not at all clear at what concentration a polymer solution is no longer semidilute, although in practice 10% (w/v) has often been used as an upper limit. For typical polymers N is quite large ($\sim 10^5$) such that c^* can actually be very small. For instance, for polystyrene chains of N $\sim 10^5$, $c^* \approx 0.005$ g/ml (0.5 % in weight) indicating that in a 1% solution, the polymer molecules are strongly overlapped, but still occupy a small volume fraction (0.01).

The Blob model is widely used to predict various static properties of semidilute solutions and to find how these properties depend on the concentration and molar mass of polymers. In dilute solutions, the single chain dynamics which involve all the interactions, such as excluded volume and hydrodynamic interactions, are referred to the monomers in the same chain.

However, in semi-dilute solutions, interactions from monomers of other chains come into effect. In semi-dilute polymer solutions, the intermolecularly and intramolecularly

coupled many-chain dynamics can be renormalized into independent motions. These independent motions are described by so-called blobs.

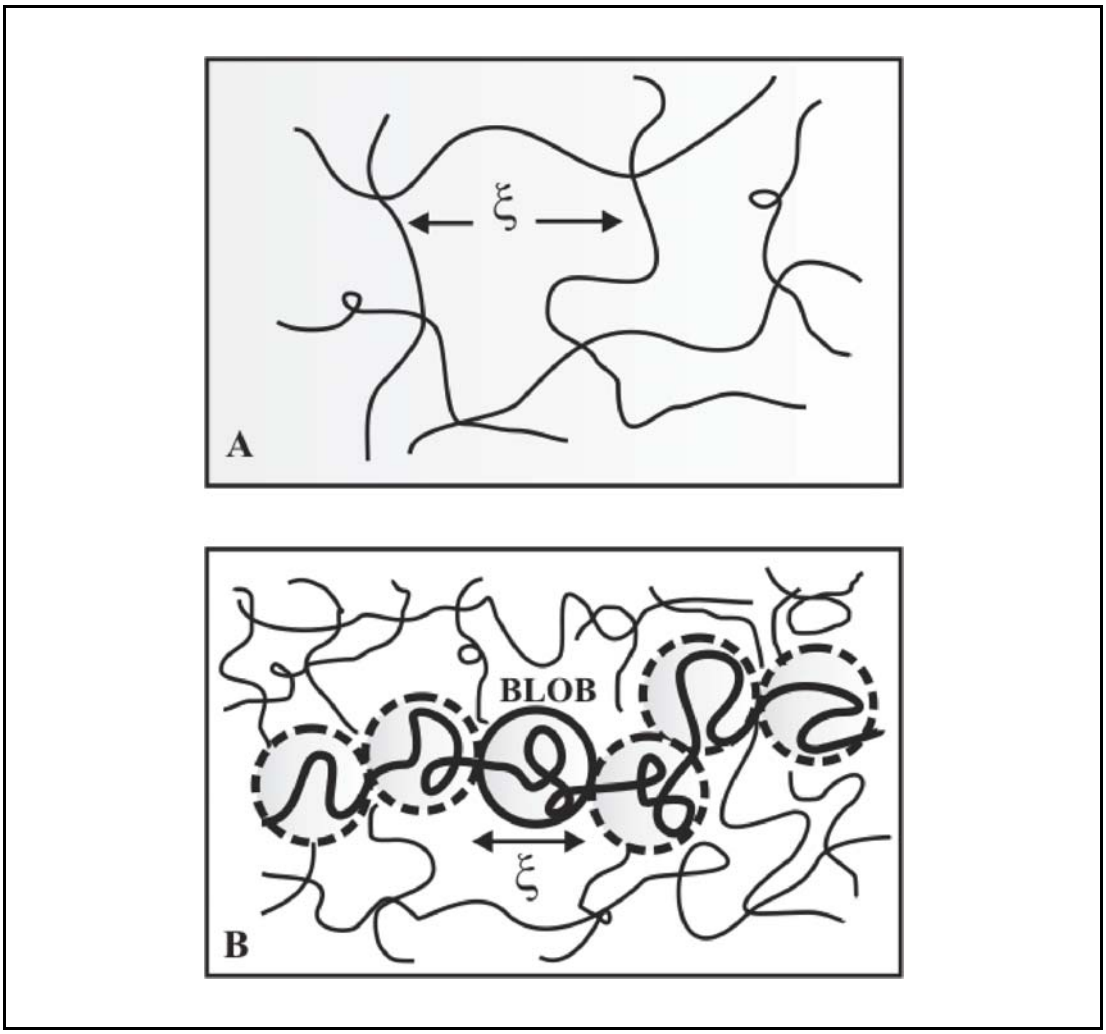

Figure 4.5: (A) Schematics of the mesh size (or correlation length) ξ of the network formed by chain contacts in a semidilute solution. (B) Schematics of the blobs in a semidilute solution.

Semidilute solution is generally considered to be a low volume fraction of polymer but a strong overlap between chains, as shown in Figure 4.5. When zoomed in, the entangled chains can be regarded as consisting of blobs. Physically, the blobs can be treated as spheres of size ξ of the correlation length. Inside the blob dynamic behavior resembles the single chain dynamics. The interactions between different chains, indicated by small dashed circles in Figure 4.5, are called the entanglement points. It is very difficult for

monomers of other chains to sneak in. In this way, the entire solution can be filled up with blobs. Figure 4.5 shows such a blob picture. The monomers contained in a blob are not necessary all from the same chain that can be a combination of segments from different chains[70].

Edwards and de Gennes have shown that in semidilute solutions, the correlation length ξ scales as the average distance between interchain contacts[70,72]. If the crosslinking occurs in these interchain contacts to form a gel, then ξ describes the mesh size of the gel network. Since ξ represents the mesh size (i.e. overlap distance) of the polymer network in semi-dilute solutions, it depends on the concentration c. The scaling assumption suggests that the functional dependence of ξ on c is universal if c is properly scaled to a fundamental scale which is assumed as c^*. Therefore ξ can take a scaling form as $\xi \approx \left(c/c^*\right)^x$, where x is a number to be determined. Because when $c \approx c^*$ where the coils are in contact (Figure 4.4), the mesh size must be comparable with the size of one coil, which is R_g, then the scaling form can written as $\xi = R_g \left(c/c^*\right)^x$.

In dilute solutions, the radius of gyration R_g of the real chain consisting of N monomers can be written as $R_g \sim N^{\nu}$, where ν is the Flory exponent, with $0.5 < \nu < 0.6$, depending on the solvent quality[32]. Introducing this relation into Equation (4.25) gives:

$$c^* \sim N^{1-3\nu} \tag{4.26}$$

Substitution of the relation $R_g \sim N^{\nu}$ and Equation (4.26) into $\xi = R_g \left(c/c^*\right)^x$ gives:

$$\xi \approx N^{\nu} N^{x(3\nu-1)} = N^{\nu+x(3\nu-1)} \tag{4.27}$$

When $c >> c^*$, ξ should not depend on N since the chains are much longer than the mesh size. Let the exponent in the above expression be zero and solve for x such as $x = \nu/1-3\nu$. For a good solvent, $\nu = 3/5$, and $\xi = R_g \left(c/c^*\right)^x$ can be rewritten as:

$$\xi = R_g \left(\frac{c}{c^*} \right)^{-0.75} \tag{4.28}$$

It should be mentioned that Equation (4.27) holds only for $c > c^*$. Below the overlap concentration, the polymer chains are isolated. The blob contains the whole chain and therefore $\xi = R_g$. Moreover, the negative exponent on c in Equation (4.28) shows that the blobs decrease with increasing the concentration and as the c exceeds its overlap concentration, ξ, approaches a straight line with a slope of -0.75. From the scaling theory, it has been shown that the blob size is closely related to the static correlation length ξ. Experimentally, ξ can be directly obtained from the angular dependence of the scattering intensity in static laser light scattering (LLS), small-angle neutron scattering (SANS), or small-angle X-ray scattering (SAXS).

4.4.3. Light Scattering From a Polymer Solution of Small Particles

Particles which are much smaller than the wavelength of the incident light are called small particles. Considering a dilute polymer solution, if all the polymer molecules are stationary, the scattered light intensity at each direction will be a constant, i.e., independent of time. As described before, all the polymer molecules in solution are undergoing Brownian motion which leads to translational and rotational diffusion. This motion gives rise to fluctuations in the concentration that are scattering light with the same phase. The fluctuations in the density and, for solutions, also in the concentration are illustrated in Figure 4.6.

The density fluctuations and the concentration fluctuations give rise to fluctuations in the polarization of the solution. Assume that, the volume element δV contains many solvent molecules and a few solute molecule with a specified concentration, c. Since the polymer molecules are randomly distributed and diffusing throughout the various volume elements, a fluctuation of concentration, δc, can occur around the average value, $\langle c \rangle$. The local variations in the total solution concentration can be written as; $c = \langle c \rangle + \delta c$.

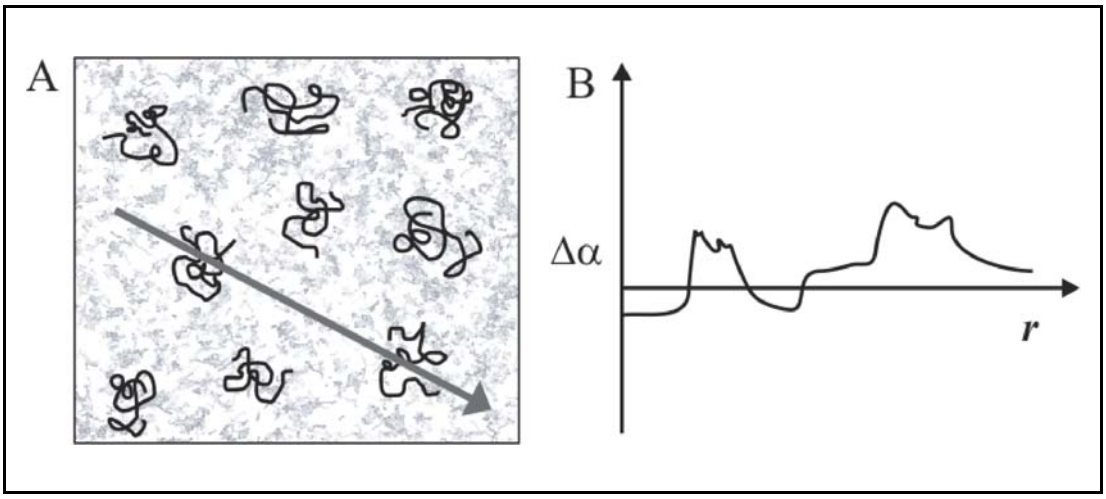

Figure 4.6: (A) Spatial variations of the local solvent density and the polymer concentration lead to fluctuation in the excess polarizability. The plot in (B) shows $\Delta\alpha$ along the gray line in (A).

The fluctuation in concentration leads to a fluctuation in the polarizability, $\delta\alpha$. The magnitude of the fluctuations in local polarizability can be expressed in terms of temperature, pressure and solute concentration:

$$\delta\alpha = \left(\frac{\partial\alpha}{\partial P}\right)_{T,C} \delta P + \left(\frac{\partial\alpha}{\partial T}\right)_{P,C} \delta T + \left(\frac{\partial\alpha}{\partial c}\right)_{T,P} \delta c \tag{4.29}$$

The first two terms on the right hand side of the latter expression are normally neglected. These terms are responsible for the density fluctuations of the solvent and Equation (4.29) becomes;

$$\delta\alpha = \left(\frac{\partial\alpha}{\partial c}\right)_{T,P} \delta c \tag{4.30}$$

and shows that the fluctuation in the concentration leads to a fluctuation in the polarizability. According to Equation (4.14), the relationship between α and $\tilde{n}$ is expressed as:

$$\Delta\alpha = \frac{\tilde{n}}{2\pi}\left(\frac{\partial\tilde{n}}{\partial c}\right)_{T,P} \Delta c \qquad \text{or} \qquad \left\langle(\Delta\alpha)^2\right\rangle = \frac{\tilde{n}^2}{4\pi^2}\left(\frac{\partial\tilde{n}}{\partial c}\right)_{T,P}^2 \left\langle(\Delta c)^2\right\rangle \tag{4.31}$$

Substitution of Equation (4.31) into Equation (4.10) provides the expression which describes the light scattered from any one volume element:

$$R_\theta = \frac{16\pi^4 \delta V \left\langle (\Delta\alpha)^2 \right\rangle}{\lambda_0^{\,4}} \tag{4.32}$$

If the solution is dilute, the density fluctuations are essentially identical to those existing in the pure solvent. Hence, the excess scattering intensity from the solution compared to the solvent arises only from the concentration fluctuation, and the excess Rayleigh ratio can be expressed as:

$$\Delta R_{\theta,E} = R_{\theta,SOLUTION} - R_{\theta,SOLVENT} = \frac{4\pi^2 \tilde{n}^2 \delta V \left(\partial \tilde{n}/\partial c\right)_{T,P}^{\,2}}{\lambda_0^{\,4}} \left\langle (\Delta c)^2 \right\rangle \tag{4.33}$$

At this point, the fluctuation theory is used to evaluate the magnitude of the concentration fluctuation. $\left\langle (\Delta c)^2 \right\rangle$ is the average value for a single volume element, or equivalently, the instantaneous value for large number of volume elements. For constant temperature and pressure, the probability of a thermodynamic variable fluctuating from its mean value is related through the Boltzman equation to the Gibb's free energy, ΔG expanded in bringing about the fluctuation.

Since the fluctuations are small in magnitude, ΔG can be expanded in a Taylor series about Δc:

$$\Delta G = \left(\frac{\partial G}{\partial c}\right)_{T,P} \Delta c + \frac{1}{2!}\left(\frac{\partial^2 G}{\partial c^2}\right)_{T,P} (\Delta c)^2 + \ldots = \frac{1}{2!}\left(\frac{\partial^2 G}{\partial c^2}\right)_{T,P} (\Delta c)^2 \tag{4.34}$$

The first term goes to zero in a closed system and the higher order terms of Δc^3 are negligible since c is small. In order to obtain a relationship for $\left\langle \Delta c^2 \right\rangle$, the fluctuation in concentration can be found by evaluating the following:

$$\left\langle \Delta c^2 \right\rangle = \frac{\int_0^\infty \left(\Delta c^2\right) \exp\left[-\left(\partial^2 G/\partial c^2\right)_{T,P}\left(\Delta c^2\right)/2kT\right] dc}{\int_0^\infty \exp\left[-\left(\partial^2 G/\partial c^2\right)_{T,P}\left(\Delta c^2\right)/2kT\right] dc} = \frac{kT}{\left(\partial^2 G/\partial c^2\right)_{T,P}} \tag{4.35}$$

All that remains is to calculate $\left(\partial^2 G/\partial c^2\right)_{T,P}$, which can be accomplished through standart thermodynamic relations. By definition the size of a volume element must be δV, and therefore $\delta n_1 \bar{V}_1 + \delta n_2 \bar{V}_2$ must equal δV, where δn_1 and δn_2 are the number of moles of solvent and solute. $\bar{V}_1$ and $\bar{V}_2$ are the partial molar volumes of the solvent and the solute, respectively. Recalling the relation that $dG = \mu_1 dn_1 + \mu_2 dn_2$, where μ is the respective chemical potential, and applying the above constraint gives,

$$\left(\frac{\partial^2 G}{\partial c^2}\right)_{T,P} = \frac{\delta V}{M}\left[\frac{\partial \mu_2}{\partial c} - \frac{\bar{V}_2}{\bar{V}_1}\frac{\partial \mu_1}{\partial c}\right] \tag{4.36}$$

where M is the molecular weight. Using the Gibbs-Duhem equation, $n_1 d\mu_1 + n_2 d\mu_2 = 0$:

$$\left(\frac{\partial^2 G}{\partial c^2}\right)_{T,P} = -\frac{\delta V}{M}\left(\frac{n_1 \bar{V}_1 + n_2 \bar{V}_2}{n_2 \bar{V}_1}\right)\left(\frac{\partial \mu_1}{\partial c}\right)_{T,P} = -\frac{\delta V}{c\bar{V}_1}\left(\frac{\partial \mu_1}{\partial c}\right)_{T,P} \tag{4.37}$$

Evaluation of the partial derivative in Equation (4.37) requires an examination of the chemical potential for a solvent in solution. The resulting expression for $\left(\partial \mu_1/\partial c\right)_{T,P}$ arises from another valuable experimental method, namely the osmotic pressure which is the pressure that polymers exert on the solution:

$$\left(\frac{\partial \mu_1}{\partial c}\right)_{T,P} = -\bar{V}_1\left(\frac{\partial \pi}{\partial c}\right)_{T,P} \tag{4.38}$$

and substituting into Equation (4.37),

$$\left(\frac{\partial^2 G}{\partial c^2}\right)_{T,P} = \frac{\delta V}{c}\left(\frac{\partial \pi}{\partial c}\right)_{T,P} \tag{4.39}$$

Hence, Equation (4.35) becomes:

$$\left\langle \Delta c^2 \right\rangle = \frac{kT}{\frac{\delta V}{c}\left(\frac{\partial \pi}{\partial c}\right)_{T,P}} = \frac{RT}{N_A \frac{\delta V}{c}\left(\frac{\partial \pi}{\partial c}\right)_{T,P}} \tag{4.40}$$

and substitution Equation (4.40) into Equation (4.33) leads to:

$$\Delta R_{\theta,E} = \frac{4\pi^2 \tilde{n}^2 \left(\partial \tilde{n}/\partial c\right)_{T,P}^{\ 2}}{N_A \lambda_0^{\ 4}} \frac{RTc}{\left(\frac{\partial \pi}{\partial c}\right)_{T,P}} \tag{4.41}$$

Rearranging Equation (4.41) by defining the optical constant $K = \frac{4\pi^2 \tilde{n}^2 \left(\partial \tilde{n}/\partial c\right)_{T,P}^{\ 2}}{N_A \lambda_0^{\ 4}}$ yields:

$$\frac{Kc}{\Delta R_\theta} = \frac{1}{RT}\left(\frac{\partial \pi}{\partial c}\right)_{T,P} \tag{4.42}$$

where the footnote "excess" in $\Delta R_{\theta,E}$ is omitted. For unpolarized incident light, the optical constant K is given by $K = \frac{2\pi \tilde{n} \left(\partial \tilde{n}/\partial c\right)_{T,P}^{\ 2}}{N_A \lambda_0^{\ 4}}$. In dilute polymer solutions, the change of osmotic pressure induced by the change in concentration can be written as:

$$\left(\frac{\partial \pi}{\partial c}\right)_{T,P} = \frac{RT}{M_w}\left(1 + A_2 c + A_3 c^2 + \ldots\right) \tag{4.43}$$

where A_2 and A_3 are the second and third osmotic virial coefficients and M_w is the weight-average molecular weight and Equation (4.42) becomes:

$$\frac{Kc}{\Delta R_\theta} = \frac{1}{M_w}\left(1 + 2A_2c + 3A_3c^2 + ...\right) \tag{4.44}$$

This is the general equation for Rayleigh scattering of vertically polarized light from a polymer solution of particles which are smaller than the wavelength of the light. In very dilute solutions, the virial coefficients from the third one A_3 onwards can be neglected. In this way, the above equation allows us to obtain easily the weight-average molecular weight of the solute and the second-order virial coefficient (A_2).

4.4.4. Light Scattering From a Polymer Solution of Larger Particles

In the previous section, Equation (4.44) was derived which is applicable only when the macromolecular size, d, is small compare to the wavelength of the incident light ($d << \lambda/20$). In this section, the light scattering by larger particles will be considered. When the size of the particle becomes larger than $\lambda / 20$, light scattered from different points of the particle will interfere at the detector. The light scattered at $\theta = 0$ has no interference and follows the same equations as light scattered from small particles ($d << \lambda/20$). However, as the angle of observation increases and therefore the magnitude of the scattered light decreases. In order to represent this decrease in the scattered light, the particle scattering function is defined as: $P(\theta) = R_\theta / R_0$, where R_θ is the scattered intensity at scattering angle, θ and R_0 is the scattered intensity at zero angle where no destructive interference is presence.

Figure 4.7 illustrates the scattering of light from a large particle. At detector number 2 (D_2), which corresponds to a scattering angle θ_2, the path length along O-P_1-D_2 is shorter than that along O-P_2 -D_2. The two scattered waves are considered to be out of phase. At the smaller scattering angle, θ_1, this difference in path length along O-P_1-D_1 and O-P_2 – D_1 is less. Hence, the waves are closer in phase but still slightly different. Finally, at a scattering angle of 0˚, assuming that the scattered light could be separated from the

incident light, the path length along O-P_1-D_0 and along O-P_2 –D_0 will be equal and no destructive interference will occur.

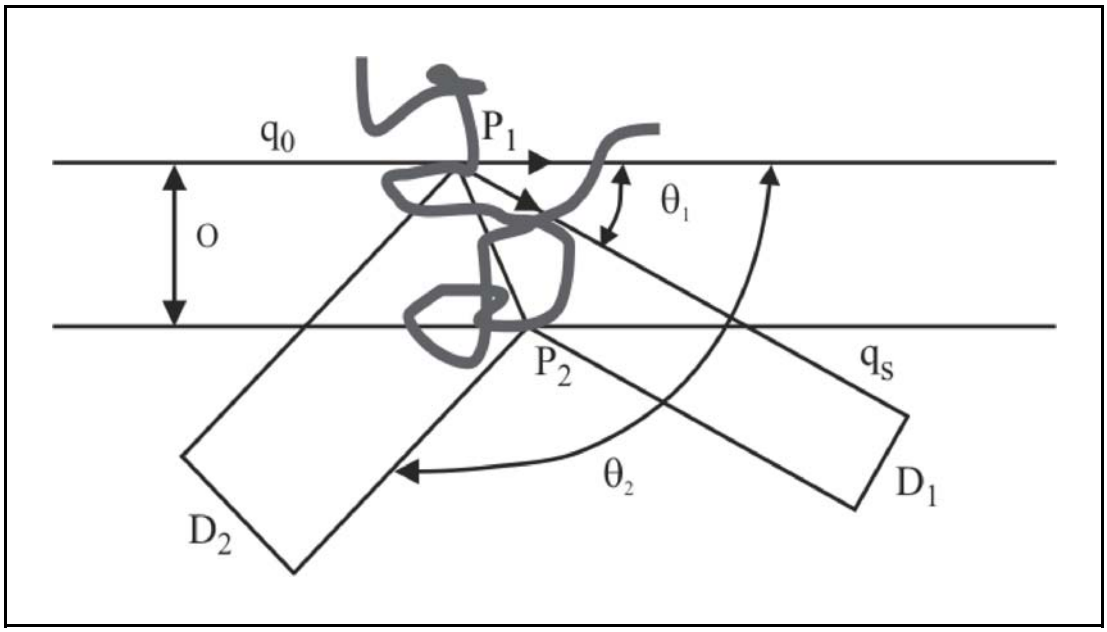

Figure 4.7: Schematic representation of the light scattering from a large particle.

The general relation between the particle scattering function P(θ) and particle configuration is given by Tanford and Flory [73,74]:

$$\frac{1}{P(\theta)} = 1 + \frac{16\pi^2 n^2}{3\lambda^2}\left(R_g{}^2\right)\sin^2\frac{\theta}{2} \tag{4.45}$$

Zimm was the first to propose that Equation (4.45) could be incorporated into the Equation (4.44) and the expression for the scattering intensity for vertically polarized light as a function of concentration and observation angle is obtained as;

$$\frac{Kc}{\Delta R_\theta} = \frac{1}{M_w P(\theta)} + 2A_2 c + \ldots = \frac{1}{M_w}\left(1 + \frac{16\pi^2 n^2}{3\lambda^2} R_g{}^2 \sin^2\frac{\theta}{2}\right) + 2A_2 c + \ldots \tag{4.46}$$

which is in the form of a grid plot[64]. The values of $Kc/\Delta R_\theta$, are plotted against the expression $\sin^2 \theta/2 + kc$ where k is a numerical constant chosen to provide a convenient

separation of the data points. Then, the $Kc/\Delta R_\theta$ values are extrapolated to the zero limits of both solute concentration and $\sin^2 \theta/2$. For the former extrapolation, Equation (4.46) becomes:

$$\left.\frac{Kc}{\Delta R_\theta}\right|_{C=0} = \frac{1}{M_w}\left(1+\frac{16\pi^2 n^2}{3\lambda^2} R_g{}^2 \sin^2\frac{\theta}{2}\right) \tag{4.47}$$

Therefore, a plot of the $Kc/\Delta R_\theta$ values against $\sin^2 \theta/2$ yields the inverse of the weight average molecular weight as the intercept and the radius of gyration from the slope. In a similar manner, for data extrapolated to an angle of 0˚, Equation (4.44) is recovered as;

$$\left.\frac{Kc}{\Delta R_\theta}\right|_{\theta=0} = \frac{1}{M_w} + 2A_2 c \tag{4.48}$$

4.5. Light Scattering From Polymer Gels

4.5.1. The Spatial Inhomogeneity in Polymer Gels

Polymer gels have unique structural inhomogeneities in the microscopic point of view. The origins of the inhomogeneity can be different depending on the crosslinking mechanisms and the phase separation behavior during the network formation. Random crosslinking, such as rubber vulcanization, radiation crosslinking of polymers, or chemical gel synthesis through multi-functional monomers result in inhomogeneous crosslink distribution in the networks.

Although there has been some diversity in defining the inhomogeneity and the heterogeneity in gels, the inhomogeneity usually means the fluctuations of the crosslink density in space whereas the heterogeneity indicates the existence of phase separated domains in polymer gels. The inhomogeneities and the heterogeneities are usual features of the polymer networks produced by free-radical polymerization reactions. Because of the Brownian motion, the concentration of a pre-crosslinked polymer (or monomer) solution randomly fluctuates in space. An introduction of crosslinks to the polymer

solution instantaneously quenches the concentration fluctuations to some extent and therefore, the final polymer networks contain an inhomogeneous distribution of crosslinkers, known as the spatial gel inhomogeneity [75,76]. This is due to the fact that the formation of a network chain by free-radical mechanism takes place within a short period of time (usually less than one second) compared to the relatively long relaxation times of the network chains. Thus, the concentration fluctuations are "frozen" in the final network. These concentration fluctuations can scatter light and reduce the transmission of visible light through the gel.

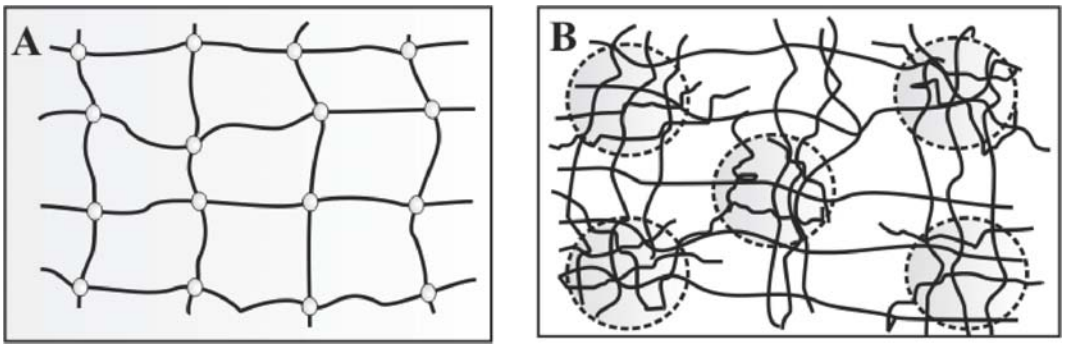

Figure 4.8: Schematic representation of an ideal gel (A) and an inhomogeneously crosslinked gel (B).

Figure 4.8 shows schematic representation of an ideal gel and an inhomogeneously crosslinked gel. In ideal gels, the length of the network chains between the crosslinks is constant and all the crosslinker molecules are consumed by effective crosslinking reactions. However, the real gels exhibit a wide distribution of chain lengths between the network junction points. In gels formed by free radical mechanism, a significant fraction of the crosslinker molecules is consumed by the cyclization and multiple crosslinking reactions. In contrast to the ideal gels with a homogeneous distribution of crosslinks, real gels exhibit an inhomogeneous crosslink density distribution, known as the spatial gel inhomogeneity[75,76].

Since the structural inhomogeneity results in a dramatic reduction in the strength of the crosslinked networks, the spatial inhomogeneity in the final materials is undesirable for applications. Therefore reducing and controlling the spatial inhomogeneities in gels is not only theoretically important, but also technologically and practically significant:

a) The mechanical properties of polymers can be adjusted by changing the crosslink density distribution or cluster sizes. The inhomogeneities in crosslink density of the networks affect orientation of chains. Increase in dispersion of the crosslink distribution causes higher percentage of chains to orient and reach their finite extensibilities, and the ultimate properties of the networks are thus increased.

b) The impact strength of coatings can be improved by adding high crosslink density reactive microgels, and the separation resolution and the efficiency of electrophoresis depend on the mesh size distribution of gels.

c) The contact lenses require low heterogeneity to reduce scattering related haze.

The presence of the spatial inhomogeneities is widely investigated through a number of modern analytical techniques such as small angle neutron scattering (SANS), small angle X-ray scattering (SAXS), nuclear magnetic resonance (NMR), dynamic light scattering (DLS) and static light scattering (SLS)[75-80].

The early research on inhomogeneity can be traced to Stein and Bueche[77,78]. They used light scattering technique to characterize inhomogeneity in the polymer networks and proposed that the inhomogeneity of the network is due to the local fluctuation in the molecular weight of chains between the crosslink junctions. Then, the static light scattering method was also used to measure the correlation size using the Debye equation [79,80]. It was found that the correlation size is related to inhomogeneity in the crosslink distribution and entanglements.

Then, dynamic light scattering and the speckle method were used to study a nonergodic solidlike medium, such as polymer gels. One obvious characteristic of the nonergodicity is the appearance of speckles; namely, the scattered intensity depends on the sample position. The speckle intensity, or the scattering intensity, is recorded as a function of the position in the sample where the laser is reflected. Higher speckle intensity is always related to more inhomogeneity in the sample [75]. The inhomogeneities of the polymer networks were also observed with neutron scattering techniques [76]. Bastide proposed “frozen blob” structures in the networks to explain the “butterfly” pattern. The network system was decribed as a random distribution of crosslinks on a lattice formed by the

interchain contact points in the solution. When two junctions were located on neighboring lattice sites, a “frozen blob” was formed.

4.5.2. Factors Affecting Spatial Gel Inhomogeneity

The existence of the spatial inhomogeneity at submicrometer scales in the hydrogels is mainly a result of the gel formation mechanism by free-radical crosslinking copolymerization of a monovinyl monomer (monomer) with a divinyl monomer (crosslinker). The most important factors for the formation of an inhomogeneous network structure can be described as follows:

i. The differences in reactivities of the monomer and the crosslinker: The different reactivities of the functional groups lead to different morphologies of the networks. The reactivity ratios of the crosslinker (divinyl) molecules are usually larger than the monomer (vinyl) molecules. In free-radical copolymerization, the crosslinker reactivity is at least twice the monomer reactivity due to the existence of two vinyl groups on each crosslinker molecule. For example, the reactivity ratios of Acrylamide and N,N’-methylenebisacrylamide monomers are 0.57 and 3.4, respectively[81]. Thus, in copolymerization, the growing chains in the pregel stage are rich in crosslinker units because of the higher reactivity of the crosslinker molecules. As a consequence of this unequal vinyl group reactivity, the crosslink density of gels fluctuates. The computer simulations made by Schröder and coworkers also showed that there is an influence of the crosslinker reactivity on the extent of the concentration fluctuations in gels[82].

ii. The cyclization, crosslinking and multiple crosslinking reactions: A schematic representation of the polymer network structures with cyclization, crosslinking, and multiple crosslinking reactions is shown in Figure 4.9. During the free-radical crosslinking copolymerization, the cyclization reactions occur when the macroradical attacks the pendant vinyl groups in the same kinetic chain. The cyclization reactions, which predominate in the early stage of polymerization, increase as the dilution increases or as the crosslinker concentration increases. The results showed that a significant fraction of the crosslinker molecules is consumed by the cyclization reactions during the gel formation process. The cycles formed due to the cyclization are elastically ineffective intramolecular links and therefore, they reduce the effective crosslink density

of gels[83-87]. The multiple crosslinks are formed when a pendant double bond reacts with a radical on a chain in which it is already crosslinked. The average number of the multiple crosslinks is zero at zero monomer conversion and it increases as the reaction proceeds because multiple crosslinking becomes the more probable the greater the molecules formed[83]. The multiple crosslinking reactions form highly crosslinked regions of the polymer networks. These elastically effective regions, where the multiple crosslinks form, have a higher density then do others so that they increase the local crosslink density of gels.

iii. The initial monomer concentration: There are two antagonistic effects of the initial monomer concentration on the spatial gel inhomogeneity. As the monomer concentration is increased, the effective density of the crosslinks increases, so that the spatial inhomogeneity becomes larger. Opposing this, increasing monomer concentration, i.e., decreasing the degree of swelling of gels after preparation reduces progressively the concentration difference between the densely and loosely crosslinked regions of the gel, so that the apparent inhomogeneity decreases. The interplay of these two opposite effects determines the inhomogeneity in gels and results in the appearance of a maximum gel inhomogeneity at a critical monomer concentration[88-89].

iv. The crosslink density: Increasing crosslink density will increase the degree of spatial inhomogeneity in gels. This phenomenon can be explained with the multiple crosslinking reactions leading to the formation of highly crosslinked regions in the final hydrogel.

v. Ionic group content: Presence of mobile ions in gels is also responsible for the homogenization of gels. The extent of the gel inhomogeneity decreases drastically with increasing charge density[90].

vi. The chain transfer agent and the primary chain length: The extent of the inhomogeneity in gels is strongly reduced by the addition of a chain transfer agent in the gel formation system. This phenomenon can be explained with decreasing primary chain length on rising chain transfer agent concentrations, which reduces the extent of the multiple crosslinking reactions and thus leads to a more homogeneous distribution of the crosslink points along the gel sample[91].

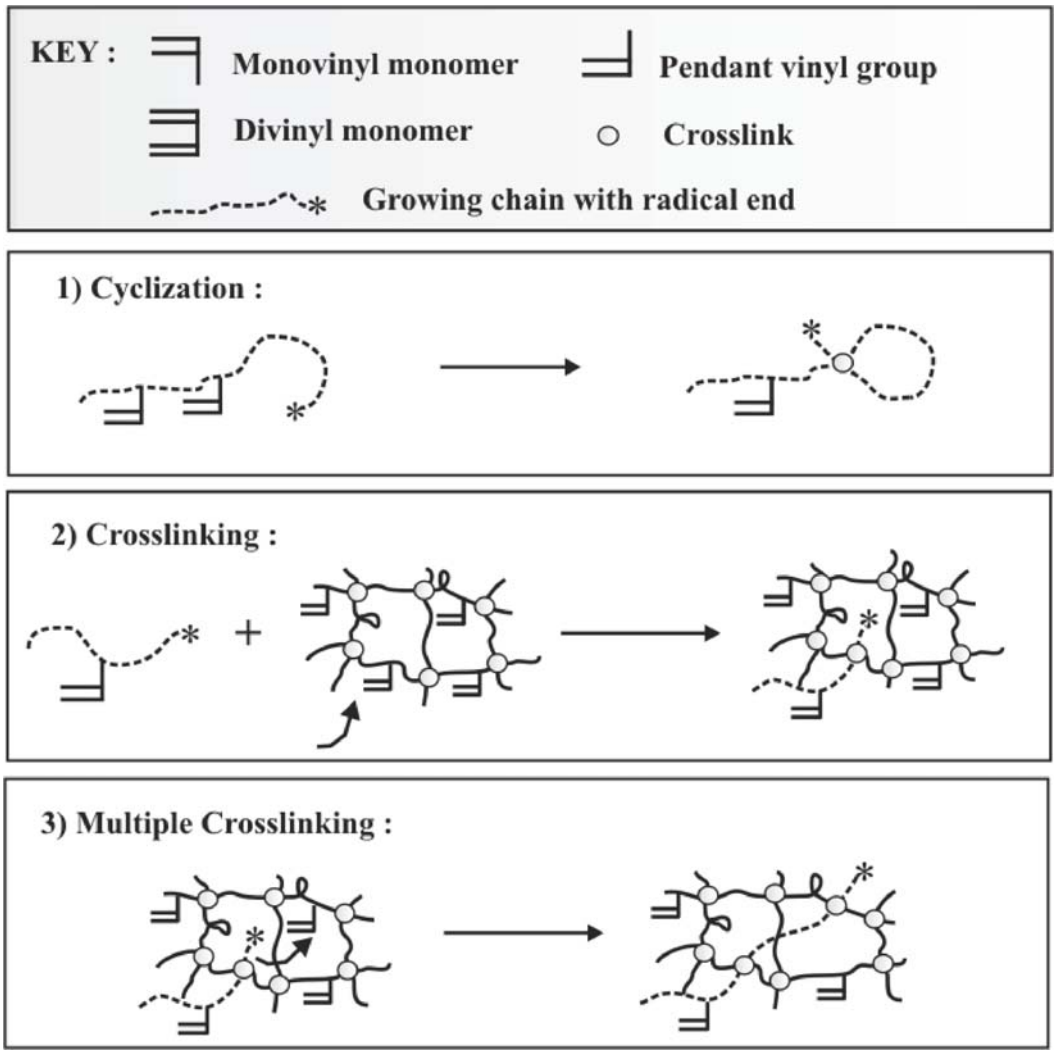

Figure 4.9: Schematic representation of cyclization, crosslinking, and multiple crosslinking reactions in free-radical crosslinking copolymerization of a monovinyl monomer with a divinyl monomer.

vii. The solvent quality: The solvating power of the solvent used in the gel formation process also affects the spatial inhomogeneity. Decreasing solvent quality increases the spatial inhomogeneity in gels. If the polymer–solvent interaction is good during crosslinking, a pendant vinyl group will be found more difficult by radicals due to the thermodynamic excluded volume effect. Thus, the presence of larger coils in the polymerization system will reduce the crosslinking and multiple crosslinking reactions. If the solvent–polymer interactions are poor, the chains will coil more rather then stretch out, and the probability of the crosslinking and multiple crosslinking is greater due to increased proximity of the pendant double bonds. As a result, a decrease in the solvent

quality during the gel formation increases both the elastic modulus and the spatial inhomogeneity of gels[91,92].

4.5.3. Debye-Bueche Theory and Scattering From Polymer Gels

For the polymer solutions in the semi-dilute regime, the scattering light intensity is given by a Lorentzian equation (or Ornstein-Zernike equation)[70,75,76,78,93-97]:

$$I(q) = \frac{I(0)}{\left(1+\xi^2 q^2\right)} \tag{4.49}$$

where I(q) is the intensity of the scattered light at the scattering vector q, I(0) is a constant and equals to I(q=0). For polymer gels, Geissler tried to separate the scattering intensity function into two contributions, i.e., the solution-like and the solid-like concentration fluctuations[98]. The solution-like concentration fluctuation was assumed to be the same as the corresponding polymer solution and is of the form of Equation (4.49). The solid-like concentration fluctuation was assumed having the form of $\exp\left[-\Xi^2 q^2\right]$. Thus the total scattering function for polymer gels is given by:

$$I(q) = I_{Solid}(0)\exp\left(-\Xi^2 q^2\right) + \frac{I_{Solution}(0)}{\left(1+\xi^2 q^2\right)} \tag{4.50}$$

where Ξ is the mean size of solid-like (static) nonuniformity or the mean size of the static concentration fluctuations. According to Equation (4.50), the scattered light intensity from gels consists of two terms, one from dynamic fluctuations and the other from frozen concentration fluctuations due to the spatial gel inhomogeneity. Similar to Equation (4.50), the total scattering intensity from gels, $R_{gel}(q)$, can be defined by the sum of the scattered intensity from a corresponding semi-dilute polymer solution, $R_{sol}(q)$, and that of the excess scattering, $R_{ex}(q)$ [76,99-100]:

$$R_{gel}(q) = R_{sol}(q) + R_{ex}(q) \tag{4.51}$$

The Rayleigh ratio $R_{gel}(q)$ in Equation (4.51) relates to the scattered light intensity (I_s) through the Equation (4.10). $R_{sol}(q)$ is reflecting the thermal fluctuations. The gel inhomogeneity is often characterized by the excess scattering $R_{ex}(q)$ from a gel sample which depends on the fluctuations of the refractive index in the sample and on the sizes of regions over which these fluctuations occur. Suitable parameters for characterizing the network inhomogeneities are the mean square fluctuations of refractive index, $\langle \eta^2 \rangle$ and the correlation length, ξ, over which these fluctuations occur. The excess scattering $R_{ex}(q)$ was expressed by Debye-Bueche as follows:

$$R_{ex}(q) = 4\pi K_{DB} < \eta^2 > \int_0^{\infty} \gamma(r) \left(\frac{\sin(qr)}{qr} \right) r^2 dr \tag{4.52}$$

where K_{DB} is the optical constant, $K_{DB} = 8\pi^2 n_0^{\,2} \lambda_0^{-4}$, $\langle \eta^2 \rangle$ is the amplitude of the fluctuation and $\gamma(r)$ is the correlation function of the fluctuation which is a number varying with the distance r. The correlation function $\gamma(r)$ which is a measure of the size of the region containing heterogeneity can be obtained from the inverse Fourier transformation of $R_{ex}(q)$, and for many systems is found to be approximated by an empirical exponential function. $\gamma(r)$ is given by [101]:

$$\gamma(r) = \exp[-r/\xi] \tag{4.53}$$

where the correlation length ξ gives a measure of the extension of the spatial inhomogeneities. The larger ξ, the larger are the extension of the inhomogeneities. Substitution of Equation (4.53) into Equation (4.52) yields:

$$R_{ex}(q) = 4\pi K_{DB} < \eta^2 > \int_0^{\infty} e^{(-r/\xi)} \left(\frac{\sin(qr)}{qr} \right) r^2 dr \tag{4.54}$$

Integrating this equation between $r = 0$ and $r = \infty$, gives:

$$R_{ex}(q) = \frac{4\pi K_{DB}\xi^3 < \eta^2 >}{(1+q^2\xi^2)^2} \tag{4.55}$$

which is known as Debye-Bueche Equation and contains very important parameters of gels[94]:

1. The correlation length of the scatterer (ξ): The size of highly crosslinked region or dense region and is a measure of the extension of the inhomogeneities.

2. The mean square fluctuation of the refractive index $\langle \eta^2 \rangle$: The mean square refractive index fluctuations $\langle \eta^2 \rangle$ relate to the concentration fluctuations in gels arising from the crosslink density fluctuations $(\Delta M_c^{\,2})$.

According to the Debye-Bueche analysis, when the inverse square of the excess scattering $(R_{ex}(q))^{-1/2}$ is plotted against q^2, a straight light is obtained as illustrated in Figure 4.10. The slope and the intercept of the plot of $R_{ex}(q)^{-1/2}$ vs q^2 (Debye-Bueche plot) gives the mean square fluctuation of the refractive index, $\langle \eta^2 \rangle$ and the correlation length, ξ according to the relation:

$$(R_{ex}(q))^{-\frac{1}{2}} = \left(2\sqrt{\pi K_{DB}\xi^3 \langle \eta^2 \rangle}\right)^{-1} + \frac{1}{2}\sqrt{\frac{\xi}{\pi K_{DB}\langle \eta^2 \rangle}}\; q^2 \tag{4.56}$$

From the slope denoted by (a) and the intercept denoted by (b) of the Debye –Bueche plot, ξ and $\langle \eta^2 \rangle$ values are calculated as:

$$\xi = \sqrt{\frac{a}{b}} \qquad \text{and} \qquad \langle \eta^2 \rangle = \left(4\pi K a^{1.5} b^{0.5}\right)^{-1} \tag{4.57}$$

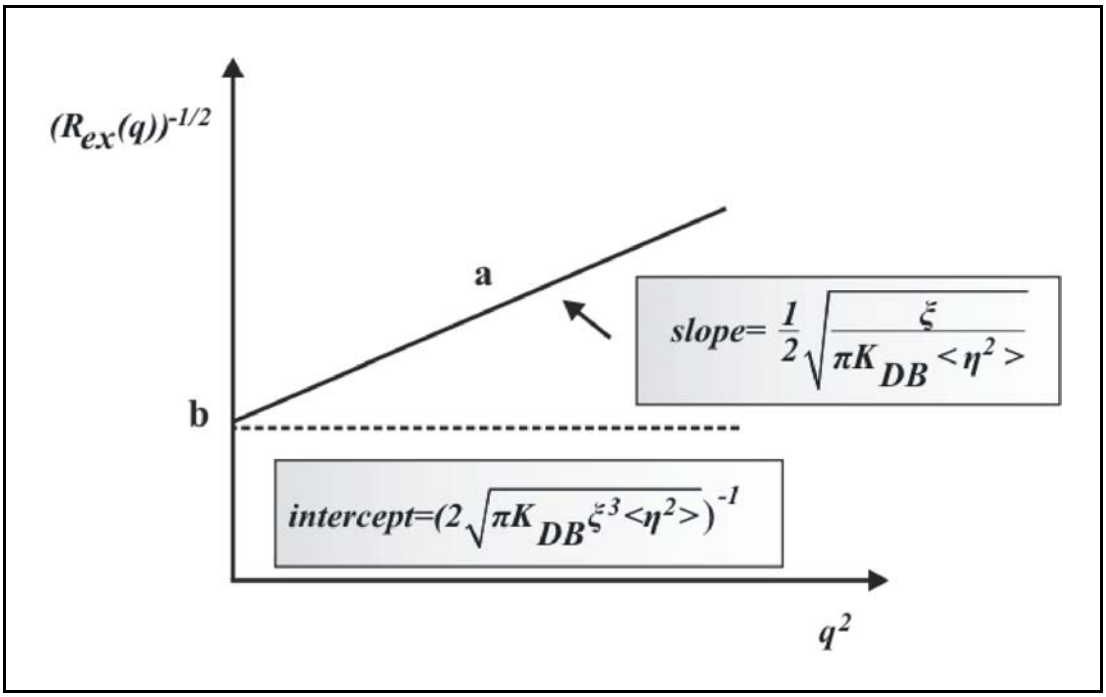

Figure 4.10: Schematic representation of the Debye-Bueche plot.

For the relationship between $\langle \eta^2 \rangle$ and $(\Delta M_c{}^2)$, a functional form can be derived[101]. The refractive index of gels, n, can be defined as follows:

$$n = n_0 + (n_1 - n_0)\nu_2 \tag{4.58}$$

where n_0 and n_1 are the refractive indices of the solvent and the polymer, respectively. Consider that two different regions in the gel sample are denoted by A and B. The refractive indices of these regions can be written as:

$$(n)_A = n_0 + (n_1 - n_0)(\nu_2)_A \quad \text{and} \quad (n)_B = n_0 + (n_1 - n_0)(\nu_2)_B \tag{4.59}$$

where $(\nu_2)_A$ and $(\nu_2)_B$ are the polymer concentrations in these regions. The refractive index difference between the regions A and B can be calculated from Equation (4.59) as follows:

$$\Delta n = (n_A) - (n_B) = (n_1 - n_0)\Delta\nu_2 \tag{4.60}$$

in which $\Delta\nu_2$ is the difference of the polymer concentration between the regions A and B. Since, there is infinite number of regions in the gels with different refractive indices, the mean square refractive index fluctuations, $\langle \eta^2 \rangle$ of the Debye-Bueche theory is equal to:

$$\langle \eta^2 \rangle \cong \langle \Delta n^2 \rangle = (n_1 - n_0)^2 \langle \Delta\nu_2 \rangle^2 \tag{4.61}$$

On the other hand, for high degrees of swelling, the Flory-Rehner Equation (2.59) can be written as:

$$\nu_2 = \left(\frac{\rho V_1 \nu_2^{0\,2/3}}{\bar{M}_c (0.5 - \chi)} \right)^{3/5} \tag{4.62}$$

Taking the derivative of ν_2 with respect to ($\overline{M_c}$), gives;

$$\frac{d\nu_2}{d\overline{M_c}} = \frac{-3}{5}\frac{dv_2}{M_c} \qquad \text{or} \qquad \Delta\nu_2 = \frac{(3/5)\nu_2}{\bar{M}_c}\Delta M_c \tag{4.63}$$

Combining Equations (4.61) and (4.63) leads to:

$$\langle \eta^2 \rangle \cong \frac{9}{25}(n_1 - n_0)^2 \nu_2{}^2 \frac{\Delta M_c{}^2}{\bar{M}_c{}^2} \tag{4.64}$$

According to the Equation (4.64), $\langle \eta^2 \rangle$ parameter of the Debye-Bueche theory is directly related to the square of the fluctuation of the crosslink density, ($\Delta M_c{}^2$), that is, to the gel inhomogeneity. Substitution of Equation (4.64) into Equation (4.54) yields:

$$R_{ex}(q) = \left(\frac{9}{25}\right) \frac{\left(n_1 - n_0\right)^2 {\nu_2}^2 \Delta {M_c}^2}{\bar{M}_c^{\,2}} \frac{4\pi K_{DB} \xi^3}{(1+q^2\xi^2)^2} \tag{4.65}$$

Equation (4.65) indicates that the excess scattering $R_{ex}(q)$ is related to the degree of inhomogeneity as well as the volume fraction of the network and the refractive index difference between the solvent and the polymer network.

5. EXPERIMENTAL

5.1. Materials

The materials used in the preparation of the hydrogels and the linear polymers are described in this section.

N,N-dimethylacrylamide (DMAAm, Fluka): It was used as a monomer in the polymerization reactions. Its molecular weight is 99.13 g/mol and it was stabilized with 0.05 % hdyroquinone monomethyl ether. It has a boiling point of 81ºC and density of 0.962 g/ml.

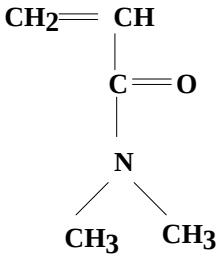

DMAAm

Acrylamide (AAm, Fluka): It was also used as a monomer in the polymerization reactions. It was used after recrystallization in acetone-ethanol mixture. It has a melting point of 84-85 ºC. Its molecular weight is 71.08 g/mol.

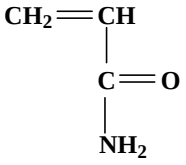

AAm

N,N'-methylenebisacrylamide (BAAm, Fluka): It was used as the crosslinking agent in the polymerization reactions and used as received. It has a melting point greater than 300 ºC. Its molecular weight is 154.17 g/mol.

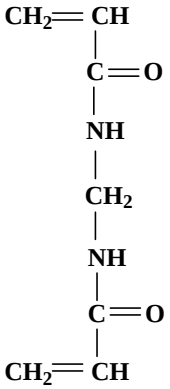

BAAm

2-acrylamido-2-methylpropane sulfonic acid (AMPS-H^+, Merck): Sodium salt of AMPS-H^+ denoted by AMPS was used as the ionic comonomer. Its molecular weight is 207 g/mol. AMPS stock solution was prepared by dissolving 20 g of AMPS-H^+ in about 40 ml of distilled water and adding to this solution 10 ml of a 30 % NaOH solution under cooling. Then the solution was titrated with 1 M NaOH to pH 7.00 and finally, the volume of the solution was made up to 100 ml with distilled water. 1 ml of AMPS stock solution thus prepared contained 0.9666 mmol AMPS.

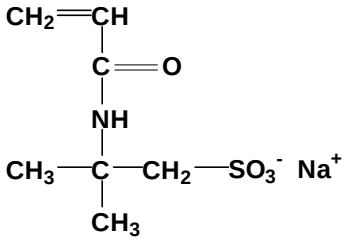

AMPS-Na

Ammonium persulfate ($(NH_4)_2S_2O_8$, APS, Merck): It was used as an initiator in the polymerization reactions and used as received. Its molecular weight is 228.20 g/mol. It has a melting point of 120 ºC.

N,N,N',N'- tetramethylethylenediamine (TEMED, Carlo Erba): It was used as an accelerator in the polymerization reactions and used as received. It has a boiling point of 120-122 ºC. Its molecular weight is 116.21 g/mol.

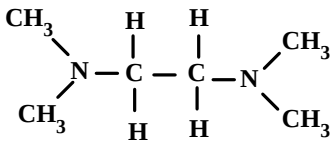

TEMED

Sodium metabisulfite ($Na_2S_2O_5$, SPS, Merck): It was used as an accelerator in the polymerization and used as received. Its molecular weight is 190.10 g/mol.

Isopropyl alcohol (IPA, Merck) was used as a chain transfer agent in the polymerization of DMAAm and used as received. HPLC-grade water and HPLC-grade acetone were used for light scattering experiments. Distilled water was used for the synthesis of the hydrogels, as well as for the swelling experiments. Reagent-grade solvents acetone, tetrahydrofuran (THF), 1,4-dioxane (dioxane), methanol, ethanol, 1-propanol, t-butanol, and dimethylsulfoxide (DMSO) were used for the swelling experiments without further purification.

5.2. Experimental Set-up and Equipment

i. Electronic Digital Compass: The diameters of the cylindrical gel samples were measured using a calibrated digital compass (Mitutoyo). The device has a measuring range between 0-150 mm with an accuracy ± 0.02 mm.

ii. pH-meter: The compact pH meter (inoLab, pH Level 2 precision) was used to perform pH measurements.

iii. Hot Water Bath: The hot water bath (Haake, Water bath FS2) with temperature control module (Haake F 4391) was used for the synthesis of the hydrogels.

iv. Digital Thermometer: The digital thermometer (Hanna, Checktemp. Pocket Thermometer) was used in the experiments.

v. Electronic Balance: The electronic balances of Sartorius (BP221S) and Precisa (205A and XB220A) were used in the experiments. They display to four decimal places and weighting capacity is 220 g.

vi. Temperature-Sensitive Oven: The oven (Nuve, EN 400) is used for the polymerization reactions. It runs in range of 0 - 80 ^oC with a sensitivity of 0.1 ^oC.

vii. Vacuum Oven: A vacuum oven (Nuve, EV 018) is used for removal of solvents from the gel and polymer samples. There is a manometer and a digital temperature control system with a sensitivity of 1 ^oC on the oven. The temperature is manually controlled and varies from 50ºC to 250ºC. The pump to provide vacuum in the oven is from Germany.

viii. Tubes: 3.90-4.09 mm internal diameter and 10 cm long glass tubes were used in experiments. Gelation occurred in these tubes.

ix. Uniaxial Compression Apparatus: In order to measure the elastic modulus of gels, a home-made uniaxial compression apparatus was used. This apparatus consists of five parts as shown in Figure 5.8.

x. Magnetic Stirrer: AREX magnetic stirrer with a heating plate was used in the experiments. The instrument is equipped by a connection for a contact Vertex thermoregulator for the direct control of temperature from ambient to 150°C with an accuracy of 0.5°C.

xi. Light Scattering Apparatus: The light scattering measurements were carried out using a commercial multi-angle light scattering DAWN EOS (Wyatt Technologies Corporation) equipped with a vertically polarized 30 mV Gallium-arsenide laser operating at 690 mV and 18 simultaneously detected scattering angles.

xii. Light Scattering Vials: The crosslinking polymerizations were carried out in the light scattering vials (a specified type of optical glass cylinders in 27 mm internal diameter and 43 mm long).

Figure 5.1: The dust-free environment used in the preparation.

xiii. Dust-Free Environment: All glassware was kept dust-free prior to the experiments. The solutions were prepared in HPLC-grade water in a dust-free environment as shown in Figure 5.1. (TELSTAR laminar flow, 1800 m^3/h HEPA filter). Horizontal laminar flow bench allowes operation in particle free conditions

due to the continuous flushing of the work area by a unidirectional horizontal and ultrafiltered air flow, thus assuring full product protection.

xiv. Dust-Free Glovebox: The Plas-Labs, Model 818-GB Basic Glove Box was used in the experiments for isolating working area from the environment. The solutions were filtered through membrane filters (pore size =0.2 μm) directly into the light scattering vials in a dust-free glovebox which is shown in Figure 5.2.

Figure 5.2: Dust-free glovebox used in the experiments.

xv. Syringe Pump: The Model A-99 Syringe Pump (Razel Instrument) was used to introduce the solution into the refractometer at an exact reproducible flow rate from a readily available syringe.

xvi. Dilatometer: The linear polymerizations of monomers were carried out in dilatometers consisting of a blown glass bulb connected to a 30 cm length of 1.5 mm precision-bore capillary tubing.

xvii. Optilab DSP Interferometric Refractometer: The Optilab DSP (Digital Signal Processing) Refractometer is used to measure dn/dc (differential refractive index increment) values at 690 nm.

5.3. Experimental Procedure

The experimental work of this thesis consists of five parts:

1. Preparation of the hydrogels and linear polymers:
    i. Non-ionic and ionic PDMAAm hydrogels and corresponding linear polymers,
    ii. Non-ionic PAAm hydrogels and corresponding linear polymers.

2. Characterization of the hydrogels and linear polymers:
    i. Gravimetric measurements to determine the gel fraction, the polymer network concentration at the stage of gel preparation and the monomer conversion,
    ii. Gel point measurements,
    iii. Dilatometric measurements to determine the fractional monomer conversion and the polymerization rate of the monomers,
    iv. The refractive index increment measurements to determine dn/dc values of linear polymers.

3. Swelling measurements in water, in solvent mixtures and in salt solutions:
    i. Volumetric measurements to determine the equilibrium volume swelling ratio q_v, and the normalized volume of the equilibrium swollen gel V_{eq},
    ii. Gravimetric measurements to determine the equilibrium weight swelling ratio q_w, and the normalized weight swelling ratio of the hydrogels with respect to their swelling ratio in water, m_{rel}.

4. Mechanical measurements:
    The uniaxial compression measurements to determine the elastic modulus of the hydrogels both after preparation and at swelling equilibrium in water.

5. Light scattering measurements:
    i. Light scattering measurements during polymerization and gelation reactions.
    ii. Light scattering measurements of hydrogels after their preparation to determine the spatial gel inhomogeneity.

5.4. Preparation of Hydrogels

The hydrogels were prepared by free-radical crosslinking copolymerization of the monomers N,N-dimethylacrylamide (DMAAm) and acrylamide (AAm) with N,N'-methylenebisacrylamide (BAAm) as a crosslinker. 2-acrylamido-2-methylpropane sulfonic acid (AMPS) was used as the ionic comonomer. The gel synthesis parameters varied were the initial molar concentration of the monomers, denoted by C_0, the ionic comonomer concentration, the crosslinker ratio denoted by X (the mole ratio of the crosslinker BAAm to the monomer DMAAm or AAm) and the type of the redox initiator system. The polymerization reactions were carried out in glass tubes, in the light scattering vials, as well as in glass dilatometers. In Figure 5.3, the formation of hydrogels by free-radical crosslinking copolymerization of acrylamide-based monomers is schematically illustrated.

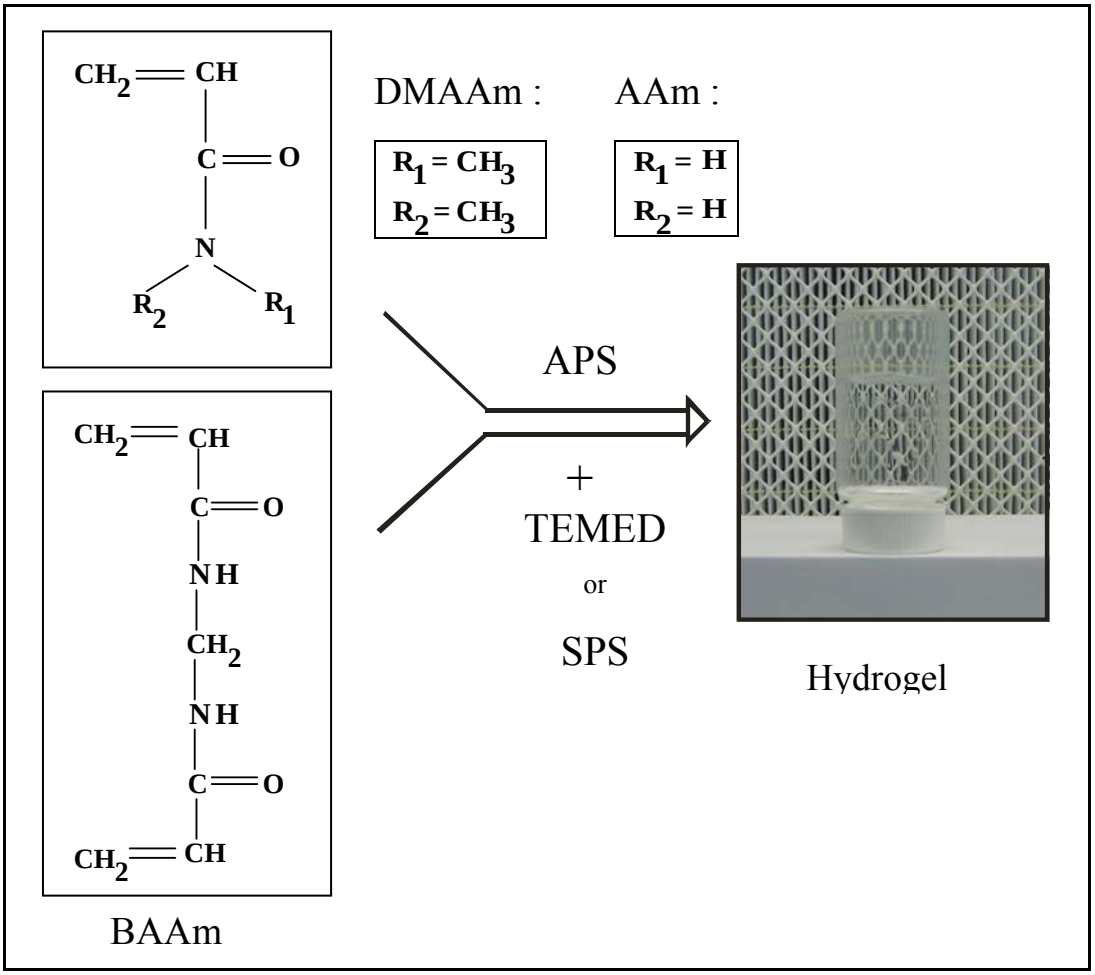

Figure 5.3: Formation of hydrogels by free-radical crosslinking copolymerization of the acrylamide derivative monomers.

Two different redox-initiator systems, namely ammonium persulfate (APS) – N,N,N',N'-tetramethylethylenediamine (TEMED) and APS – sodium metabisulfite (SPS) were used to initiate the gelation reactions:

1) APS –TEMED redox initiator system: This pair is widely used as redox initiator system in the free-radical crosslinking copolymerization (FCC). Tanaka proposed that the first step in the polymerization is a reaction between APS and TEMED in which the TEMED molecule is left with an unpaired valance electron[24]. In order to make clear whether TEMED could produce the initial free radical in the reaction with APS, Feng and coworkers used spin trapping technique and ESR spectra[102]. The following initiation mechanism of the APS/TEMED system was proposed via contact charge transfer complex and cyclic transition state (Figure 5.4).

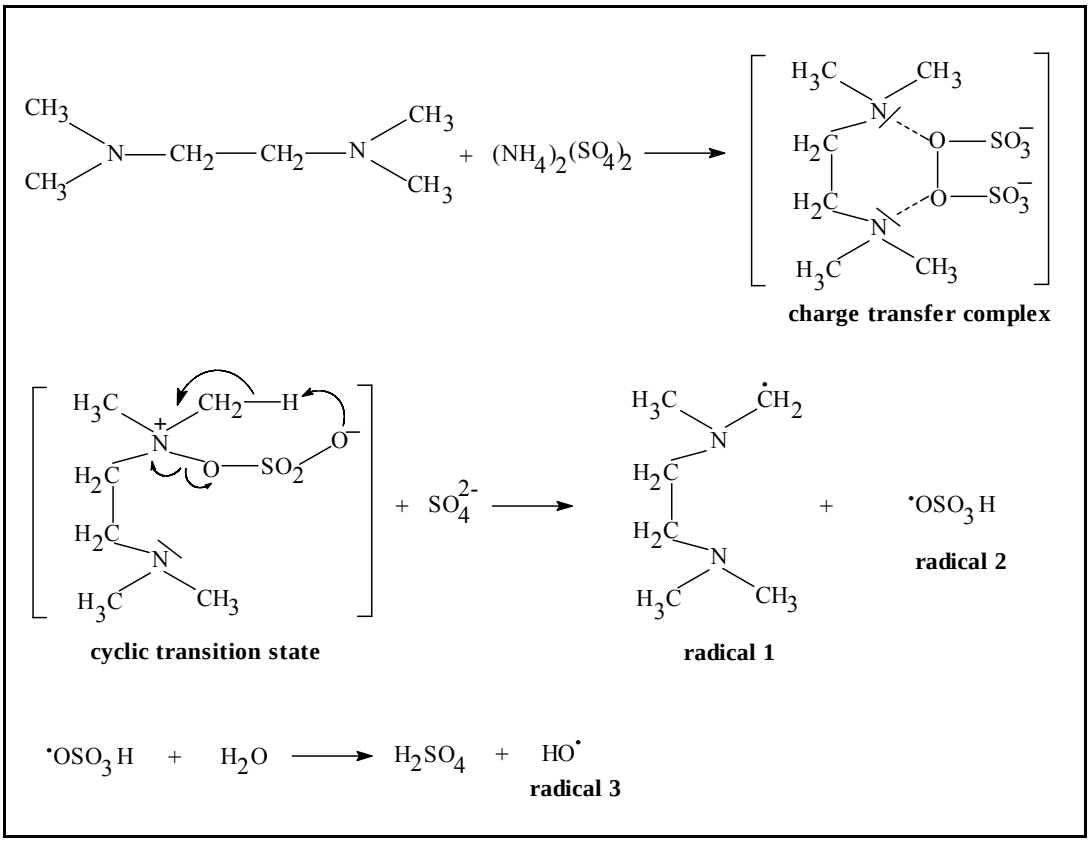

Figure 5.4: Initiation mechanism of the vinyl polymerization with the system APS/TEMED.

It was found that the free radicals 1, 2 and 3 are responsible for the initiation of the polymerization. However, the result of amino end group analysis confirmed the fact that the free radical 1 initiates the polymerization and becomes the end group of the resulting polymers. The polymerization mechanism can be seen in Figure 5.5.

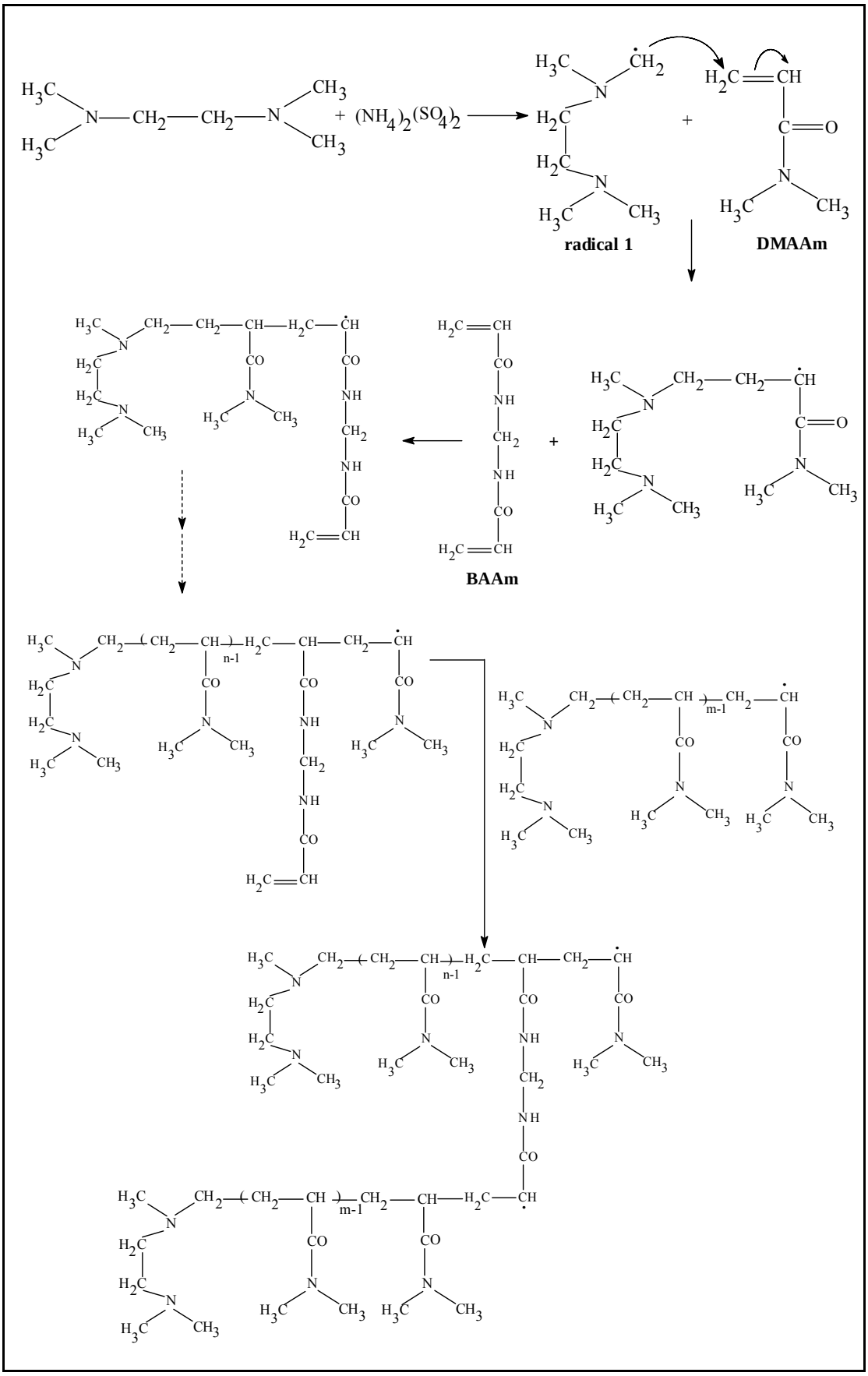

Figure 5.5: Formation of PDMAAm hydrogels.

The activated TEMED molecule can combine with an N,N-dimethylacrylamide or N,N'-methylenebisacrylamide (BAAm) monomer; in the process, the unpaired electron is transferred to the N,N-dimethylacrylamide unit, so that it turn becomes reactive. As the chain of N,N-dimethylacrylamide units grows, the active site shifts to the free end. Another monomer can therefore be attached and activated in the same way. The polymer can continue growing indefinetly and a BAAm molecule can be incorporated into two growing chains simultaneously to form a permanent link between them. Hence, the presence of BAAm leads to the formation of crosslinks between the chains. In Figure 5.6, 3-dimensional structure of the non-ionic PDMAAm gels was shown. The carbon, nitrogen, oxygen and hydrogen atoms were represented by blue, dark blue, red and black colors, respectively.

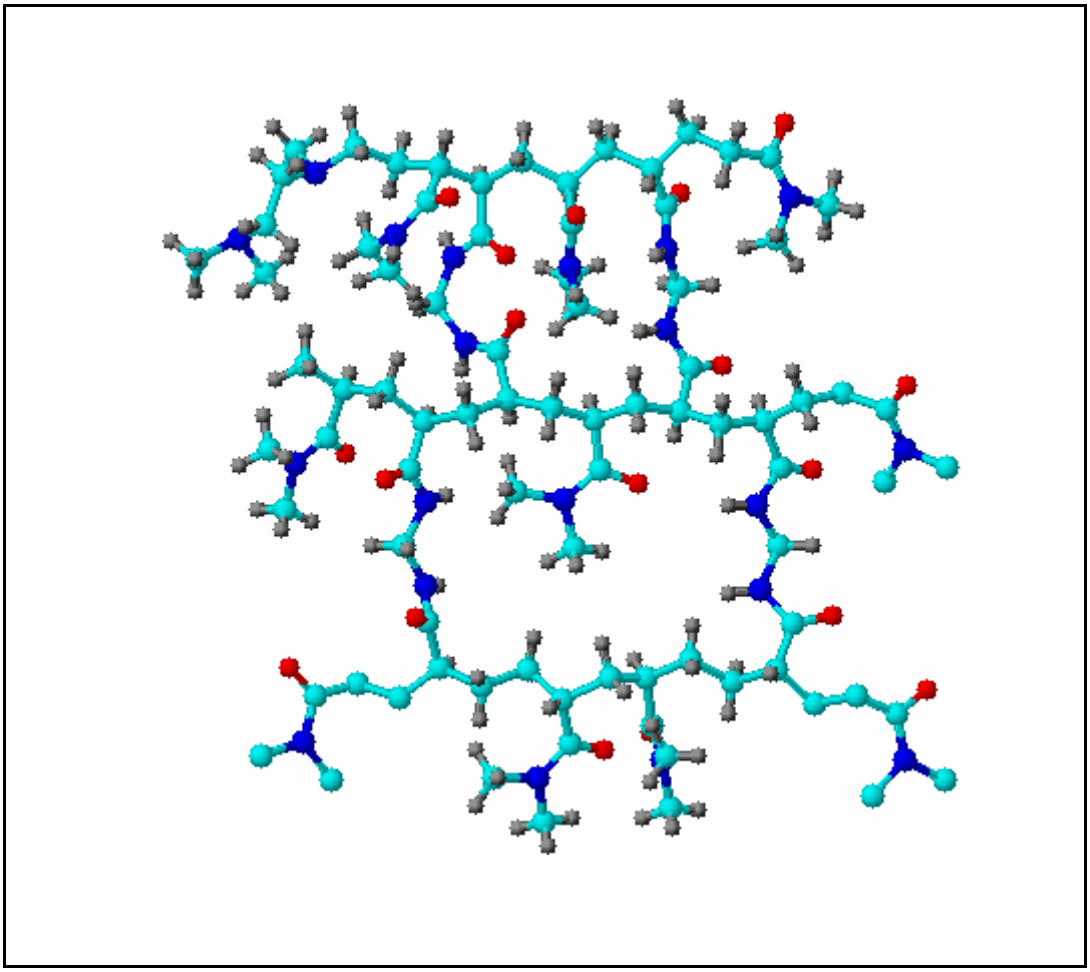

Figure 5.6: 3-Dimensional representation of the non-ionic PDMAAm hydrogels.

2) APS – SPS redox initiator system: The second initiator system used in the gel preparation is APS – sodium metabisulfite (SPS) redox pair. Although the mechanism have not yet been established undoubtedly, the free-radical generation by this redox pair occurs using metabisulfite as well as bisulfite anions[103,104]. The equation used for describing the free-radical generation by APS-SPS redox pair can be given as:

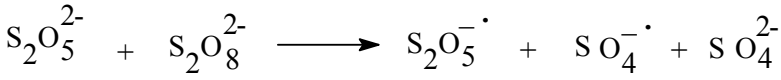

(5.1)

Based on the end-group analysis, it is proposed that the reductant in the redox reaction is bisulfite anion, that is in equilibrium with metabisulfite anion in the aqueous medium:

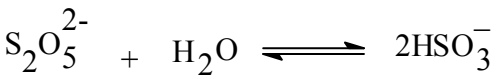

(5.2)

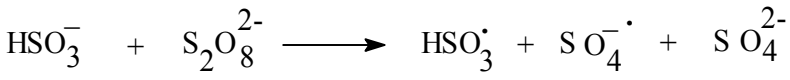

(5.3)

Therefore, it is considered that the bisulfite anion in Equation(5.3) rather than the metabisulfite anion in the Equation (5.1) initiates the polymerization reaction. Further, in the presence of oxygen, the bisulfite ion can also couple with oxygen to form a redox pair to generate free-radicals, initiating the polymerization:

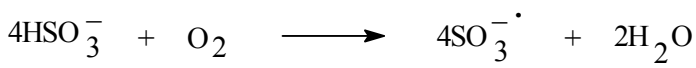

(5.4)

Therefore, the free-radical polymerization initiated by APS-SPS redox pair in the presence of oxygen consists of several competitive initiation steps. However, the preliminary experiments showed that the polymerization rates of both AAm and DMAAm monomers in the presence of APS – SPS and air are initially slow but then rapid, as in the APS – TEMED initiated reactions[102-104].

5.4.1. Preparation of Non-ionic and Ionic Poly(N,N-dimethylacrylamide) Hydrogels

PDMAAm hydrogels were prepared by free-radical crosslinking copolymerization of DMAAm and N,N'-methylenebisacrylamide (BAAm) in aqueous solution at 5 ^{o}C. To initiate the polymerization, the redox pairs consisting of APS - TEMED as well as APS - SPS were used in the experiments. PDMAAm hydrogels were prepared as the following:

i. Non-ionic PDMAAm hydrogels were prepared by using APS (3.51 mM) - TEMED (0.25 v/v%) redox initiator system. The initial molar concentration of the monomers, C_0, was varied between 0.36 and 9.54 M while the crosslinker ratio X (mole ratio of the crosslinker BAAm to the monomer DMAAm) was fixed at 1/83. APS and TEMED stock solutions were prepared by dissolving 0.080 g APS and 0.250 ml TEMED separately in 10 ml of water. The amounts of the chemicals used in the hydrogel preparation are compiled in Table 5.1.

Table 5.1: Feed compositions for the preparation of non-ionic PDMAAm hydrogels.

C_0, M	DMAAm (ml)	BAAm (g)	APS (g)	TEMED (ml)
0.36	0.37	0.0660	0.008	0.025
0.48	0.49	0.0088	0.008	0.025
0.58	0.60	0.0108	0.008	0.025
0.73	0.74	0.0132	0.008	0.025
1.45	1.47	0.0264	0.008	0.025
1.97	2.00	0.0359	0.008	0.025
2.90	2.94	0.0529	0.008	0.025
3.93	4.00	0.0717	0.008	0.025
4.92	5.00	0.0897	0.008	0.025
5.90	6.00	0.1077	0.008	0.025
6.88	7.00	0.1255	0.008	0.025
7.87	8.00	0.1435	0.008	0.025
8.75	8.90	0.1597	0.008	0.025
9.54	9.70	0.1741	0.008	0.025

To illustrate the synthetic procedure in the glass tubes, the details for the preparation of a non-ionic PDMAAm hydrogel at C_0 = 1.45 M can be given as follows: APS stock solution (1.0 ml), DMAAm (1.47 ml) and BAAm (0.0264 g) were mixed in a 10 ml graduated flask. After bubbling nitrogen for 15 minutes in order to eliminate

oxygen from the system, TEMED stock solution (1.0 ml) was added and then, the reaction solution was completed to 10 ml with distilled water in a volumetric flask. After shaking the flask, the solution was poured into several glass tubes. The tubes were sealed, and the polymerization reaction was conducted at 5 ^{o}C for one day. For the preparation of hydrogels at C_0 > 8.8 M, the reactions were carried out one day at 5 ^{o}C and another day at 70 ^{o}C.

ii. Ionic PDMAAm hydrogels were prepared using AMPS as ionic comonomer. To initiate the polymerization, the same amount of the initiator system consisting of APS and TEMED were used as in the preparation of non-ionic PDMAAm hydrogels. The mole fraction of ionic comonomer AMPS in the monomer mixture x_i was varied between 0 and 1. The initial concentration of the total monomers was held constant at 5.1 w/v %. The crosslinker ratio X (mole ratio of the crosslinker BAAm to the monomers DMAAm + AMPS) was fixed at 1/83. BAAm stock solution was prepared by dissolving 0.3 g BAAm in 50 ml of water. The amount of chemicals used in ionic PDMAAm hydrogels preparation are compiled in Table 5.2.

Table 5.2: Feed compositions for the preparation of ionic PDMAAm hydrogels.

x_i AMPS	DMAAm (ml)	AMPS (g)	BAAm stock ml	APS (g)	TEMED (ml)
0	0.51	0.0000	1.55	0.008	0.025
0.005	0.50	0.0025	1.54	0.008	0.025
0.01	0.50	0.0050	1.53	0.008	0.025
0.02	0.49	0.0099	1.51	0.008	0.025
0.05	0.46	0.0248	1.46	0.008	0.025
0.07	0.44	0.0347	1.42	0.008	0.025
0.10	0.41	0.0496	1.37	0.008	0.025
0.20	0.32	0.0992	1.23	0.008	0.025
0.30	0.26	0.1488	1.12	0.008	0.025
0.40	0.20	0.1984	1.02	0.008	0.025
0.50	0.16	0.2480	0.94	0.008	0.025
0.60	0.12	0.2976	0.87	0.008	0.025
0.70	0.08	0.3472	0.82	0.008	0.025
0.80	0.05	0.3967	0.76	0.008	0.025
0.90	0.02	0.4463	0.72	0.008	0.025
1.00	0.00	0.4959	0.68	0.008	0.025

iii. Non-ionic PDMAAm hydrogels were also prepared by using APS - SPS (both 1.50 mM) redox initiator system. The free-radical crosslinking copolymerization reaction of DMAAm/BAAm was carried out in aqueous solutions at 21^{o}C in the light scattering vials. APS and SPS stock solutions were prepared by dissolving 0.1143 g APS and 0.0951 g SPS separately in 20 ml of water. These optimum concentrations of the redox pairs, providing gelation times in the reaction systems of less than one hour, were determined by the preliminary experiments. The stock solution of BAAm was prepared by dissolving 0.4 g BAAm in 50 ml of water. The initial concentration of the total monomers C_0 was fixed at 5.0 w/v % while the crosslinker ratio, X, was varied between 1/80 and 1/50. The amounts of the chemicals used in the gel preparation are given in Table 5.3.

Table 5.3: Feed compositions for non-ionic PDMAAm hydrogels prepared using APS – SPS redox pair.

X	DMAAm (ml)	BAAm (ml stock)	APS (ml stock)	SPS (ml stock)
50	0.50	1.87	0.60	0.60
60	0.50	1.56	0.60	0.60
70	0.50	1.34	0.60	0.60
80	0.50	1.17	0.60	0.60

The details for the preparation of the non-ionic PDMAAm hydrogel at X = 1/50 and C_0 = 5 w/v % using APS-SPS redox pair are given in the following scheme: The stock solutions of APS (0.60 mL), DMAAm (0.50 mL), and BAAm (1.87 mL) were mixed in a 10 mL graduated flask. Then, SPS stock solution (0.6 mL) and HPLC-grade water were added to give a total volume of 10 mL. The light scattering vials were sealed, and the polymerization was conducted at 21^{o}C for 24 h.

5.4.2. Preparation of Non-ionic Poly(acrylamide) (PAAm) Hydrogels

Poly(acrylamide) (PAAm) hydrogels were also prepared by free-radical crosslinking copolymerization of AAm and BAAm in aqueous solution at 21^{0}C. Mainly two sets of experiments were carried out:

i. Non-ionic PAAm hydrogels were prepared using the redox pairs consisting of APS (3.51 mM) - TEMED (24.9 mM) as well as APS-SPS (both 1.50 mM). The free-radical crosslinking copolymerization reaction of AAm/BAAm was carried out in aqueous solutions at 21^{o}C at a total monomer concentration C_0 of 5.1 w/v %. The

crosslinker ratio was varied between 1/80 and 1/50. The stock solution of AAm was prepared by dissolving 9.62 g AAm in 50 ml of HPLC-grade water. The amounts of the chemicals used in the gel preparation are given in Table 5.4.

Table 5.4: Feed compositions for the preparation of PAAm hydrogels using APS – SPS redox pair.

X	AAm (ml stock)	BAAm (ml stock)	APS (ml stock)	SPS (ml stock)
50	2.50	2.61	0.60	0.60
60	2.50	2.18	0.60	0.60
70	2.50	1.87	0.60	0.60
80	2.50	1.64	0.60	0.60

ii. Non-ionic PAAm hydrogels with varying amounts of the crosslinker BAAm were prepared at various initial monomer concentrations C_0 (mass of AAm + BAAm in 100 mL reaction solution). 2.63 mM APS and 24.9 mM (0.375 v/v %) TEMED were used as the redox initiator system. The stock solutions of the monomers and the initiator system in water were prepared using the following concentrations: AAm (10g / 50 mL), BAAm (0.3 g / 50 mL), APS (0.060 g / 10 mL), and TEMED (0.75 mL / 20 mL). The reactions were carried out in glass tubes as well as in the light scattering vials. The amounts of the chemicals used in the gel preparation are given in Table 5.5.

To illustrate the synthetic procedure in glass tubes, the details for the preparation of a PAAm gel at C_0 = 4 w/v % and 1 mol % BAAm can be given as: The stock solutions of AAm (1.96 mL), BAAm (1.43 mL), APS (1.00 mL), were mixed in a 10 mL graduated flask. After cooling in ice-water bath and bubbling nitrogen for 15 min, TEMED stock solution (1.0 ml) was added to the mixture. The polymerization reaction was conducted at 21^{o}C for one day.

Table 5.5: Feed compositions for the preparation of PAAm hydrogels prepared at various initial monomer concentrations C_0.

		C_0 = 3 w/v %		C_0 = 4 w/v %		C_0 = 5 w/v %		C_0 =6 w/v %		C_0 = 7 w/v %		C_0 = 8 w/v %	
X	BAAm mol %	AAm (ml)	BAAm (ml)	AAm (ml)	BAAm (ml)	AAm (ml)	BAAm (ml)	AAm (ml)	BAAm (ml)	AAm (ml)	BAAm (ml)	AAm (ml)	BAAm (ml)
500	0.2	1.49	0.22	1.99	0.29	2.49	0.36	2.99	0.43	3.48	0.51	3.98	0.58
249	0.4	1.49	0.43	1.98	0.58	2.48	0.72	2.97	0.86	3.47	1.01	3.97	1.15
166	0.6	1.48	0.65	1.97	0.86	2.47	1.08	2.96	1.29	3.45	1.51	3.95	1.72
124	0.8	1.47	0.86	1.97	1.15	2.46	1.43	2.95	1.72	3.44	2.01	3.93	2.29
99	1.0	1.47	1.07	1.96	1.43	2.45	1.79	2.94	2.15	3.42	2.50	3.91	2.86
82	1.2	1.46	1.28	1.95	1.71	2.44	2.14	2.92	2.57	3.41	3.00	3.90	3.43
70	1.4	1.46	1.5	1.94	1.99	2.43	2.49	2.91	2.99	3.40	3.49	3.88	3.99
61	1.6	1.45	1.71	1.93	2.27	2.41	2.84	2.90	3.41	3.38	3.98	3.86	4.55
54	1.8	1.44	1.91	1.92	2.55	2.40	3.19	2.89	3.83	3.37	4.47	3.85	5.10

5.5. Preparation of Linear Polymers

Linear PDMAAm was prepared by free-radical polymerization of DMAAm in aqueous solution at 5°C without using the crosslinker BAAm. Linear PAAm was also prepared by free-radical polymerization of AAm in aqueous solution at 21°C without using the crosslinker BAAm. To initiate the linear polymerization reactions, the redox pairs consisting of APS - TEMED as well as APS - SPS were used in the experiments.

5.6. Characterization of Hydrogels

5.6.1. Polymer Network Concentration at The Stage of Gel Preparation

All the hydrogel samples after preparation were subjected to the gravimetric tests to determine the monomer conversions and the gel fractions. The mechanical properties and the swelling behavior of hydrogels sensitively depend on the degree of dilution at which they are formed. The degree of dilution of the networks after their preparation was denoted by ν_2^0, the volume fraction of crosslinked polymer after the gel preparation. In order to determine ν_2^0, the hydrogels after preparation were first swollen in water to extract non-polymerizable or soluble components and then carefully deswollen in a series of water–tetrahydrofuran (THF) mixtures with increasing THF (poor solvent) contents and finally, in pure THF. This solvent exchange process facilitated final drying of the hydrogel samples at 80 °C under vacuum to constant mass. In Figure 5.7 photographs of a gel sample after preparation, after swelling and then after drying process are shown. As seen from Figure 5.7, the equilibrium swollen hydrogel exhibits a large volume, i.e., it contains a large amount of water. Drying of such swollen hydrogel without a solvent exchange procedure resulted trapped water inside the gel sample. The experimental values of ν_2^0 were calculated using the Equation (2.14). Moreover, assuming that the monomer conversions were complete after the crosslinking copolymerization, the theoretical values of ν_2^0 were also calculated using the Equation (2.13). For ionic hydrogels, the molar volume of the polymer repeat units $\overline{V}_r$ (in ml/mole) was calculated from the molar volumes DMAAm and AMPS repeat units as:

$$\bar{V}_r = \left[229x_i + 99.13(1-x_i)\right]/\rho \qquad (5.5)$$

where ρ is the PDMAAm density (1.213 g/ml) and x_i is the mole fraction of the ionic comonomer AMPS in the monomer mixture.

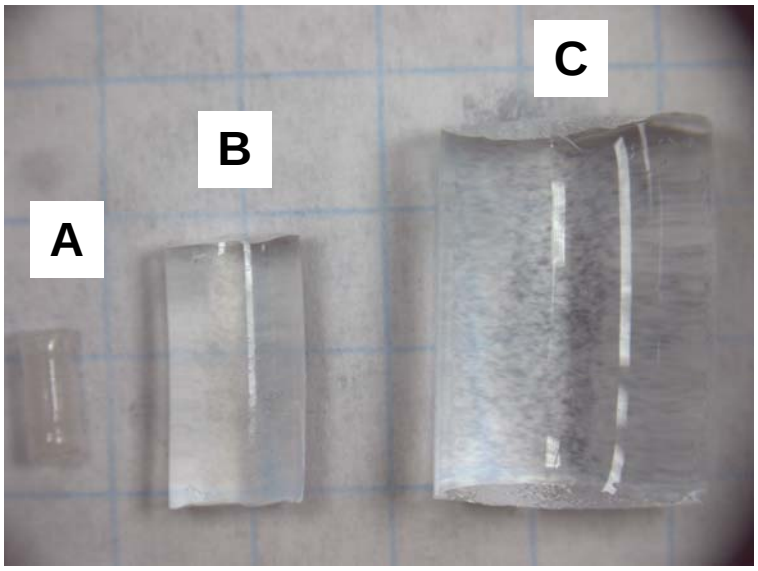

Figure 5.7: Photographs of the gel samples after drying (A), after preparation (B) and after equilibrium swelling (C).

5.6.2. Swelling Measurements

The swelling behaviors of the hydrogels were investigated in water, in solvent mixtures as well as in aqueous salt solution. After the preparation, the hydrogels in the form of rods of 4 mm in diameter were cut into samples of about 10 mm length. The gel samples were immersed in an excess of distilled water or solvent mixtures for at least two weeks to reach the swelling equilibrium at room temperature. The swelling ratios of the hydrogels were measured by using volumetric and gravimetric techniques.

i. Volumetric measurements: The swelling equilibrium was tested by measuring the diameter of the gel samples by a calibrated digital compass. To achieve good precision, three measurements were carried out on samples of different length taken from the same gel. The normalized volume of the equilibrium swollen gel V_{eq} (volume of equilibrium swollen gel/volume of the gel just after preparation) was calculated as;

$$V_{eq} = \left(\frac{D}{D_o} \right)^3 \tag{5.6}$$

where D and D_0 are the diameters of hydrogels after equilibrium swelling in water and after synthesis, respectively. The volume fraction of crosslinked polymer in the equilibrium swollen gel $\nu_{2,eq}$ was calculated as:

$$\nu_{2,eq} = \frac{\nu_2^0}{V_{eq}} \tag{5.7}$$

The equilibrium volume swelling ratio q_v (volume of swollen gel/volume of dry gel) was calculated using the Equation (2.5).

ii. Gravimetric measurements: The weight of the gel samples after preparation (m_0) and after swelling (m_{sw}) were measured by the electronic balance. The equilibrium weight swelling ratio q_w of the gel samples with respect to the after preparation state was calculated using the Equation (2.2).

For ionic gels, the swelling measurements in solvent mixtures were only carried out gravimetrically due to the deformation of the gel samples during their deswelling period under poor solvent condition. For this purpose, the weight of the hydrogels equilibrium swollen in solvent mixtures was measured after blotting the excess surface solvent. The normalized weight swelling ratio of the hydrogels with respect to their swelling ratio in water, m_{rel}, was calculated as:

$$m_{rel} = \frac{m_{solvent}}{m_{water}} \tag{5.8}$$

where $m_{solvent}$ and m_{water} are the masses of the equilibrium swollen gel sample in a solvent mixture and in water, respectively.

5.6.3. Mechanical Measurements

For the mechanical measurements, the hydrogels were prepared in glass tubes of about 100 mm long. After the reaction, the hydrogels were cut into specimens of approximately 7 mm in length. Uniaxial compression measurements were performed

on the hydrogels after their preparation and at their swelling equilibrium in water. The key parts of the apparatus used for mechanical measurements of gels are shown in Figure 5.8.

A cylindrical gel sample of 5 mm in diameter and 7 mm in length was placed on a digital electronic balance (Sartorius BP221S, readability and reproducibility: 0.1 mg). A load was transmitted vertically to the gel through a rod fitted with a PTFE (Teflon) end-plate. The force acting on the gel F was calculated from the reading of the balance m as F=mg, where g is gravitational acceleration (g = 9.8030 m.s^{-2}). The resulting deformation $\Delta l = l_o - l$, where l_o and l are the initial undeformed and deformed lengths, respectively, was measured using a digital comparator (IDC type Digimatic Indicator 543-262, Mitutoyo) which was sensitive to displacements of 10^{-3} mm. The force and resulting deformation were recorded after 20 sec of relaxation. The measurements were conducted up to about 20% compression. Reversibility of the isotherms was tested by recording the force and the resulting deformation during both force-increasing and force-decreasing processes. The two processes yielded almost identical stress-strain relations. From the repeated measurements, the standard deviations in the modulus value were less than 3%. The deformation ratio α (deformed length/initial length) was calculated as:

$$\alpha = 1 - \frac{\Delta l}{l_o} \tag{5.9}$$

The corresponding stress f was calculated as f = F / A, where A is the cross-sectional area of the specimen, A = π (D_o/2)^2, where D_o is its initial diameter. As pointed out in the theoretical section, for uniaxial deformation, the statistical theories of rubber elasticity yield for Gaussian chains an equation of the form:

$$f = G_0\left(\alpha - \alpha^{-2}\right) \tag{5.10}$$

where G_0 is the elastic modulus of the gel sample and can be determined from the slope of the linear dependence of stress-strain isotherms by using this equation. The computer program used to calculate the corrected slope of the stress-strain isotherms is given in Appendix A.

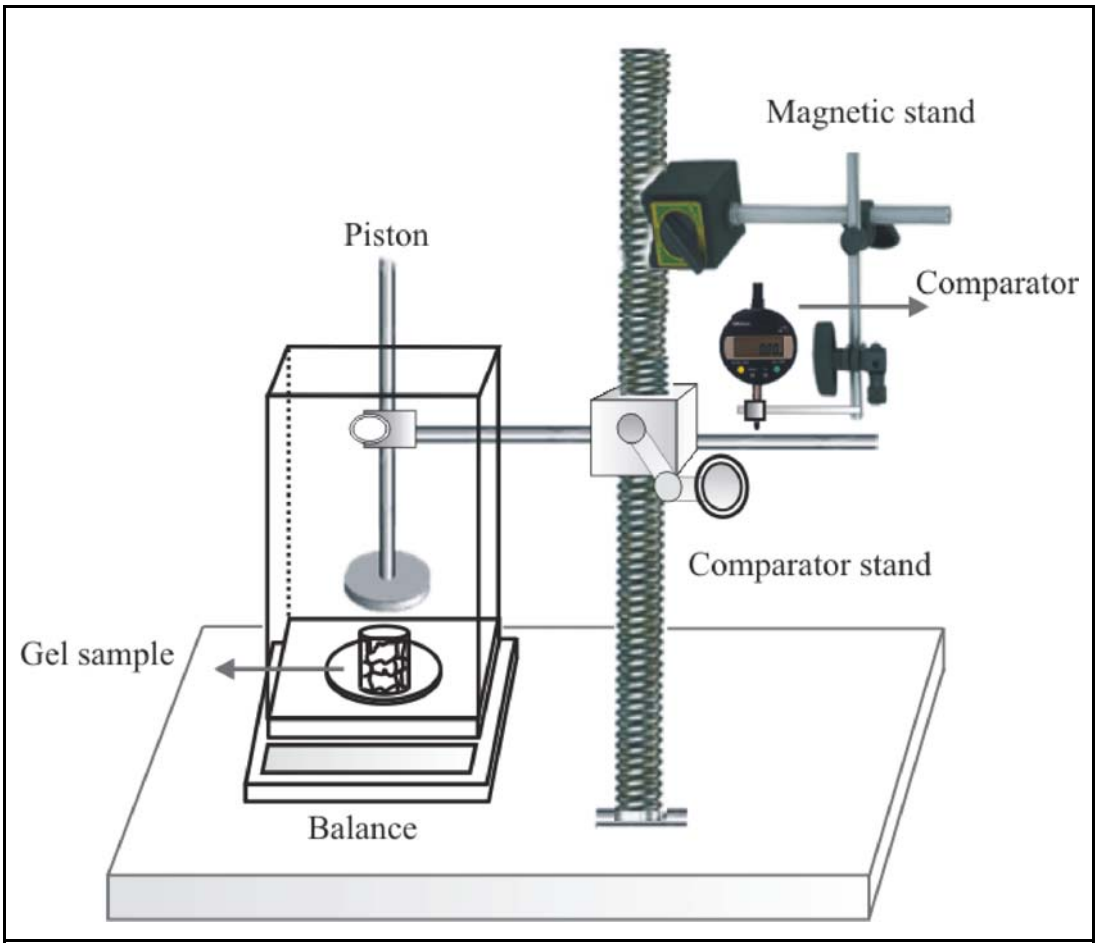

Figure 5.8: Uniaxial compression apparatus for measuring stress-strain data.

5.6.4. Light Scattering Measurements

The light scattering measurements were carried out at 21 ± 0.5 ^{o}C using a commercial multi-angle laser light scattering DAWN EOS (Wyatt Technologies Corporation) equipped with a vertically polarized 30 mW Gallium-arsenide laser operating at $\lambda = 690$ nm and 18 simultaneously detected scattering angles. In Figure 5.9, the light scattering apparatus was illustrated schematically.

The 18 discrete photo-detectors spaced around the DAWN EOS Batch's in a unique multi-angle geometry is shown in Figure 5.10. The measurements can be made simultaneously over a broad range of scattering angles θ (between 19 and 149^{0}). DAWN EOS works by sending laser light of 690 nm through the sample and detecting scattering caused by molecules or impurities. The detectors convert the reading to an electrical impulse which is sent to computer. When collecting the data from the instrument, periodically calibration, normalization and dark offset

measurements were made to ensure accurate measurements. Also, whenever collecting data on gel samples, firstly solvent offset measurements were made.

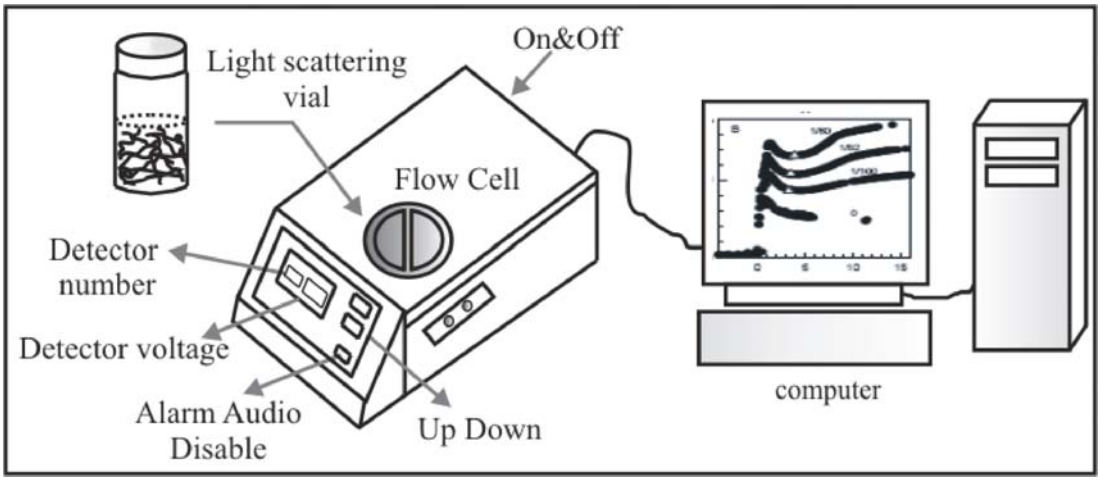

Figure 5.9: Schematic representation of the light scattering apparatus.

1- Calibration: The instrument was calibrated to compute the calibration constant. The calibration measurements were made with great care as the accuracy of all other measurements depends upon them. Only the 90^0 detector was calibrated against a toluene standard. The other detectors were normalized with respect to the 90^0 detector during the normalization step. Toluene was used for calibration because it is a dust-free solvent and it has a relatively large, well known Rayleigh ratio (Rayleigh ratio at 690 nm = 9.7801×10^{-6} cm^{-1}, DAWN EOS software). HPLC-grade toluene filtered through 0.2 μm filter was used for the calibration. During the calibration, the vial was rotated four times; an average of these measurements was taken as the calibration constant.

2- Dark offset: Even without light, detectors pick up voltage inside the instrument. Dark offset measurements were made to record these identical voltages so that they can be subtracted from the light scattering data.

3- Solvent offset: Solvent offset measurements were made with filtered (0.2 μm) HPLC-grade water. The cleanliness of the filtered solvent was checked by noting how much it scatters light at low angles that at high angles.

4-Normalization: The photodiode detectors at all scattering angles other than 90^0 were normalized relative to the 90^0 detector using HPLC-grade filtered toluene.

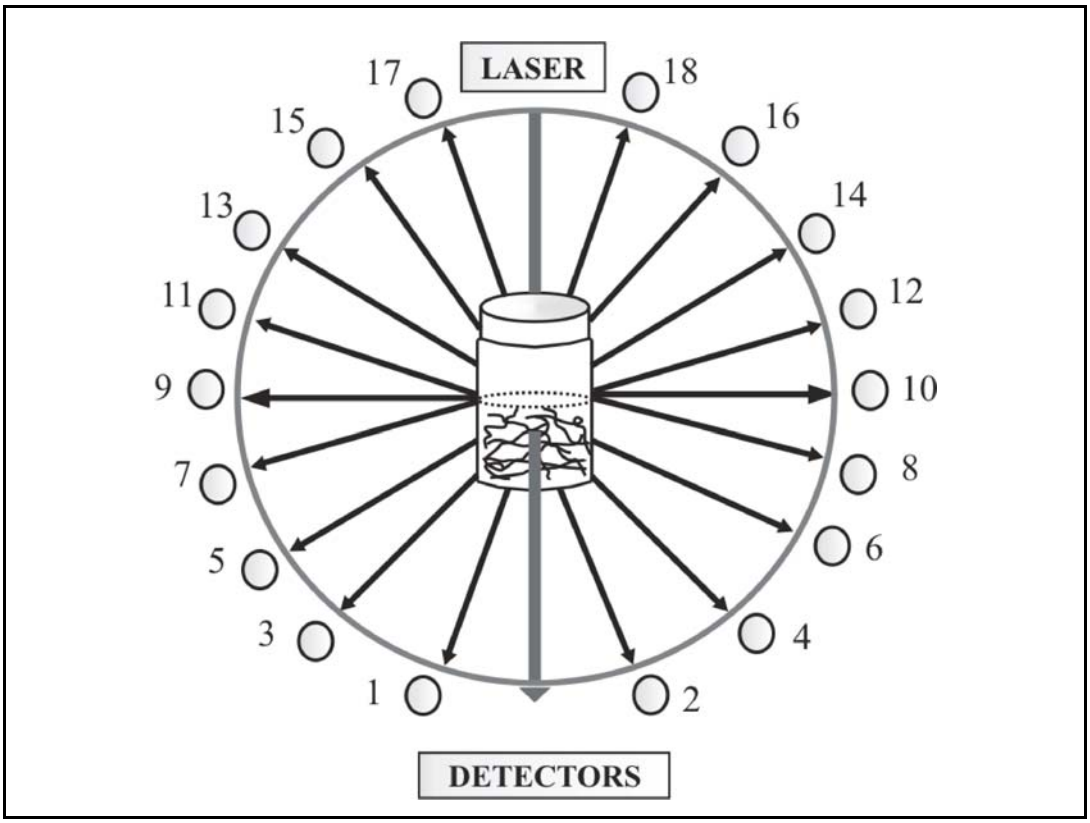

Figure 5.10: Schematic representation of DAWN light scattering photometer.

Light scattering measurements were carried out on gel samples just after various reaction times. The polymerization reactions were carried out in the light scattering vials. The reaction solutions were prepared in HPLC-grade water. The reaction solutions were filtered through membrane filters (pore size = 0.2 μm) directly into the light scattering vials. This process was carried out in a dustfree glovebox (The Plas-Labs, Model 818-GB Basic Glove Box 220/50Hz) (Figure 5.2). All glassware was kept dustfree by rinsing in hot acetone prior using. All the solutions subjected to light scattering measurements were clear and appeared homogeneous to the eye.

The scattered light intensities as a function of the reaction time were only recorded from a scattering angle $\theta = 90^{o}$. For the light scattering measurements on completely formed hyrdogels, i.e., after one day of reaction time, the scattered light intensities were recorded from angles $\theta = 14.5^{0}$ to 163.3^{0} which correspond to the scattering vector q range $3.1\text{x}10^{-4}$ – $2.4\text{x}10^{-3}$ $A^{o\ -1}$, where $q = (4\pi n/\lambda)\sin(\theta/2)$, n is the refractive index of the medium. To obtain the ensemble averaged light scattering intensity of gels, eight cycles of measurements with a small rotation of the vial between each cycle were averaged. For the calculation of excess scattering from

gels, all the crosslinking polymerizations were repeated under the same experimental conditions except that the crosslinker BAAm was not used. The excess scattering $R_{ex}(q)$ of the gel samples was determined by subtracting the scattering intensity of solution samples $R_{soln}(q)$ from the scattering intensities of gels $R_{gel}(q)$, both having the same concentration. Employing the Debye–Bueche analysis, the values of the mean square fluctuations of refractive index $\langle \eta^2 \rangle$, and the correlation length ξ, were obtained by means of the linear regression of Equation (4.56).

5.6.5. Gel Point Measurements

Gel point measurements were carried out in light scattering vials containing the reaction solution and a PTFE-covered steel sphere of 4.8 mm diameter. The record of the reaction time was started after crossing the induction period, at which an abrupt increase in the scattered light intensity was observed. The midpoint between the last time at which the sphere moved magnetically and that at which it stopped moving was taken as the gel point.

5.7. Characterization of Linear Polymers

5.7.1. Dilatometric Measurements

The linear polymerizations of DMAAm and AAm in the presence of APS-TEMED as well as APS-SPS redox initiator systems were also carried out in dilatometers. Figure 5.11 shows the dilatometer which was constructed in the laboratory. It consists of a blown glass bulb, approximately 25 ml in volume connected to a 30 cm length of 1.5 mm precision-bore capillary tubing with a ground-glass joint. The radius of the capillary was calibrated using mercury.

In the experiments, the zero reaction time was taken as the time at which the solution in the capillary starts to drop. The meniscus of the polymerizing solution was measured throughout the experiment with a millimetric paper to 0.2 mm as shown in Figure 5.11(right). The reproducibility of the kinetic data was checked by repeating the experiments as well as by the gravimetric measurement of the monomer conversions at certain time intervals[58,83]. The deviation in the time versus conversion data was always less than 3%. The non-isothermal condition during the warm up period of the reaction solution must be mentioned as the main source of

error in the dilatometric studies. The conversion of monomers x at the reaction time t was calculated as:

$$x = \frac{\pi r^2}{V_0 \alpha_C} \Delta h \tag{5.11}$$

where r is the radius of the capillary, V_0 is the volume of monomers in the dilatometer, α_C is the contraction factor, and Δh is the height change of the liquid column in the capillary between time zero and time t, respectively. The contraction factors α_C for DMAAm and AAm polymerizations were found by gravimetric determination of the monomer conversions as 0.245 and 0.330, respectively. The excel worksheet contains macro for the calculation of monomer conversion is given in Appendix B.

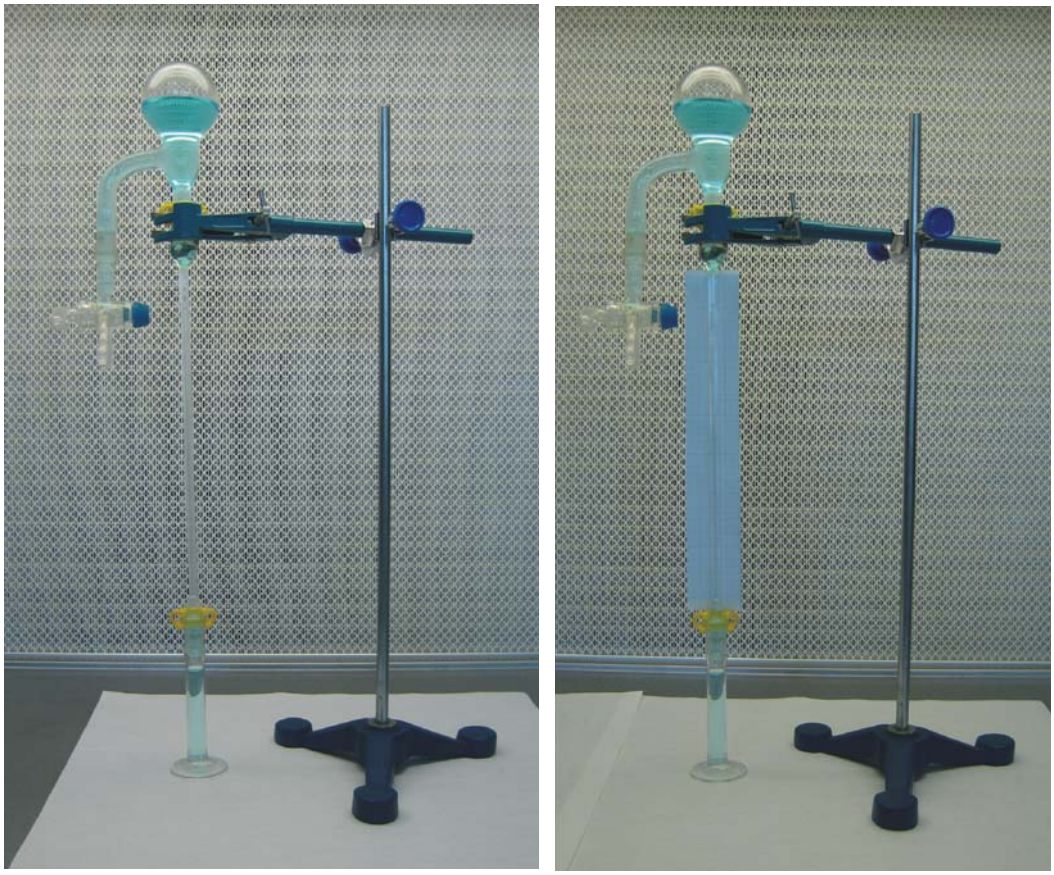

Figure 5.11: The dilatometer consisting of a blown glass bulb connected to a 30 cm length of 1.5 mm precision-bore capillary tubing (left). A millimetric paper was connected to capillary tubing (right).

Linear PDMAAm and PAAm were isolated after a reaction time of 24h by precipitation of the diluted reaction solutions in Acetone and methanole, respectively. The linear polymers were then dried in vacuum at room temperature to constant weight. The standart solutions of the polymers with concentrations in the range of $5x10^{-5}$ – $2.5x10^{-4}$ g/mL in water were prepared from the dry polymer samples. The solutions were filtered and the refractive index increment measurements as well as the light scattering measurements were carried out to determine dn/dc values and Zimm plots of linear PDMAAm and PAAm, respectively.

Light scattering measurements of linear PDMAAm and PAAm prepared in the presence of APS-TEMED as well as APS-SPS redox initiator systems were carried out using the DAWN EOS at λ = 690 nm at scattering angles between 34° and 132°. The weight-average molecular weight $\overline{M}_w$ and the radius of gyration $\left\langle R_g^2 \right\rangle^{1/2}$ of linear PDMAAm and PAAm were calculated from Zimm plots which are shown in Figures 6.40 and 6.41.

5.7.2. Refractive Index Increment Measurements

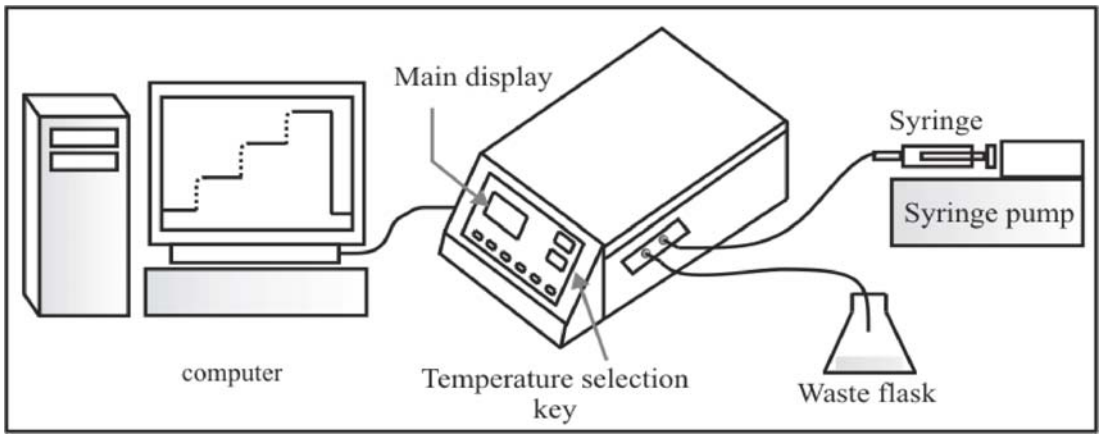

Figure 5.12: Schematic representation of the DAWN Optilap DSP Refractometer apparatus.

The refractive index increment dn/dc of standart polymer solutions was determined using DAWN Optilap DSP (Digital Signal Processing) Refractometer at 690 nm as shown in Figure 5.12. The Optilap DSP is a differential refractometer based on a wavefront shearing technique used somewhat similarly in interference microscopy. Two nearly coherent and linearly polarized beams of light pass through two

flow cells: one contains a reference fluid and the other contains a test fluid. Any difference in refractive index between the two fluids results in a phase shift of one beam relative to the other. This phase shift is directly proportional to the refractive index difference.

Calibration: The instrument was calibrated using sodium chloride dissolved in water, which has a dn/dc of 0.172 mL/gr at a wavelength of 690 nm. The solution standards of 1.1×10^{-3}, 1.02×10^{-3}, 8.48×10^{-4}, 6.34×10^{-4}, 4.7×10^{-4} and 1.86×10^{-4} g/mL were prepared from a 2×10^{-3} g/mL NaCl stock solution using prefiltered water. The solutions were prepared in HPLC-grade water filtered through 0.2 μm membrane filters. The slope of the best straight line through the refractive indexes of the NaCl solution standards versus the auxiliary detector voltages of the standards gave the calibration constant dn/dV as 2.2451e-04. Figure 5.13 shows the calibration curve of NaCl solution standards.

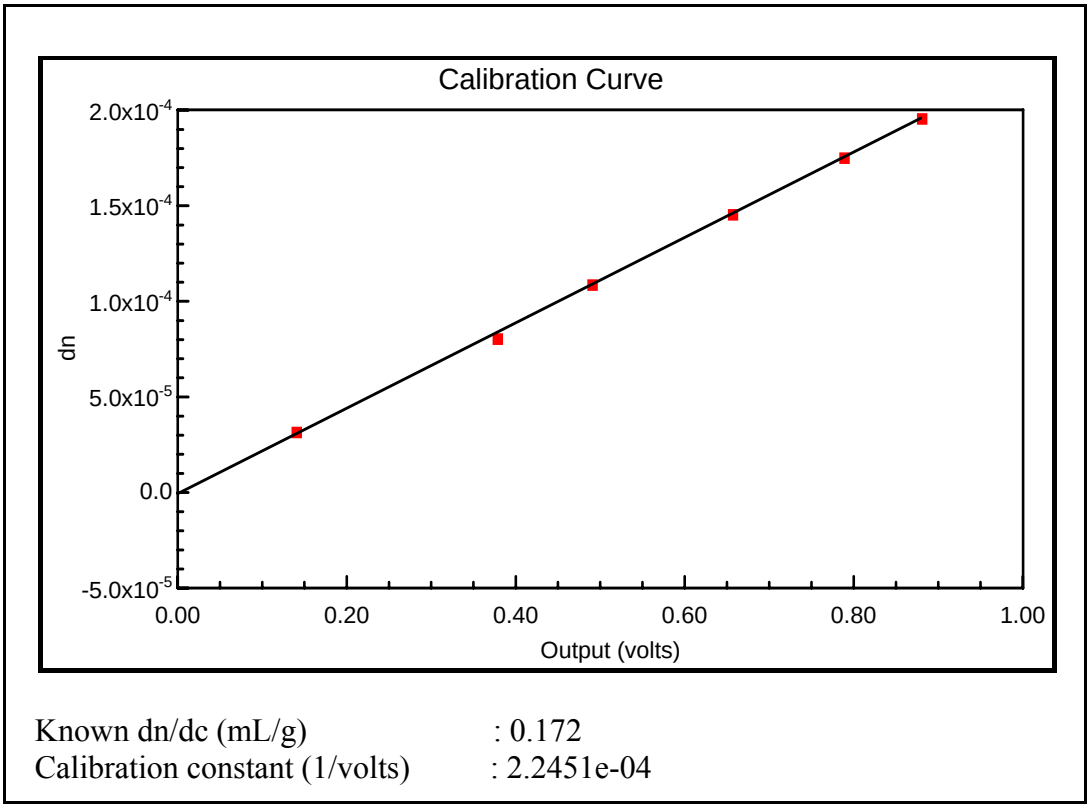

Figure 5.13: The calibration curve of NaCl solution standards.

The refractive index increment, dn/dc, of linear PDMAAm and PAAm was determined from the slope of the plot of the refractive indexes versus concentrations. The auxiliary detector voltage of the laser photometer was first stabilized against

filtered water. The sample and reference cell were flushed with filtered water for some time before making measurements. The polymer solutions were analyzed by injection of about 3.0 mL of each of the standards, starting with the lowest concentration, into the injection loop of the instrument. The detector voltage was recorded one minute after the voltage signal increased rapidly, and several minutes were required for the signal stabilize. This occurs when the solution has been completely rinsed out of the cell. Each solution yields a plateau on the screen. After all of the concentrations have been measured, filtered water was injected again to clear any remaining polymer solution and to confirm that there was no baseline drift during the measurement.

Figure 5.14 and 5.15 shows the dn/dc curves of the linear PDMAAm and PAAm, respectively. The upper plots show refractive index change dn versus concentration c, and is used for dn/dc calculation, whereas the lower plots show dn/c versus c. The dn/dc values of the polymers in water were found as 0.166 and 0.163 mL/g for PDMAAm and PAAm, respectively.

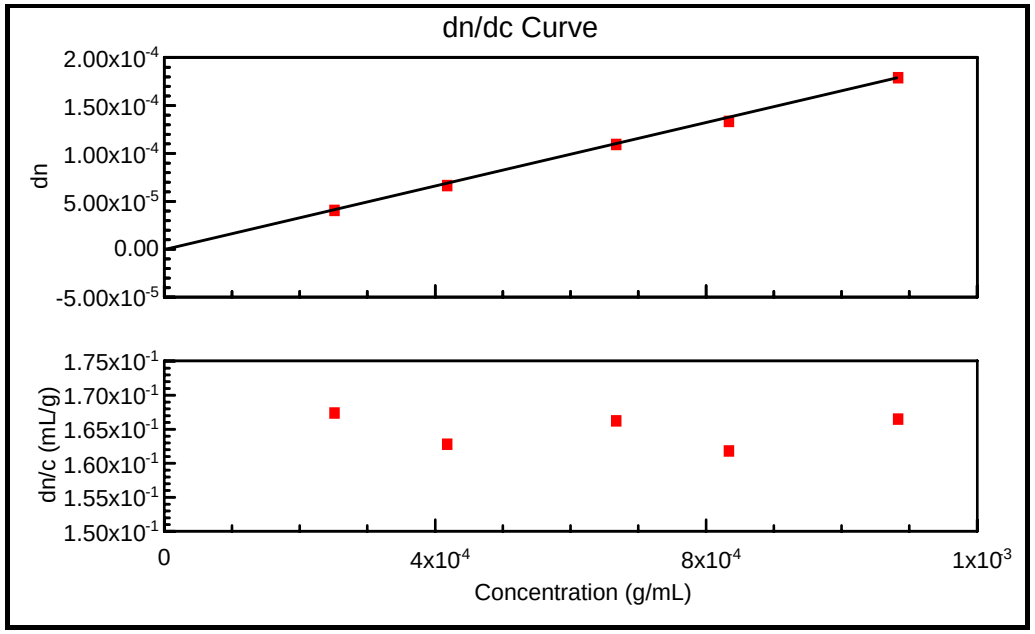

Known Calibration constant (1/ volts) : 2.2451e-04
dn/dc (mL/g) : 0.1656 ± 0.0029

Figure 5.14: The dn/dc curve for linear PDMAAm.

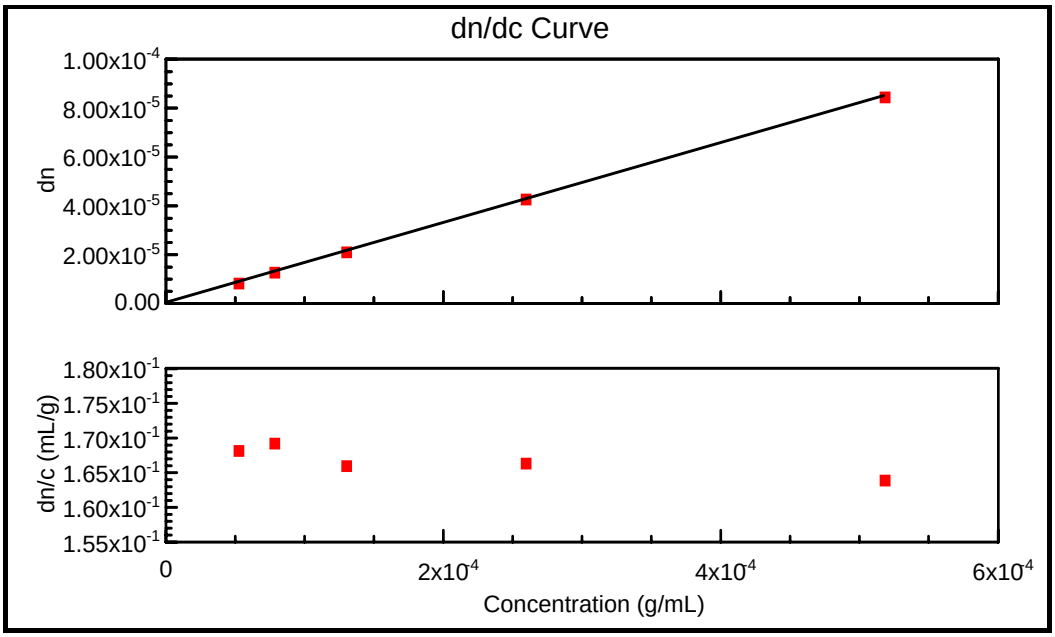

Known Calibration constant (1/volts) : 2.2451e-04
dn/dc (mL/g) : 0.1635 ± 0.0006

Figure 5.15: The dn/dc curve for linear PAAm.

6. RESULTS AND DISCUSSION

The main aim of this thesis was to determine the swelling, elasticity and the degree of the spatial inhomogeneity of PDMAAm hydrogels. For this purpose, swelling and elasticity tests as well as light scattering measurements were carried out on the hydrogel samples formed under various conditions. In this section;

i. The swelling behavior of both non-ionic and ionic PDMAAm hydrogels in water, in solvent mixtures as well as in aqueous salt solutions were discussed.
ii. The elastic behavior of both non-ionic and ionic PDMAAm hydrogels after preparation and after equilibrium swelling in water were discussed.
iii. The formation process and the spatial inhomogeneity in PDMAAm and PAAm hydrogels were also discussed as a function of the initial monomer concentration, the ionic comonomer concentration and the redox-initiator systems used to initiate the gelation reactions.

6.1. Swelling of PDMAAm Hydrogels

A series of gels based on N,N-dimethylacrylamide (DMAAm) monomer was prepared throughout this study. As pointed out before, the selection of DMAAm as a monomer is due to the fact that it is a liquid at room temperature and fully miscible with water. Thus, PDMAAm hydrogels could be prepared in aqueous solutions at monomer concentrations from a few percent up to 100 % (without the use of a solvent). In this way, it is possible to investigate the hydrogel properties over the whole range of the polymer concentration.

The hydrogels were prepared by free-radical crosslinking copolymerization reactions of DMAAm and BAAm crosslinker. Ammonium persulfate - N,N,N',N'-tetramethylethylenediamine (TEMED) redox initiator system was used to initiate the polymerization reactions. Sodium salt of 2-acrylamido-2-methylpropane sulfonic acid (AMPS) was used as the ionic comonomer for the preparation of ionic

hydrogels. To make a comparison, PAAm hydrogels were also prepared under the same experimental condition except that AAm monomer was used in the gel preparation. In the following, the swelling behavior of non-ionic and ionic PDMAAm hydrogels will be discussed as a function of the initial monomer concentration and the ionic comonomer concentration.

6.1.2. Swelling of Non-ionic PDMAAm Hydrogels in Water

A series of non-ionic PDMAAm hydrogels was prepared at a fixed crosslinker ratio X = 1/83 (the mole ratio of the crosslinker BAAm to the monomer DMAAm) but at various initial monomer concentration, denoted by C_0, between 0.36 and 9.54 M. The hydrogel prepared at C_0 less than 0.36 M was too weak to withstand the swelling and mechanical measurements. Thus, this gel was only subjected to the light scattering measurements. The swelling and the elasticity measurements were conducted on the hydrogel samples. The characteristics of non-ionic PDMAAm hydrogels are complied in Table 6.1. The examples of calculations of the characteristic data of hydrogels from swelling measurements are given in Appendix C.

All the hydrogel samples after preparation were subjected to the gravimetric tests to determine the monomer conversions and the gel fractions. In the second column of Table 6.1, the weight swelling ratios of the hydrogels after their preparation q_F (mass of gel preparation / mass of dry gel) calculated using Equation (2.15) are collected. It is seen that q_F decreases with increasing initial monomer concentration of the hydrogels from 25.19 to 1.17. From the q_F values, the volume fraction of crosslinked polymer after the gel preparation ν_2^0 was calculated using Equation (2.14). The experimental values $\nu_{2,\text{exp}}^0$ of the hydrogels are also shown in column 4 of the Table 6.1. Assuming that the monomer conversions and the gel fractions are complete after the crosslinking DMAAm polymerization the theoretical values $\nu_{2,\text{theo}}^0$ of the hydrogels can be calculated using the Equation (2.13).

In Figure 6.1, the experimental ν_2^0 values of PDMAAm hydrogels ($\nu_{2,\text{exp}}^0$) are plotted against its theoretical value ($\nu_{2,\text{theo}}^0$). The straight line in Figure 6.1 shows the relation $\nu_2^0 = \nu_{2,\text{theo}}^0$. It is seen that the experimental ν_2^0 is close to its theoretical

value, indicating that, under the reaction conditions, the monomer conversions and the gel fractions are complete, as long as $\nu^0_{2,\text{theo}} < 1$[105].

PDMAAm hydrogels formed at various polymer network concentrations were subjected to the swelling measurements in water. The measurements were carried out at room temperature (24 ± 0.5°C). The linear swelling ratio α was determined by measuring the diameter of the hydrogel samples after equilibrium swelling in water D and after synthesis D_0 by a calibrated digital compass ($\alpha = D/D_0$). The volume fraction of the crosslinked polymer in the equilibrium swollen gel $\nu_{2,eq}$ and the normalized volume of the equilibrium swollen hydrogels V_{eq} (volume of equilibrium swollen gel/volume of the gel just after preparation) were also calculated using Equations (5.7) and (5.6), respectively. These data are collected in column 5 and 6 of Table 6.1.

Table 6.1: The characteristic data of non-ionic PDMAAm hydrogels.

C_0, M	q_F	$\nu^0_{2,\text{theo}}$	$\nu^0_{2,\text{exp}}$	$\nu_{2,eq}$	*Veq*	G_0 /*Pa*	*G* / *Pa*	v_e
0.36	25.19	0.029	0.033	0.0145	2.0671	864.09	729.30	21.273
0.48	19.23	0.040	0.046	0.0214	1.8511	2015.50	1832.14	35.297
0.58	13.84	0.049	0.060	0.0267	1.8143	3699.90	3314.33	49.608
0.73	11.07	0.061	0.076	0.0443	1.7084	7165.67	6354.78	76.661
1.45	5.99	0.123	0.142	0.0695	2.0377	32237.70	25673.80	184.338
1.97	3.06	0.169	0.195	0.0877	2.2238	51757.50	40084.50	214.886
2.9	4.40	0.253	0.285	0.1151	2.4792	90238.43	79860.57	256.050
3.93	2.23	0.353	0.401	0.1272	3.1523	123892.80	83805.10	250.175
4.92	1.84	0.451	0.496	0.1426	3.4817	143617.00	99437.71	234.313
5.9	1.514	0.555	0.616	0.1502	4.1019	154654.70	107678.60	203.288
6.88	1.33	0.663	0.717	0.1574	4.5513	179162.60	114482.80	202.506
7.87	1.14	0.777	0.853	0.1659	4.6964	524633.70	102892.30	498.459
8.75	1.12	0.885	0.829	0.1552	5.6831	217006.90	139690.70	211.989
9.54	1.17	1	0.882	0.1551	5.3412	302755.70	169644.70	278.151

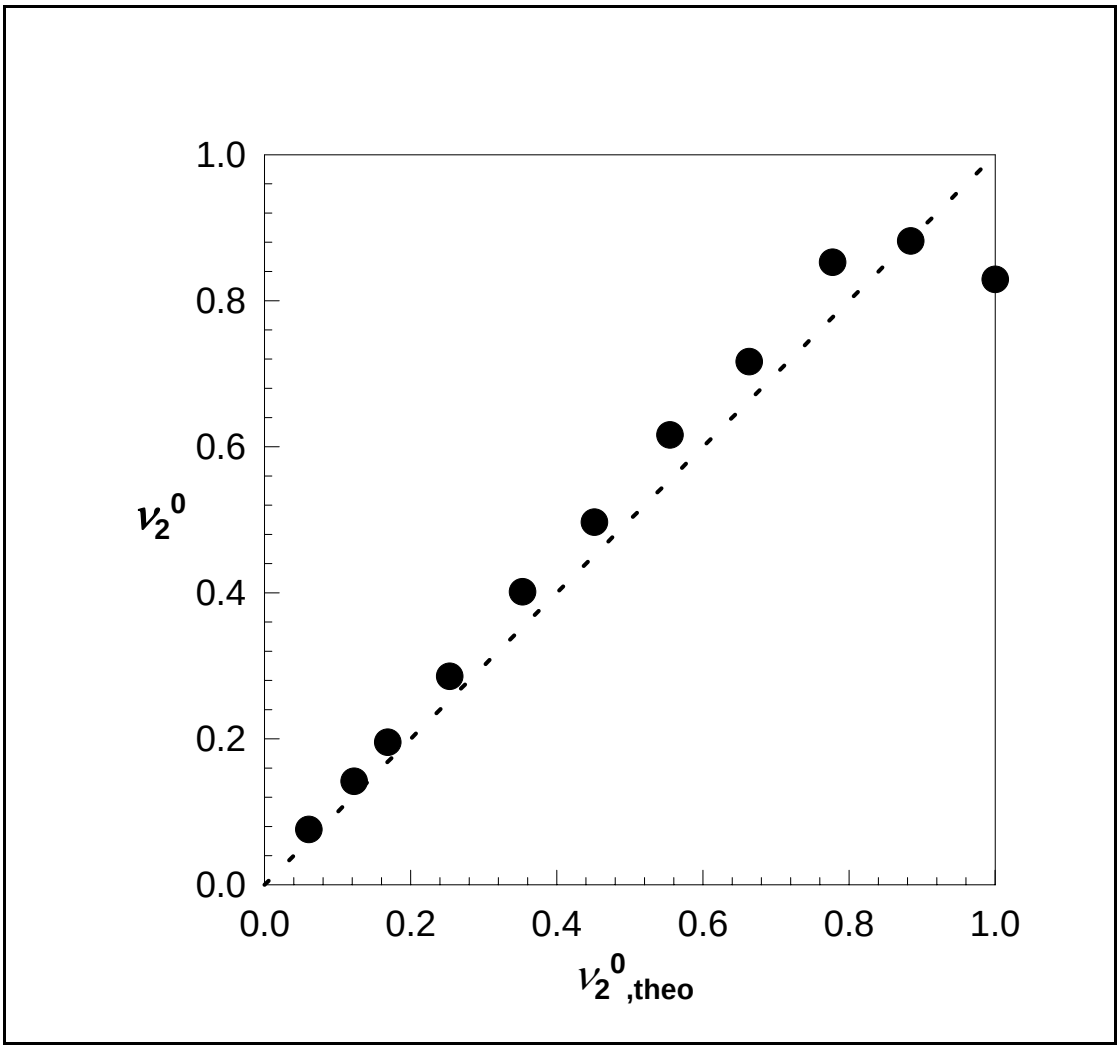

Figure 6.1: Experimental values ν_2^0 of the hydrogels shown as a function of its theoretical value ($\nu_{2,\text{theo}}^0$). The dotted line shows the relation $\nu_2^0 = \nu_{2,\text{theo}}^0$.

In Figure 6.2, the linear swelling ratio α of non-ionic PDMAAm hydrogels is plotted as a function of the crosslinked polymer concentration at the gel preparation ν_2^0 by the filled symbols. For comparison, swelling data for non-ionic PAAm hydrogels of crosslinker ratios *X* varying between 1/50 and 1/100 taken from the literature are also shown in the Figure by the open symbols[88,90]. The dotted lines in Figure 6.2 represent the scaling parameters –0.2 and 0.2 predicted by Equations (2.84) and (2.85), respectively. It is seen that the dotted lines agree well with the experimental swelling behavior of the hydrogels. Figure 6.2 shows that α is not a monotonic function of the polymer concentration ν_2^0. The dependence of α on ν_2^0 exhibits three different regimes:

1- For ν_2^0 < 0.10, α is a decreasing function of ν_2^0. In this regime, increasing the initial monomer concentration results in decreased expansion ratios of the gels with respect to after preparation state.

2- In a rather narrow range of ν_2^0 around 0.10, α is ν_2^0 independent. The constancy of α in this regime is in agreement with the observation of Shibayama et al. on PNIPA gels[21].

3- For ν_2^0 > 0.10, α increases continuously with increasing ν_2^0 up to the bulk polymerization condition[105,106].

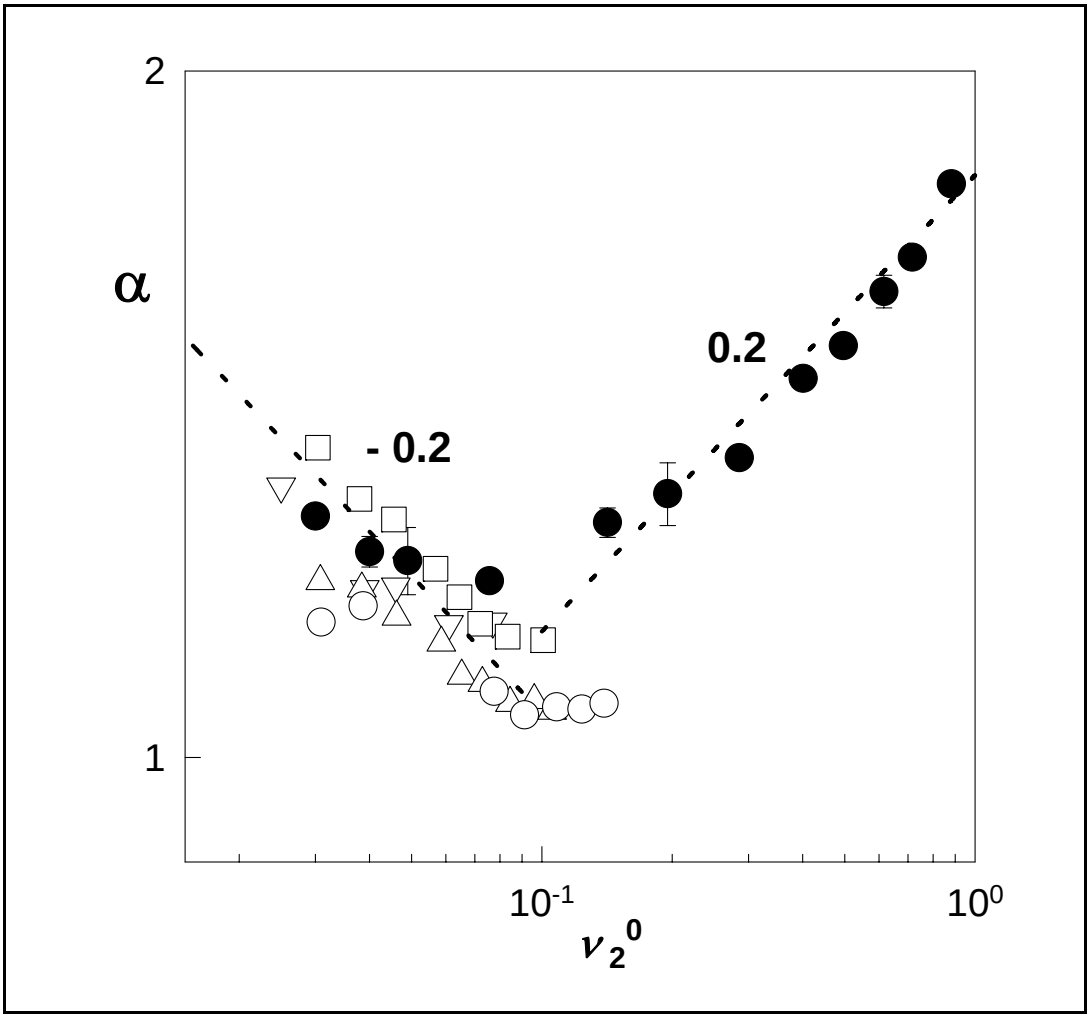

Figure 6.2: Linear swelling ratio α of PDMAAm hydrogels with X = 1/83 (filled symbols) and of PAAm hydrogels (open symbols) shown as a function of ν_2^0. X = 1/50 (○), 1/61.5 (△), 1/66 (▽), and 1/100 (□). The corresponding slopes of the dotted lines are shown.

In section 2.4.5, a scaling relation between α and ν_2^0 was derived to discuss the monomer concentration dependence of the linear swelling ratio α and it was found that ν_2^0-dependence of α is due to the variation of the network chain length N depending on the initial monomer concentration. The increase of the linear swelling ratio with the network chain length follows the relationship $\alpha \approx \left(\nu_2^0 N\right)^{1/5}$ (Equation (2.81)). At low polymer concentrations, i.e., for ν_2^0 < 0.1, N is very sensitive to the initial monomer concentration due to decreasing probability of cyclization as the monomer concentration is increased and varies as $N \approx \left(\nu_2^0\right)^{-2}$ and hence, α scales with ν_2^0 through the relation $\alpha \approx \left(\nu_2^0\right)^{-1/5}$ (Equation (2.84)). At high polymer concentrations, i.e., for ν_2^0 > 0.1, N varies only slightly with ν_2^0 due to the reducing reactivity of pendant vinly groups during crosslinking as well as due to the increasing extent of the chain entanglements and hence, α scales with ν_2^0 through the relation $\alpha \approx \left(\nu_2^0\right)^{1/5}$, (Equation (2.85)).

6.1.2.1. The Interaction Parameter Between PDMAAm Hydrogels and Water

The interaction parameter between PDMAAm hydrogels and water χ was calculated from the Flory-Rehner equation for phantom chains as:

$$\chi = -\frac{\ln\left(1-\nu_{2,eq}\right) + \nu_{2,eq} + 0.5\,\nu_e\,V_1\left(\nu_{2,eq}\right)^{1/3}\left(\nu_2^0\right)^{2/3}}{\left(\nu_{2,eq}\right)^2} \tag{6.1}$$

In the Flory-Rehner Equation, χ parameter is assumed to be concentration dependent, i.e.;

$$\chi = \chi_1 + \chi_2\,\nu_2 + \chi_3\,\nu_2^2 + ... \tag{6.2}$$

where the coefficients χ_1, χ_2, and χ_3,.. are the functions of the molecular characteristics of the polymer-solvent system[107]. The calculation results of χ are shown in Figure 6.3 plotted against the equilibrium polymer volume fraction $\nu_{2,eq}$.

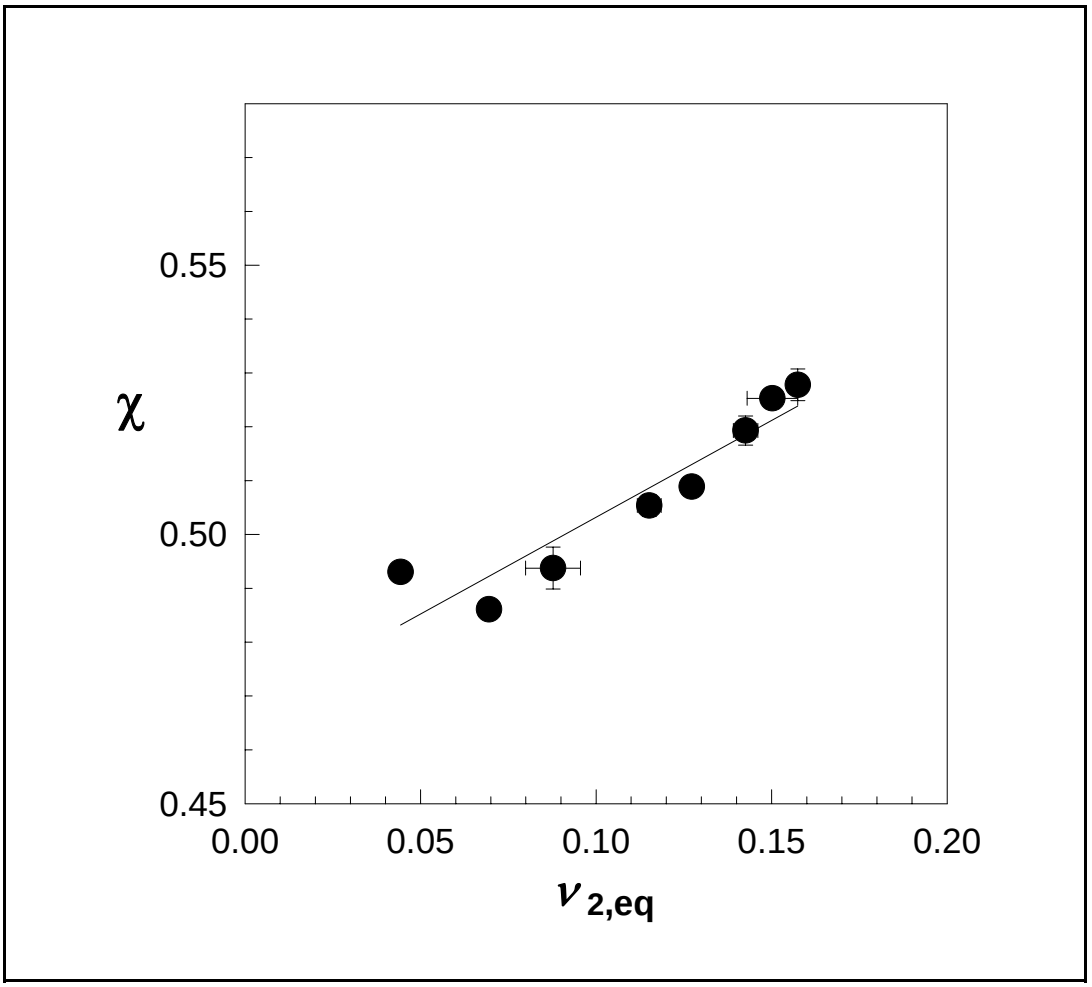

Figure 6.3: The interaction parameter χ of PDMAAm – water system shown as a function of the concentration $\nu_{2,eq}$.

In Figure 6.3, the straight line through the experimental points is obtained by least squares as:

$$\chi = \chi_1 + \chi_2 \nu_{2,eq} \tag{6.3}$$

where χ_1 = 0.47 and χ_2 = 0.36 and they are subject to uncertainties of $\pm$ 0.01 and $\pm$ 0.06, respectively. The expressions assuming the affine network behavior for gels give similar χ parameter values (χ_1 = 0.48 and χ_2 = 0.33). Equation (6.3) indicates that χ of PDMAAm – water system strongly depends on concentration. Erman and Flory showed that when the χ parameter is expressed as a linear function of $\nu_{2,eq}$, a necessary condition for the nonionic gels to go through critical conditions is to have $\chi_1 < 1/2$ and $\chi_2 > 1/3$ [107]. Although the indicated requirements for the hydrogel

collapse is rare for real polymer-solvent systems, Equation (6.3) shows that both these conditions are satisfied for PDMAAm - water system. Thus, the present gel system is a suitable candidate for the first – order volume phase transition studies. For this reason, swelling behavior of non-ionic PDMAAm hydrogels in solvent mixtures was investigated.

6.1.3. Swelling of Non-ionic PDMAAm Hydrogels in Solvent Mixtures

The swelling behavior of non-ionic PDMAAm hydrogels was investigated in aqueous organic solvent mixtures as functions of the solvent species and the concentration. The hydrogels were subjected to the swelling measurements in the following organic solvent–water mixtures: Acetone–water, dimethylsulfoxide (DMSO)–water, THF–water, 1,4-dioxane–water, ter-butanol–water, methanol–water, ethanol–water and propanol-water. The composition of the solvent mixtures was varied between 0 and 100%. The measurements were carried out at room temperature $24 \pm 0.5°C$.

In Figure 6.4, the swelling behavior of non-ionic PDMAAm hydrogels immersed in acetone-water mixtures is illustrated. Here, the equilibrium swelling ratio V_{eq} of the hydrogels in acetone-water mixtures is plotted as a function of the acetone volume fraction ϕ in the external solution. For comparison, the swelling behavior of the non-ionic PAAm hydrogel is also shown in the Figure 6.4 by the open symbols.

It is seen that the PAAm hydrogel slightly undergoes a deswelling transition as the acetone concentration of the solvent mixture increases and finally attains a collapsed state in pure acetone with a volume $V_{eq} \cong 10^{-1}$. In contrast, PDMAAm hydrogel first remains in the swollen state up to $\phi = 0.65$. As ϕ crosses 0.65, the gel exhibits the reentrant phase transition, in which the gel first deswells up to $V_{eq} \cong 10^{-1}$, then rapidly reswells if ϕ is monotonically increased. The reswelling of the collapsed PDMAAm hydrogel occurs in a narrow of ϕ above $\phi = 0.97$[108]. Since the only difference between the PDMAAm and PAAm hydrogels is the existence of the methyl groups in PDMAAm networks, the results indicate that the hydrophobic interactions are responsible for the reentrant conformation transition in PDMAAm hydrogels immersed in acetone-water mixtures.

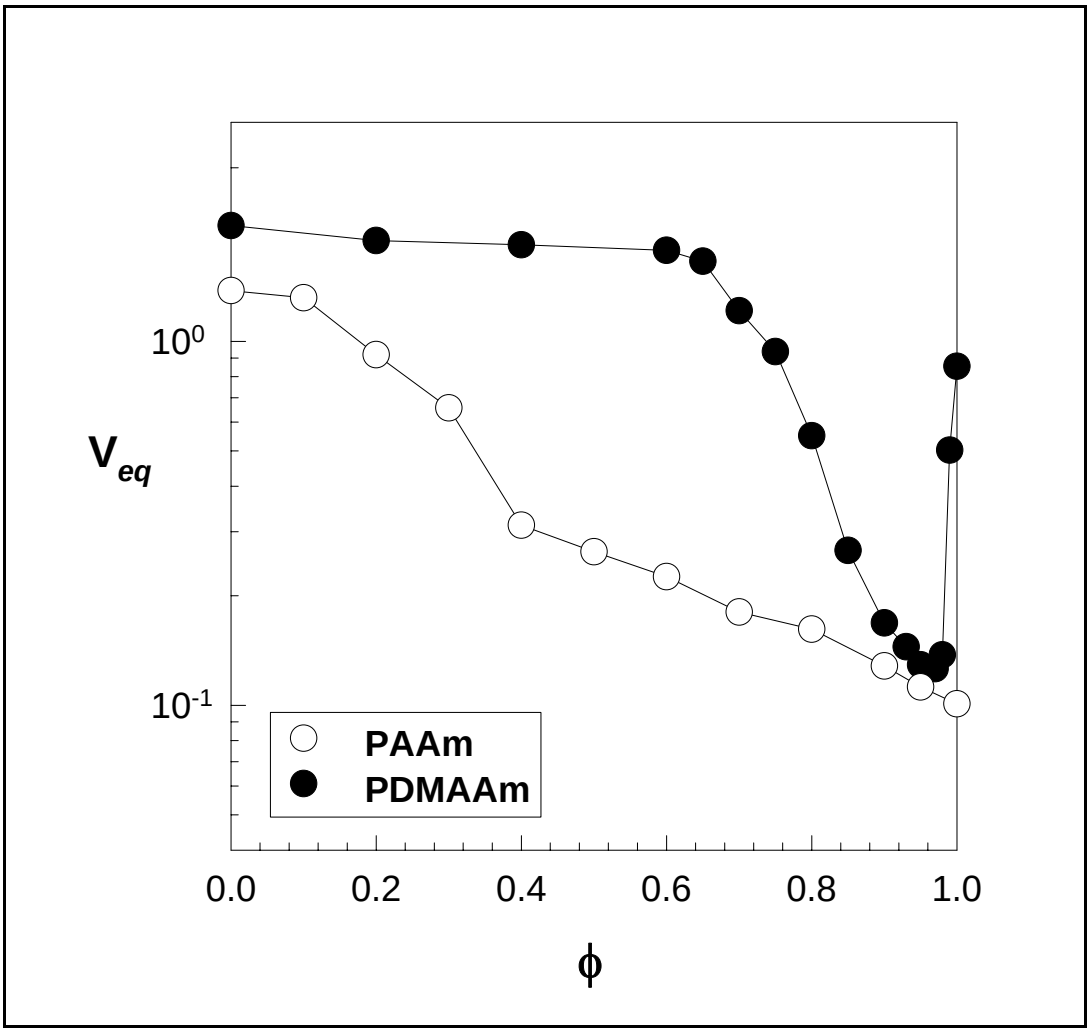

Figure 6.4: The equilibrium swelling ratio V_{eq} of PDMAAm (filled symbols) and PAAm (open symbols) hydrogels shown as a function of the acetone volume fraction ϕ in the external aqueous solution.

As can be seen from Figure 6.4, the volume of PDMAAm hydrogel in acetone (ϕ = 1) is about ten fold larger than that of PAAm hydrogel. This means that the incorporation of the methyl groups on the network chains creates attractive hydrophobic interactions between PDMAAm segments and acetone molecules.

Moreover, from the large swelling ratio of PDMAAm hydrogel in water, it can be concluded that DMAAm segments and water molecules also attract each other due to the hydrogen bonding interactions. Thus, the water and acetone molecules taken separately are good solvents for PDMAAm network. However, in mixtures prepared in the range of ϕ value between 0.65 and 1, the attractive acetone-water interactions together with the intramolecular hydrophobic forces within the PDMAAm network seem to dominate over the water - PDMAAm or acetone- PDMAAm interactions.

As a result, in this range of ϕ, addition of acetone to water or water to acetone decreases the solvent content of the gel, so that the gel contracts and attains a minimum volume at ϕ = 0.97 (Figure 6.4).

The experimental works in the literature also shows the importance of hydrogen bonding and the hydrophobic interactions in the solutions and gels of poly(N-monoalkylacrylamide) as well as in poly(N,N-dialkylacrylamide)[109–112]. Maeda et al. showed by IR spectroscopy that most of the C=O groups of poly(N,N-diethylacrylamide) (PDEAAm) in water or in water/methanol mixture are associated with water and methanol molecules through hydrogen bonds, even above the lower critical solution temperature (LCST). Although the ethyl groups of PDEAAm are also hydrated below the LCST, upon phase transition, most of these groups are dehydrated and associate through hydrophobic interaction [112].

To understand the relative magnitude of the intermolecular forces responsible for the reentrant conformation transition in PDMAAm hydrogels, their swelling behavior was also investigated in various organic solvent–water mixtures. In Figures 6.5 and 6.6, the experimental results are collected.

Figure 6.5(A) shows the equilibrium swelling ratio V_{eq} of PDMAAm hydrogels plotted against the volume fraction ϕ of DMSO, dioxane, and THF in the external aqueous solution. For comparison, the data obtained in acetone–water mixtures are also included in the figure. It is seen that except the DMSO–water system, all the organic solvent–water mixtures induce strong reentrant transitions in PDMAAm hydrogels. The deswelling of gel starts at ϕ between 0.4 and 0.65 while the reswelling of the collapsed gel occurs at ϕ values close to unity. In Figure 6.5(B), the magnified observation of the high ϕ range of Figure 6.5(A) is shown and the Figure indicates that the reswelling mainly occurs above ϕ = 0.97–0.99.

Thus, it can be concluded that the addition of a small amount of water into one of these organic solvents induces a collapse transition in PDMAAm hydrogel. These results also suggest that the trace amount of water existing in these organic solvents can be determined by monitoring the volume change of PDMAAm hydrogels.

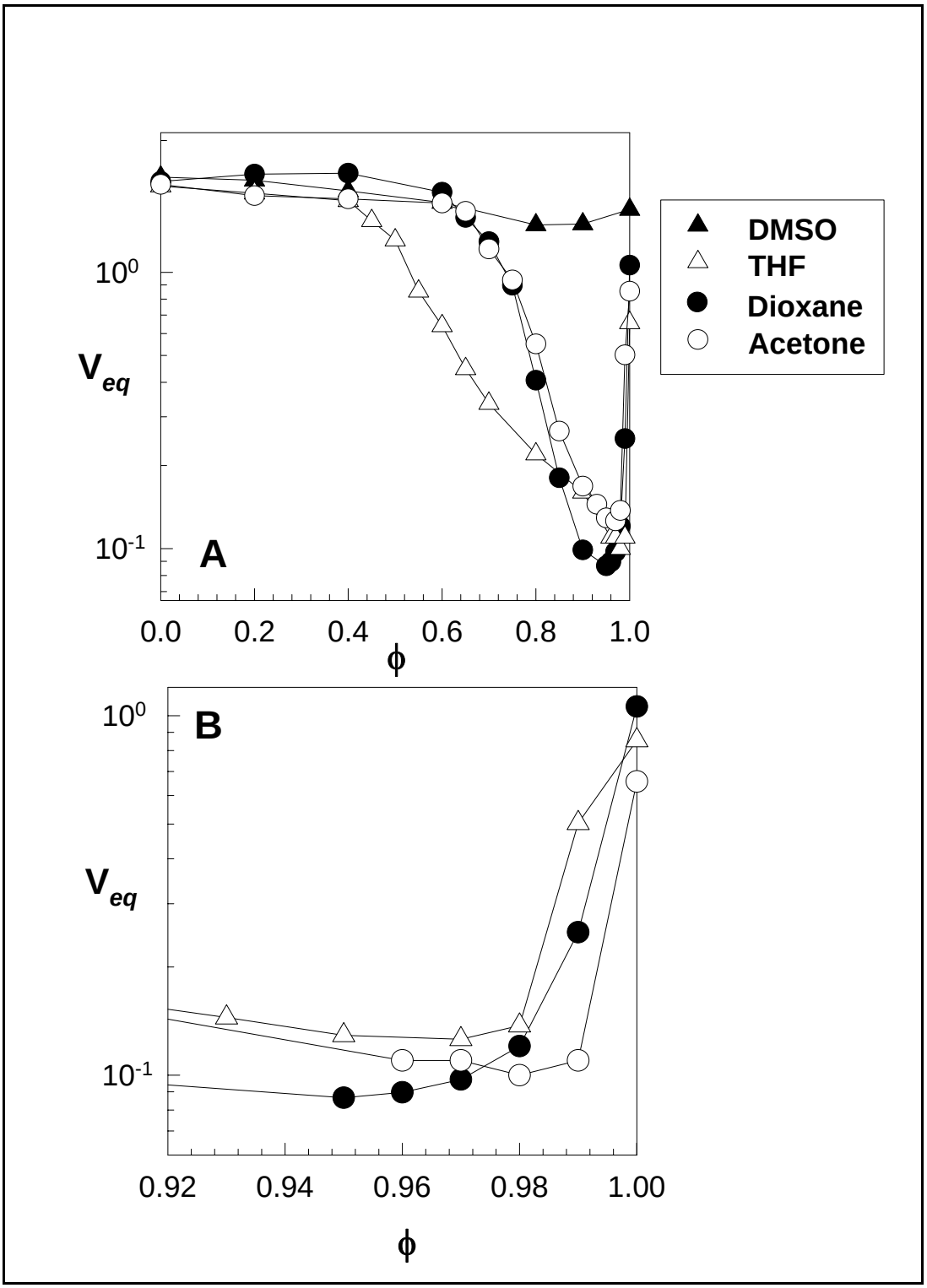

Figure 6.5: (A) The equilibrium swelling ratio V_{eq} of PDMAAm hydrogels shown as a function of the organic solvent volume fraction ϕ in the external aqueous solution. **(B)** shows the magnified observation of the high ϕ range of Figure 6.5A.

In Fig. 6.6, the swelling behavior of non-ionic PDMAAm hydrogels in aqueous solution of various alcohols is shown as a function of the alcohol volume fraction ϕ in the external aqueous solution. It is seen that in methanol or ethanol solutions, the

hydrogel remains in the swollen state over the entire range of ϕ. The reentrant transition in hydrogels appears in aqueous solutions of 1-propanol and t-butanol.

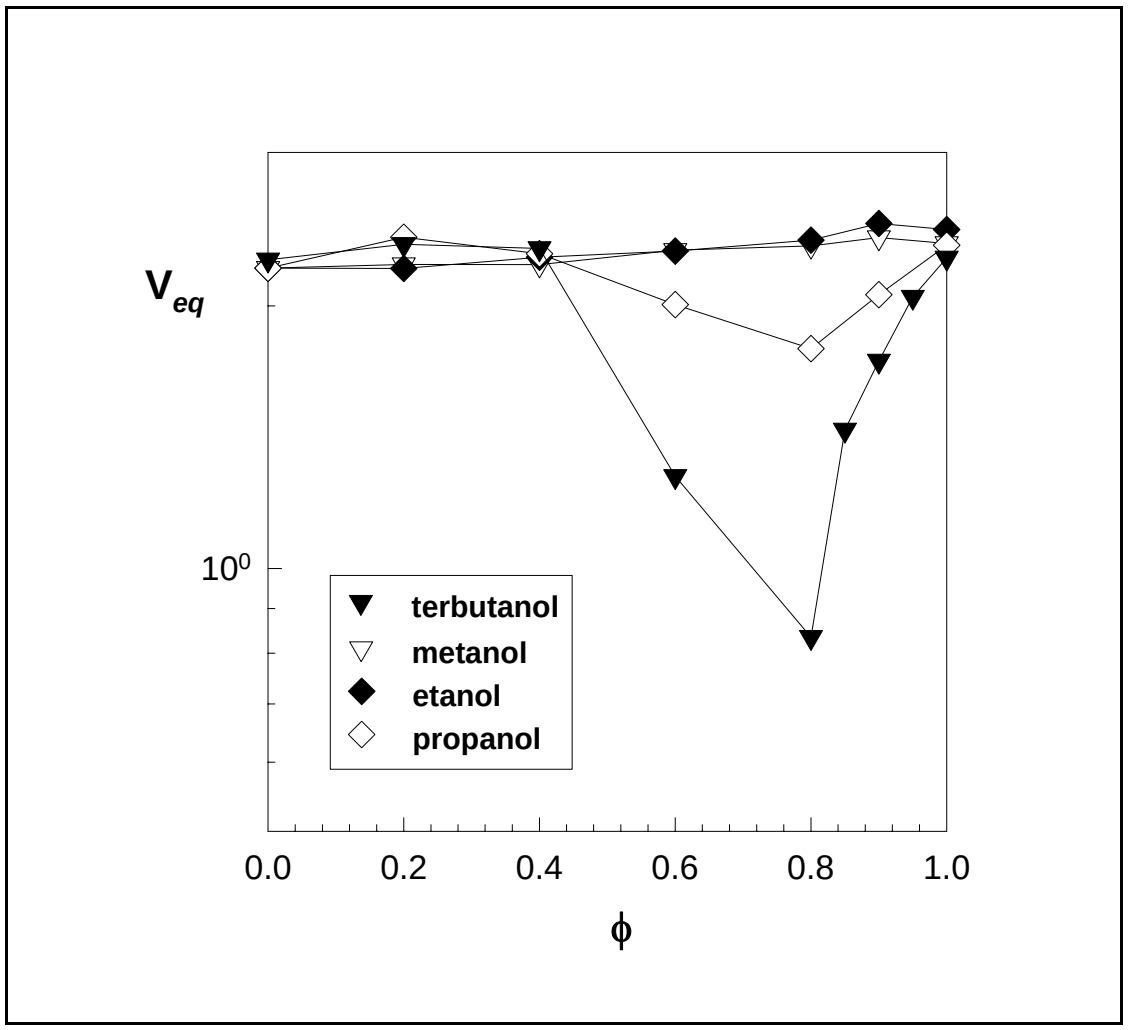

Figure 6.6: The equilibrium swelling ratio V_{eq} of PDMAAm hydrogels shown as a function of the alcohol volume fraction ϕ in the external aqueous solution. The alcohols used are indicated in the figure.

6.1.3.1. The Effect of Solvent Specificity on The Reentrant Transition

In order to understand the effect of the solvent specificity on the reentrant transition in PDMAAm hydrogels, the solubility parameters provide an easy numerical method to predict the extent of interactions in the system components. According to the Hildebrand theory, the properties of solvents are classified in terms of the solubility parameter δ[113]. Hansen separates the solubility parameter into three components due to dispersion forces δ_d, polar forces δ_p, and hydrogen bonding interactions δ_h [114]. It was observed that the polar and the hydrogen bonding components of the solubility parameter values vary depending on the type of the organic solvent used in

the swelling tests. For example, δ_p decreases from 12.3 to 5.7 $Mpa^{1/2}$ as the number of carbon atoms of the alcohols increases from one to four. Thus, the experimental results in Figure 6.6 shows that decreasing the polarity of the alcohols increases the extent of reentrant transition of PDMAAm hydrogels in aqueous alcohol solutions.

In the following, the extent of the reentrant transition is represented by V_{min}, which is the minimum volume of PDMAAm hydrogels recorded in a given water–organic solvent mixture. Thus, the lower V_{min}, the larger the volume change in the water–organic solvent mixture and the larger the extent of reentrant transition. Figure 6.7(A) shows V_{min} plotted against the hydrogen bonding component of the solubility parameter δ_h of the organic solvent. As δ_h decreases, the gel passes to a more collapsed state in the water–organic solvent mixture. Thus, acetone, THF, or dioxane forming moderate hydrogen bonds in the mixtures with water compared to alcohols and DMSO induce a strong reentrant conformation transition in PDMAAm hydrogels.

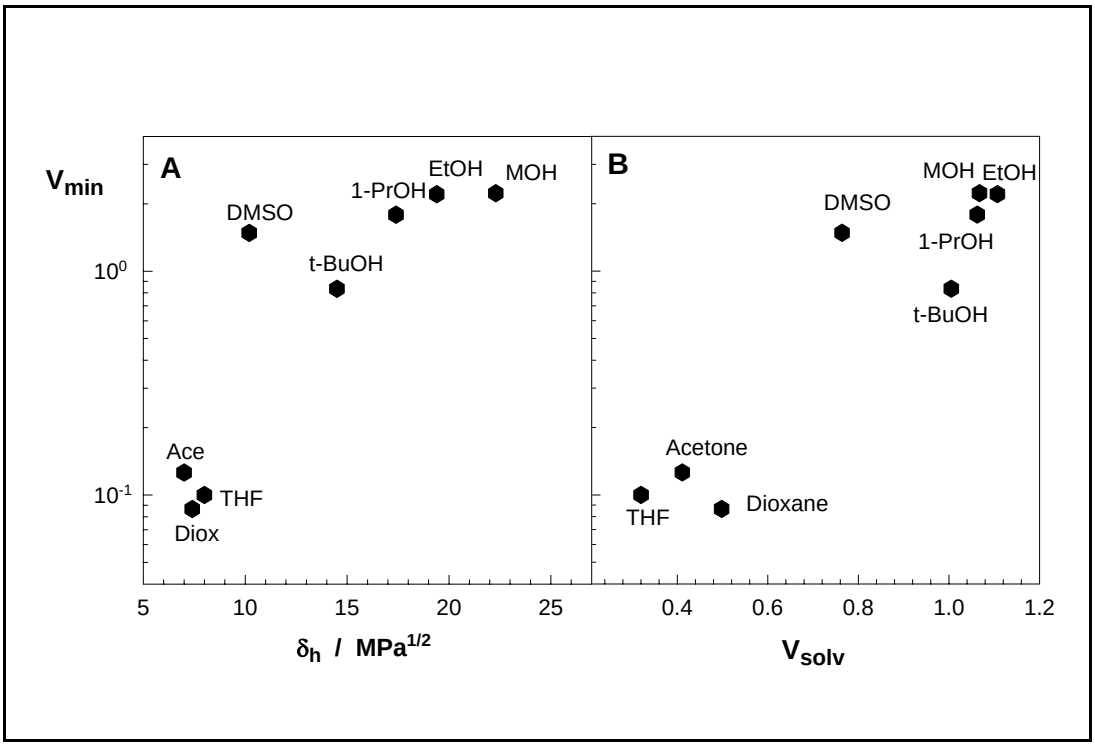

Figure 6.7: (A) The minimum gel volume V_{min} recorded in a given organic solvent – water mixture is shown as a function of the hydrogen bonding component of the solubility parameter δ_h of the organic solvent. **(B)** V_{min} is plotted against the normalized swelling ratio V_{solv} of PDMAAm hydrogels. MOH = methanol, EtOH = ethanol, 1-PrOH= 1-propanol, t-BuOH = t-butanol.

In Figure 6.7(B), V_{min} is plotted against the normalized swelling ratio V_{solv} of PDMAAm hydrogel in the pure organic solvent. It is seen that V_{min} decreases with decreasing swelling ratio of the gel in the organic solvent. Thus, the strong attractive interactions between the organic solvent and PDMAAm network represented by a high value of V_{solv} prevents the reentrant transition in PDMAAm hydrogels. The reentrant transition requires weak attractive interactions between PDMAAm network and the organic solvent.

The results thus suggest that a reentrant conformation transition in PDMAAm hydrogels requires a moderate hydrogen bonding organic solvent so that hydrophobic interactions dominate the swelling behavior of gels in the organic solvent. Although PDMAAm hydrogels remain in the swollen state in aqueous solutions of methanol or ethanol, PNIPA as well as TBA/AAm hydrogels exhibit strong reentrant conformation transitions in these solvent mixtures[11,17,18]. It seems that due to the less hydrophobic character of PDMAAm compared to PNIPA and TBA/AAm networks, less hydrogen bonds are needed between the organic solvent and water for the observation of the reentrant phenomenon in PDMAAm networks.

The phenomena shown in Figs. 6.4–7 can be explained as follows: The organic solvents acetone, THF, and dioxane are attracted by water through the hydrogen–bonding interactions. These organic solvents are also attracted by the PDMAAm hydrogel due to the hydrophobic interactions between the methyl groups of PDMAAm and the methyl or methylene groups of the organic solvent. The competing weak interactions between the organic solvent–water and organic solvent–PDMAAm network results in the reentrant swelling behavior of the hydrogel. Thus, when the organic solvent is added to water, the organic solvent molecules like to stay in the solution due to the interaction between the organic solvent and water, which reduces the gel swelling. The decrease in the gel swelling will increase the intramolecular hydrophobic interactions of the methyl groups of PDMAAm, which may promote further shrinkage of the PDMAAm hydrogel. Furthermore, at high values of ϕ, the attractive PDMAAm–organic solvent interactions dominate over the organic solvent–water interactions due to the increased number of contacts between organic solvent molecules and PDMAAm segments. As a result, organic solvent enters into the gel phase and results in gel swelling.

6.1.3.2. The Interaction Parameters and Partition of Organic Solvent Between Gel and Solution Phases

In this section, a theoretical investigation of the conditions for the reentrant phase transition of non-ionic PDMAAm networks immersed in an aqueous solution of organic solvents was presented. For this purpose, the three component gel system consisting of PDMAAm network, water and organic solvent was examined using the Flory-Huggins theory, as discussed in Section 2.4.4. In the following, the calculation results using Equations (2.75) and (2.76) are presented in terms of the partition parameter φ, and the interaction parameter χ_{13} between the organic solvent and the water. The parameters required for the solution of Equations (2.75) and (2.76) were evaluated as follows: Both ν_2^0 and *N* were determined experimentally. The values ν_2^0 = 0.056 and $N = 1.6\times10^3$ were used for the present simulation. In Section 6.1.2.1., the interaction parameter χ_{12} between the PDMAAm network and water was evaluated as $\chi_{12} = 0.48 + 0.33\nu_2$.

The interaction parameters χ_{23} between the PDMAAm network and the organic solvent was calculated from the swelling ratios of the hydrogels in pure organic solvents (Figures 6.4 – 6.7) together with the following equation:

$$\ln\left(1-\nu_2\right)+\nu_2+y\chi_{23}\nu_2^2+yN^{-1}\nu_2\left(\alpha^2-0.5\right)=0 \qquad (6.4)$$

The values found were χ_{23} = 0.124, 0.107, 0.116, and 0.114 for acetone, dioxane, THF, and DMSO, respectively. Also, y was calculated from the molar volumes of the solvents as 4.1, 4.7, 4.5, and 3.9 for acetone, dioxane, THF, and DMSO, respectively. After finding these parameters, the equations contain three unknown parameters: the polymer concentration in the gel phase ν_2, the partition parameter φ, and the interaction parameter χ_{13} between the organic solvent and water. Therefore, Equations (2.75) and (2.76) were solved for χ_{13} and φ as a function of ϕ in order to reproduce the experimental polymer concentrations ν_2 of non-ionic gels in solvent mixtures. The computer program which was used to calculate the critical parameters for the reentrant phase transition of non-ionic PDMAAm networks are already given in Appendix D.

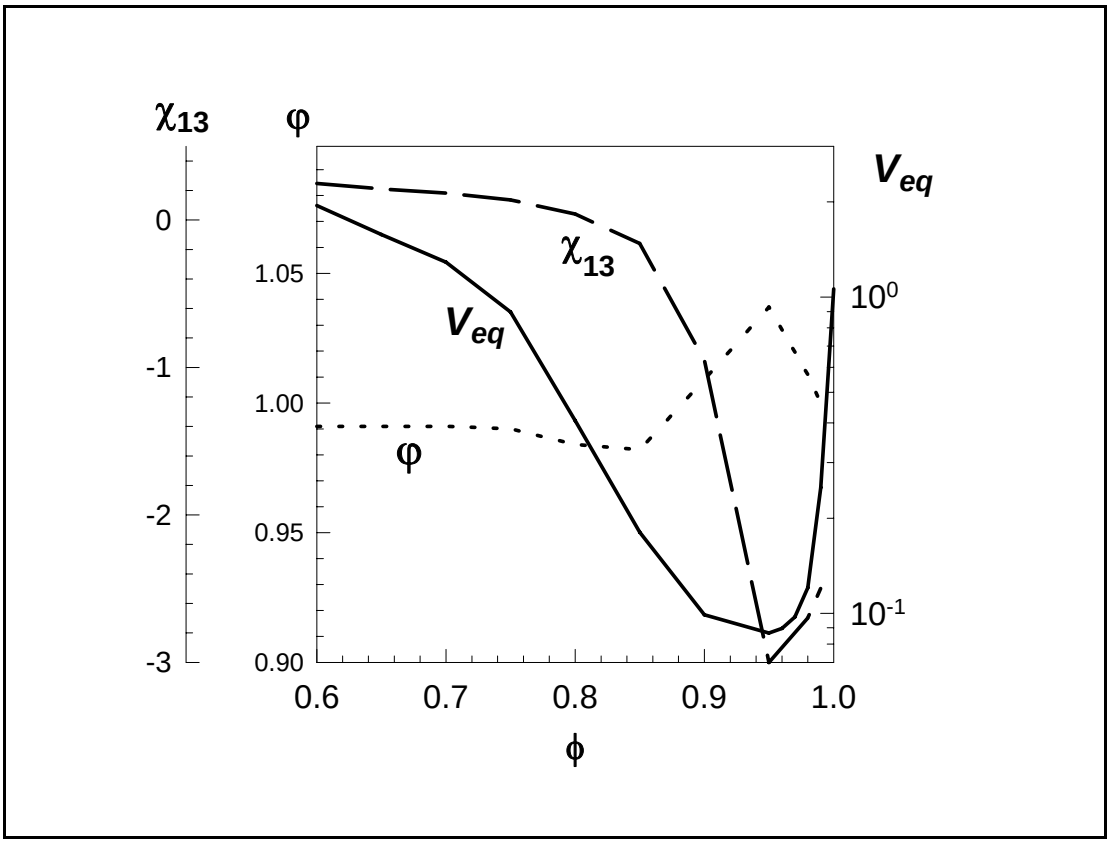

Figure 6.8: The interaction parameter between water and dioxane χ_{13} (dashed curve) and the partition parameter φ of dioxane between the gel and the solution phases (dotted curve) shown as a function of dioxane concentration ϕ in the external solution.

In Figure 6.8, the calculated values of χ_{13} (dashed curve) and φ (dotted curve) are plotted as a function of the dioxane volume fraction ϕ in the external solution. For comparison the experimental gel volume V_{eq} vs. ϕ dependence is also shown in the figure by the solid curve. Depending on the value of ϕ, three different regimes can be distinguished from Figure 6.8:

1. Between ϕ = 0.60 and 0.85, both the partition parameter φ and χ_{13} are decreasing functions of ϕ. Thus, the fraction of dioxane molecules penetrating into the PDMAAm network decreases as ϕ is increased. This is due to the predominant attraction of dioxane by water molecules locating in the external solution, which lowers both the swelling degree V_{eq} and the partition parameter φ.

2. Between ϕ = 0.85 and 0.95, χ_{13} rapidly decreases while the partition parameter φ increases, i.e. the solution inside the gel is enriched by dioxane as ϕ is increased. The opposite behavior of the partition parameter φ in this regime is due to the collapsed state of PDMAAm hydrogel. High polymer segment concentration inside the gel

together with the high dioxane concentration in the external solution increases the number of contacts between PDMAAm and dioxane so that dioxane molecules reenter the collapsed gel phase.

3. For $\phi > 0.95$, the collapsed gel starts to swell again due to the favorable PDMAAm–dioxane interactions now dominating the swelling process. In this regime, the gain in energy due to the increased number of contacts between PDMAAm and dioxane exceeds the attraction forces between water and dioxane. As a result, χ_{13} increases on rising ϕ, so that the volume of the network increases. At the same time, φ decreases again and approaches to unity due to the increase of the gel volume that facilitates the penetration of both water and dioxane molecules into the gel network.

In the case of PNIPA and TBA/AAm networks, the increase of the partition parameter φ is accompanied with the gel swelling [10,17,18,115]. As a result, the reswelling of the collapsed PNIPA or TBA/AAm gels occurs at a much lower concentration of the organic solvent than the PDMAAm gels do. Therefore, in the presence of these more hydrophobic networks, the reentrance of the organic solvent into the network and the associated energy gain compensate more than the water–organic solvent attractions so that the volume of the network increases.

However, due to the less hydrophobicity of PDMAAm network, a much higher organic solvent concentration is required to reswell the gel. This is the main characteristic of PDMAAm networks.

In Figure 6.9, the calculated values of χ_{13} and φ for PDMAAm hydrogels in aqueous solutions of acetone, THF, DMSO, are shown as a function of ϕ. Except the DMSO–water system, the shape of the dependence of χ_{13} and φ on ϕ is similar to that shown in Figure 6.8. The organic solvent molecules flow from the solution to the gel phase or vise versa depending on ϕ and results in the reentrant transition in PDMAAm hydrogels. In DMSO–water mixtures, χ_{13} does not change much with ϕ, so that the gel remains in the swollen state over the whole range of ϕ.

Moreover, the partition parameter φ remains below unity due to the conformational entropy of DMSO molecules. Since the penetration of DMSO with a size of $y = 3.9$

is accompanied by a loose of entropy of the DMSO molecules, DMSO concentration in the solution remains always higher than its concentration in the gel solution[108].

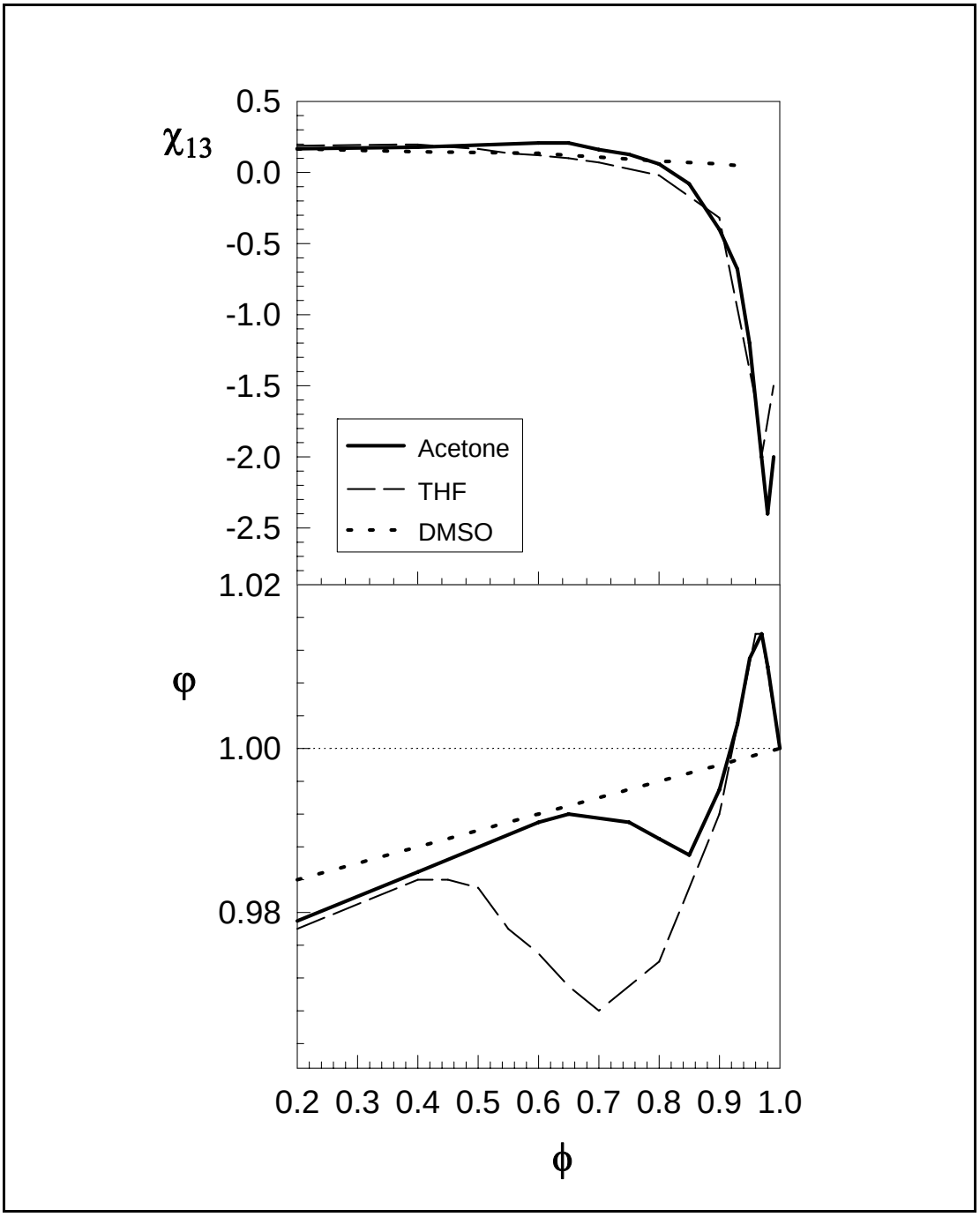

Figure 6.9: The interaction parameter between water and the organic solvent χ_{13} (A) and the partition parameter φ of the organic solvent between the gel and the solution phases (B) shown as a function of the organic solvent concentration ϕ in the external solution. The thin dotted line in Fig. 6.9B represents the relation φ =1.

6.1.4. Swelling of Ionic PDMAAm Hydrogels in Water and in Aqueous Salt Solutions

A series of ionic PDMAAm hydrogels were prepared by free-radical crosslinking copolymerization. Sodium salt of 2-acrylamido-2-methylpropane sulfonic acid (AMPS) was used as the ionic comonomer.

The crosslinker ratio X = 1/83 (the mole ratio of the crosslinker BAAm to the monomers DMAAm + AMPS) and the total monomer concentration was also fixed at 5.1 w/v% throughout the study. In order to obtain hydrogels with different charge densities, the mole fractions of the ionic comonomer AMPS in the monomer mixture x_i was varied between 0 and 1.

The swelling behavior of ionic hydrogels was investigated in water and in aqueous NaCl solutions. The concentration of NaCl solutions ranged from 10^{-5} to 1.0 M. The hydrogels equilibrium swollen in water were transferred to vials containing aqueous NaCl solution. The gel samples were allowed to swell in the solution for two weeks, during which aqueous NaCl was refreshed to keep the concentration as needed.

After the swelling equilibrium is established, swelling measurements were carried out by weighing the samples, or by measuring their diameters. The measured swelling data of ionic PDMAAm hydrogels in water were compared with that measured in aqueous salt solutions. The elastic modulus of the hydrogels were also measured both after preparation and after equilibrium swelling in water.

The results from swelling and elasticity tests are complied in Table 6.2. It is seen that the swelling ratio V_{eq} of the hydrogels increases from 1.55 to 253 with increasing AMPS content. Thus, ionic PDMAAm hydrogels are highly swollen in water.

A series of photographs taken from the equilibrium swollen hydrogels are also shown in Figure 6.10 illustrates the the effect of charge density on the swelling capacity of hydrogels.

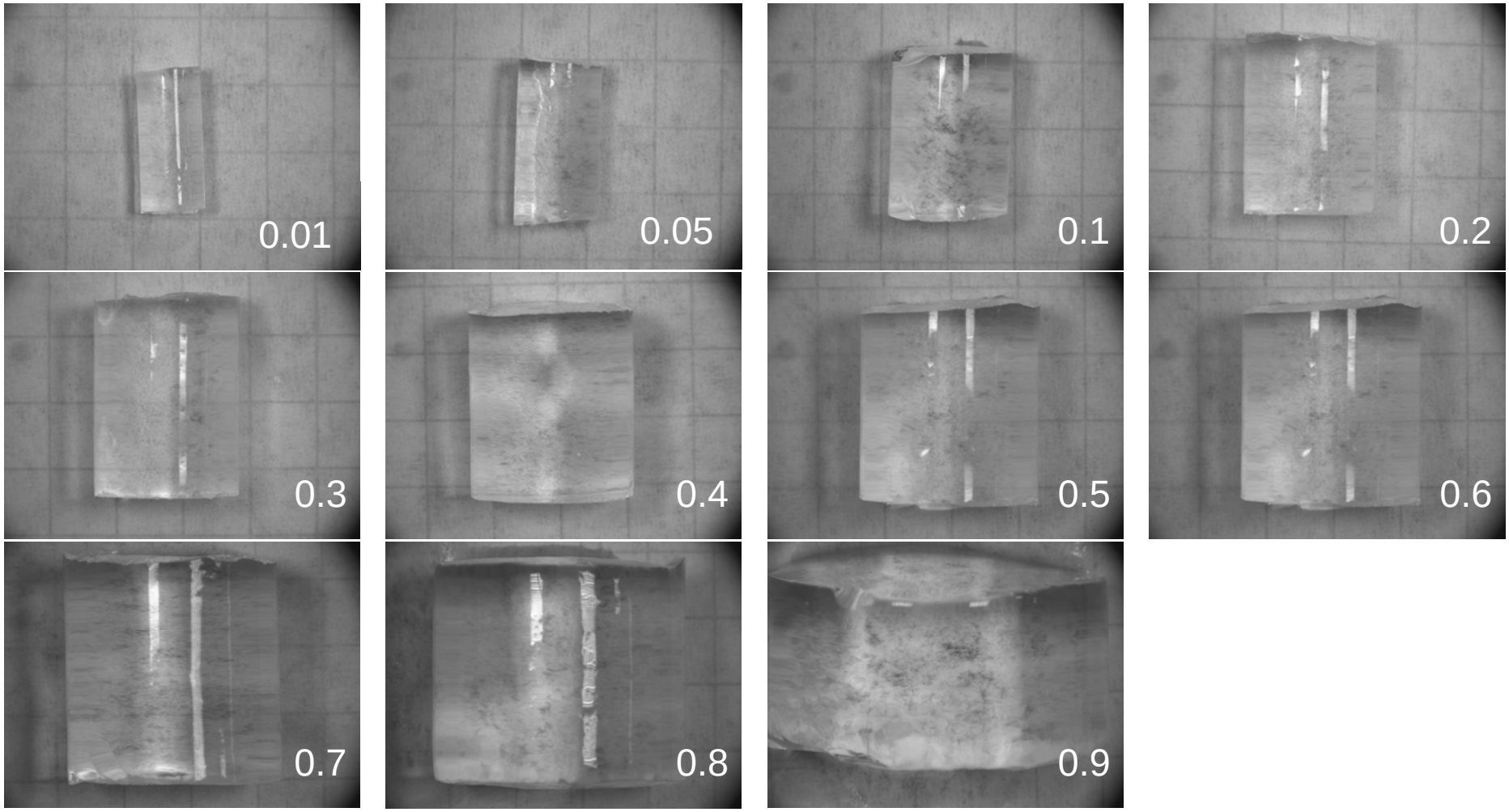

Figure 6.10: A series of photographs taken after the equilibrium swelling of ionic PDMAAm hydrogels. The mole fractions of AMPS in the monomer mixture x_i, are indicated in the figure.

Table 6.2: The characteristic data of ionic PDMAAm hydrogels in water. x_i = the mole fraction of the ionic comonomer AMPS in the monomer mixture, q_v = the equilibrium volume swelling ratio of the hydrogels in water.

x_i	$\nu^0_{2,theo}$	G_0 / Pa	G / Pa	V_{eq}	q_v	$\nu_{2,eq}$
0	0.04086	4188.62	3861.54	1.5513	37.9666	0.02634
0.01	0.041395	4435.49	3426.49	2.7310	65.9744	0.01516
0.05	0.043537	4500.07	4116.06	6.5097	149.522	0.00669
0.07	0.044607	4531.34	4131.32	7.7940	174.727	0.00572
0.1	0.046213	4297.75	5095.04	11.1340	240.938	0.00415
0.2	0.051566	3633.36	7656.68	16.6040	321.99	0.00311
0.3	0.056919	3328.05	8040.99	21.6300	380.008	0.00263
0.4	0.062272	2599.52	7660.26	28.0910	451.101	0.00222
0.5	0.067625	2458.22	7313.37	36.3640	537.725	0.00186
0.6	0.072978	1920.51	5298.37	47.1140	645.59	0.00155
0.7	0.078331	1464.17	4105.05	60.0770	766.968	0.0013
0.8	0.083684	976.277	2115.87	117.1500	1399.87	0.00071
0.9	0.089037	523.84	706.49	253.0400	2841.98	0.00035
1	0.09439	98.83	*a*	*a*	*a*	*a*

a- This sample was too weak to withstand the mechanical and swelling measurements at the swelling equilibrium.

In Figure 6.11, the equilibrium volume swelling ratio q_v of ionic PDMAAm hydrogels in water and in aqueous NaCl solutions is plotted as a function of the mole fraction of AMPS in the comonomer feed x_i. Figure 6.11 shows that the equilibrium degree of swelling of the hydrogels in water increases slightly with increasing ionic group content. This is a consequence of the osmotic pressure exerted by the counterions of AMPS units in the network chains.

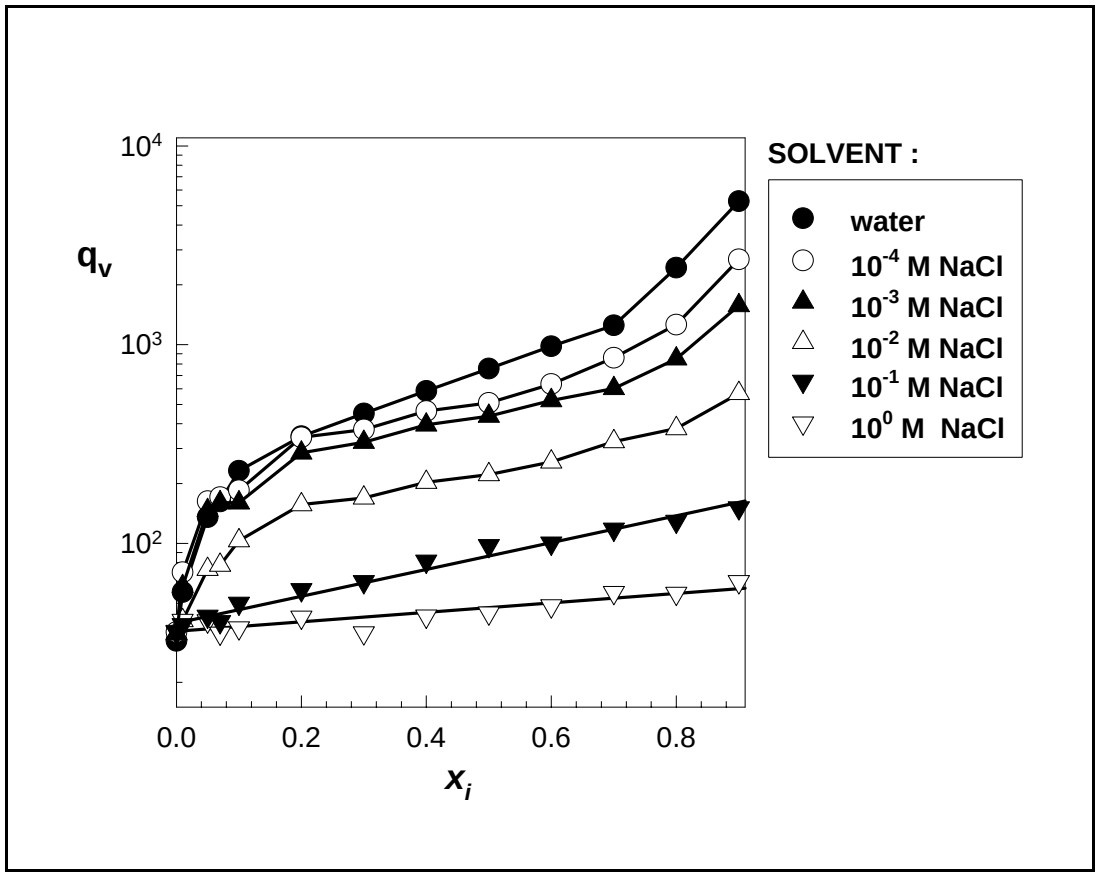

Figure 6.11: Variation of the volume swelling ratio q_v of ionic PDMAAm hydrogels in water and in aqueous NaCl solutions with the mole fraction of AMPS in the comonomer feed x_i.

Increasing the ionic group content of the hydrogels increases the number of the fixed charges in the gel ($-SO_3^{2-}$). Moreover, as x_i increases, the mobile counterion concentration (Na^+) inside the gel also increases to maintain the electroneutrality condition. As a result, the difference between the mobile ion concentration inside and outside the gel increases with increasing x_i, which creates an additional osmotic pressure that expands the gel. According to Equation (2.64), this osmotic pressure increases as the concentration of the counterions increases. The degree of equilibrium swelling of the hydrogels increases with increasing ionic group content or with decreasing salt concentration in the external solution as was expected.

In Figure 6.12, q_v values of the hydrogels is shown as a function of the NaCl concentration in the external solution. The swelling ratio of hydrogels decreases with increasing salt concentration in the external solution; this is due to a decrease in the concentration difference of counterions inside and outside the hydrogel. The decrease in q_v is first rapid up to 10^{-2} M NaCl concentration. As the NaCl concentration

further increases, the decrease in q_v slows down and between 10^{-1} and 10^0 M NaCl, q_v values remains almost constant or slightly decreases with increasing salt concentration.

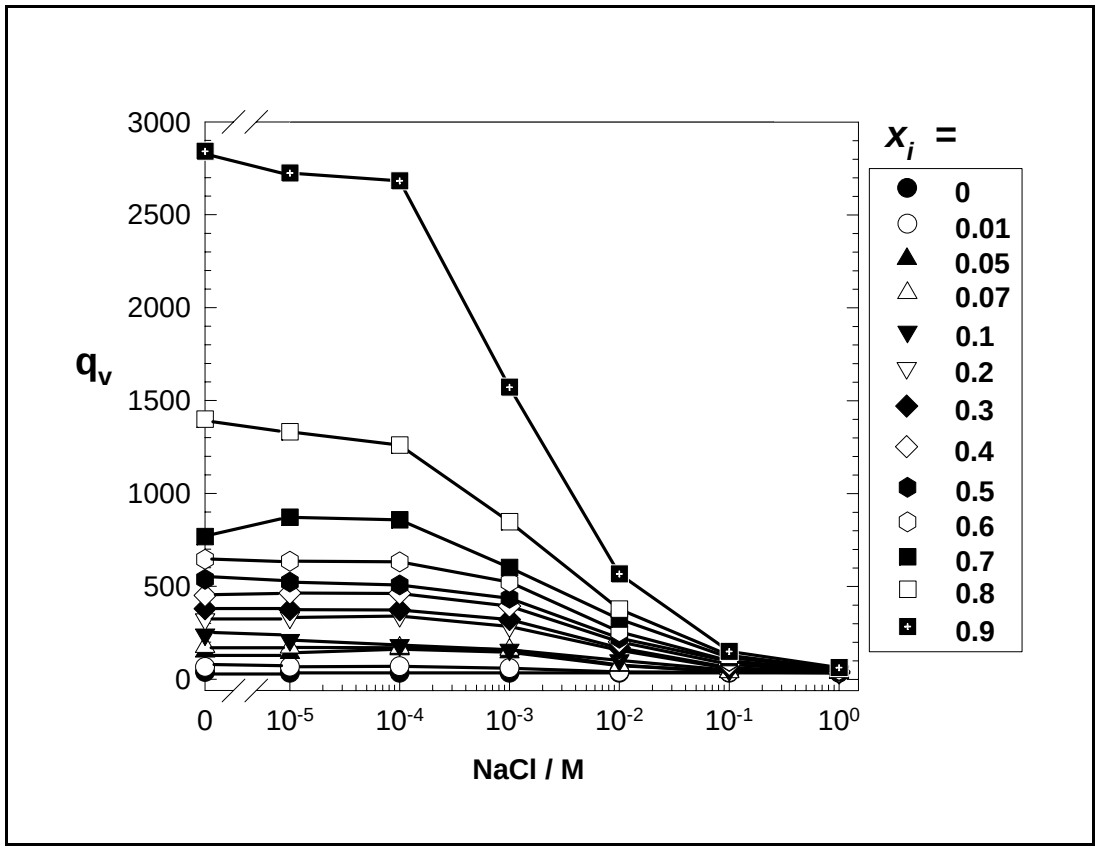

Figure 6.12: The equilibrium volume swelling ratio q_v of the hydrogels shown as a function of the NaCl concentration in the external solution. The solid curves only show the trend of the data.

During the swelling of ionic PDMAAm hydrogels in water, the charge density in PDMAAm network is higher than in the external solution (water). Thus, water molecules tend to enter the gel phase and the gel swells. However, in case of swelling of the ionic hydrogels in concentrated NaCl solutions, the mobile counterion concentration (Na^+) in the external solution is higher than in the gel phase, which results in an osmotic pressure that water molecules inside the gel flow from the gel to the solution phase so that the gel deswells.

6.1.5. Swelling of Ionic PDMAAm Hydrogels in Solvent Mixtures

The swelling measurements of ionic PDMAAm hydrogels in solvent mixtures were carried out gravimetrically due to the deformation of the gel samples during their

deswelling period under poor solvent condition. The weight of the hydrogels equilibrium swollen in solvent mixtures was measured after blotting the excess surface solvent. The normalized weight swelling ratio of the hydrogels with respect to their swelling ratio in water m_{rel} was calculated using the Equation (5.8).

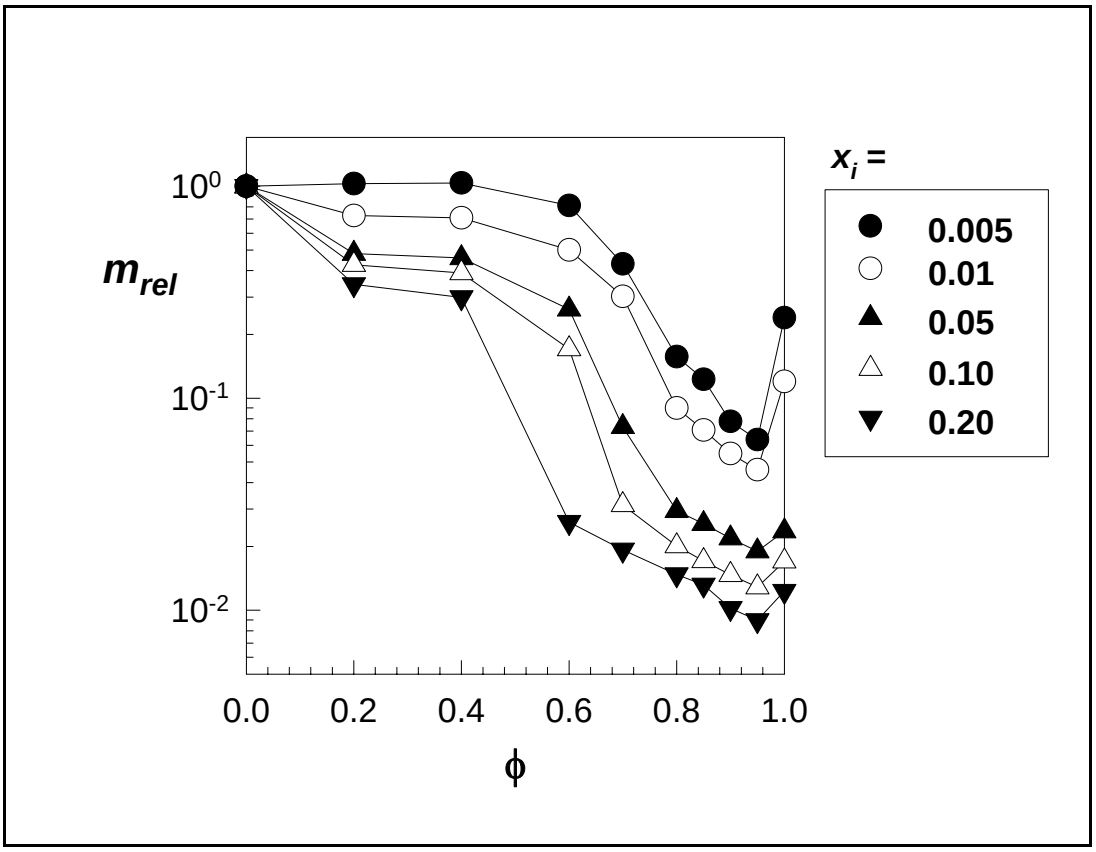

Figure 6.13: The relative weight swelling ratio m_{rel} of ionic PDMAAm hydrogels shown as a function of acetone volume fraction ϕ in the external aqueous solution.

Figure 6.13 shows the effect of the charge density on the swelling behavior of PDMAAm gels in acetone–water mixtures. The relative weight swelling ratio m_{rel} of gels of various charge densities is plotted against the acetone volume fraction ϕ in the external solution. As shown in the figure, ionic PDMAAm hydrogels exhibit reentrant transition at low charge densities. However, the reentrant transition gradually disappears and becomes a deswelling transition at high charge densities. Also, the acetone concentration ϕ required for the deswelling transition shifts to smaller values while the reswelling transition becomes weaker as the gel charge density is increased.

The swelling behavior of ionic PDMAAm hydrogels in water–acetone mixtures is closely related with the ion pair formation. As is well known, the fraction of ions

forming ion pairs in the gel strongly depends on the dielectric constant of the gel phase[116]. The formation of ion pairs is more pronounced for solutions with a lower solvent dielectric constant ε. A decrease in ε increases the probability of ion pairing and results in the deswelling of the gel. Because ε of acetone is 21 compared to the value of ε=80 for water, the counterions that are free in water bind tightly in the acetone environment to the AMPS units to form ion pairs.

Thus, ionic PDMAAm gels deswell with increasing acetone content in the solution so that the reentrant transition gradually becomes a deswelling transition at high AMPS contents.

6.2. Elasticity of PDMAAm Hydrogels

The uniaxial compression measurements were performed on both non-ionic and ionic PDMAAm hydrogels just after their preparation as well as after equilibrium swelling in water. All the mechanical measurements were conducted in a thermostated room at 24 ± 0.5°C. The elastic modulus of the hydrogels was determined from the slope of stress-strain isoterms by using Equation (5.10). The examples of calculations of the characteristic data of hydrogels from mechanical measurements are given in Appendix C.

6.2.1. The Elasticity of Non-ionic PDMAAm Hydrogels After Their Preparation

PDMAAm gels formed at various polymer network concentrations were subjected to the elasticity tests just after their preparation. Typical stress-strain are shown in Figure 6.14 for non-ionic PDMAAm hydrogels with varying polymer network concentrations ν_2^0.

The results from the swelling measurements and the elastic modulus measurements of non-ionic PDMAAm hydrogels formed at various polymer network concentrations after preparation are collected in Figure 6.15. In Figure 6.15A, the volume fraction of crosslinked polymer in the equilibrium swollen gel $\nu_{2,eq}$ is plotted as a function of ν_2^0. In Figure 6.15B, the elastic modulus after preparation G_0 is shown as a function of the volume fraction of crosslinked polymer after preparation ν_2^0.

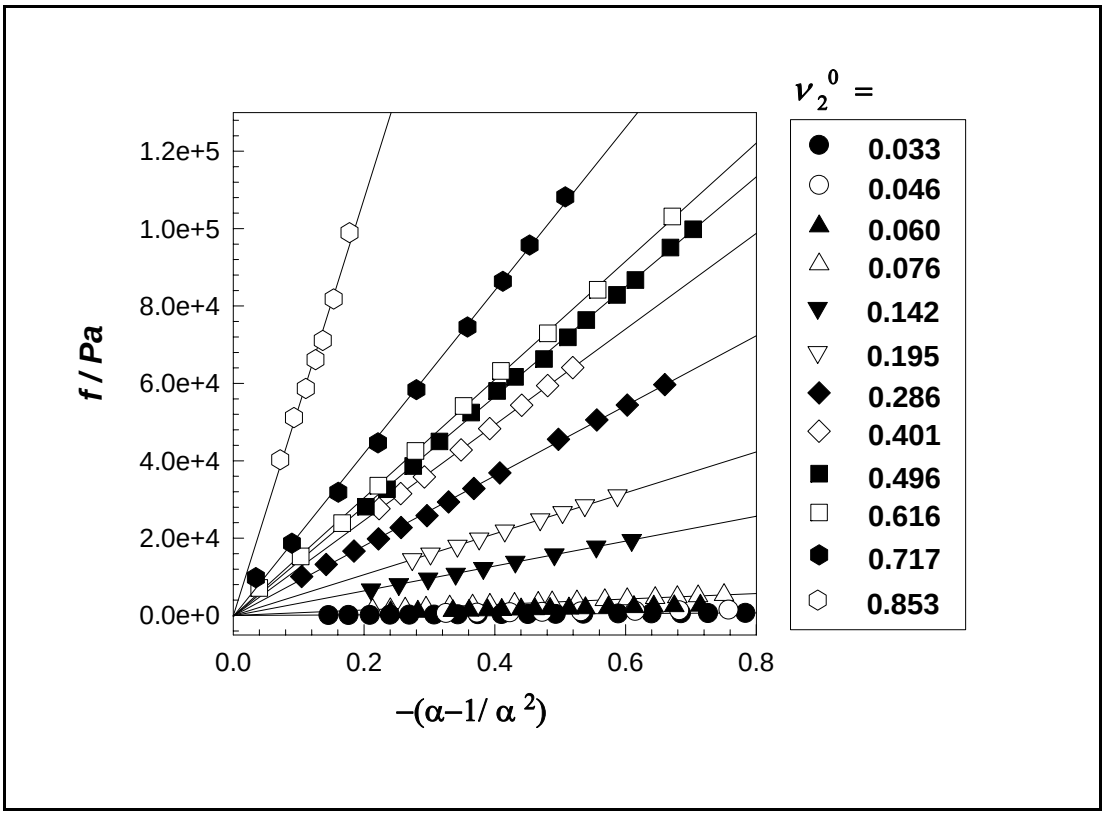

Figure 6.14: Typical stress – strain data for PDMAAm hydrogels just after their preparation. The crosslinked polymer concentrations ν_2^0 are indicated in the Figure.

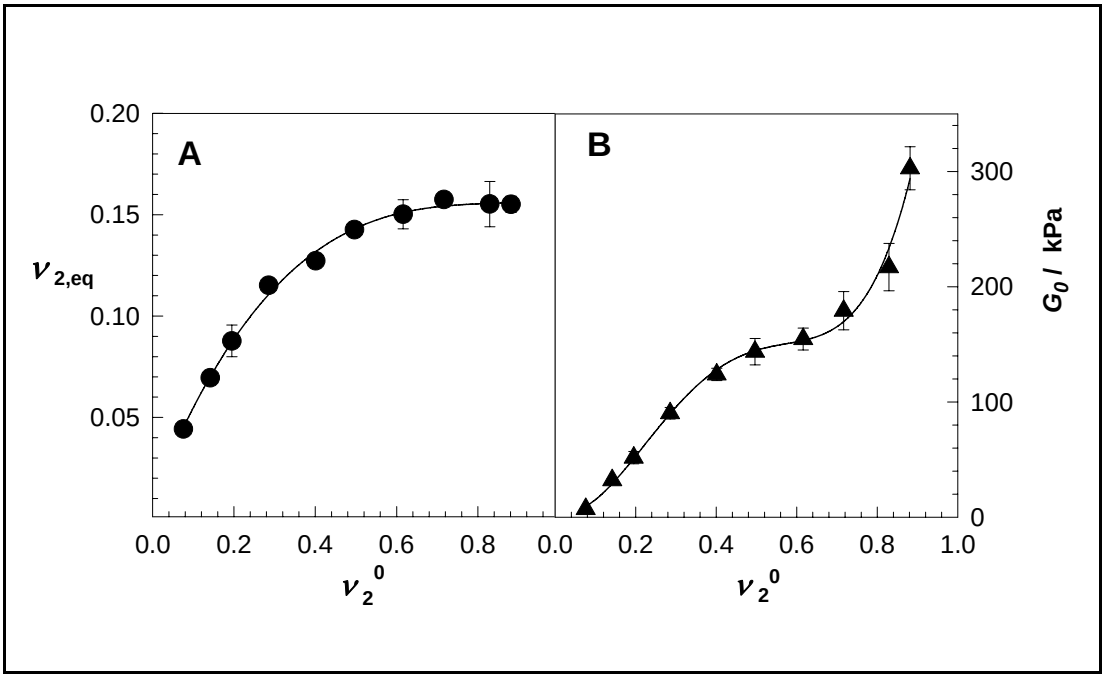

Figure 6.15: (A) The volume fraction of crosslinked polymer in the equilibrium swollen hydrogel $\nu_{2,eq}$ shown as a function of ν_2^0. (B) Elastic modulus of hydrogels after preparation G_0 shown as a function of ν_2^0.

6.2.1.1. The Crosslinking Efficiency and Effective Crosslink Density of Non-ionic PDMAAm Hydrogels

The crosslinking efficiency ε_{xl} that is the fraction of BAAm forming effective crosslinks can be calculated as:

$$\varepsilon_{xl} = \frac{\nu_e}{\nu_{chem}} \tag{6.5}$$

where ν_e the effective crosslink density and ν_{chem} is the chemical crosslink density of the hydrogels. Assuming phantom network behavior ($\phi = 4$), the effective crosslink densities ν_e of the hydrogels were calculated using the G_0 and ν_2^0 of the hydrogels together with Equation (3.61). These data are collected in the last column of Table 6.1. The results of calculations are also shown in Figure 6.16 as symbols plotted against ν_2^0.

The chemical crosslink density of the hydrogels ν_{chem} is defined as the BAAm % used in the gel preparation. If one assumes that all the crosslinker molecules from effective crosslinks in the final network, the chemical value of ν_{chem} can be calculated from the following equation;

$$\nu_{chem} = \rho \frac{2X}{M_r} \tag{6.6}$$

where X is the crosslinker ratio, i.e., the molar ratio of crosslinker to the monomer, and M_r is the molecular weight of the polymer repeat unit. (Since X = 1/82, ν_{chem} = 298 mol.m^{-3} and constant over all ν_2^0 range). Thus, ε_{xl} gives the fraction of the crosslinker BAAm molecules consumed in the formation of the effective crosslinks. In Figure 6.16, the dashed curve represents the crosslinking efficiency ε_{xl} as a function of ν_2^0. As seen from Figure 6.16, the effective crosslink density ν_e is not a monotonic function of the polymer concentration ν_2^0. The nonlinear curve fit to the experimental ν_e vs. ν_2^0 data given in Figure 6.16 gives the following relation:

$$\nu_e \text{ (mol.m}^{-3}) = -69 + 2389\nu_2^0 - 5389\left(\nu_2^0\right)^2 + 3610\left(\nu_2^0\right)^3 \quad (\text{for } \nu_2^0 < 0.7) \qquad (6.7)$$

Depending on the value of ν_2^0, three different regimes can be distinguished from Figures 6.15 and 6.16:

1. Regime: For ν_2^0 < 0.3, both $\nu_{2,eq}$ and ν_e are increasing functions of ν_2^0. Thus, increasing the polymer network concentration at the gel preparation ν_2^0 results in decreased swelling ratios and increased effective crosslink densities of the hydrogels. This is expected due to the fact that increasing polymer concentration during the gel formation decreases the probability of the cyclization and the multiple crosslinking reactions. Therefore, the crosslinking efficiency ε_{xl}, shown in Figure 6.16 by the dashed curve, rapidly increases from 0.2 to 0.9 on rising ν_2^0. The importance of cyclization at low ν_2^0 can also be seen from the ν_e vs. ν_2^0 dependence, which intersects the abscissa at a nonzero ν_2^0 value.

2. Regime: For 0.3 < ν_2^0 < 0.7, $\nu_{2,eq}$ increases slightly, while both the effective crosslink density and the crosslinking efficiency decrease with increasing ν_2^0. In this regime, since the polymer concentration is relatively high (30-70 % after complete monomer conversion), the pendant vinyl groups during the gel formation tend to have lower relative reactivities because of the steric hindrance. The experimental works in the literature also show that the accessibility of the pendant vinyl groups for other polymer molecules is strongly reduced at high monomer concentrations[7,11,43-45]. The calculations indicate a 1-2 orders of magnitude decrease in the average reactivity of the pendant vinyls for intermolecular reactions compared to the monomeric vinyls. As a result, a fraction of pendant vinyl groups remains unreacted in the final hydrogel leading to the observed decrease in the crosslink density of gels on rising ν_2^0. The results thus show that the gel passes from the first to the second regime at ν_2^0 = 0.3, at which the gel crosslink density becomes maximum. The crosslinking efficiency ε_{xl} decreases as going downward from the maximum point to the lower or higher polymer concentrations, due to the cyclization and steric effects, in the first and second regimes, respectively [83,85,117,118].

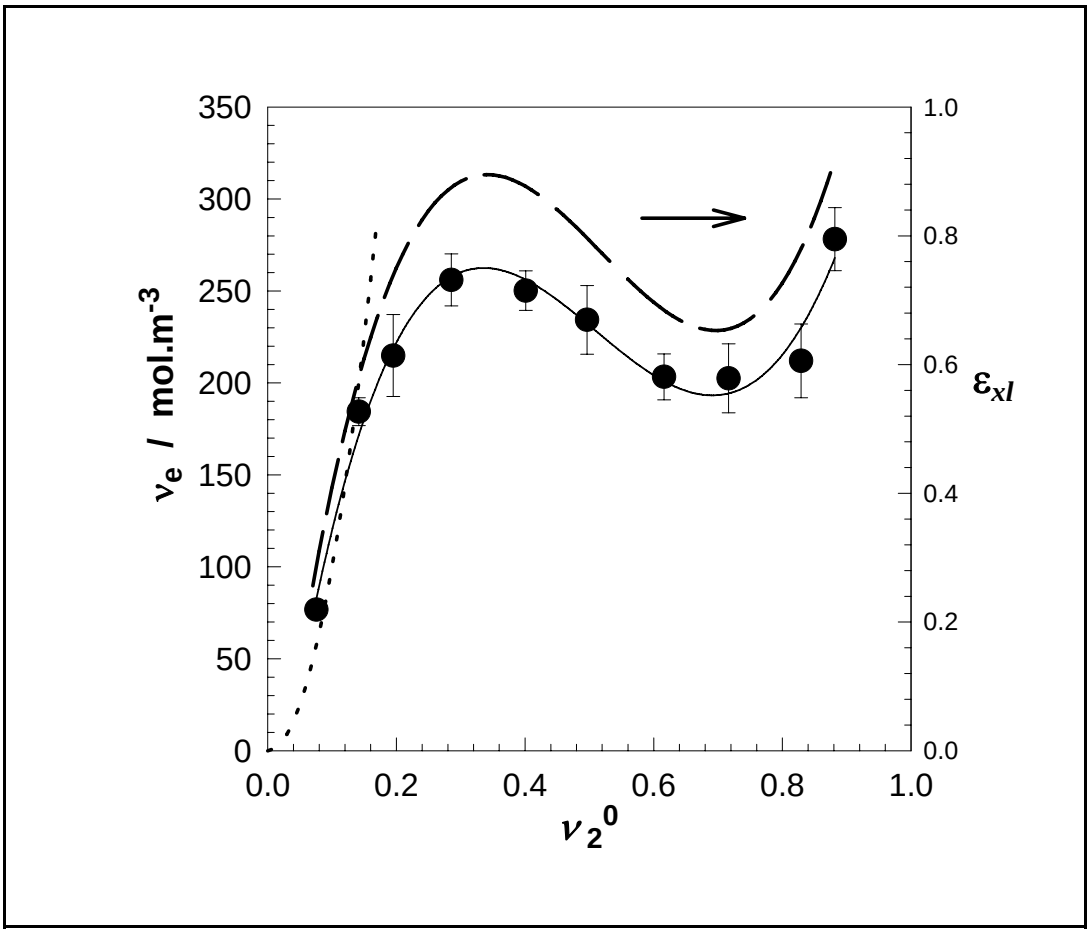

Figure 6.16: The effective crosslink density ν_e of the hydrogels shown as a function of ν_2^0. The solid curve shows the trend of data. The crosslinking efficiency of BAAm ε_{xl} is also shown in the Figure by the dashed curve. The dotted curve was calculated using Equation (3.68).

3. Regime: For $\nu_2^0 > 0.7$, $\nu_{2,eq}$ does not change with ν_2^0 but the modulus of gels after preparation G_0 and therefore, the effective crosslink density ν_e increase sharply with increasing ν_2^0. The rapid increase of G_0 with increasing monomer concentration in this high concentration regime may be interpreted as the transition of the polymer from the rubbery to the glassy state by decreasing the water content of the system. However, $\nu_2^0 = 0.7 - 0.9$ corresponds to a water content of 10 to 30 %. This means that the hydrogels are in the rubbery state during the mechanical measurements, and the observed behavior cannot be explained with the overall rubbery-to-glassy transition of the gels. A more plausible explanation is the effect of spatial gel inhomogeneities. Since the glass transition temperature increases with an increasing degree of crosslinking because more thermal energy will be needed for the system to become rubbery, the highly crosslinked regions will pass from the rubbery

to the glassy state earlier (i.e., at lower ν_2^0 values) than the other regions. The rapid increase in the gel modulus with ν_2^0 in this regime can thus be explained with the glassy transition of the highly crosslinked and therefore less swollen regions of the hydrogel sample.

In order to quantify the dependence of the effective crosslink density of PDMAAm gels on the monomer concentration ν_2^0, the statistical model proposed by Bromberg et al. was used[54]. In this model, the effective crosslink density of the hydrogels scales with the second power of the monomer concentration ν_2^0 through the relation, $\nu_e \approx (\nu_2^0)^2$ which was derived in Section 3.7. The dotted curve in Figure 6.16 represents ν_e versus ν_2^0 dependence predicted by Equation (3.68). It is seen that the model only predicts the initial increase of the crosslink density with concentration ν_2^0. Over the whole range of ν_2^0, real behavior of gels strongly deviates from the prediction of Equation (3.68). This is mainly due to Equation (3.66), which assumes a constant probability *p* for the growing chain to form crosslink. In real systems, *p* varies depending on the microenvironment of the growing chains because of the intramolecular crosslinking reactions as well as conversion dependent reactivities of the pendant vinyl groups, which were not considered in the model. Therefore, the experimental results show three different regimes for the dependence of the gel properties on the monomer concentration, which have not been predicted by the theories[105].

6.2.2. The Elasticity of Non-ionic PDMAAm Hydrogels After Equilibrium Swelling in Water

The PDMAAm gels were also subjected to the elasticity test after equilibrium swelling in water. In Figure 6.17, the elastic modulus of the hydrogels after equilibrium swelling in water *G* are shown as a function of ν_2^0. For comparison the modulus of the hydrogels after preparation G_0 are also shown in the Figure.

It is seen that, the elastic modulus of gels after equilibrium swelling in water *G* are lower than that of after preparation G_0. This result is expected since the swelling of gels reduces the polymer network concentration so that *G* becomes smaller than G_0 for Gaussian chains. For a homogeneous network of Gaussian chains, the elastic

modulus of gels swollen to equilibrium G relates to the network crosslink density through the Equation (3.63). Since $\nu_2 < \nu_2^0$ for hydrogels swollen to equilibrium, the elastic modulus of gels swollen to equilibrium G should be less than that of the same gel after its preparation.

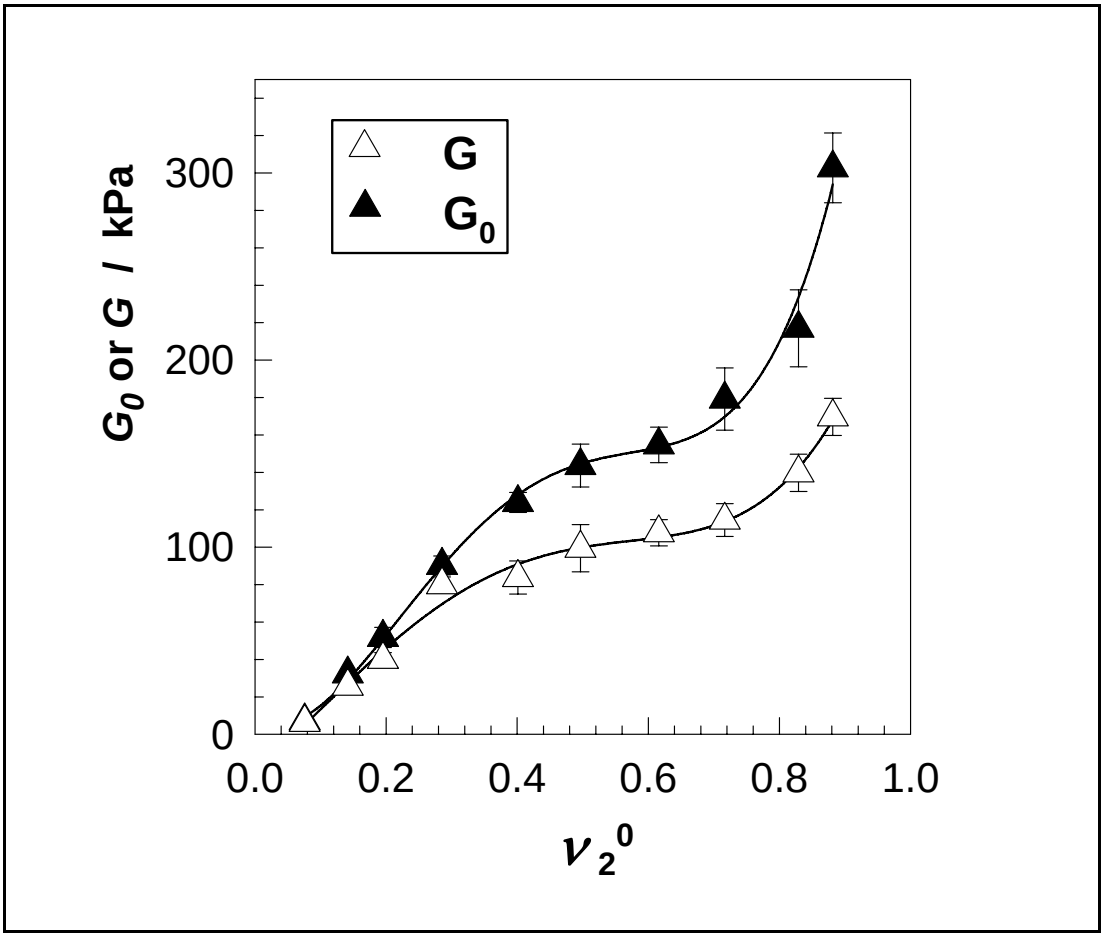

Figure 6.17: The elastic modulus of non-ionic PDMAAm hydrogels after preparation G_0 (filled symbol) and after equilibrium swelling in water G (open symbols) shown as a function of ν_2^0.

6.2.2.1. Gaussian Behavior of Swollen PDMAAm Hydrogels

The reduced modulus of gels at a given degree of swelling was calculated using the Equation (3.62) and the results were collected in Table 6.1. In Figure 6.18, the reduced modulus G_r of non-ionic PDMAAm hydrogels is plotted against the equilibrium gel volume V_{eq}.

For a network of Gaussian chains, one may expect a continuous decrease of G_r with the gel swelling due to the decrease of the concentration of the elastically effective

network chains. Figure 6.18 shows good relation with the theory. The modulus monotonically decreases as the gel swells beyond its swelling degree after preparation.

According to Equation (3.62), the double-logaritmic G_r versus V_{eq} plot should exhibit a slope of -1/3 for Gaussian chains. The solid curve is the best fit to the experimental data, which gives an exponent –0.32, close to the theoretical value of -1/3. Thus, it can be concluded that non-ionic PDMAAm hydrogels swollen to equilibrium in water behave as Gaussian[105].

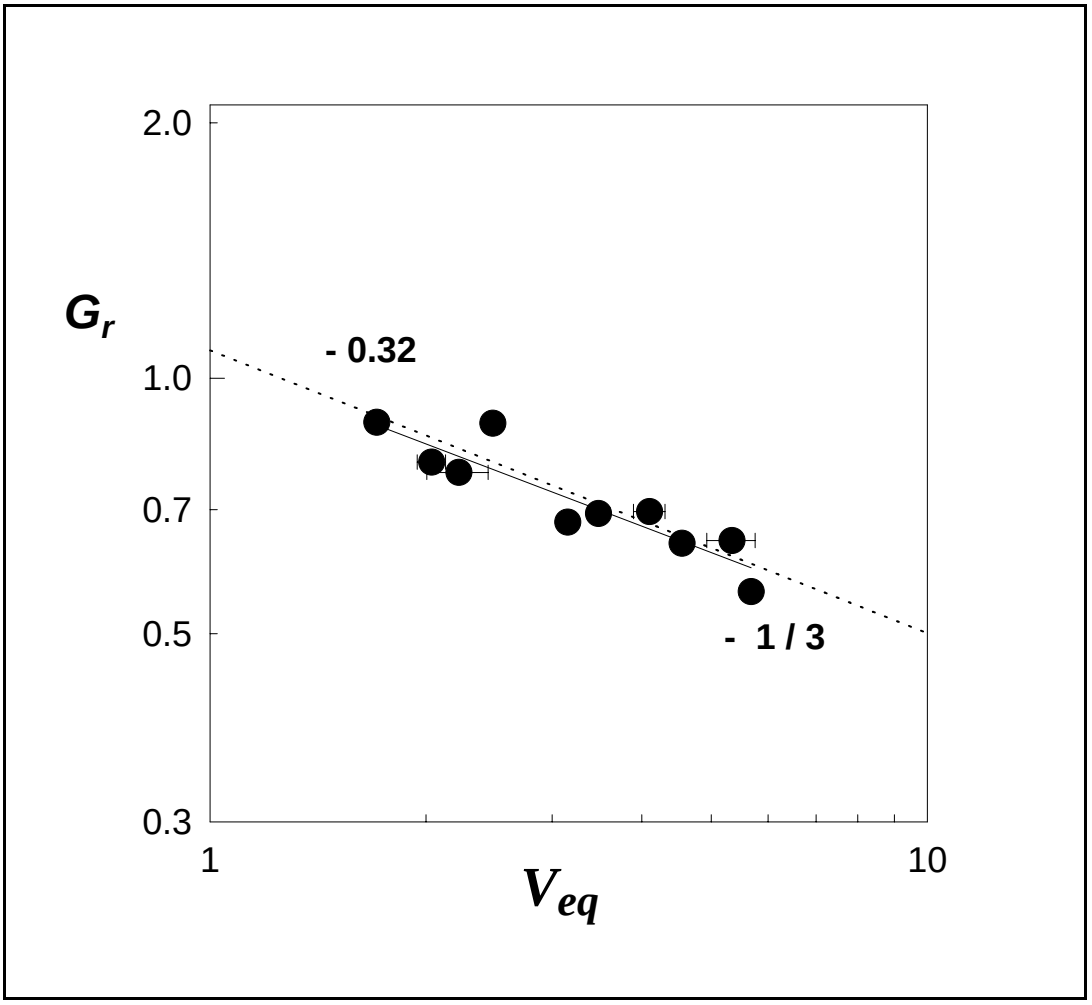

Figure 6.18: The reduced modulus G_r, shown as a function of the normalized volume V_{eq} of the equilibrium swollen PDMAAm hydrogel. The solid curve is the best fit to the experimental data. The dotted curve represents the prediction of Equation (3.62).

6.2.3. The Elasticity of Ionic PDMAAm Hydrogels After Their Preparation

The uniaxial compression measurements were performed on the ionic PDMAAm hydrogels just after their preparation. In Figure 6.19A, the elastic modulus of the hydrogels after preparation G_0 is plotted as a function of the mole fraction of AMPS in the comonomer feed x_i. As seen from the Figure, G_0 first increases slightly with ionic comonomer concentration up to about x_i = 0.07 - 0.10, then decreases continuously. Theoretically, increasing the charge density should monotonically decrease the elastic modulus of the hydrogels. The initial increase of the modulus G_0 with increasing charge density shown in Figure 6.19 is connected with the condensation of counterions to ion pairs. The ion pairs attract each other due to the dipole-dipole interactions and form multiplets[119]. After the gel preparation, the concentration of the polymer inside the gel is high enough to make formation of multiplets more favorable. The multiplets act as additional (physical) crosslinks in the hydrogel and thus contribute to the elastic modulus by increasing the effective crosslink density of the network. Moreover, the decrease of modulus at higher ionic group content is connected with the contribution of electrostatic interactions to the conformational change of the network chains.

Results similar to those of Figure 6.19 have been reported by Tong and Liu for N,N'-dimethylacrylamide-AMPS hydrogels[120]. Ilavsky and coworkers also investigated the elastic properties of a series of hydrogels with various types of ionic comonomers over the range of x_i between 0 and 0.20[121]. Their data also indicate an increase in G_0 with increasing charge density of the network.

In order to explain the charge density dependence of G_0 shown in Figure 6.19A, the variation of the dilution degree of the network after the gel preparation should be considered. Although the initial monomer concentration C_0 was fixed in the experiments, the volume concentration ν_2^0 changes due to the different molar volumes of the monomers DMAAm and AMPS. For example, calculations using Equations (2.13) and (5.5) show that, with an increase of x_i from 0 to 0.10, ν_2^0 increases from 0.0408 to 0.0462. Moreover, according to Equation (3.61), this will increase the modulus of the ionic hydrogels.

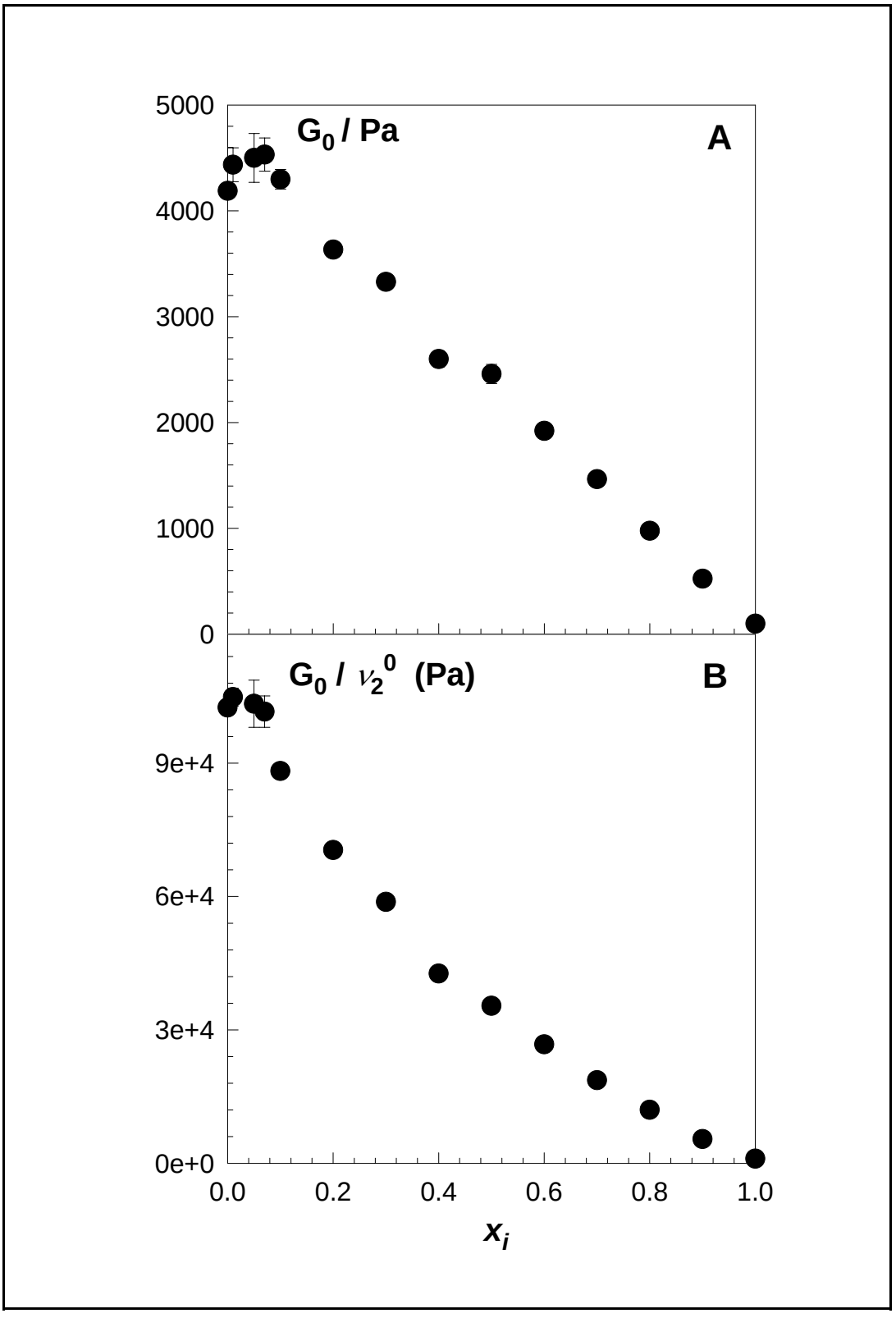

Figure 6.19: Variations of the elastic modulus of non-ionic PDMAAm hydrogels after preparation G_0 (A) and G_0/ν_2^0 (B) with the mole fraction of AMPS in the comonomer feed x_i.

In order to eliminate this effect, the ratio G_0/ν_2^0 was calculated, which only depends on the effective crosslink density of the network. However, G_0/ν_2^0 versus x_i data illustrated in Figure 6.19B show the same type of dependence as in Figure 6.19A. Thus, the shape of the dependence of G_0 on x_i is real and, according to Equation (3.61), this dependence originates from the variation of the effective crosslink density of the network depending on its charge density.

6.2.3.1. The Effective Crosslink Density of Ionic PDMAAm Hydrogels

The effective crosslink densities of the hydrogels in terms on *N*, the number of segments between two successive crosslinks can be calculated by using the values of G_0 and ν_2^0 of the hydrogels together with Equation (3.61). In Figure 6.20, the effective crosslink densities of the networks in terms of *N* are shown as a function of x_i. The filled and open symbols are calculation results for phantom ($\phi = 4$) and affine network models, respectively. The dotted line in the figure represents the chemical cross-link density, N_{chem}, which would result if all the crosslinker (BAAm) molecules formed effective cross-links in the hydrogel. N_{chem} was calculated from the cross linker ratio *X* used in the gel preparation using the equation:

$$N_{chem} = \frac{X^{-1}}{2}\frac{\bar{V}_r}{V_1} \tag{6.8}$$

For non-ionic PDMAAm hydrogel ($x_i = 0$), *N* equals 669 or 1338 for phantom or affine network models, respectively, compared to its chemical value of 186. Also, the effective crosslink densities of non-ionic hydrogels in terms on M_c, equals to 14609 and 29218 g mol^{-1} for phantom and affine network models, respectively, compared to the value of 4114 g mol^{-1}, calculated from the molar ratio of the monomers to the crosslinker used in the gel synthesis (83). It is seen that the effective value of *N* is much larger than its chemical value N_{chem} and the difference between *N* and N_{chem} further increases at high charge densities. The difference between the effective and chemical crosslink densities and also, the experimental and theoretical M_c values of PDMAAm hydrogels indicates that a significant fraction of the crosslinker BAAm is wasted during the cross-linking copolymerization, probably due to the cyclization and multiple cross-linking reactions. The fraction of wasted BAAm units in PAAm

gels was previously reported to be as 80% using the determination of pendant vinyl group conversions[122]. This value was also calculated as 95% from the swelling measurements[123]. Thus, previous analytical and swelling measurements together with the present mechanical measurements show that at least 80% of BAAm present in the feed are involved in ineffective crosslinks in the PDMAAm hydrogels.

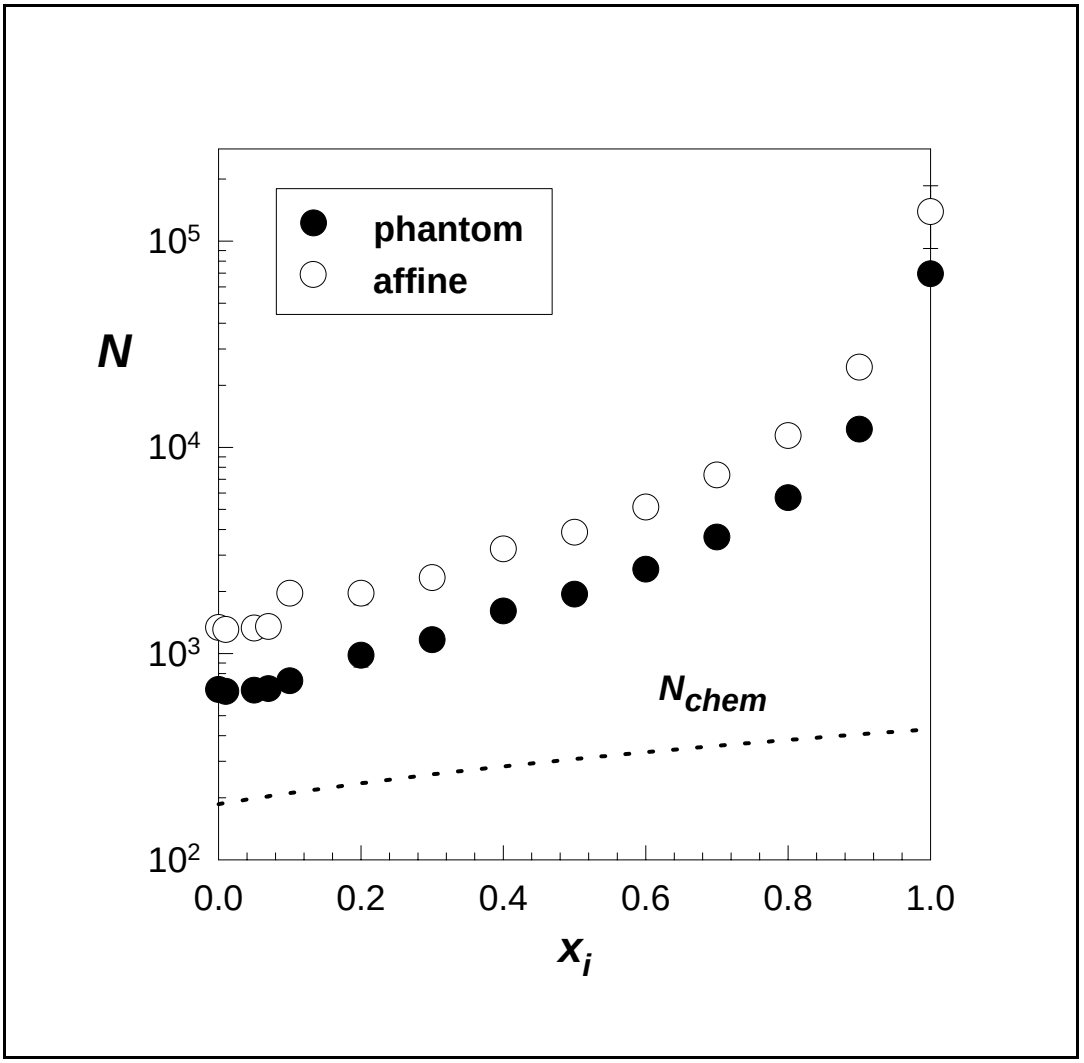

Figure 6.20: The effective crosslink densities *N* of ionic PDMAAm hydrogels shown as a function of the mole fraction of AMPS in the monomer mixture x_i. The filled and open symbols are calculation results for phantom (ϕ = 4) and affine network models, respectively. The dotted line was calculated using Equation (6.8).

Figure 6.20 shows that increasing the content of the ionic comonomer in the feed from x_i = 0.07 up to 1 increases continuously the number of segments between the crosslinks *N*, i.e., decreases the cross-link density of PDMAAm hydrogels. This is a consequence of the simultaneous decrease of the chemical crosslink density, as shown by the dotted line in Figure 6.20. Moreover, the contribution of electrostatic

interaction of charged groups to the elastic free energy of ionic gels may also be responsible for this variation. It is seen that N slightly decreases for $x_i < 0.07$; that is, the crosslink density increases with an increasing charge density.

This type of variation of the crosslink density with x_i at small charge densities was also reported and it is connected with the condensation of counterions to ion pairs[55,121]. The ion pairs form multiplets which act as physical crosslinks in the hydrogel and thus increases the effective crosslink density of the network[119].

6.2.4. The Elasticity of Ionic PDMAAm Hydrogels After Equilibrium Swelling in Water

The uniaxial compression measurements were also performed on the ionic PDMAAm hydrogels after equilibrium swelling in water. In Figure 6.21, the modulus G of the hydrogels swollen to equilibrium in water is shown as a function of the mole fraction of AMPS x_i.

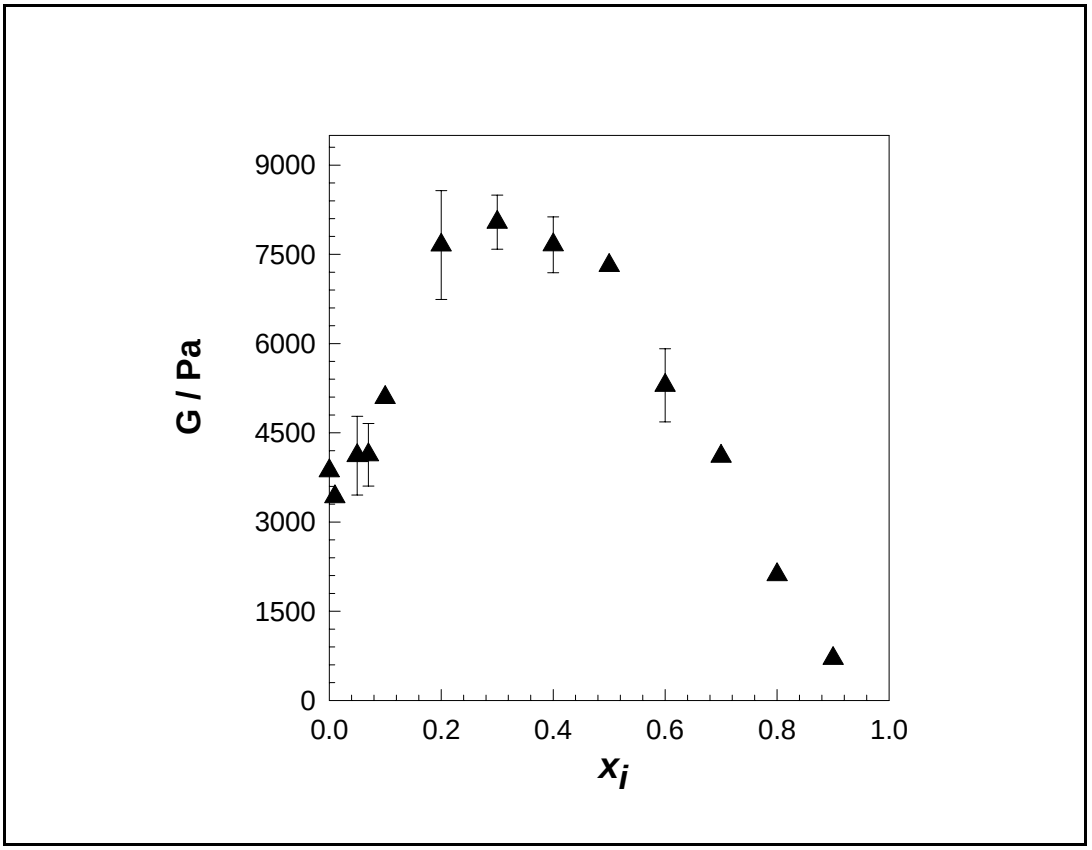

Figure 6.21: The modulus G of the hydrogels swollen to equilibrium in water shown as a function of the mole fraction of AMPS in the monomer mixture x_i.

The modulus of equilibrium swollen ionic hydrogels G increases with increasing x_i up to about 0.30. The increase of the elastic modulus is connected with the high stretching of the network chains. For x_i > 0.30, the modulus decreases with the charge density of the network. The hydrogels in this regime were also too weak to withstand the mechanical measurements. The network chains in these swollen hydrogels are in the expanded configuration with respect to dry state, so that a destruction of the chains may occur during the measurements. The modulus G rapidly decreases due to the effect of the electrostatic interaction of charged groups on the elastic free energy.

In Figure 6.22, the reduced modulus G_r is plotted against the normalized gel volume V_{eq}. For Gaussian chains, the slope of G_r versus V_{eq} plot equals to -1/3 (Equation (3.62)), which is represented in the figure by the dotted curve.

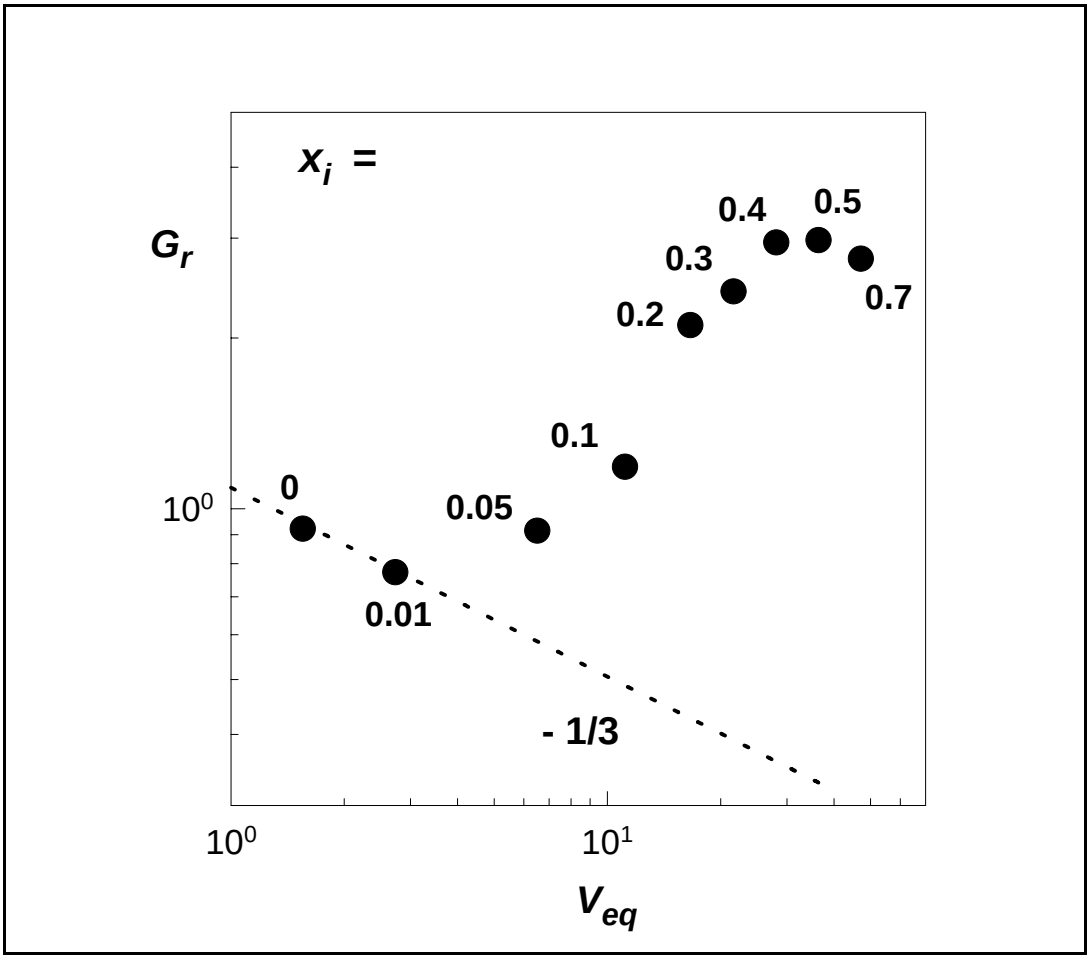

Figure 6.22: The reduced modulus G_r, shown as a function of the normalized gel volume V_{eq}. The dotted curves represents the slope -1/3 predicted for Gaussian chains. The mole fractions of AMPS in the monomer mixture x_i, are indicated in the figure.

As seen from Figure 6.21, the modulus G of the hydrogels swollen to equilibrium in water decreases with increasing x_i from 0 to 0.01. The slope of G_r versus V_{eq} plot (Figure 6.22) which is close to the theoretical value of -1/3 indicates that the hydrogels prepared in this regime behave Gaussian. Over the range of x_i from 0.01 to 0.50, the reduced modulus G_r increases rapidly with increasing gel volume V_{eq}. This behavior is an indication of the limited extensibility of the network chains and is connected with the non-Gaussian behavior of high stretched the network chains.

6.2.4.1. The Charge Density of Ionic PDMAAm Hydrogels

The Flory-Huggins theory assumes an equivalent size for both the solvent molecules and the network segments. However, because of the different molar volumes of the monomer units and solvent of the present system, the mole fraction of AMPS units in the network x_i does not correspond to the charge density of the network f. The values of the charge density of the network f can be obtained from the relation; $f = x_i V_1 / V_r$.

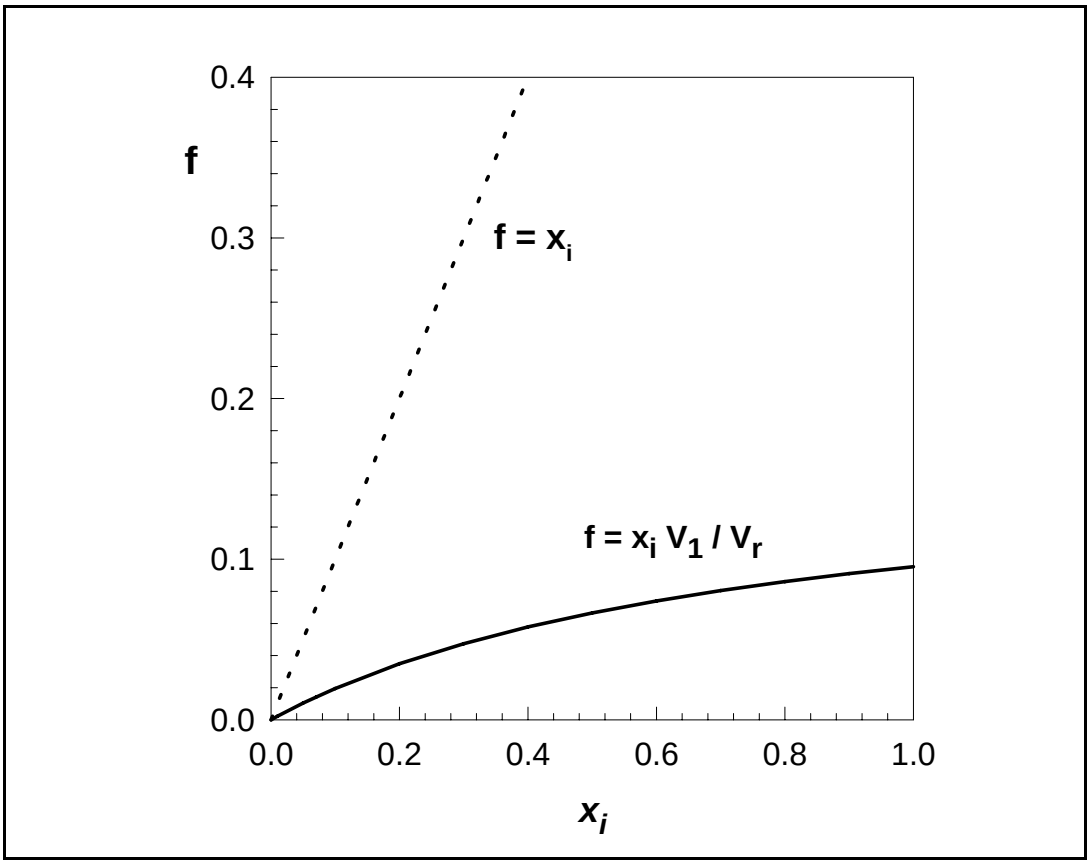

Figure 6.23: The charge density of the networks f shown as a function of the mole fraction of AMPS x_i. Due to the different molar volumes of the monomer units and solvent, f deviates from x_i, as shown by the solid curve.

The calculated f values are shown in Figure 6.23 as the solid curve plotted as a function of the mole fraction of AMPS units in the network x_i. It is seen that f is much smaller than x_i. This is due to the fact that each AMPS unit in the gel occupies a volume equal to 9-fold volume of a solvent molecule; i.e., each AMPS unit forms 9 segments but produces only one mobile ion in the gel. This size effect of the ionic comonomer results in a considerable lower charge density than expected from the chemical composition of the network chains.

6.2.4.2. Non-Gaussian Behavior of Swollen PDMAAm Gels at Various Charge Densities

The elasticity of non-ionic PDMAAm gels after equilibrium swelling in water was examined in Section 6.2.2.1. and it was found that non-ionic PDMAAm gels swollen to equilibrium in water behave as Gaussian. In the following, the elastic behavior of swollen PDMAAm gels at various charge densities will be discussed.

Flory-Huggins theory assumes that the polymer network is a collection of Gaussian chains, which can be extended to infinity. As seen in Table 6.2, for ionic-PDMAAm hydrogels, the volume fraction of crosslinked polymer in the equilibrium swollen gel $\nu_{2,eq}$ values vary between 0.02634 and 0.00035 depending on the charge density. This indicates that the network chains in the equilibrium swollen hydrogels are extended conformation according to dry state. At such high swelling ratios, deviation from the Gaussian statistics may appear due to the finite extensibility of the network chains[125,126]. According to the Equation (3.35) and the theory of rubber elasticity of Gaussian chains, the free energy of elastic deformation ΔG_{el} scales with the deformation ratio as:

$$\Delta G_{el} \approx N^{-1}\alpha^2 \tag{6.9}$$

where α is the linear deformation ratio,($\alpha = (D/D_0) = V^{1/3}$). According to the non-Gaussian theory of rubber elasticity, the change of elastic free energy of gels due to swelling is given by[39,57].

$$\Delta G_{el} \approx N^{-1}\alpha n^{1/2} L^{-1}\left(\alpha n^{-1/2}\right) \tag{6.10}$$

where L^{-1} is the inverse Langevin function, and n is the number of flexible units between crosslinks, which includes the non-Gaussian properties of the network. The inverse Langevin function can be accurately approximated by a Pade equation[124];

$$L^{-1}(x) = x\left(3 - x^2\right)/\left(1 - x^2\right) \tag{6.11}$$

Substituting Eq. (6.11) in Eq. (6.10) gives:

$$\Delta G_{el} \approx N^{-1}\alpha^2\left(1 + \frac{2}{1 - \alpha^2/n}\right) \tag{6.12}$$

Serial expansion of the second term of Eq. (6.12) and truncating at α^4 yield the following equation for the elastic free energy of non-Gaussian chains:

$$\Delta G_{el} \approx N^{-1}\alpha^2\left(3 + 2\alpha^2/n + 2\alpha^4/n^2\right) \tag{6.13}$$

For $\alpha^2/n \ll 1$, that is for moderate degrees of swelling, or at the onset of deviations from the Gaussian statistics, Equation (6.13) reduces to:

$$\Delta G_{el} \approx N^{-1}\left(\alpha^2 + \alpha^4/n\right) \tag{6.14}$$

According to Equation (6.14), when n approaches infinity, the equation reduces to the Gaussian description (Equation (6.9)). For finite values of n (i.e., as the network chains deviate from the Gaussian statistics), elastic free-energy ΔG_{el} will increase with a higher power of α.

At the swelling equilibrium of highly swollen ionic hydrogels, the gel rubberlike elasticity given by Equation (6.13) is balanced by the ionic free energy due to the mixing entropy of the counterions. The ionic contribution to the free-energy ΔG_i may be written as[32];

$$\Delta G_i \approx f \ln\left(f\nu_2^0/\alpha^3\right) \tag{6.15}$$

where *f* is the effective charge density of the network (i.e., the fraction of segments bearing ionic groups. Balancing the two opposite free-energy contributions represented by ΔG_{el} (Eq. (6.13)) and ΔG_i (Eq. (6.15)) by minimizing their sum with respect to α and, because $\alpha = V_{eq}^{1/3}$ at the swelling equilibrium, then it gives:

$$6V_{eq}^{2/3} + 8\frac{V_{eq}^{4/3}}{n} + 12\frac{V_{eq}^{2}}{n^2} \approx fN \tag{6.16}$$

For the Gaussian chains, that is, when *n* approaches infinity, Eq. (6.16) reduces to:

$$V_{eq} \approx \left(fN\right)^{3/2} \tag{6.17}$$

which indicates a scaling parameter of 1.5 between the equilibrium swollen volume V_{eq} of the hydrogels and the number of charges per network chain *fN*. The scaling parameter predicted by Equation (6.17) decreases below 1.5 as the number of flexible units between crosslinks represented by *n* decreases (i.e., as the network chains deviate from Gaussian behavior).

Figure 6.24 shows a double-logarithmic plot of the equilibrium gel volume V_{eq} against the number of charges per network chains *fN*. Experimental data are shown by symbols. The values of *N* were calculated using the phantom network model. The dotted curve in the figure represents the prediction of Equation (6.17) with a scaling parameter of 1.5.

The solid curve in the figure are the best fitting curve to the experimental swelling data of the hydrogels, which gives a scaling parameter; 0.94 ± 0.03 for ionic PDMAAm hydrogels. The calculations using the affine model do not change the value of the exponent. It is seen that the scaling parameter 0.94 found for ionic PDMAAm hydrogels deviates from the prediction of the FH theory (Equation (6.17)) and indicates non-Gaussian behavior of the network chains in ionic PDMAAm hydrogels.

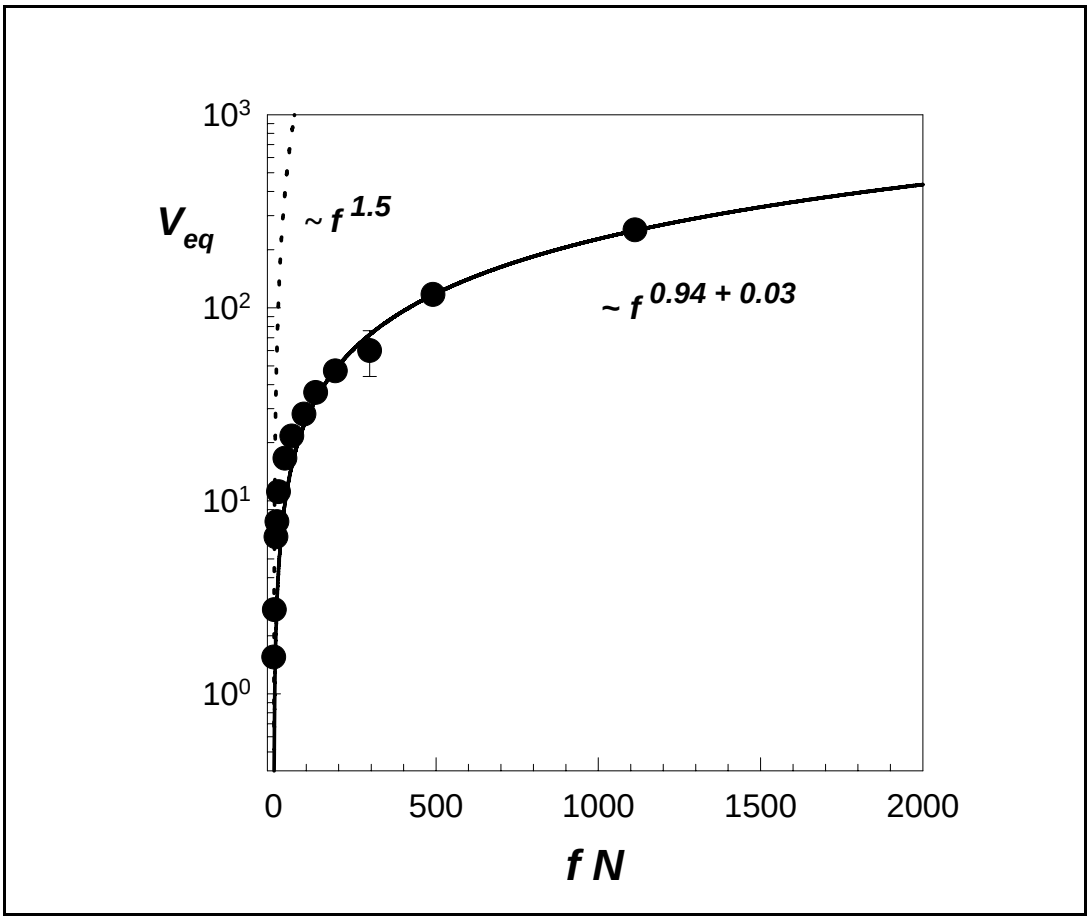

Figure 6.24: The equilibrium volume of the hydrogels normalized with respect to the after preparation state V_{eq} of ionic PDMAAm hydrogels shown as a function of the number of charges per network chain *fN*.

6.3. Spatial Inhomogeneity in PDMAAm Hydrogels

The extent of the spatial inhomogeneity in PDMAAm hydrogels was investigated as a function of various gel synthesis parameters. The experimental parameters varied were: the initial monomer concentration, i.e., the polymer concentration, the ionic comonomer concentration and the redox-initiator systems used to initiate the gelation reactions. To make a comparison, PAAm hydrogels were also prepared under the same experimental condition. Besides the static light scattering measurements on the hydrogels after one day of polymerization time, the time-resolved light scattering measurements were also carried out to obtain the scattering intensity profile of hydrogels during their formation process.

6.3.1. The Effect of Polymer Concentration on The Spatial Inhomogeneity of Non-ionic PDMAAm Hydrogels

The light scattering measurements were carried out on non-ionic PDMAAm hydrogels prepared at various polymer network concentration, i.e., ν_2^0 between 0.019 and 0.16. The scattered light intensities both from hydrogels and solutions were recorded in the range of the scattering vector q between 1×10^{-3} and 2.2×10^{-3} A^{0-1}. The results are collected in Figure 6.25 which shows the Rayleigh ratio *R(q)* versus the scattering vector *q* plots for PDMAAm hydrogels (filled symbols) and for the corresponding linear PDMAAm solutions (open symbols). The polymer concentrations ν_2^0 are indicated in the Figure. As seen in Figure 6.25, the light scattering intensity does not change much with the scattering vector *q* in the range of $\nu_2^0 \leq 0.12$ and so, linear Rayleigh ratio *R(q)* vs. *q* plots were obtained. However, at higher values of ν_2^0, non-linear scattering plots were obtained. For example, at ν_2^0= 0.16, a marked curvature appears in the *R(q)* vs. *q* curves, especially at low angles. Also, *R(q)* of the polymer solution even exceeds *R(q)* of the polymer gels in this range of ν_2^0. Due to the high polymer concentration in this regime, in addition to the concentration fluctuations, the density fluctuations also play an important role in the scattering intensity which seems to be responsible for the strong *q*-dependence of the Rayleigh ratios at $\nu_2^0 > 0.12$[127]. Figure 6.25 also shows that, for $\nu_2^0 \leq 0.12$, the scattering light intensity from polymer solutions decreases with increasing

concentration ν_2^0. The most important point shown from the Figure 6.25 is that compared to solutions, the light scattering intensity from gels first increases slightly up to ν_2^0 = 0.06 but then rapidly decreases[105].

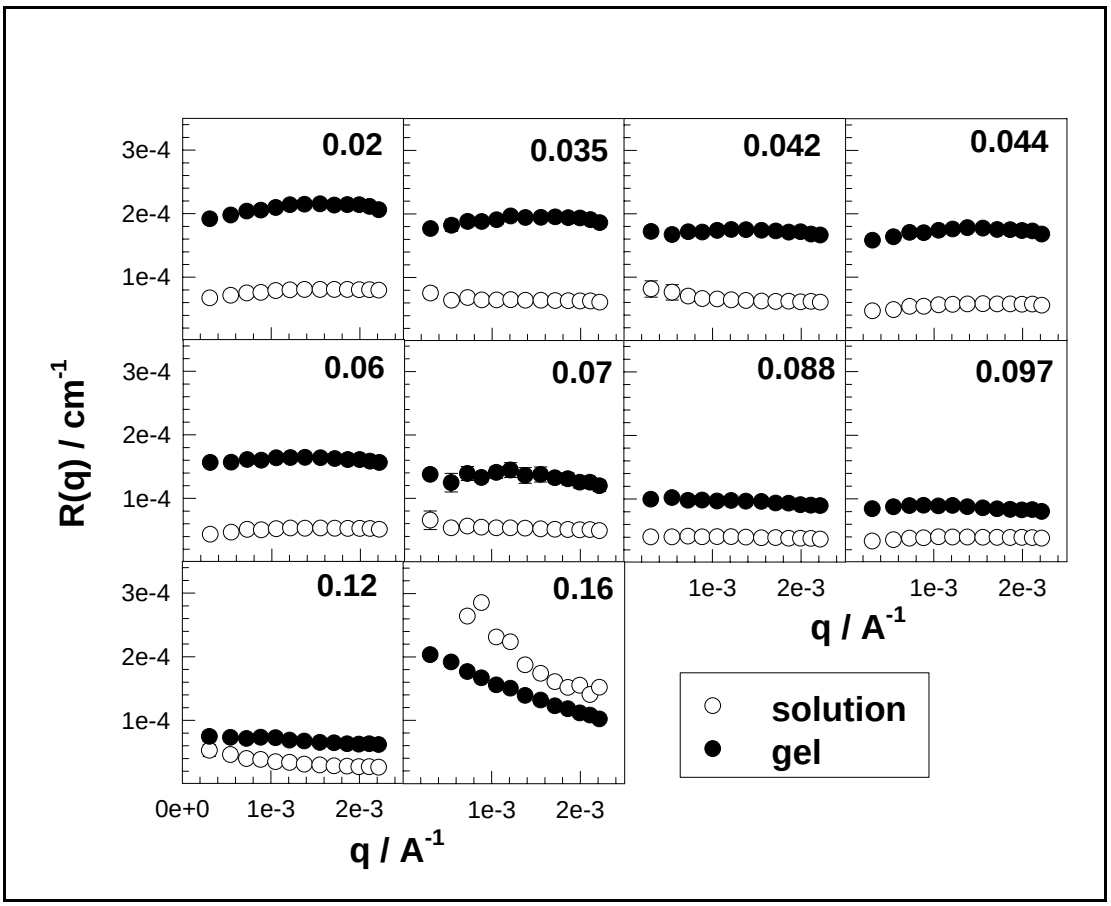

Figure 6.25: The Rayleigh ratio *R(q)* versus scattering vector *q* plots for PDMAAm hydrogels (filled symbols) and for the corresponding linear polymer solutions (open symbols). The ν_2^0 values are indicated in the Figures.

By using Equation (4.51) together with the data points shown in Figure 6.25, the excess scattering of gels over the scattering from polymer solution $R_{ex}(q)$ was calculated through the relation; $R_{ex}(q) = R_{gel}(q) - R_{sol}(q)$. In Figure 6.26, the excess scattering $R_{ex}(q)$ vs. scattering vector q plots are shown for PDMAAm hydrogels of various polymer network concentration ν_2^0. To compare the excess scattering of hydrogels, the scattering intensity measured at a fixed scattering vector at $q = 1\times10^{-3}$ A° $^{-1}$ was considered.

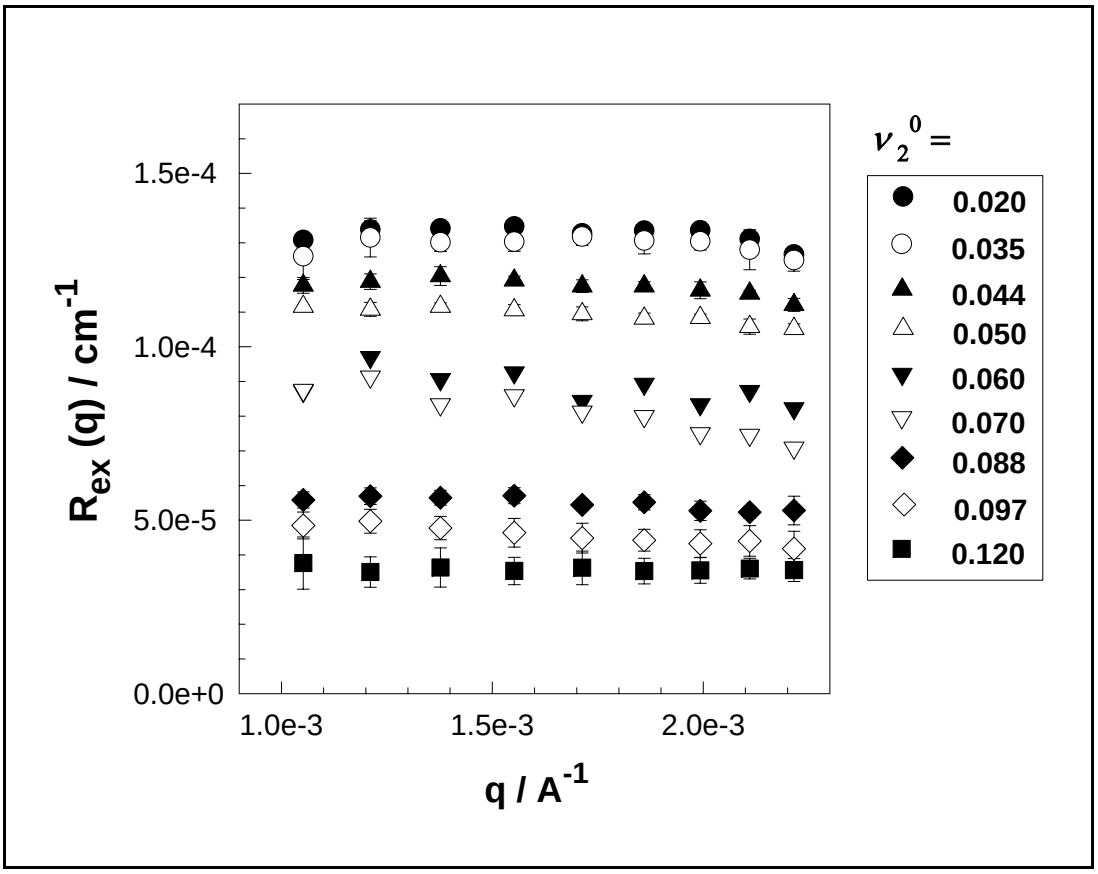

Figure 6.26: The excess scattering $R_{ex}(q)$ with scattering vector q plots for PDMAAm hydrogels. The polymer network concentration ν_2^0 indicated in the Figure.

In Figure 6.27, the scattering light intensities from polymer solutions $R_{sol,q}$ (open circles) and the excess scattering $R_{ex,q}$ from gels (filled circles) at $q = 1 \times 10^{-3}$ A$^{o\ -1}$ are plotted as a function of the polymer network concentration ν_2^0. Several interesting features can be seen in Figure 6.27. Although the scattered light intensity from solution decreases with rising ν_2^0, the excess scattering from gels $R_{ex,q}$ first increases with increasing ν_2^0 becomes maximum at a critical polymer concentration $\nu_{2,cr}^0$ (= 0.06), then decreases continuously with a further increase in ν_2^0. Since the thermal fluctuations are eliminated in the excess scattering, R_{ex} is a measure of the spatial inhomogeneity in the gel. Thus, the results in Figure 6.27 show that the PDMAAm gels prepared at a critical polymer network concentration exhibit the highest degree of inhomogeneity. The experimental work in the literature also indicates such a maximum degree of spatial inhomogeneity at a critical polymer concentration in PAAm gels[88].

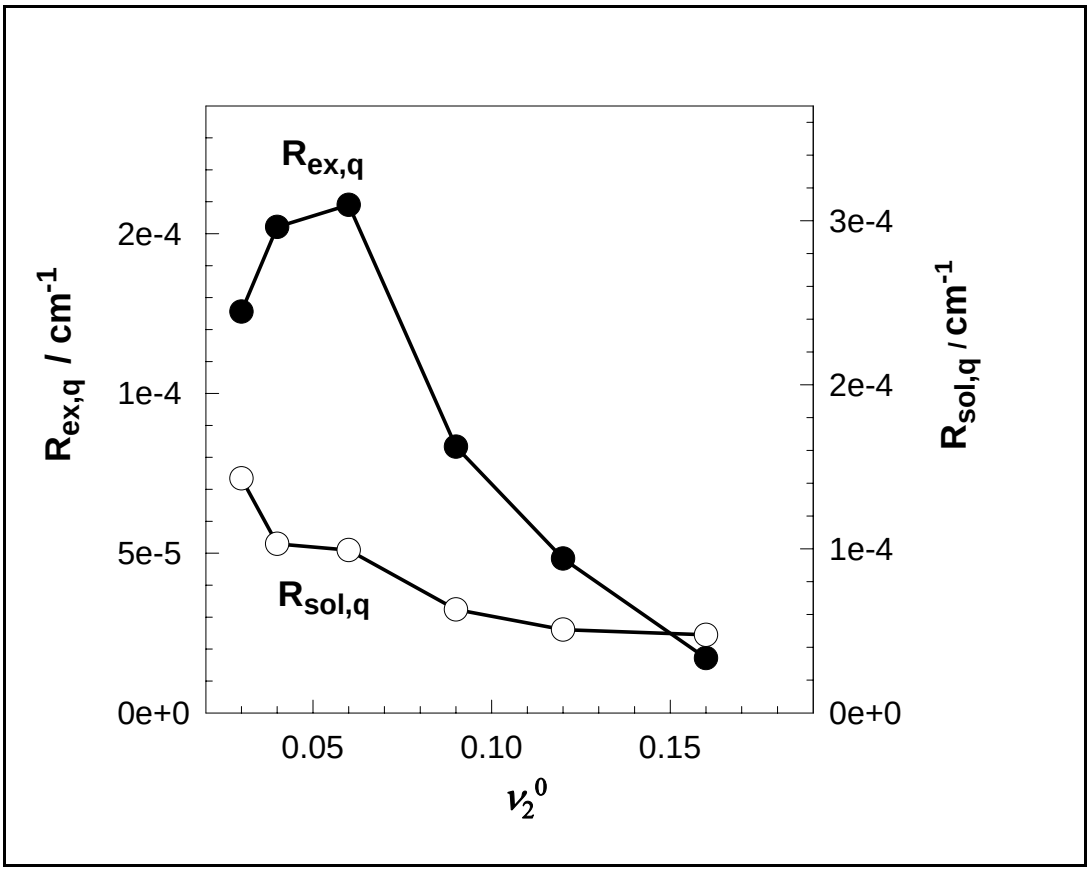

Figure 6.27: The scattering intensity from PDMAAm solutions $R_{sol,q}$ (open symbols) and the excess scattering from gels $R_{ex,q}$ from PDMAAm hydrogels (filled symbols) measured at $q = 1\text{x}10^{-3}$ A^{o-1} shown as a function of ν_2^0.

The appearance of a maximum degree of spatial inhomogeneity in PDMAAm hydrogels can be explained with two different effects of the monomer concentration on the extent of spatial inhomogeneity. These effects are also shown schematically in Figure 6.28;

1- The effect of the crosslink density: As seen from Figure 6.16, the effective crosslink density ν_e of non-ionic PDMAAm hydrogels increases with ν_2^0 in the first regime, which is the range of the light scattering measurements. Thus, increasing ν_2^0 increases the effective crosslink density of gels, so that the spatial inhomogeneity becomes larger on rising ν_2^0.

2- The effect of the polymer concentration: Increasing polymer network concentration reduces progressively the concentration difference between the densely and loosely crosslinked regions of gels, so that the apparent spatial inhomogeneity decreases on rising ν_2^0.

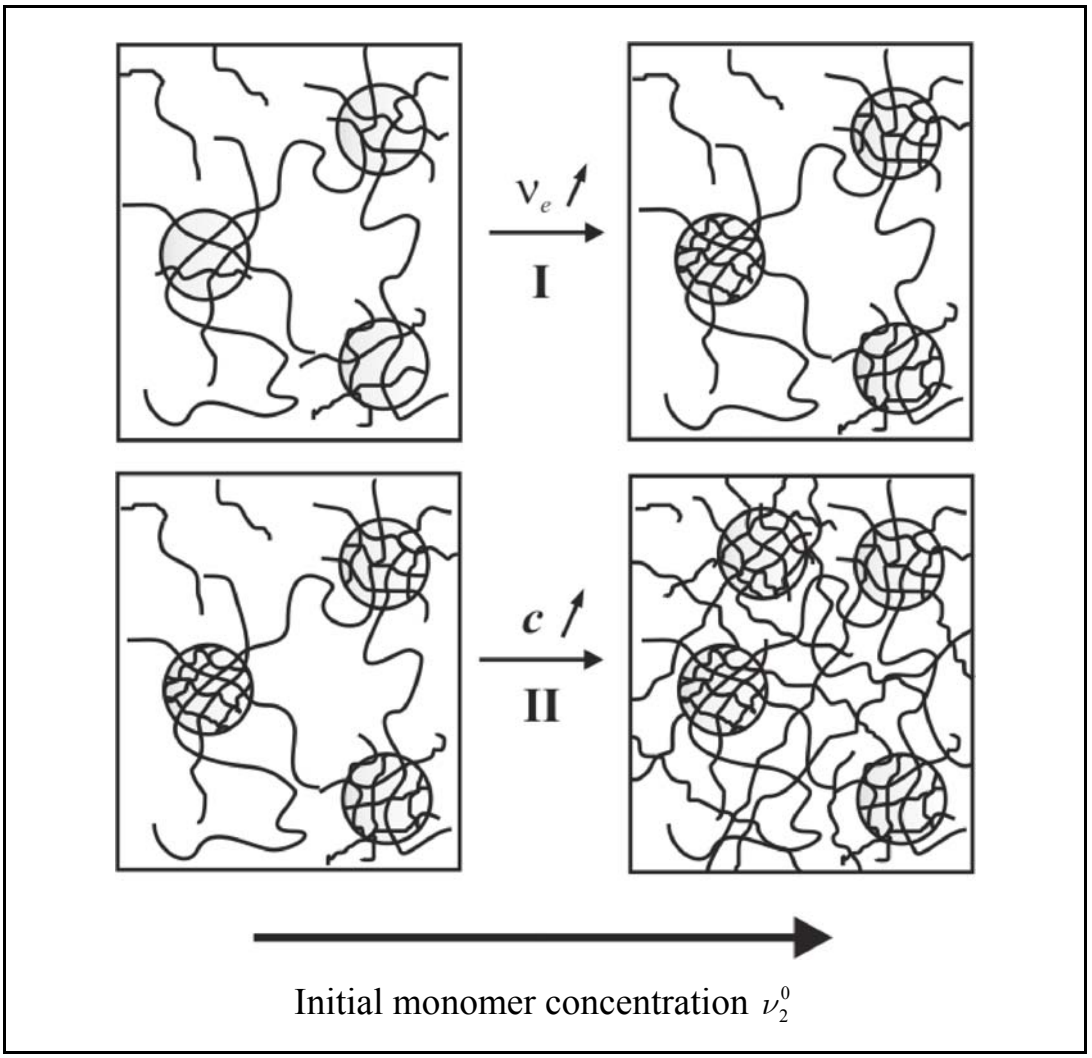

Figure 6.28: Schematic representation of various effects determining the spatial inhomogeneity in PDMAAm gels: the crosslink density effect (ν_e), and the concentration effect (c).

The dependence of the gel inhomogeneity on the monomer concentration is thus determined by a competition of these two opposite effects. At low monomer concentrations, i.e., $\nu_2^0 < 0.06$, the crosslink density effect dominates over the concentration effect so that the gel inhomogeneity increases with ν_2^0 (Figure 6.28.I). At higher values of monomer concentrations, i.e., $\nu_2^0 > 0.06$, the concentration effect is more dominant than the crosslink density effect so that the gel inhomogeneity decreases with ν_2^0 (Figure 6.28.II). The location of the maximum in the excess scattering vs. monomer concentration ν_2^0 plot represents the transition point between these two regimes. Thus, it can be concluded that the interplay of these two effects mentioned above determines the spatial inhomogeneity in PDMAAm hydrogels at

the state of their preparation and they are responsible for the appearance of a peak in the $R_{ex,q}$ versus ν_2^0 dependence.

In Figure 6.29, the excess scattering data of hydrogels are given in the form of Debye-Bueche plots. By using Equation (4.57), the mean square fluctuation of the refractive index $\langle \eta^2 \rangle$ and the correlation length of the scatterers ξ were calculated from the slope and the intercept of the straight lines shown in Figure 6.29. The results showed that, in the range of ν_2^0 = 0.06 to 0.12, the correlation length of the scatterers remains almost constant at $\xi = 10 \pm 1$ nm, while the mean square fluctuations $\langle \eta^2 \rangle$ decreases slightly with increasing ν_2^0 from 10×10^{-7} up to 5×10^{-7}. At high values of ν_2^0, Debye-Bueche function gave negative slopes, so that these parameters cannot be calculated.

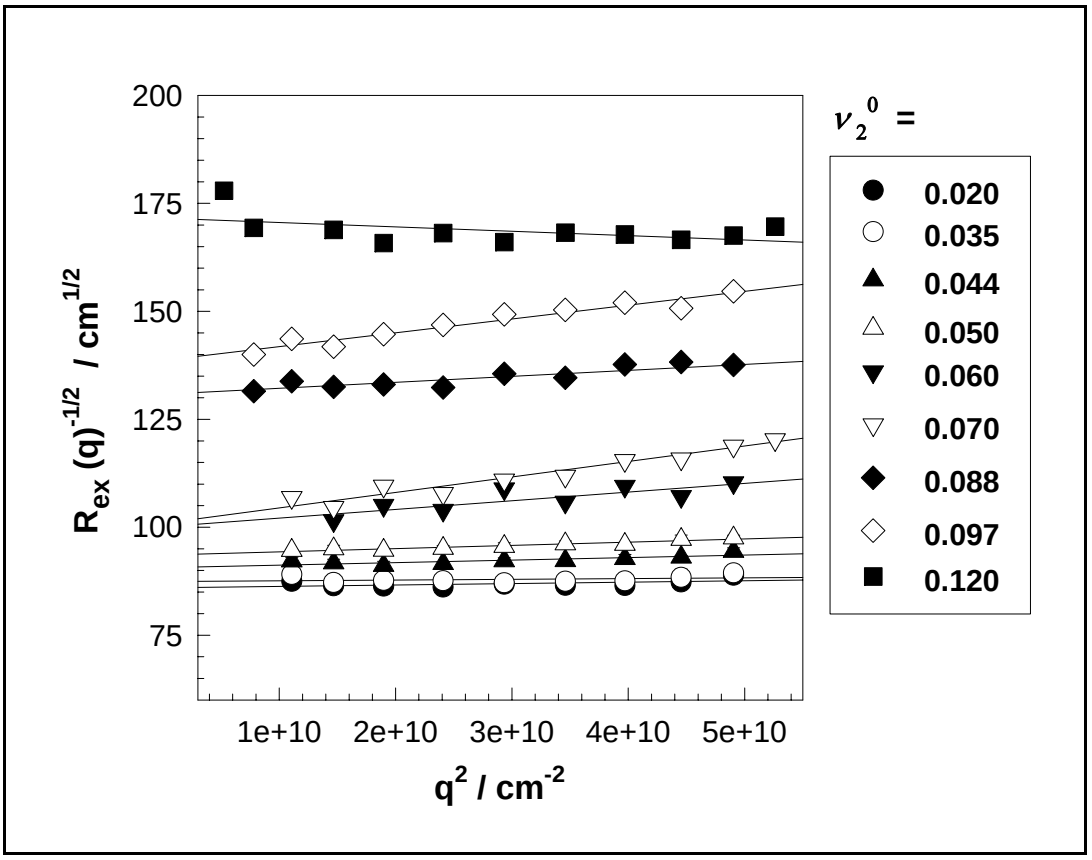

Figure 6.29: Debye - Bueche plots for non-ionic PDMAAm hydrogels prepared at various ν_2^0 indicated in the Figure.

As pointed out before, the correlation length ξ of the Debye–Bueche theory is a characteristic length scale in the gel. It shows the average distance over which the

local variation in the polymer concentration can be considered not to change appreciably. Thus, ξ is a measure of the spatial extent of the fluctuation[93,94]. The larger the ξ values, the larger are the extension of the inhomogeneities. Because of the scatterers in gels are highly crosslinked regions, the correlation length corresponds to the size of these regions. Thus, the results indicate that the correlation length remains almost constant over the entire range of the polymer concentration while the extent of the concentration fluctuations of PDMAAm hydrogels $\langle \eta^2 \rangle$ decreases slightly[105].

6.3.2. The Effect of Ionic Comonomer Concentration on The Spatial Inhomogeneity of Ionic PDMAAm Hydrogels

The effect of the ionic comonomer concentration on the spatial inhomogeneity of ionic PDMAAm hydrogels was investigated by use of the light scattering technique. The ionic PDMAAm hydrogels containing ionic comonomer AMPS in the range of the mole fraction x_i between 0 and 0.30 were prepared as described in Section 5.4.1.

The light scattering measurements from ionic PDMAAm hydrogels and solutions were conducted after one day of polymerization time. The scattered light intensities both from gels and solutions were recorded from angles $\theta = 14.5^0$ to 163.3^0 which correspond to the scattering vector q in the range between 1×10^{-3} and $2.5\times10^{-3}\ A^{0-1}$. The results are collected in Figure 6.30 which shows the Rayleigh ratio from PDMAAm hydrogels $R_{gel}(q)$ and from PDMAAm solutions $R_{sol}(q)$ plotted against the scattering vector q for AMPS mole fraction x_i between 0 and 0.30. The mole fractions of AMPS in the comonomer feed x_i are indicated in the Figure.

It is seen that the scattered light intensities both from polymer solution $R_{sol}(q)$ and from hydrogels $R_{gel}(q)$ decrease with increasing mole fraction of AMPS (x_i). A general observation from the Figure is that even the presence of a small amount of the ionic comonomer AMPS decreases drastically the scattering light intensity from the samples. Another point shown in Figure 6.30 is that the hydrogels with low AMPS contents scatter much more light than the corresponding polymer solution of the same concentration. Moreover, the Rayleigh ratios from PDMAAm hydrogels and PDMAAm solutions are almost independent on q over the range of q between 1×10^{-3} and $2.5\times10^{-3}\ A^{0-1}$.

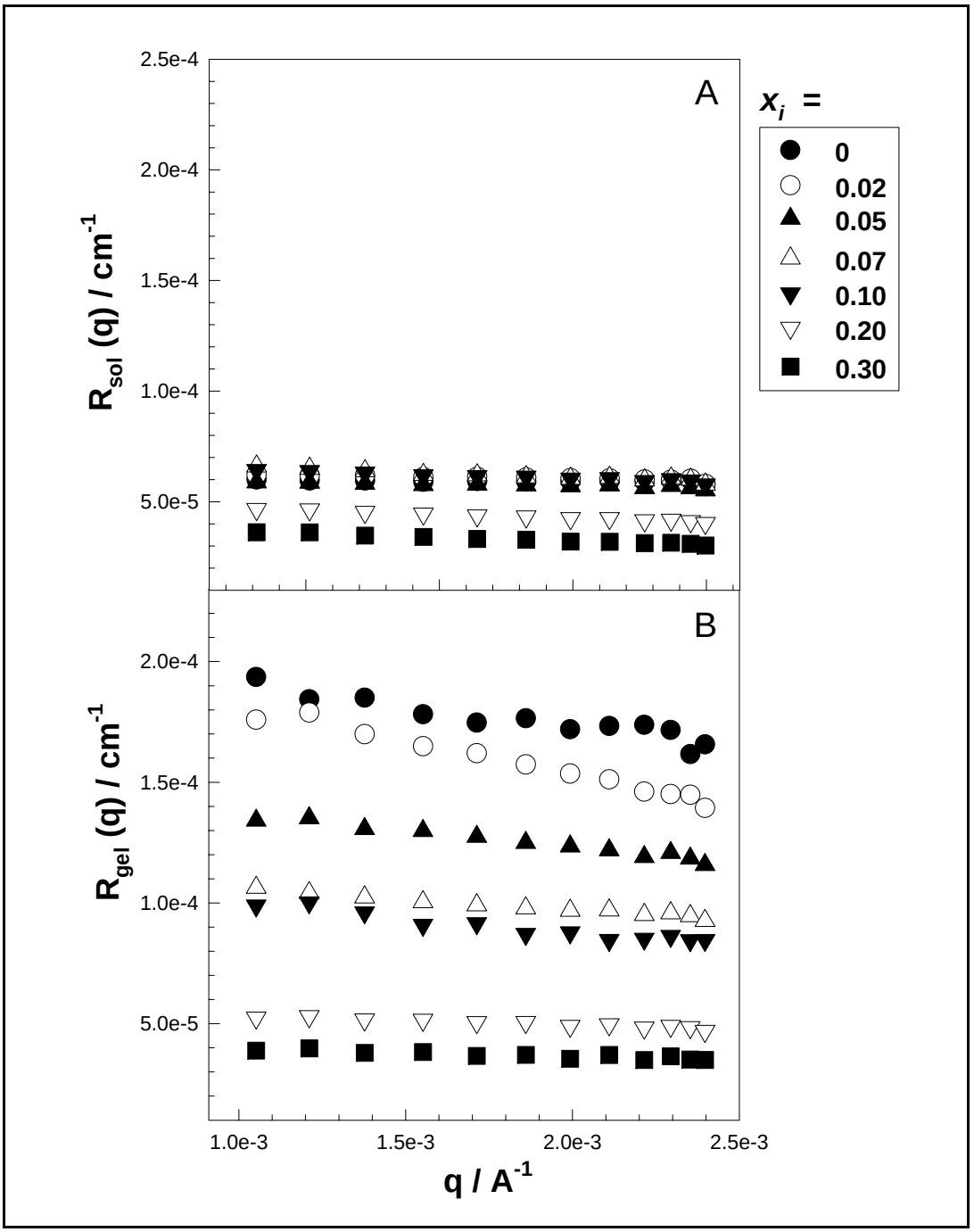

Figure 6.30: The scattering light intensities from ionic PDMAAm hydrogels R_{gel}(q) **(A)** and from polymer solutions R_{sol}(q) **(B)** shown as a function of the scattering vector q for PDMAAm hydrogels at various charge densities. AMPS mole fractions (x_i) are indicated in the Figure.

In the following, the scattering intensity R_q measured at a fixed scattering vector, $q = 1 \times 10^{-3}\, A^{0-1}$, or $\theta = 90^0$, which will be denoted by $R_{q,90}$ is focused to compare the scattered light intensities of various gels.

Figure 6.31 shows $R_{q,90}$ of PDMAAm hydrogels (filled symbols) and of PDMAAm solutions (open symbols) plotted against the mole fraction of AMPS. It is seen that $R_{q,90}$ of gels decreases first rapidly up to about $x_i = 0.10$ but then slightly decreases with a further increase in the AMPS content. $R_{q,90}$ of the linear polymer solutions remains nearly constant in this range of AMPS content. Moreover the scattering light intensities from PDMAAm hydrogels become equal to the scattering intensities from PDMAAm solutions at $x_i = 0.30$. Thus the gel with 30 mol% AMPS is homogeneous like a polymer solution. This observation is very important for many industrial applications such as contact lenses, where the optical clarity determines the quality of the product.

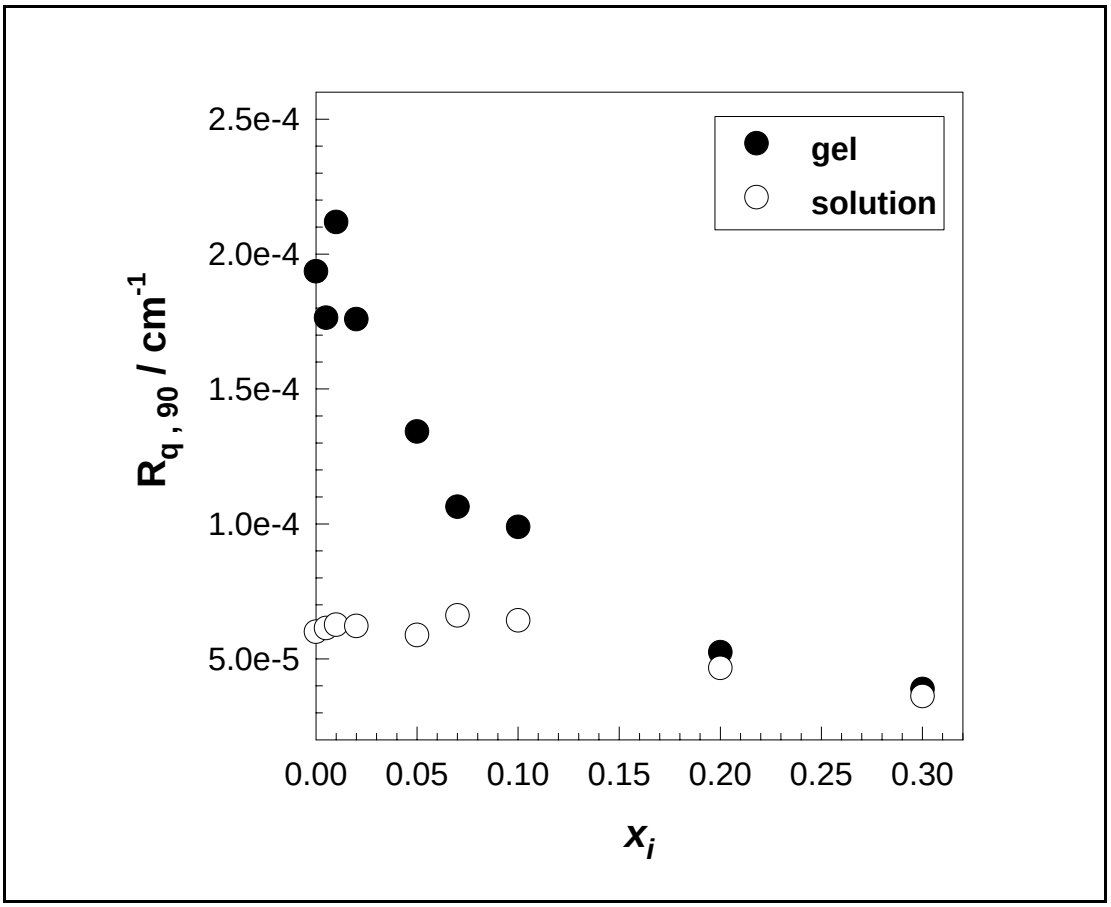

Figure 6.31: The scattering light intensities from PDMAAm solutions $R_{sol}(q)$ (open symbols) and from PDMAAm hydrogels $R_{gel}(q)$ (filled symbols) measured at 90^0 shown as a function of the mole fraction of AMPS x_i.

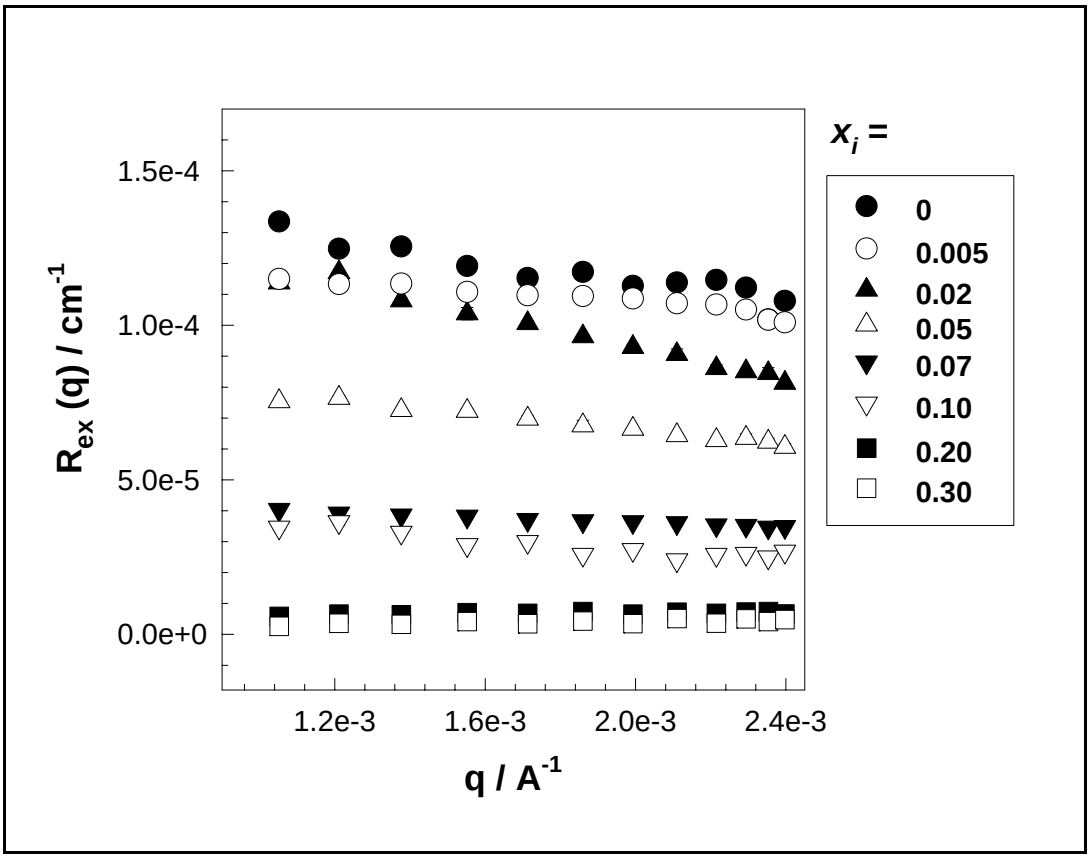

Figure 6.32: The excess scattering $R_{ex}(q)$ with scattering vector q plots for PDMAAm hydrogels of the mole fractions of AMPS x_i indicated in the Figure.

The excess scattering intensities $R_{ex}(q)$ were calculated from the data shown in Figure 6.30 through the relation; $R_{ex}(q) = R_{gel}(q) - R_{sol}(q)$. In Figure 6.32, the excess scattering $R_{ex}(q)$ vs scattering vector q plots are shown for PDMAAm hydrogels of various AMPS content x_i. It is seen that the excess scattering from hydrogels decreases continuously with increasing mole fraction of AMPS. In Figure 6.33, the excess scattering at $\theta = 90^o$ for PDMAAm hydrogels ($R_{ex,q}$) is plotted as a function of the mole fraction of AMPS x_i. It is seen that $R_{ex,q}$ decreases first rapidly up to about $x_i = 0.10$ but then slightly decreases with increasing AMPS content. As shown in the inset to Figure 6.33, a good linear behavior was obtained if the data points are redrawn in a semi-logarithmic plot, indicating an exponential law between $R_{ex,q}$ and x_i. Since $R_{ex,q}$ is a measure of the spatial inhomogeneity in the gel, this indicates that PDMAAm hydrogel becomes increasingly homogeneous with increasing mole fraction of AMPS in the network chains.

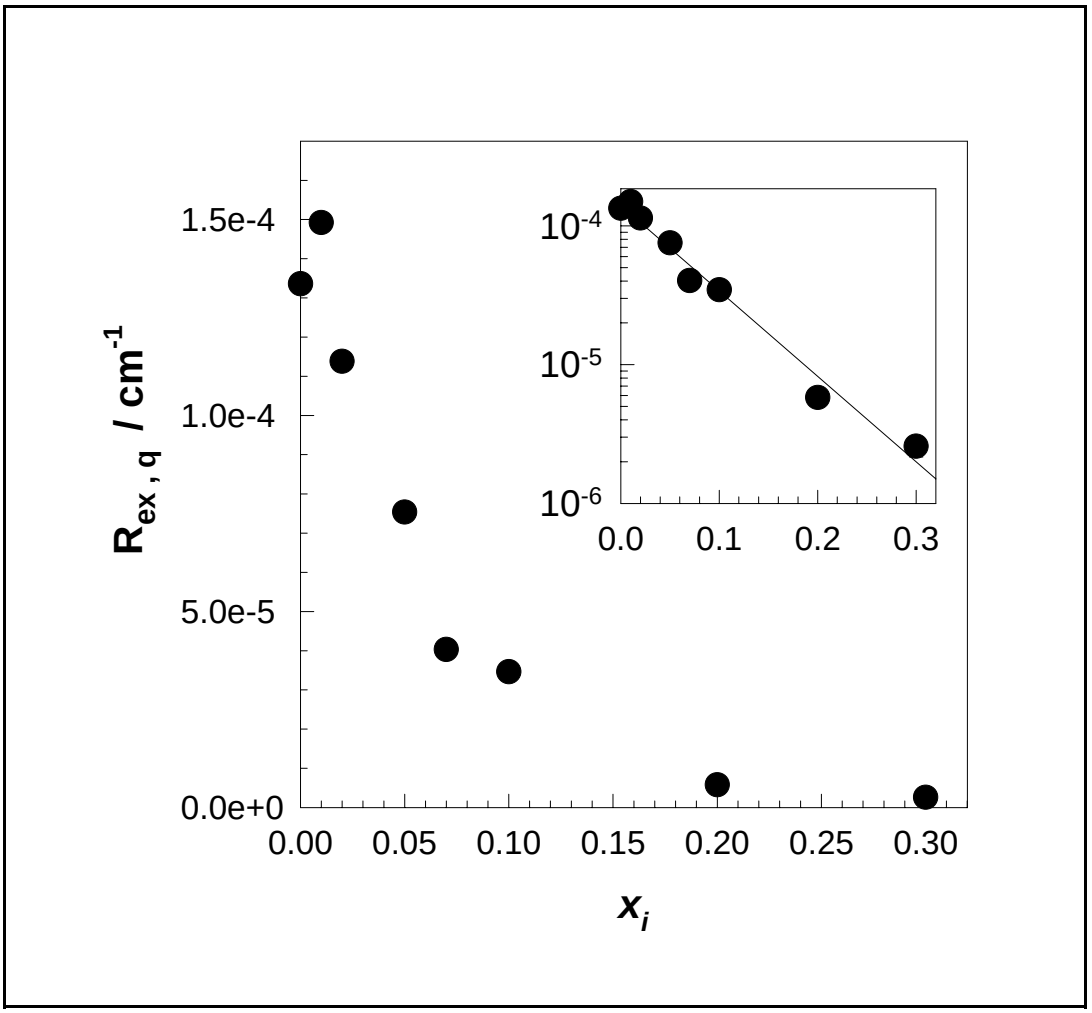

Figure 6.33: The excess scattering $R_{ex,q}$ measured at $\theta = 90^{o}$ shown as a function of the mole fraction of AMPS. The inset to the Figure is a semi-logarithmic plot of the data points.

The data points shown in Figure 6.32 are replotted in the form of Debye-Bueche plots. Linear $R_{ex}(q)^{-1/2}$ vs. q^2 plots were obtained, from which the inhomogeneity parameters ξ and $\langle \eta^2 \rangle$ of PDMAAm hydrogels were calculated using Equation (4.57). The mean square fluctuation of the refractive index $\langle \eta^2 \rangle$ and the correlation length of the scatterers ξ thus calculated are collected in Figure 6.34 plotted against the mole fraction of AMPS in the monomer mixture x_i. The Debye-Bueche function gave negative slopes for $x_i \geq 0.10$, so these parameters cannot be calculated. Figure 6.34 shows that the correlation length of the scatterers ξ is in the range of 10-20 nm for PDMAAm gels while the mean square fluctuation of the refractive index $\langle \eta^2 \rangle$ is in the range 10^{-8}-10^{-6} and decreases rapidly with increasing mole fraction of AMPS.

Combining the observations from Figure 6.33 and Figure 6.34B, it has been established that the excess scattering $R_{ex}(q)$ and the mean square fluctuation of the refractive index $\langle \eta^2 \rangle$ decrease with increasing mole fraction of AMPS. The results suggest that the degree of gel inhomogeneity in ionic PDMAAm hydrogels decreases with increasing AMPS content.

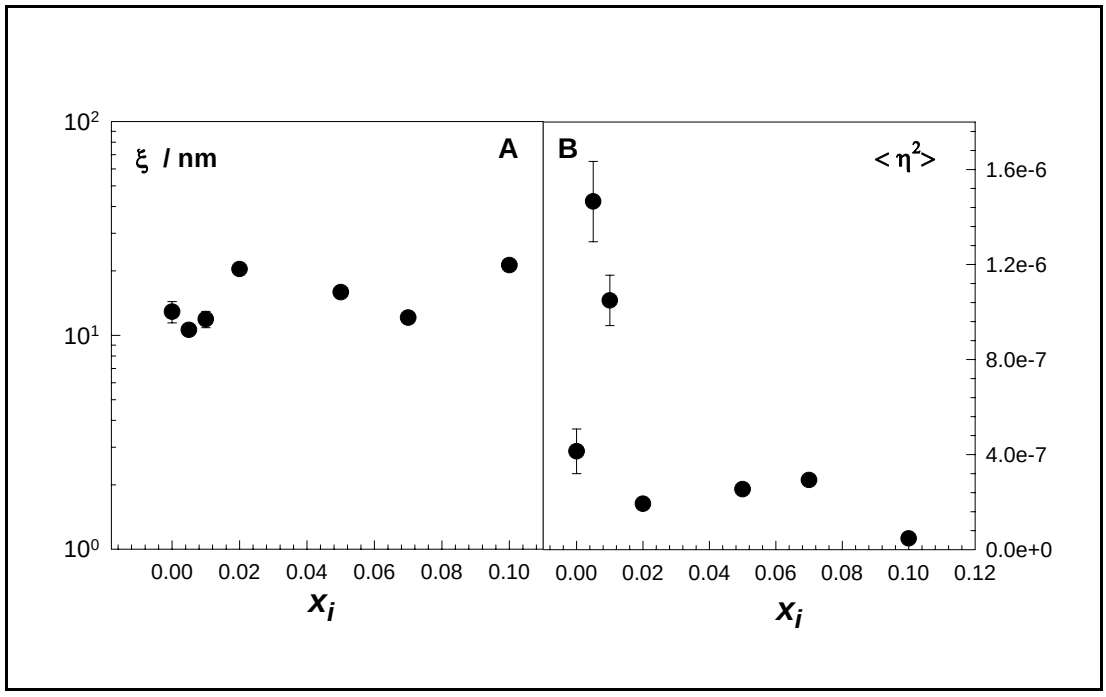

Figure 6.34: The correlation length of the scatterers ξ (A), the mean square fluctuation of the refractive index $\langle \eta^2 \rangle$ (B) in ionic PDMAAm hydrogels shown as a mole fraction of AMPS.

The results thus obtained can be explained as follows: As shown in Figure 6.35, the gel consists of highly crosslinked (dense) regions, which are interconnected by the less crosslinked (dilute) interstitial regions. Thus, the gel consists of regions of high and low polymer concentrations. The local charge density (the number of ionic units per unit gel volume) will thus be higher in the dense regions compared to the dilute regions, as schematically illustrated in the figure. Due to the condition of electroneutrality, the concentration of the mobile counterions will also be higher in the dense regions. This unequal distribution of counterions between the inside and outside the dense regions of gel will create an osmotic pressure resulting in the swelling of the dense regions. This means that, in ionic gels, water diffuses from dilute to the dense regions of the gel due to the additional osmotic pressure of excess

counterions. As a result, the size of the dense regions ξ increases while the extent of the concentration fluctuation $\langle \eta^2 \rangle$ decreases with increasing AMPS content of the hydrogels[90].

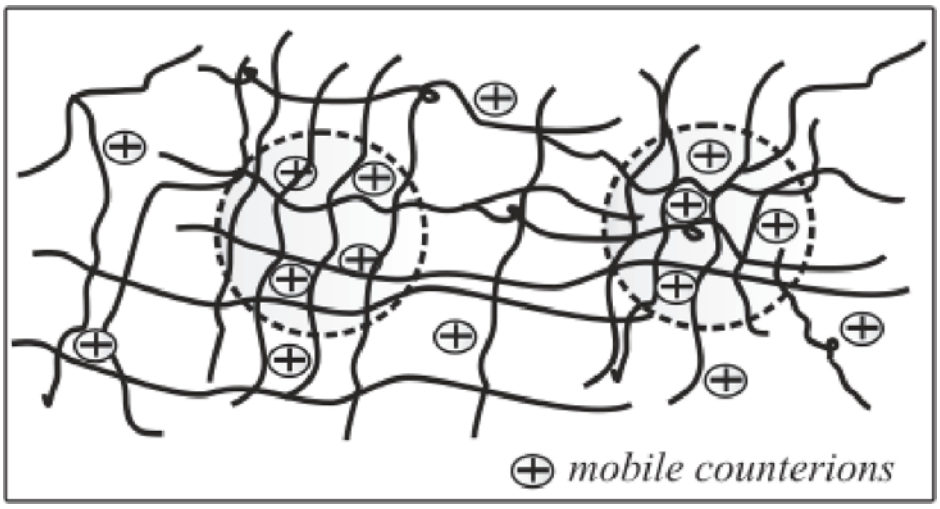

Figure 6.35: Schematic representation of the dense and dilute regions of the hydrogel. Mobile counterions (cations) are also indicated in the figure.

One of the purpose of this thesis is to obtain a correlation between the macroscopic (elastic) and microscopic (scattering) properties of hydrogels. Indeed, a comparison of the elasticity results with the results of the light scattering measurements shows an interesting feature of ionic PDMAAm hydrogels: In the range of x_i between 0 and 0.10, the modulus of elasticity G_0 increases with increasing ionic group content of the hydrogels (Figure 6.19A). In the same range of x_i, the excess scattering, that is, the spatial gel inhomogeneity rapidly decreases (Figure 6.33). Thus, the results indicate that the increase of the elastic modulus with the ionic group content is not due to the ion-pair formation but due to the homogenization of gels in the presence of the counterions. Therefore, it can be suggested that the variation of the degree of the spatial inhomogeneity is mainly responsible for the charge density dependence of the elastic modulus of PDMAAm hydrogels. Thus, the macroscopic elastic property of PDMAAm hydrogels can be controlled by the microscopic gel structure determined by the scattering measurements.

6.3.3. The Effect of Initiator System on The Spatial Gel Inhomogeneity

The effect of the type of the initiator system used in the preparation on the spatial inhomogeneity in PDMAAm and poly(acrylamide) (PAAm) hydrogels were investigated by light scattering measurements. The hydrogels were prepared by free-radical crosslinking copolymerization of the monomers DMAAm and AAm with BAAm as a crosslinker as described in Section 5.4. To initiate the gelation reactions of DMAAm as well as AAm monomers in the presence of BAAm as a crosslinker, two different redox-initiator systems were used:

1- Ammonium persulfate (APS) – N,N,N',N'-tetramethylethylenediamine (TEMED).
2- APS – sodium metabisulfite (SPS).

6.3.3.1. Linear Polymerizations of DMAAm and AAm Monomers

The linear polymerization reactions of the monomers DMAAm and AAm were first investigated by dilatometric and light scattering measurements. The linear polymers of DMAAm and AAm were prepared by free-radical polymerization reactions of both monomers in aqueous solutions at 21^{o}C at a total monomer concentration C_0 of 5.0 w/v%. The polymerization reactions were conducted in the absence of the crosslinker BAAm. To initiate the polymerization, the redox pairs consisting of APS (3.51 mM) - TEMED (24.9 mM) as well as APS - SPS (both 1.50 mM) were used in the experiments.

The linear polymerization reactions of DMAAm and AAm monomers were first followed by dilatometry. The details for this measurement was already given in Section 5.7.1. The results of the dilatometric measurements are shown in Figure 6.36 where the fractional monomer conversion x is plotted against the reaction time t in DMAAm (triangles) and AAm (circles) polymerizations. The filled and open symbols are the data points obtained using APS-TEMED and APS-SPS initiator systems, respectively. The duration of the induction period was found to be 15 and 5 min in DMAAm and AAm polymerizations, respectively. By repeated measurements, a variation of ± 2 min was observed in the induction period. However, it was found that the polymerization rate was unchanged from these variations. The prolonged induction period in DMAAm polymerization is observed due to the presence of the inhibitor hydroquinone monomethylether in the DMAAm

monomer. In order to test the effect of the existance of the inhibitor, the same inhibitor was added to the AAm polymerization system and it was found that the addition of the same inhibitor also prolonged the induction period without changing the time-conversion curve of the AAm polymerization system.

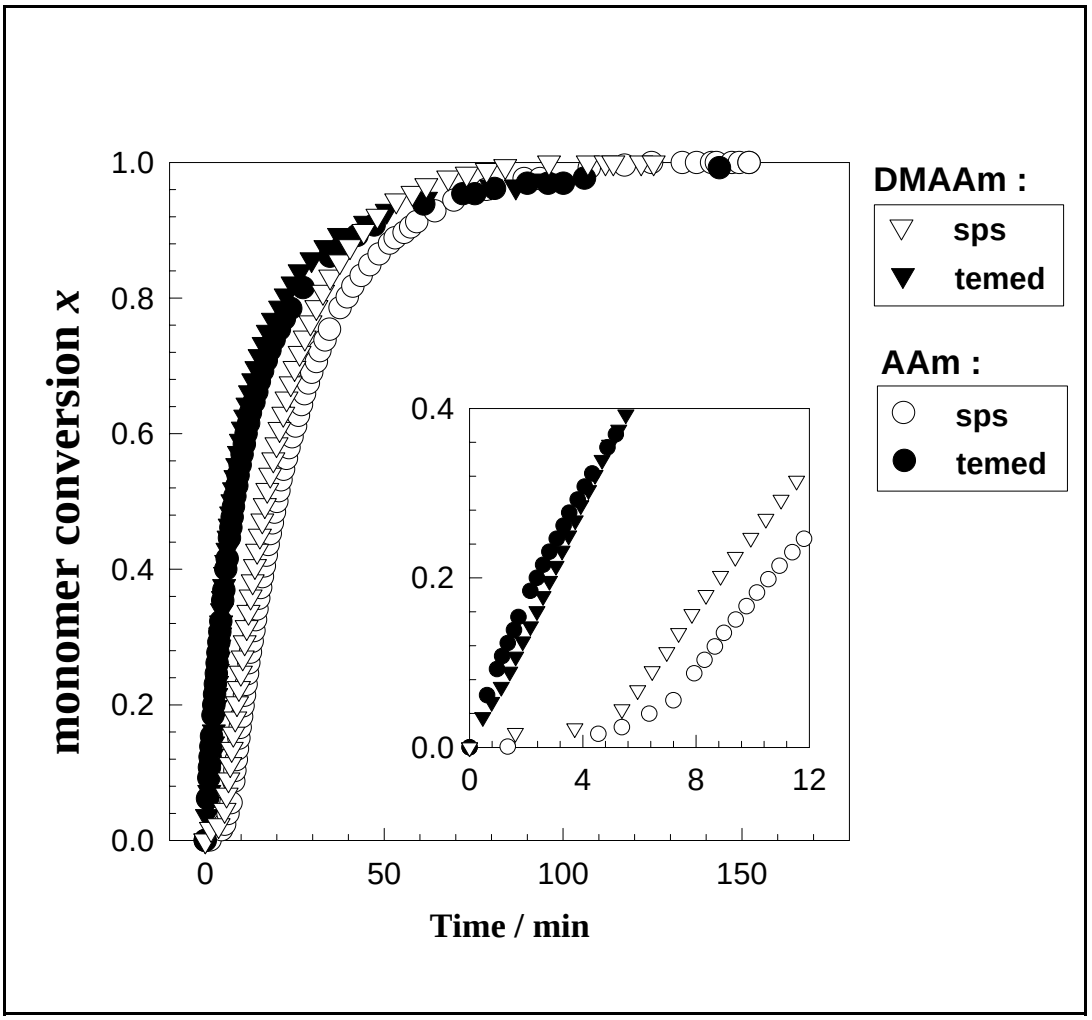

Figure 6.36: The fractional monomer conversion *x* plotted against the reaction time in linear DMAAm (triangles) and AAm (circles) polymerizations. Initiator system: APS-TEMED (filled symbols), APS-SPS (open symbols). The inset shows the initial period of the reactions.

Another point shown from the Figure 6.36 is that the complete monomer conversions were obtained after a reaction time of 90 min and, the polymerization rates are almost equal for DMAAm and AAm polymerizations. The inset to Figure 6.36 shows the initial period of the reactions. It is seen that the polymerization of both DMAAm and AAm monomers in the presence of APS – SPS initiator system is initially slow up to about 5 – 7 min. The monomer conversion attained after this slow period is about 2-4 %. Thereafter, the polymerization occurs very rapidly, as in the

presence of APS – TEMED redox pair and, a complete monomer conversion was obtained after a reaction time of 90 min[128,129]. As discussed in the experimental section, the existence of various consecutive reactions for the radical generation by APS-SPS redox pair seems to be responsible for this behavior.

The linear polymerization reactions of DMAAm and AAm were also followed by real-time light scattering technique. The scattered light intensity I_s at $\theta = 90^0$ was measured during the course of the linear polymerization reactions. In Figure 6.37A, the scattered light intensity I_s recorded at $\theta = 90^o$ is shown as a function of the reaction time in the linear DMAAm and AAm polymerizations in the presence of APS-TEMED redox pair. In order to make a comparison, the conversion curves obtained from dilatometric measurements are also shown in Figure 6.37B. The dotted vertical lines indicate the reaction times at the maximum intensity. The arrow shows the corresponding monomer conversion. As shown in the Figure 6.37, no intensity rise was observed during the induction period of the reactions. Therefore, to interpret the results from the real-time light scattering measurements the reaction time is defined as the total time elapsed minus the time needed for the induction period. The start of the polymerization is accompanied with a rapid increase in I_s, which reaches a maximum after a certain reaction time. It was found that the polymerization reaction in the presence of APS-TEMED initiator system reaches a maximum after 0.4 and 0.6 min for DMAAm and AAm polymerization. After passing the maximum intensity, I_s gradually decreases with the reaction time or monomer conversion and finally, attains a plateau value after about 10 min or 60 % monomer conversion.

Figure 6.37B shows that the maximum intensity occurs at a monomer conversion x = 0.04 ± 0.02, indicating that the polymer concentration in the reaction system is 0.2 ± 0.1 w/v %. The maximum in the scattering curves can be interpreted as the point at which the polymer concentration in the reaction system attains the critical overlap concentration c^* (in w/v %). By using the molecular weight $\overline{M}_w$ and the radius of the polymer chains $\left\langle R_g^2 \right\rangle^{1/2}$ listed in Table 6.3 together with Equation (4.25), the overlap concentrations c^* were calculated and are shown in the fifth column of Table 6.3. For the PAAm solution in water, c^* equals 0.37 (0.08), indicating that the reaction system attains this concentration at x = 0.026. Thus, c^* for the PAAm system is close to the polymer concentration of AAm reaction system at the peak

maximum. Further, c^* for PDMAAm in water is lower than that of found for PAAm system (Table 6.3). Therefore, the maximum intensity in the DMAAm system appears earlier, i.e., in shorter reaction times.

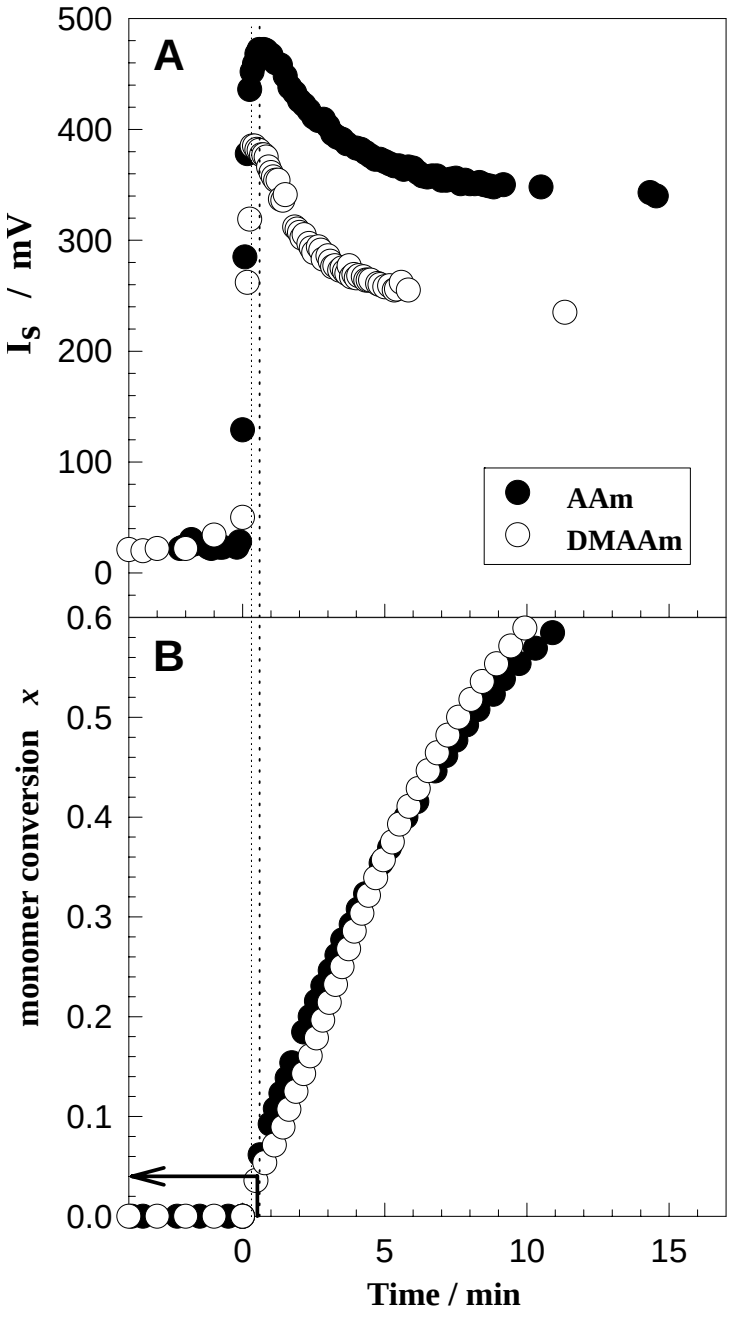

Figure 6.37: The scattered light intensity I_s recorded at $\theta = 90^o$ (A) and the monomer conversion x (B) shown as a function of the reaction time in linear DMAAm (open symbols) and AAm (filled symbols) polymerizations in the presence of APS-TEMED redox pair.

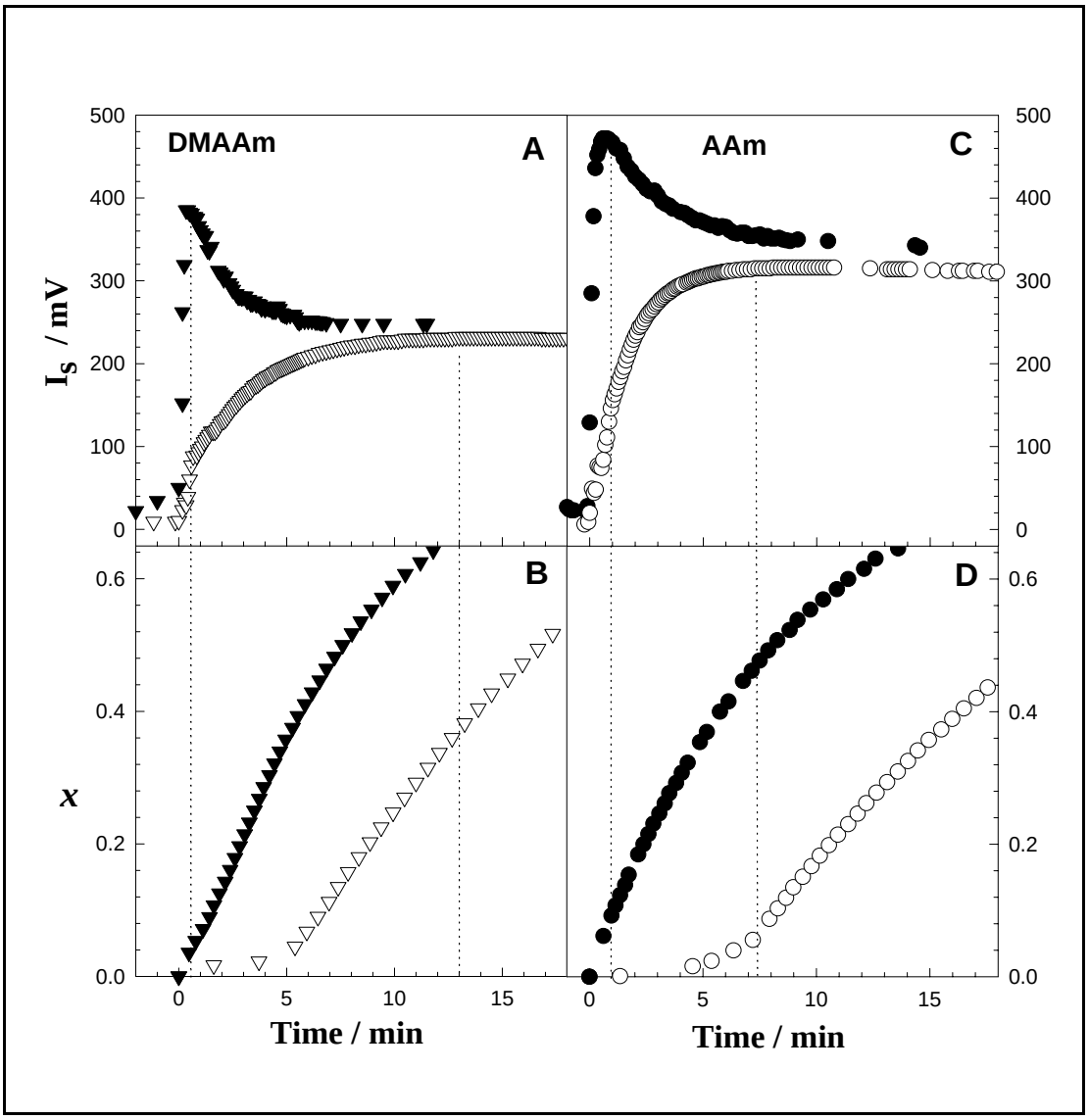

Figure 6.38: The scattered light intensity I_s recorded at $\theta = 90^o$ (A,C) and the monomer conversion x (B,D) shown as a function of the reaction time in linear DMAAm (triangles) and AAm (circles) polymerizations using APS-TEMED (filled symbols) and APS-SPS (open symbols) redox pairs. The dotted vertical lines indicate the critical reaction times t* at the chain overlap.

In Figure 6.38, the scattered light intensity I_s, recorded at $\theta = 90^o$ is shown as a function of the reaction time in the linear DMAAm and AAm polymerizations using APS-TEMED and APS-SPS redox pairs. In order to make a comparison, the conversion curves are also shown in the Figures. As shown in the Fig. 6.38A-D, similar to the APS-TEMED redox pairs, no intensity rise was observed during the induction period of the reactions initiated by APS-SPS redox pairs.

The rapid increase in I_s is again accompanied with the start of the polymerization. Also, the scattered light intensity I_s reaches the maximum after a certain reaction

time. However, a somewhat different behavior observed in the presence of APS-SPS redox pairs. Compared to TEMED, SPS as an accelerator produces only a smooth maximum in the scattered light intensity I_s at much longer reaction times. After passing the maximum intensity, I_s gradually decreases with the reaction time or monomer conversion and finally, attains a plateau value after about 15 min.

The shape of the scattering curves shown in Figures 6.37 and 6.38 can be explained as follows:

i. The rapid increase of I_s in short reaction times (< 35 s) is due to the very short life time of the radicals in FCC so that the polymer chains immediately start to form. The polymer chains formed during the reactions are initially in a highly dilute solution so that the polymer concentration c is below the so-called overlap threshold c^* where the chains start to overlap. As a result, the single coils scatter light intensively and, an abrupt intensity rise is observed with the onset of reactions due to the increasing number of coils with time.

ii. The number of individual polymer coils attains a maximum value at the overlap concentration so that the scattering curve exhibits a peak at this concentration. Therefore, the maximum in the scattering curves can be interpreted as the point at which the polymer concentration in the reaction system attains the critical overlap concentration c^*.

iii. As the reactions proceed, the polymer concentration c increases and, when c becomes larger than c^*, a semidilute polymer solution forms in the reaction system, where the chains overlap and the average mesh size is the characteristic size of the entangled chains. In this regime, only the mesh size of the polymer solution is detectable by light scattering and not the size of the individual polymer coils. Since the mesh size is much smaller than the size of molecules, and scattered light intensity decreases with the reaction time[128,129].

In order to check this point, the critical reaction times t^* for the onset of chain overlap were calculated using the c^* concentrations listed in Table 6.3 together with the time conversion curves. The calculated values of t^* together with the reaction times t at the peak maxima are listed in Table 6.3. The vertical dotted lines in Figure 6.38 also represent t^* values on the time axes. It is seen that, for all the reaction systems studied, the maximum in the scattering curves coincides with c^* of the

polymerization systems. These results also demonstrate that the combination of dilatometric and real-time light scattering techniques provides an experimental tool for the determination of the critical overlap concentration in linear polymerization systems. Thus, the scattering curves display three regimes of the linear polymerization systems, as schematically illustrated in Figure 6.39:

1) Induction period ($t^* = 0$),
2) Dilute concentration regime ($t^* = 0$ to about 0.8), and,
3) Semi-dilute regime ($t^* > 0.8$).

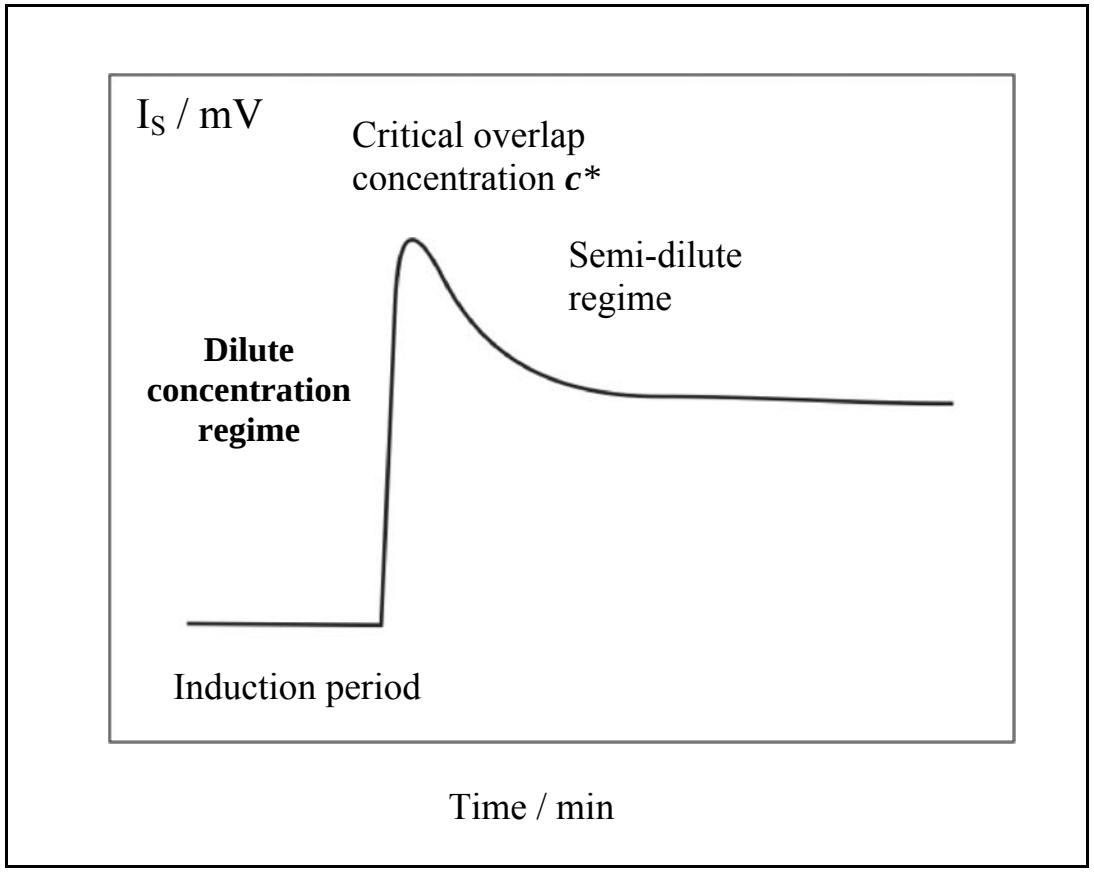

Figure 6.39: Schematic illustration of the scattering intensity profile I_s obtained during the linear polymerization reactions.

To interpret the linear polymerization results, Zimm plots obtained by light scattering measurements of linear PDMAAm and PAAm prepared in the presence of APS-TEMED and APS-SPS redox pairs are given in Figures 6.40 and 6.41.

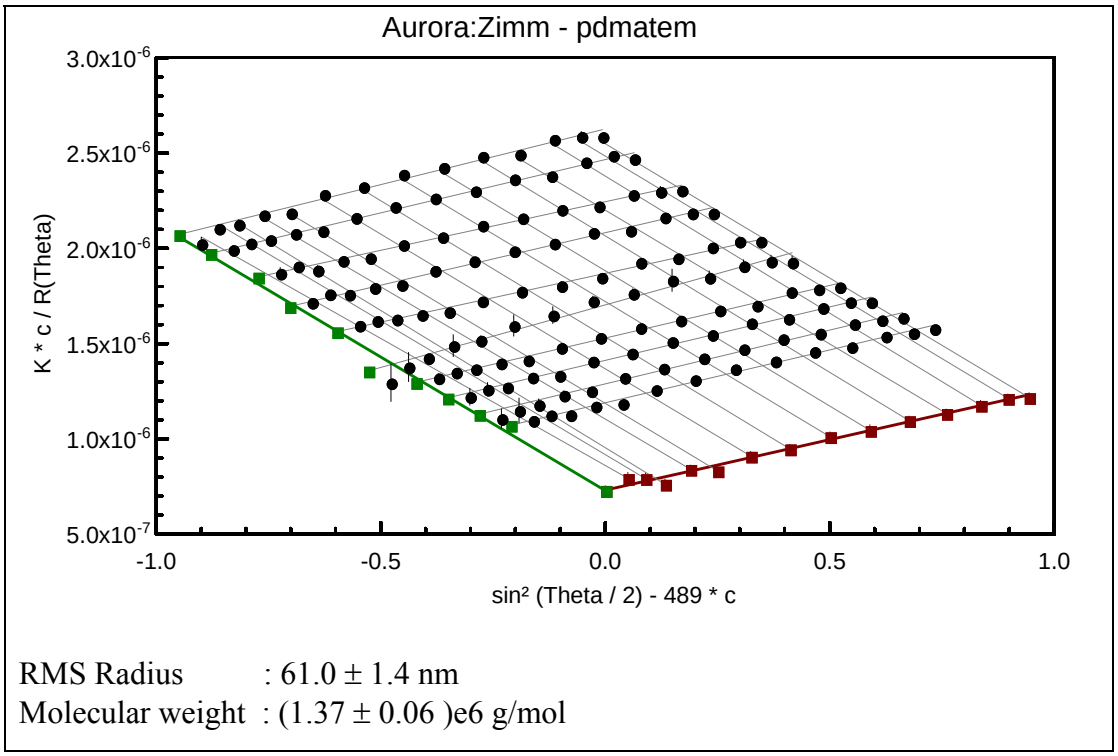

RMS Radius : 61.0 ± 1.4 nm
Molecular weight : (1.37 ± 0.06)e6 g/mol

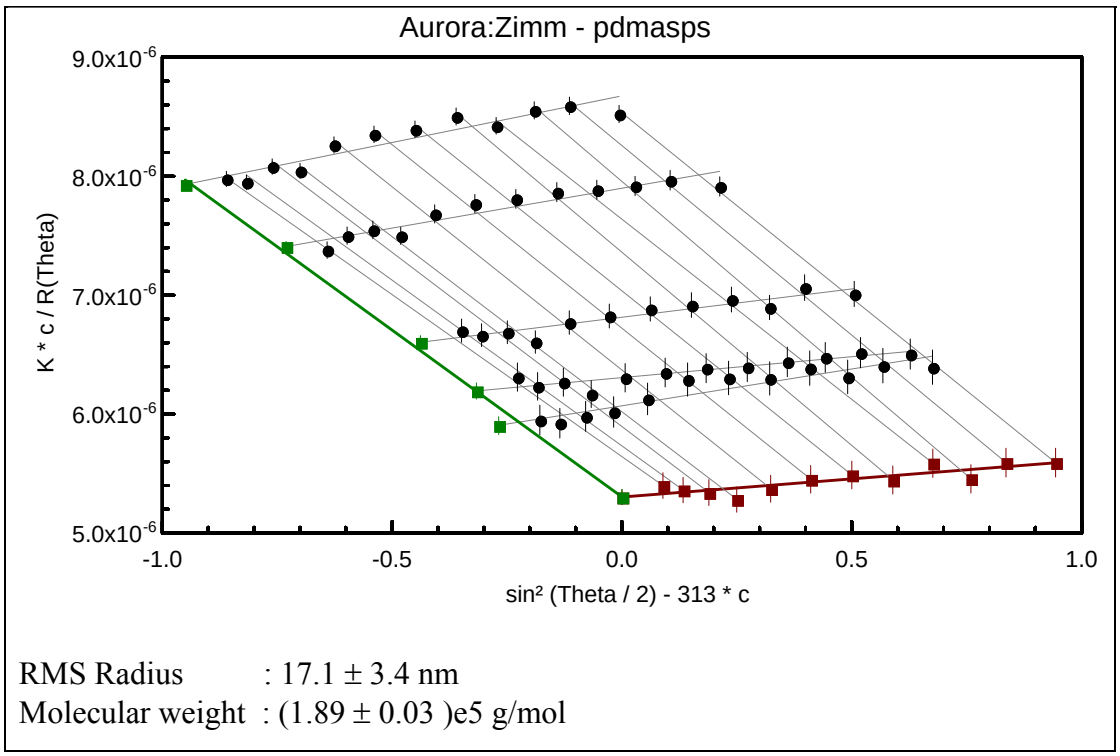

RMS Radius : 17.1 ± 3.4 nm
Molecular weight : (1.89 ± 0.03)e5 g/mol

Figure 6.40: Zimm plots for linear PDMAAm. Initiator system: APS-TEMED (upper plot), APS-SPS (lower plot).

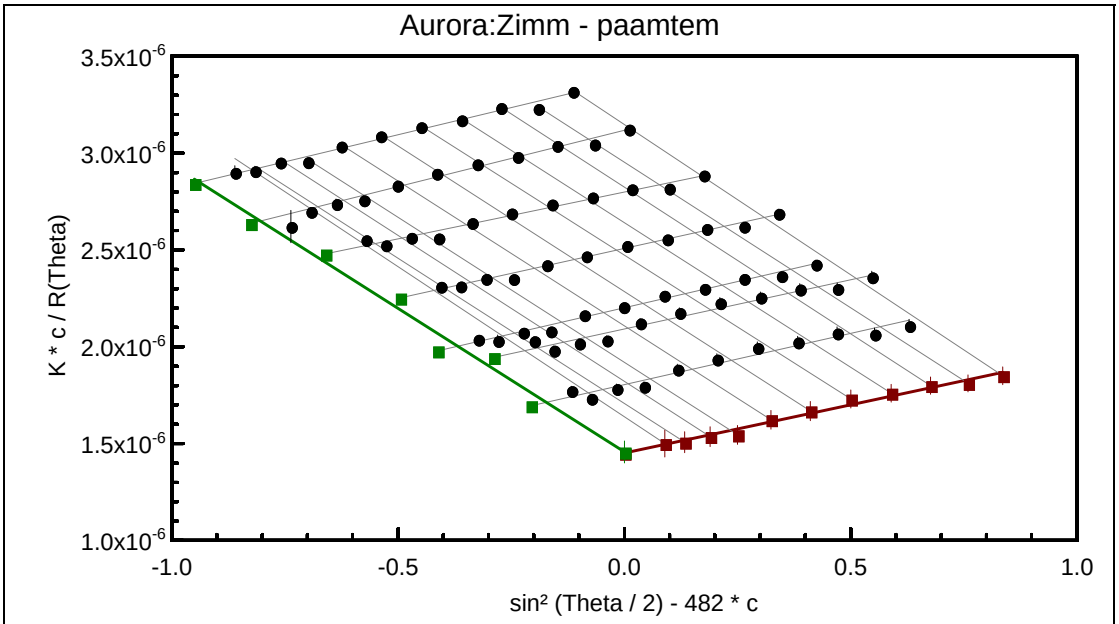

RMS Radius : 41.9 ± 2.64 nm
Molecular weight : (6.88 ± 0.33)e5 g/mol

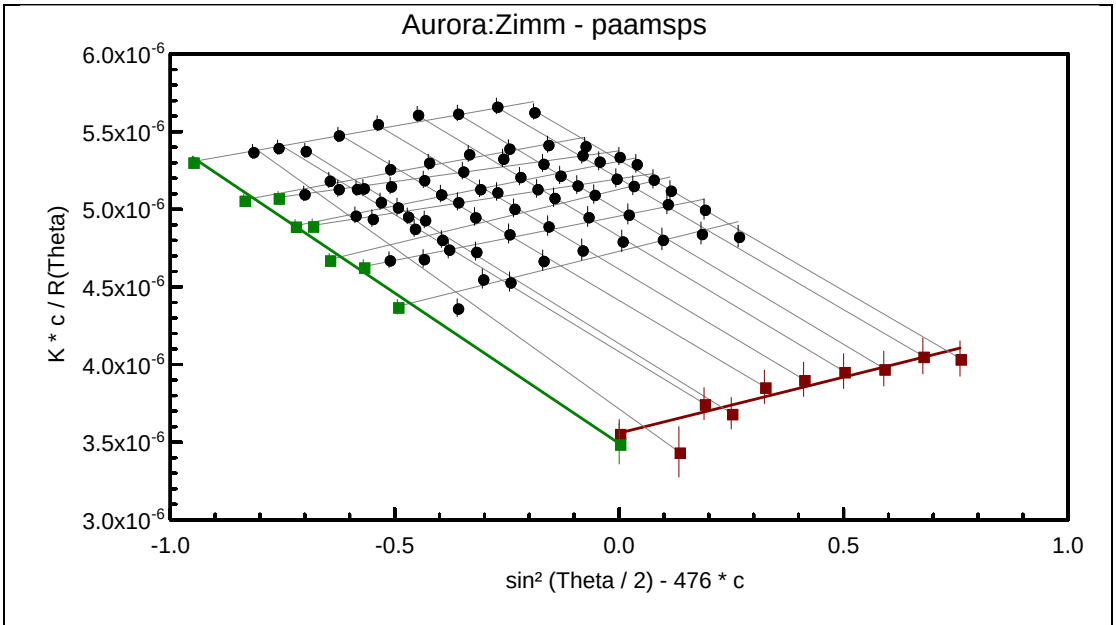

RMS Radius : 32.2 ± 4.2 nm
Molecular weight : (2.84 ± 0.1)e5 g/mol

Figure 6.41: Zimm plots for linear PAAm. Initiator system: APS-TEMED (upper plot), APS-SPS (lower plot).

The weight-average molecular weight $\overline{M}_w$ and the radius of gyration $\left\langle R_g^2 \right\rangle^{1/2}$ of the polymers obtained from the Zimm plots are collected in the third and fourth columns of Table 6.3, respectively. Table 6.3 shows that the average size of PDMAAm coils formed using APS-SPS is much smaller compared to those formed using APS-TEMED redox pair. As a consequence, PDMAAm chains in APS-SPS initiated reactions start to overlap at a longer reaction time (12 vs. 0.7 min), so that the maximum of the scattering curve shifts toward a later reaction time. In AAm polymerization, however, the decrease in the coil size is not as significant as in the DMAAm polymerization so that *c** does not change much when with the initiator system was changed (Table 6.3). However, in this case, since the initial rate of APS-SPS initiated polymerization is slow, *t** also shifts toward a longer reaction time.

Table 6.3: Characteristics of the linear PDMAAm and PAAm prepared using APS-TEMED and APS-SPS redox pairs: t* = the critical reaction time at the chain overlap and t = the reaction times at the peak maximum in the scattering curves. The numbers in parenthesis are the standard deviations.

Polymer Type	Initiator Type	$10^{-5}\ \overline{M}_w$ (g/mol)	$\left\langle R_g^2 \right\rangle^{1/2}$ (nm)	*c** (g/100 mL)	t* (min)	t at $I_{s,max}$ (min)
PAAm	APS-TEMED	6.9 (0.3)	42 (3)	0.37 (0.08)	0.8 (0.1)	0.6 (0.1)
	APS - SPS	2.8 (0.1)	32 (4)	0.34 (0.10)	7.5 (0.3)	9 (0.5)
PDMAAm	APS-TEMED	14 (1)	62 (2)	0.23 (0.02)	0.7 (0.05)	0.4 (0.2)
	APS-SPS	1.9 (0.03)	17 (3)	1.6 (0.6)	12 (1)	12.5 (1)

6.3.3.2. Crosslinking Polymerizations of DMAAm and AAm Monomers

By using free-radical crosslinking copolymerization, PDMAAm and PAAm hydrogels were prepared in the presence of APS (3.51 mM)-TEMED (24.9 mM) as well as APS-SPS (both 1.50 mM) redox initiator systems. In order to investigate the spatial inhomogeneity in PDMAAm and PAAm hydrogels, the light scattering experiments were performed on the hydrogels. The uniaxial compression measurements were also performed on the hydrogels to interpret light scattering results. The results from the mechanical measurements are complied in Tables 6.4.

Table 6.4: The characteristic data of PDMAAm and PAAm hydrogels prepared using APS-SPS and APS-TEMED redox pairs. C_0 = 5 w/v%. X = the crosslinker ratio, G_0 = the elastic modulus of gels after their preparation, G_{theo} = theoretical elastic modulus of the gels, and ε_{xl} = the crosslinking efficiency.

APS-SPS	PDMAAm			PAAm		
X	G_0 / Pa	G_{theo}	ε_{xl}	G_0 / Pa	G_{theo}	ε_{xl}
50	238	23900	0.0100	1265	34393	0.0368
60	177	19917	0.0089	1042	28660	0.0363
70	163	17071	0.0096	919	24566	0.0374
80	134	14937	0.0089	716	21495	0.0333

APS-TEMED	PDMAAm			PAAm		
X	G_0 / Pa	G_{theo}	ε_{xl}	G_0 / Pa	G_{theo}	ε_{xl}
50	4005	23900	0.1676	3389	34393	0.0985
60	2789	19917	0.1400	2522	28660	0.0880
70	2485	17071	0.1455	2293	24566	0.0933
80	2263	14937	0.1515	1912	21495	0.0889

The uniaxial compression measurements were also performed on PDMAAm and PAAm hydrogels prepared using APS-TEMED redox pair at predetermined reaction times. To obtain the modulus of the hydrogels as a function of the reaction time, only six records were taken during the elasticity tests, which required 2 min. During the measurements, the reaction time was taken as the time period between the onset of the polymerization reactions (end of the induction period) and the start of the compression of the gel sample. In Figure 6.42, the elastic modulus G_0 of both PDMAAm and PAAm hydrogels prepared in the presence of APS-TEMED redox pair are plotted against the reaction time. For these hydrogels C_0 =5.0 w/v% and the crosslinker ratio X =1/82. It is seen that PDMAAm hydrogels exhibit slightly larger elastic moduli compared to PAAm hydrogels. The difference observed just beyond the gel point (G_0 < 1 kPa) shown in the inset is due to the early onset of the gelation in AAm polymerization so that the growth of PAAm hydrogel starts earlier.

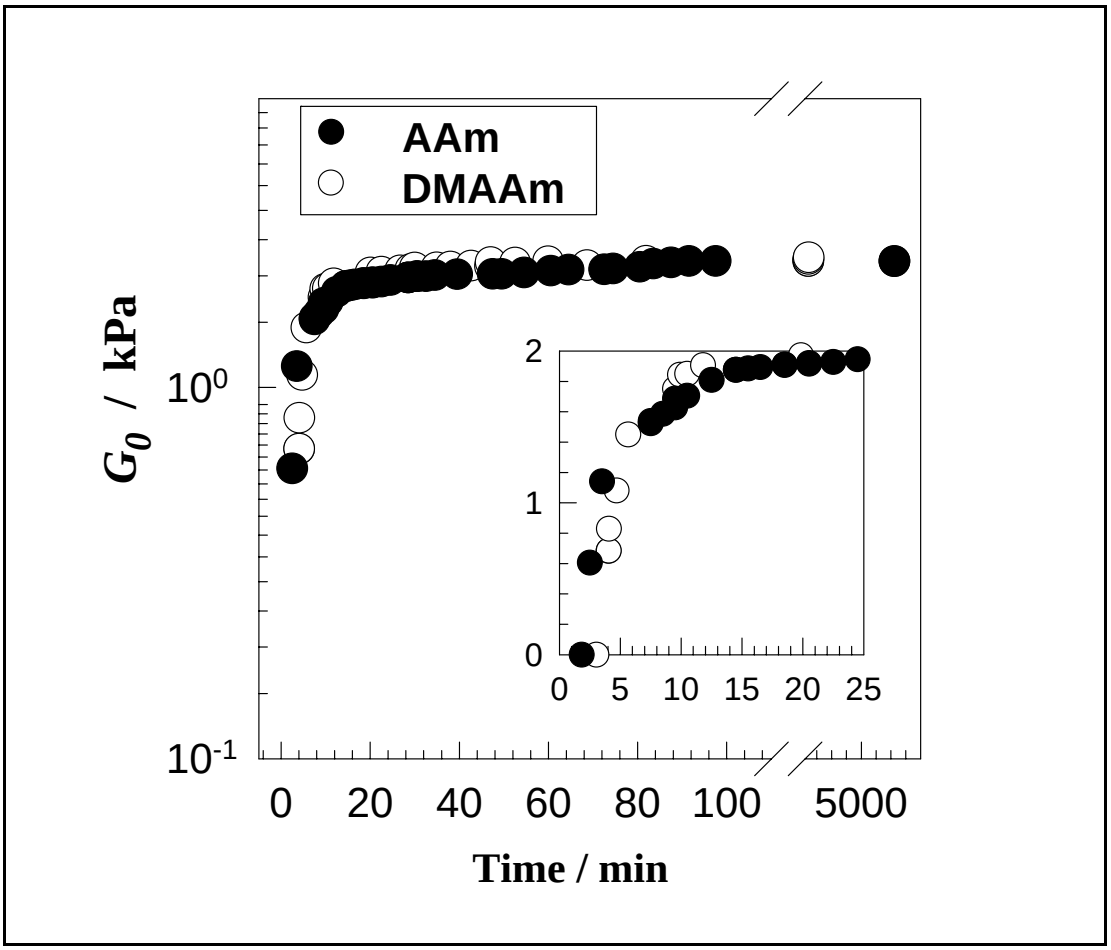

Figure 6.42: The elastic modulus of hydrogels after preparation G_0 plotted against the reaction time for crosslinking DMAAm polymerizations (open symbols) and AAm (filled symbols). The inset shows the initial reaction period beyond gelation.

The mechanical measurements were also performed on PDMAAm and PAAm hydrogels after their preparation. In Figure 6.43, the elastic modulus G_0 of PDMAAm (triangles) and PAAm (circles) hydrogels are plotted against the inverse crosslinker ratio $1/X$. The filled and open symbols represent data from gels obtained using APS-TEMED and APS-SPS redox-pairs, respectively. It is seen that, G_0 increases with the crosslinker concentration. Moreover, the hydrogels formed using APS-TEMED exhibit larger elastic modulus compared to those formed using APS-SPS initiator system. Assuming phantom network behavior ($\phi = 4$), G_{theo} of the hydrogels are shown in Figure as the dotted curves. It is seen that G_{theo} is much higher than G_0 of the hydrogels. Assuming that all BAAm molecules used in the gel synthesis participate in forming effective crosslinks, the theoretical elastic modulus G_{theo} of the hydrogels can be calculated as[32,39]:

$$G_{theo} = A\frac{2\rho X}{M_r} RT \nu_2^0 \qquad (6.18)$$

where the front factor A equals to 1 for an affine network and 1- 2 / ϕ for a phantom network, ϕ is the functionality of the crosslinks, ρ is the polymer density (1.21 and 1.35 g/mL for PDMAAm and PAAm gels, respectively) and M_r is the molecular weight of repeat unit (99 and 71 g/mol for DMAAm and AAm, respectively), ν_2^0 is the polymer concentration just after the gel preparation, R and T are in their usual meanings.

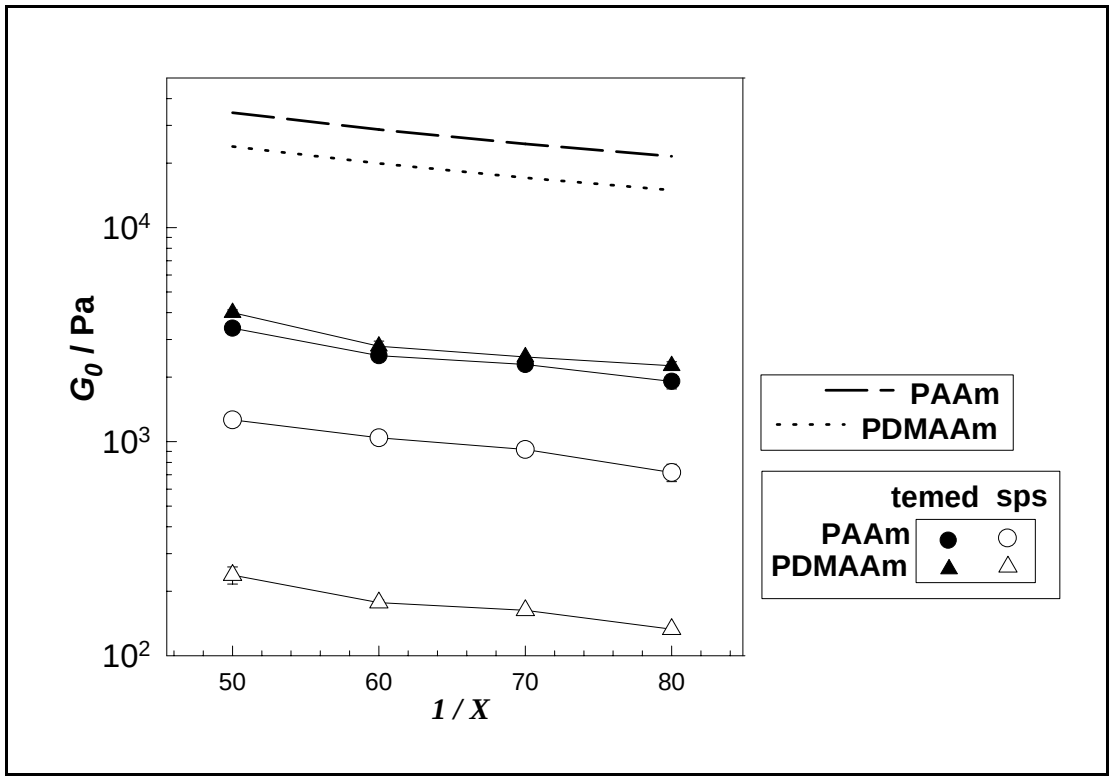

Figure 6.43: The elastic modulus of hydrogels after preparation G_0 shown as a function of $1/X$ for PAAm (circles) and PDMAAm gels (triangles). Initiator system: APS-TEMED (filled symbols), and APS-SPS (open symbols). The theoretical elastic modulus G_{theo} vs $1/X$ plot is shown by the dotted curves.

In Fig. 6.44, the crosslinking efficiency of BAAm $\varepsilon_{xl} = G_0 / G_{theo}$, that is the fraction of BAAm forming effective crosslinks is shown as a function of $1/X$. When TEMED is used as an accelerator, ε_{xl} is in the range 0.10 – 0.15. This value is in good agreement with that found from the equilibrium swelling measurements of gels[130], as well as from the determination of the pendant vinyl group content of pre-gel polymers[117]. The low efficiency of crosslinking ε_{xl} is mainly due to the cyclization

and the multiple crosslinking reactions during gelation, leading to the formation of the elastically ineffective loops as well as the clusters of crosslinks in the final network. However, if SPS is used as an accelerator, ε_{xl} further reduces to $10^{-2} - 10^{-3}$, indicating that only 0.1 to 1 % of BAAm used in the hydrogel preparation form effective crosslinks in the final hydrogels.

Figure 6.44 also shows that the decrease in the crosslinking efficiency due to use of SPS is particularly significant in the DMAAm polymerization. This very low efficiency of crosslinking in APS-SPS system is probably due to the formation of low molecular weight polymers (Table 6.3). Thus, as the primary molecules become shorter, the number of terminal chains, which make no contribution to the network elasticity, increases, so that the crosslinking efficiency decreases.

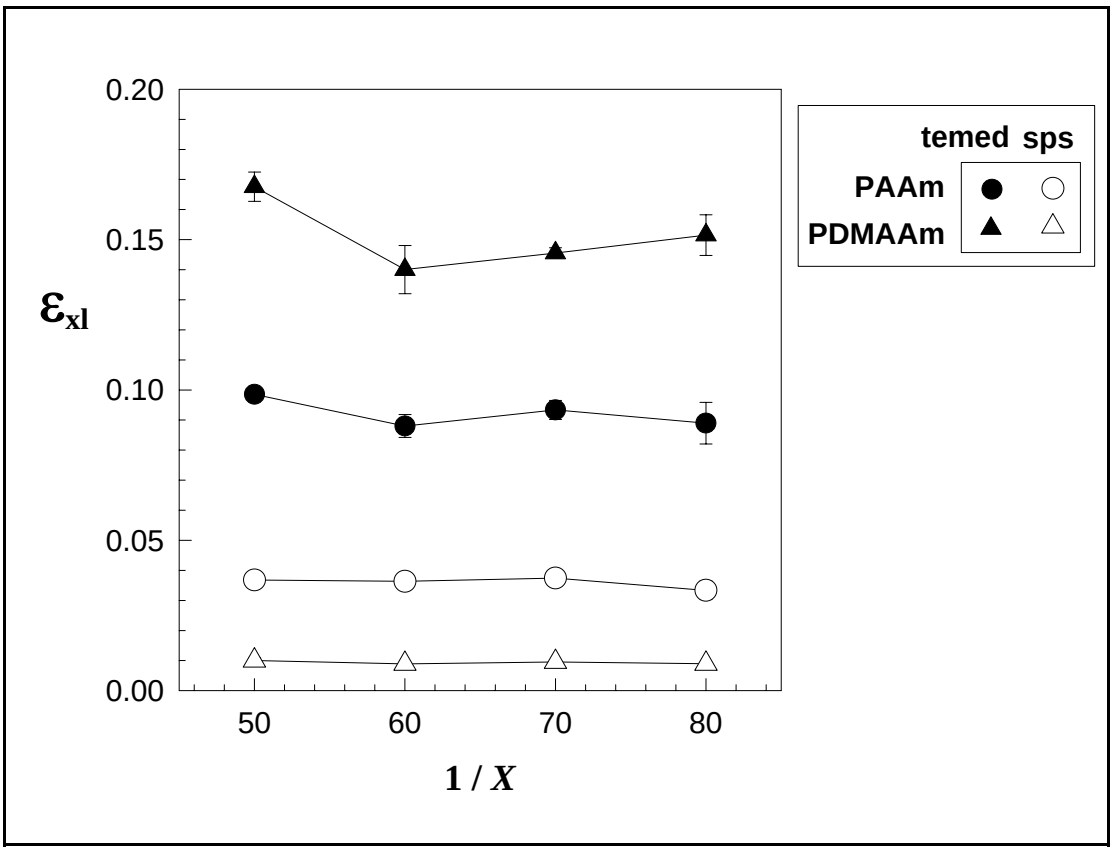

Figure 6.44: The crosslinking efficiency of BAAm ε_{xl} during the gel preparation shown as a function of $1/X$ for PDMAAm (triangles) and PAAm (circles) gels. Initiator system: APS-TEMED (filled symbols), and APS-SPS (open symbols).

6.3.3.3. Light Scattering Measurements of Hydrogels

The light scattering measurements of PDMAAm and PAAm hydrogels were carried out during the gelation reactions as well as after a reaction time of one day. The results are presented in two parts depending on the redox initiator systems used in the hydrogel synthesis. The results for PDMAAm and PAAm hydrogels prepared using APS –TEMED redox pair will be discussed at first and then the results for both hydrogels prepared using APS –SPS redox pair will be discussed in the second part.

i. PDMAAm and PAAm hydrogels prepared using APS –TEMED

In Figure 6.45, the scattered light intensity I_s is plotted against the reaction time for crosslinking DMAAm polymerizations. The crosslinker ratio X was varied between 1/100 and 1/50 keeping the total monomer concentration C_0 at 5 w/v %.

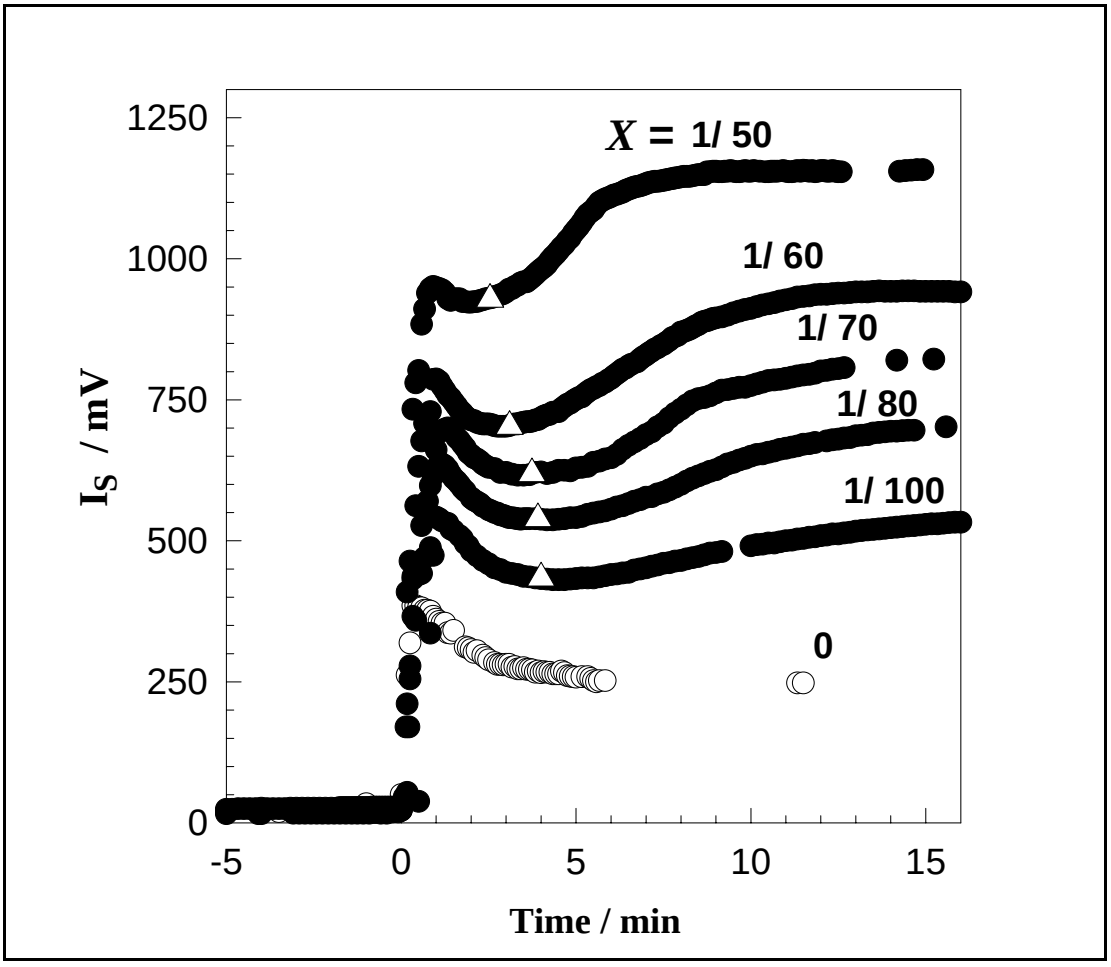

Figure 6.45: The scattered light intensity I_s at $\theta = 90^o$ plotted against the reaction time for crosslinking DMAAm polymerizations (filled symbols) and linear PDMAAm polymerizations (open symbols). The open triangles illustrate the gel points in terms of the reaction times.

The data obtained in linear polymerization reaction of DMAAm monomer ($X = 0$) is also shown in the Figure by open symbols. The first point seen from the Figure 6.45 is that, the scattering intensity profiles of the crosslinking DMAAm polymerizations differ from that of the linear polymerization. In Figure 6.45, the scattering curves of DMAAm polymerizations show the existence of both a maximum and a minimum in the scattering curves of the DMAAm system. The open triangles in Figure 6.45 illustrate the gel points in terms of the reaction times. It is seen that gelation in the DMAAm system occurs at reaction times corresponding to the minima in the scattering curves. It should be noted that, in contrast to the classical gel point at which the system changes from liquid to solid-like state, the sol-gel transitions in gelation system occurred not abrupt and took about 30 s. Therefore, the gel point is defined as the average of two reaction times where the gel starts to form at the lower part of the reaction mixture and where the gel occupies the whole available volume. Another point shown from the Figure 6.45 is that the larger is X the stronger is the increase of I_s, which is obviously due to the crosslinking reactions prior to gelation leading to the formation of larger molecules.

In order to make a comparison, PAAm hydrogels were also prepared under the same experimental condition with the PDMAAm hydrogels and the crosslinking AAm polymerizations were also followed by time-resolved light scattering measurements. In Figure 6.46, the scattered light intensity I_s is plotted against the reaction time for crosslinking AAm polymerizations. The crosslinker ratio X was varied between 1/200 and 1/50 keeping the total monomer concentration C_0 at 5 w/v %. The data obtained in the linear polymerization reaction of AAm monomer ($X = 0$) is also shown in the Figure by open symbols. As seen from Figure 6.46, for AAm polymerization, the shape of the scattering intensity I_s versus time plots is the same with and without crosslinker. However, the scattering curves of AAm polymerizations show the existence of only a maximum in the scattering curves of the AAm system. Similarly, the open triangles in Figure 6.46 illustrate the gel points in terms of the reaction times. It is seen that the gelation in the AAm system occurs at reaction times corresponding to the maxima in the scattering curves indicating that the gelation occurs at a polymer concentration in the vicinity of the chain overlap concentration c^*. Moreover, it was found that similar to the DMAAm system, the larger the X, the stronger the scattered intensity I_s along the AAm polymerization.

The experimental works indicated that the gelation occurs below overlap at high crosslinker ratios while it occurs later at low values of the crosslinker ratios.

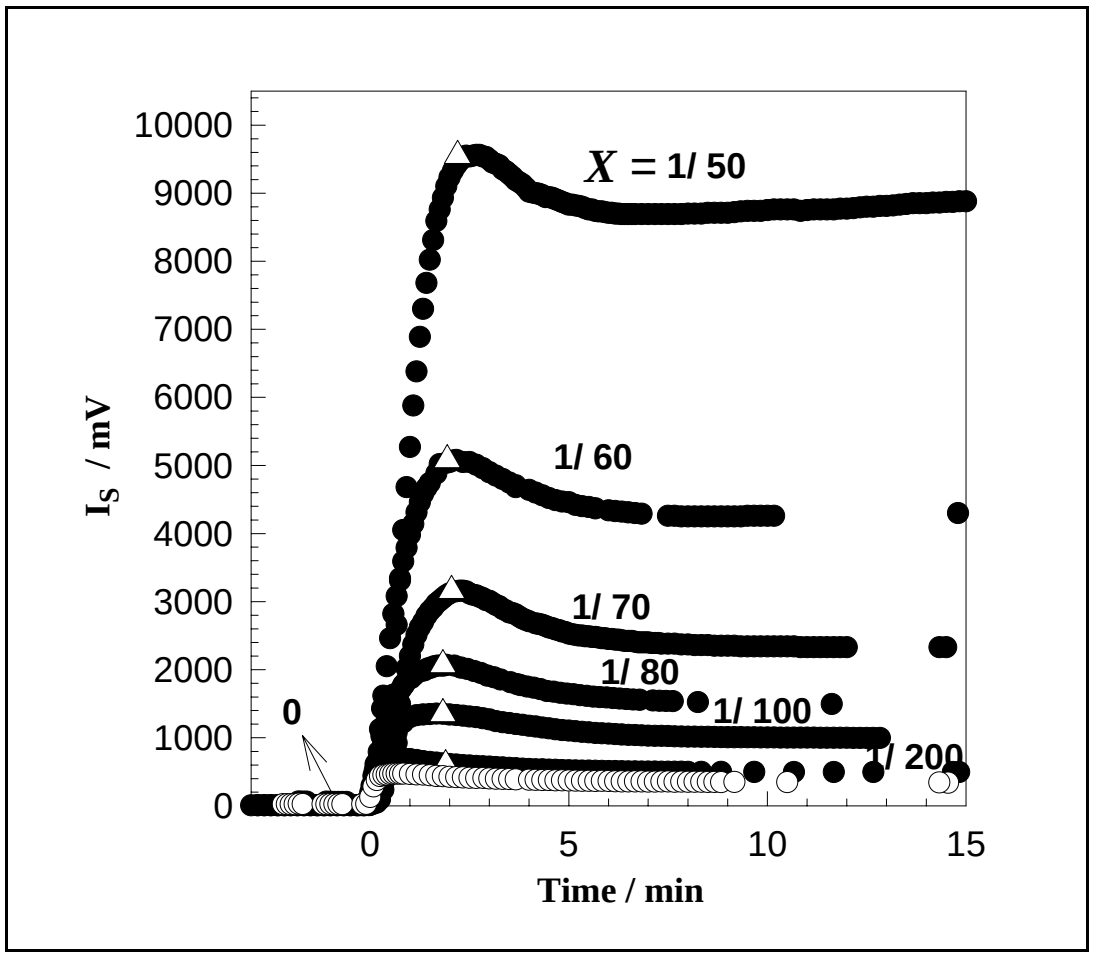

Figure 6.46: The scattered light intensity I_s at $\theta = 90^o$ plotted against the reaction time for crosslinking AAm polymerizations (filled symbols) and linear PAAm polymerizations (open symbols). The open triangles illustrate the gel points in terms of the reaction times.

In Figure 6.47 the scattering intensity I_s for crosslinking AAm polymerization at two different initial monomer concentrations C_0 (A) and crosslinker ratios X (B) are plotted as a function of reaction time in a semi-logarithmic scale. The shape of the curves is similar to those observed in linear polymerization. In Figure 6.47A, the plateau value of the scattered light intensity I_s increases with decreasing monomer concentration due to the unfolding of concentration fluctuations in gels.

Moreover, I_s also increases with the crosslinker ratio X due to the increasing degree of spatial gel inhomogeneity on rising the crosslink density of gels in a good solvent (Figure 6.47B). For reaction times longer than 10^3 min (>17 h), a decrease in the scattered light intensity was observed. This is due to the partial hydrolysis of AAm

units of the network chains into acrylic acid units. The use of TEMED as the accelerator during the gelation process leads to the formation of charged groups in the aged PAAm gels whose number increases with increasing time of aging of gels in the polymerization reactor. Since increasing charge density reduces the apparent degree of spatial gel inhomogeneity, I_s gradually decreases at longer reaction times. Thus, the scattering curves visualize the effects of various gel preparation parameters on the extend of spatial inhomogeneity in PAAm hydrogels[8,90].

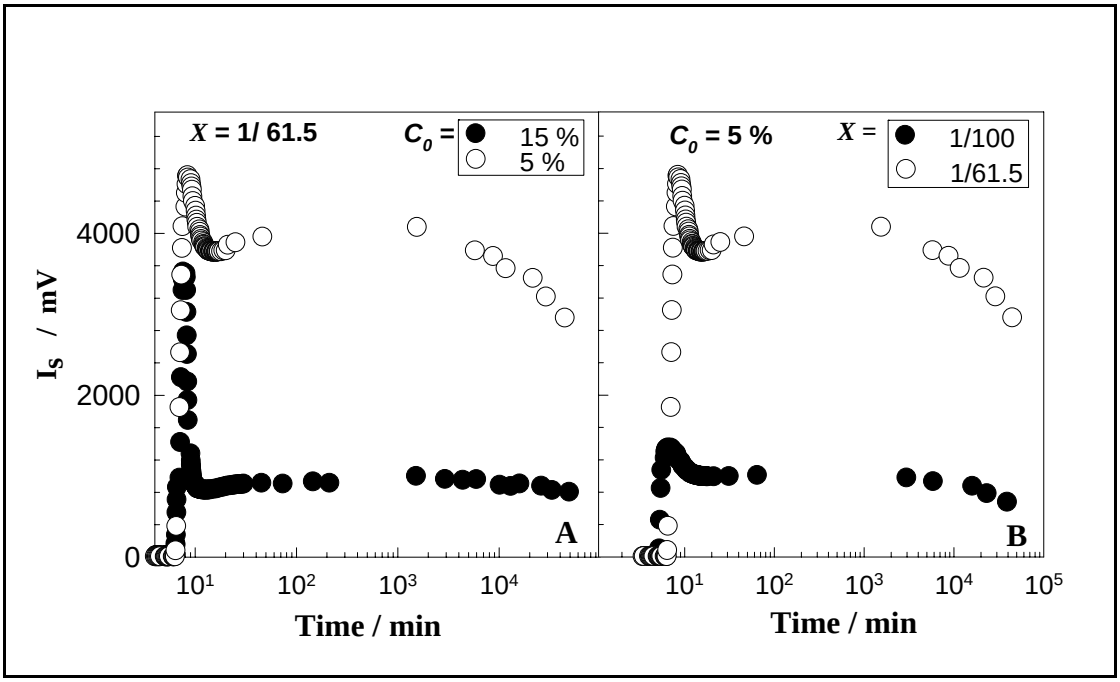

Figure 6.47: The scattered light intensity I_s at $\theta = 90^o$ versus reaction time plots, in a semi-logarithmic scale, for crosslinking AAm polymerization. (A) X=1/61.5, C_0= 5% (○) and 15% (●). (B) C_0= 5%, X=1/61.5 (○) and 1/100 (●).

In the following paragraphs, a comparison between the results of the time-resolved light scattering measurements of both crosslinking DMAAm and AAm polymerizations in the presence of APS-TEMED redox pair will be given. In Figure 6.48, the scattered light intensity change I_s at $\theta = 90^o$ with the reaction time is collected for crosslinking DMAAm polymerizations and AAm polymerizations in the presence of APS-TEMED redox pair. It is seen that no significant intensity rise was observed in DMAAm polymerization systems. The shape of the scattering intensity curves is quite different for DMAAm and AAm systems, both a maximum and a minimum appear in the scattering curves of the DMAAm system whereas only a maximum point appear in the scattering curves of the AAm system.

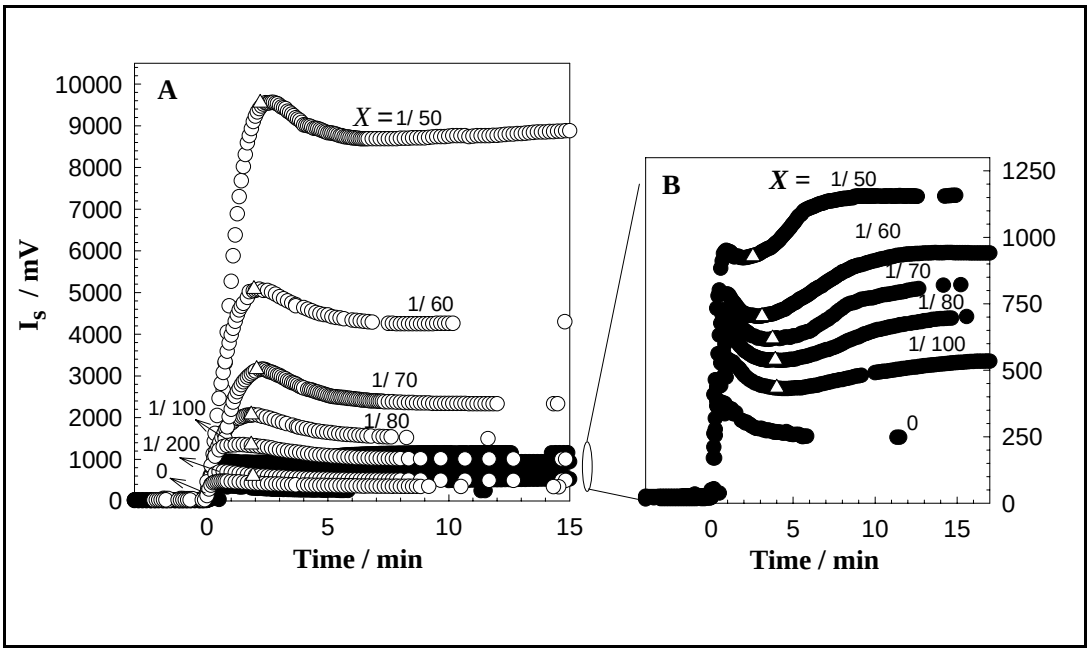

Figure 6.48: Variation of the scattered light intensity I_s at $\theta = 90^o$ with the reaction time for crosslinking DMAAm polymerizations (filled symbols) and AAm polymerizations (open symbols).

The location of the gel point is also different for DMAAm and AAm crosslinking copolymerizations. In AAm system, the gel point is close to the reaction time at the peak position. However, in DMAAm system, the gelation occurs at reaction times corresponding to the minima in the scattering curves. A comparison of the gel points in DMAAm and AAm systems also shows that the gel formation is retarded by replacing AAm with the DMAAm monomer. In Figure 6.49, the results of the real-time scattering light intensity I_s of both linear and crosslinking polymerization reactions of PDMAAm and PAAm was illustrated schematically and the differences in the scattering light intensity profiles during the polymerization reactions were also shown.

Similar to the AAm system, the larger the X, the stronger the scattered intensity I_s along the DMAAm polymerization. However, the intensity increase with the crosslinker ratio is much less than that observed in AAm polymerization. One possible explanation for the reduced degree of the scattered light intensity from PDMAAm hydrogels is their lower effective crosslink density leading to a reduced degree of the spatial inhomogeneity. In order to check this point, the mechanical measurements on both PAAm and PDMAAm hydrogels formed at various reaction times were conducted as described before. It was found that the reduced scattering from DMAAm system compared to the AAm system cannot be explained with the

effect of the crosslink density (Figure 6.42). It is rather a result of very different microscopic structure of PDMAAm hydrogel compared with that of PAAm hydrogel. As shown in Figure 6.48A, this difference is increasing with increasing crosslink density. A plausible explanation of this difference is the late onset of gelation in DMAAm polymerization. As seen in Figure 6.48B, gelation occurs in the DMAAm system in the semi-dilute regime, while in the AAm system, it occurs around the overlap concentration. The delay of gelation in DMAAm system is probably due to the bulky side groups in PDMAAm chains which reduce the reaction rates between macromolecules. Thus, the crosslinking reactions between the growing PDMAAm chains and the pendant vinyl groups occur at a slower rate so that the gel point is shifted to higher conversions. The much higher molecular weight of polymers formed in the DMAAm polymerization compared to the AAm system is also a result of the reduced rate of terminations reactions. The experimental works in the literature shows that the higher the DMAAm content of the comonomer feed in DMAAm/AAm copolymerization, the higher the molecular weight of the polymers[131].

Thus, for PAAm hydrogels, microgel-like clusters form during the gelation process due to the extensive cyclization reactions as well as due to the different reactivities of AAm and BAAm monomers. As a result, PAAm represents a typical inhomogeneous gel formed by free-radical crosslinking mechanism. On the contrary, in DMAAm polymerization, a solution of linear and branched polymers crosses the semi-dilute regime prior to the onset of gelation and therefore, this system resembles gel formation from a preformed polymer solution. Since the crosslinks are introduced relatively randomly in space during the crosslinking of preformed polymer chains PDMAAm hydrogel is much more homogeneous than PAAm hydrogel of the same effective crosslink density, so that it scatters much less light than the corresponding PAAm gel[76].

Figure 6.42 also shows that the appearance of a minimum in the scattering curve of the DMAAm system is due to the increase of the gel elasticity during the post-gelation period of the reactions. Since the spatial inhomogeneity becomes larger on raising the crosslink density, scattering intensity beyond the gel point increases up to a reaction time of 10 min due to the simultaneous increase of the elastic modulus. The minima do not appear in the scattering curves of AAm system as seen in the

Figure 6.49. This is due to the fact that the gelation time is close to the time at the peak maximum so that the increase in I_s due to the increasing moduli of gels is masked by the decrease in I_s due to the transition to the semi-dilute regime. Thus, the concentration effect decreasing the mesh size of polymer chains dominates over the crosslink density effect, resulting in a continuous decrease in I_s beyond the peak maximum in AAm polymerization. This point also shown schematically in Figure 6.49.

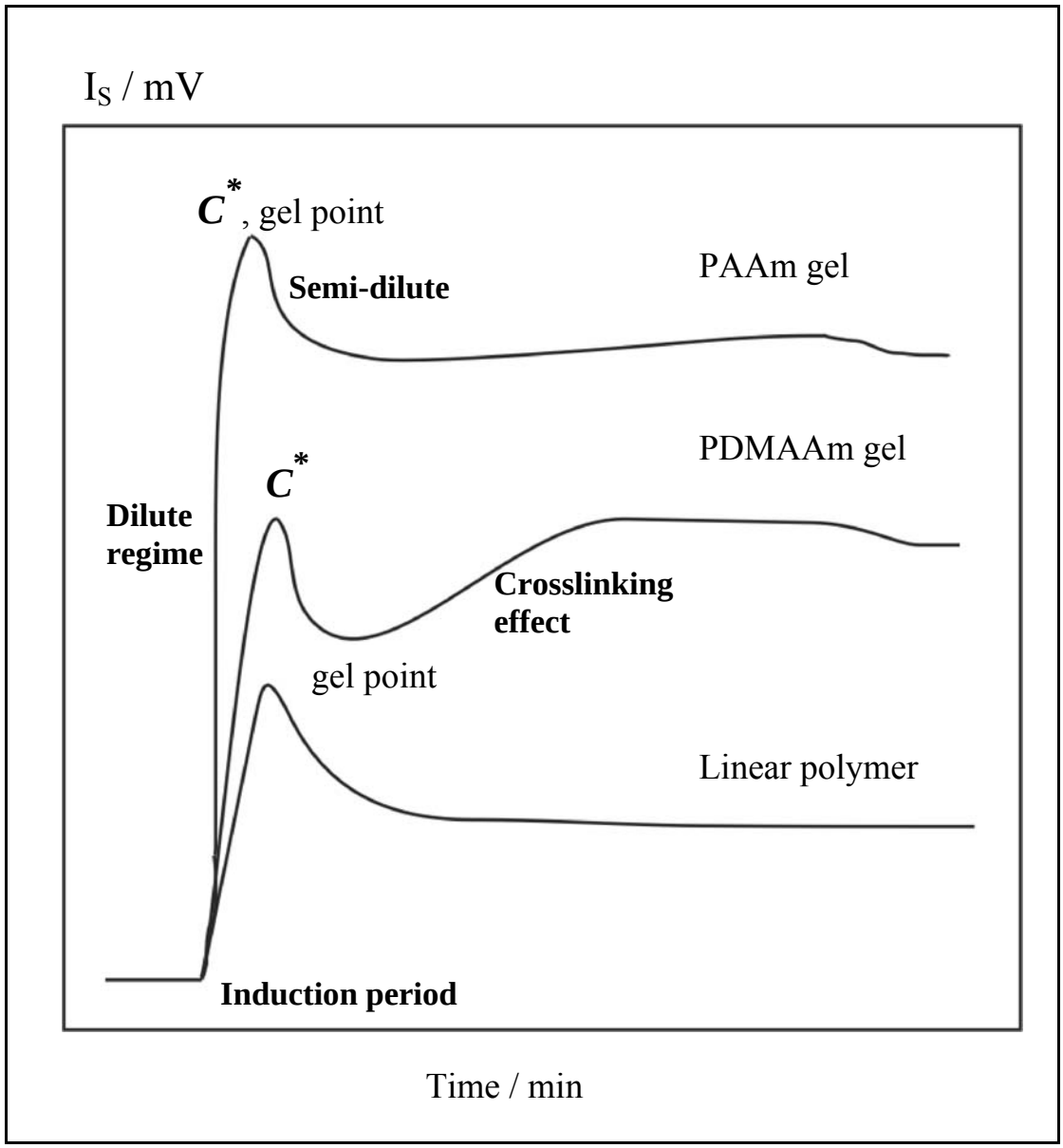

Figure 6.49: Schematic illustration of the scattering intensity profiles I_s during linear and crosslinking polymerization reactions.

According to these results, it was concluded that factors reducing the crosslink density of gels should also weaken the minima of the scattering curves in the DMAAm system. This behavior is indeed seen in Figure 6.48B, where the minima become weaker as the crosslinker ratio *X* is decreased.

Thus, it was considered that the addition of a chain transfer agent (CTA) in DMAAm system should also reduce the intensity rise after the gel point so that the minima should disappear at high CTA concentrations. This is due to fact that CTA decreases the molecular weights of the primary molecules so that the gelation occurs later and the gels formed exhibit a lower modulus of elasticity with increasing amount of CTA[91,123].

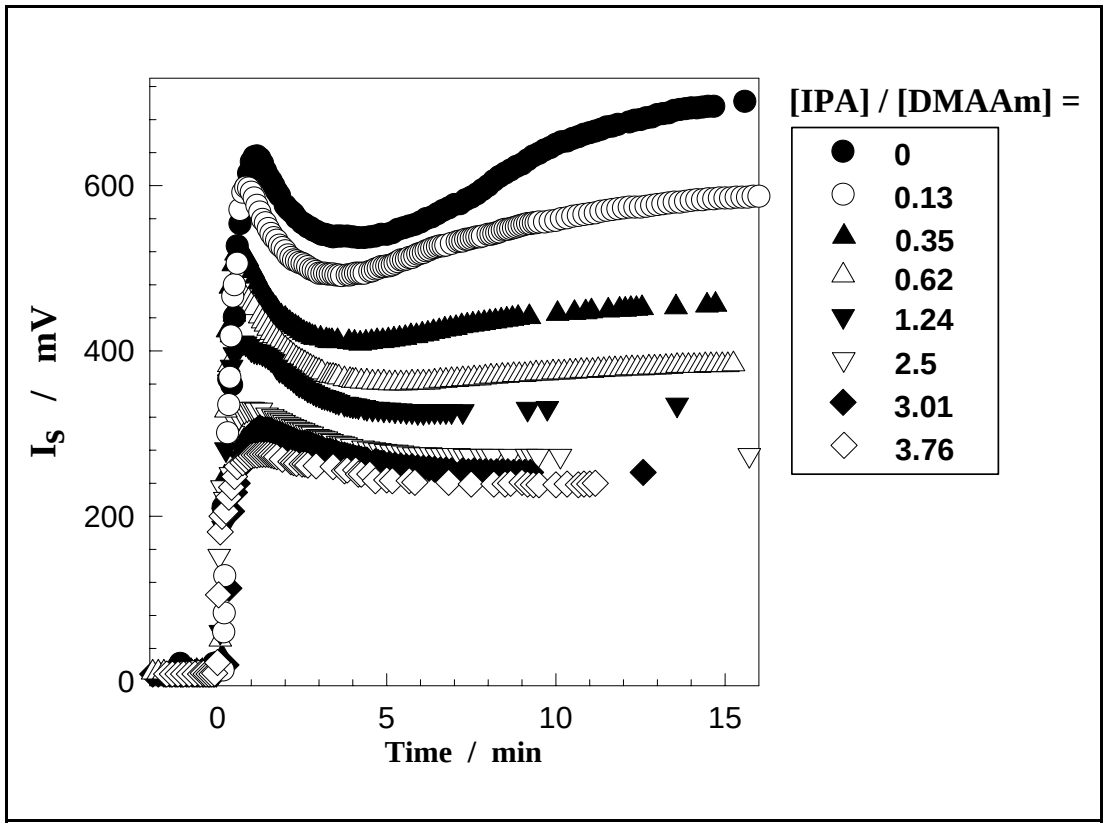

Figure 6.50: The scattered light intensity I_s at $\theta = 90^o$ plotted against the reaction time for crosslinking DMAAm polymerizations in the presence of various amounts of IPA. The mole ratios of IPA to DMAAm are indicated.

To test the validity of this assumption, the crosslinking polymerization of DMAAm was monitored in the presence of various amounts of isopropyl alcohol (IPA) as a CTA. During the synthesis, the crosslinker ratio was kept as 1/82 and the initial monomer concentration was chosen again as 5.0 w/v %. The scattering intensity I_s versus reaction time was monitored just after the preparation of the hydrogels. In

Figure 6.50, the scattered light intensity I_s at $\theta = 90^o$ is plotted against the reaction time for crosslinking DMAAm polymerizations in the presence of various amounts of IPA. It is seen that the gelation times are shifted to larger values as the IPA content is increased as expected. For example, gelation times were 3.9, 7, and 12 min for 0, 2.5, and 3.0 mol IPA/mol DMAAm, respectively. As seen from the figure, the shift of the gel point is accompanied with the gradual disappearance of the minimum of the scattering curves. Simultaneously, the initial rise of I_s in the dilute regime becomes smaller due to the decreasing molecular weight of the sol molecules[128].

Moreover, it was also considered that the addition of ionic comonomer should reduce the intensity rise after the gel point in the DMAAm system so that the gel becomes more homogeneous. For this reason, the crosslinking polymerization of DMAAm in the range of ionic comonomer AMPS mole fraction x_i between 0 and 0.30 was monitored by time-resolved light scattering technique. In Figure 6.51, the scattered light intensity I_s, recorded at $\theta = 90^o$ is shown as a function of the reaction time for crosslinking DMAAm-AMPS copolymerizations.

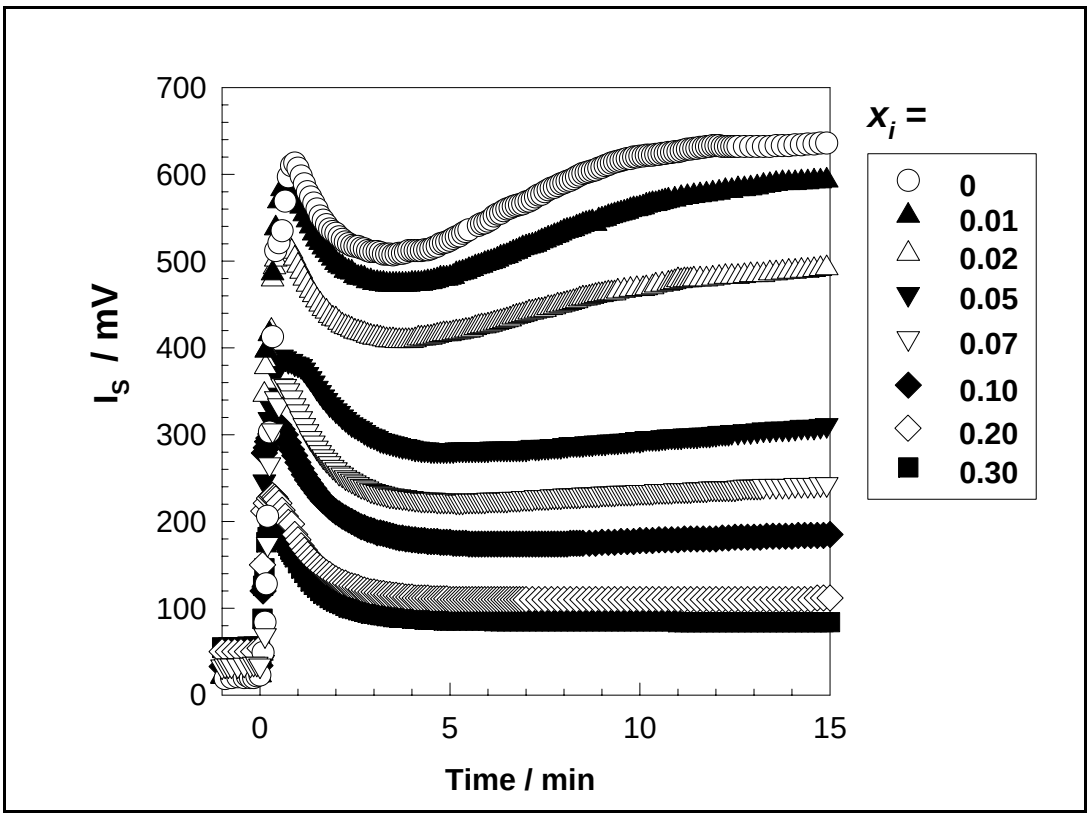

Figure 6.51: The scattered light intensity I_s recorded at $\theta = 90^o$ shown as a function of the reaction time for crosslinking DMAAm-AMPS polymerizations. The mole fraction of AMPS in the comonomer feed x_i is indicated in the Figure.

As seen from the figure, the addition of ionic comonomer in the DMAAm system reduces the intensity rise after the gel point so that the minima disappear at high ionic comonomer concentrations. Thus, the hydrogel becomes more homogeneous as the ionic comonomer concentration is increased. As the charge density of the network chains increases, they rearrange themselves as far as possible due to the repulsion of the charged groups as well as due to the inhomogeneous distribution of mobile counterions in the gel. Those of the chains in the dense regions of gel move apart to assume a new, less inhomogeneous structure.

The results thus obtained show that PDMAAm hydrogels formed at C_0 = 5 %, X = 1/82 and up to a reaction time of 15 min are less inhomogeneous compared to PAAm gels. In order to generalize these findings, the light scattering measurements were carried out on PDMAAm hydrogels formed at various initial monomer concentrations and crosslinker ratios. The reaction time was set to 24 h. and so, the measurements were conducted after one day of polymerization time. The scattered light intensities both from hydrogels and solutions were recorded in the range of the scattering vector q between 8.8×10^{-4} and 2.3×10^{-3} A^{0-1}.

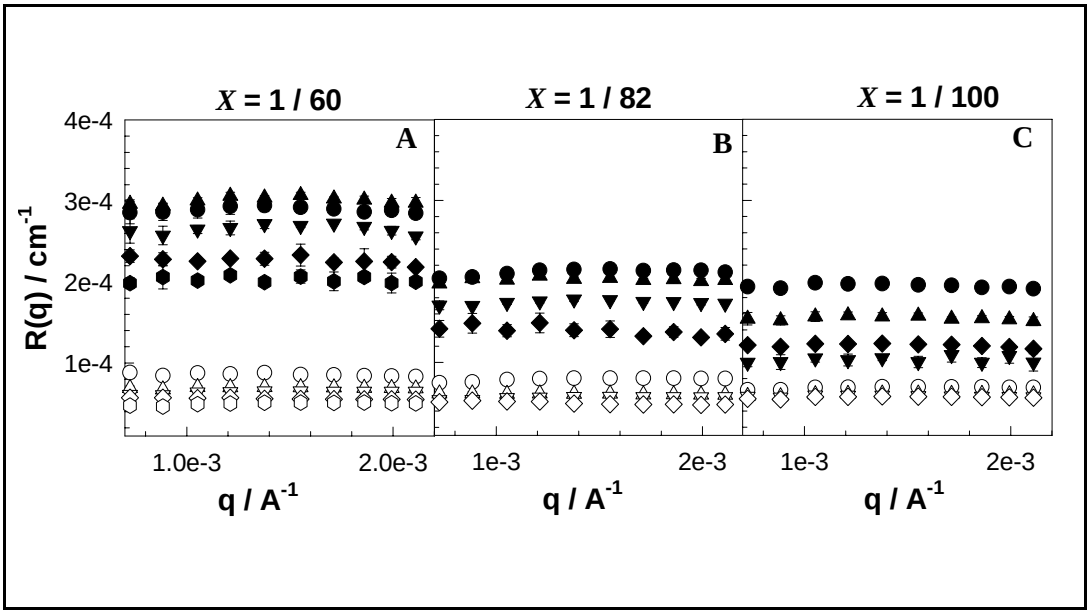

Figure 6.52: Rayleigh ratio *R(q)* versus scattering vector *q* plots for the PDMAAm gels (filled symbols) and for the corresponding linear PDMAAm solutions (open symbols). (A) X =1/60, C_0 =2.4 (●, ○), 3.6 (▲, △), 4.2 (▼, ▽), 6.1 (◆, ◇), 7.3% (■, □). (B) X =1/82, C_0 = 2.4 (●, ○), 4.7 (▲, △), 5.3 (▼, ▽), 7.3% (◆, ◇) (C) X =1/100, C_0 =3.6 (●, ○), 4.7 (▲, △), 6.1 (▼, ▽), 7.3% (◆, ◇)

In Fig. 6.52, the Rayleigh ratio *R(q)* for PDMAAm hydrogels at three different crosslinker ratios (filled symbols) and for the corresponding linear PDMAAm solutions (open symbols) are plotted as a function of the scattering vector *q*. The initial monomer concentrations C_0 are indicated in the Figure. From the data shown in Figure 6.52, for both PDMAAm hydrogels and solutions, the Rayleigh ratio *R(q)* is almost independent on the scattering vector *q* over the range of the light scattering measurements. This is expected due to the semi-dilute regime for PDMAAm solutions. Therefore, the scattering intensities measured at a fixed scattering vector *q* = $1x10^{-3}$ A^{o-1} was considered in the following paragraphs. Another point shown in Figure 6.52 is that the scattering intensity from PDMAAm hydrogels is larger than that from the polymer solution. From the data points shown in Figure 6.52, the excess scattering over the scattering from polymer solution $R_{ex}(q)$ was calculated. In Figure 6.53 the excess scattering $R_{ex}(q)$ of PDMAAm gels is plotted as a function of C_0.

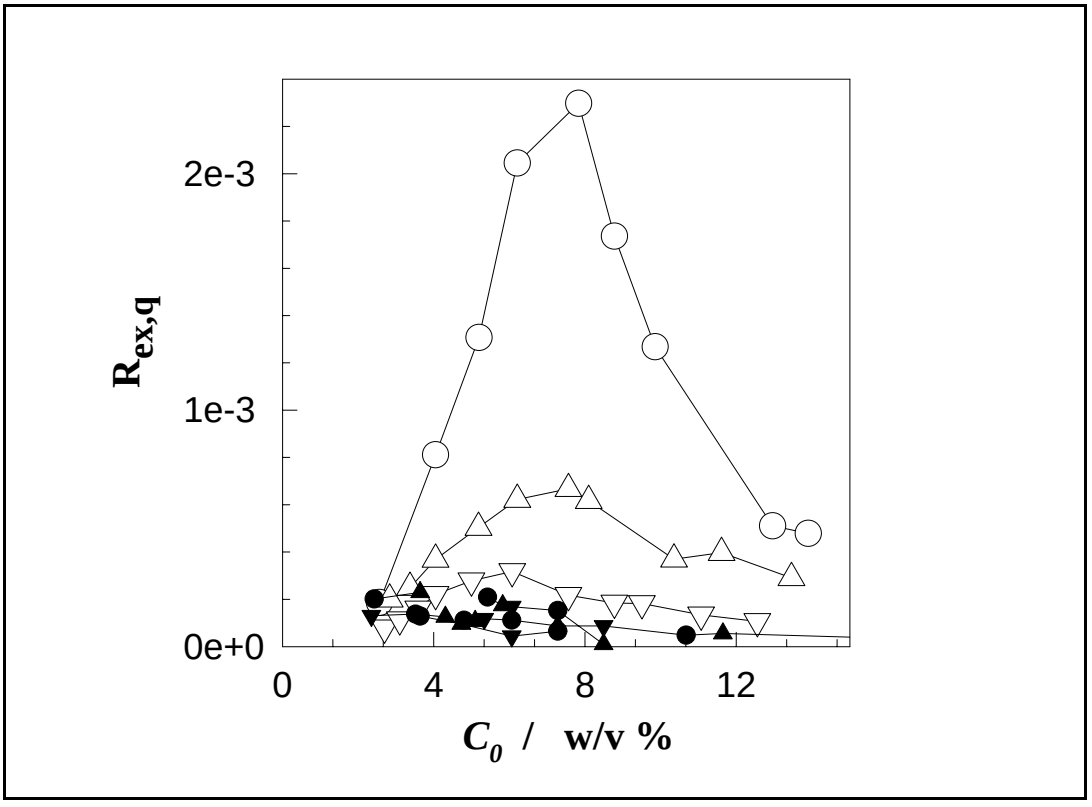

Figure 6.53: The excess scattering $R_{ex,q}$ measured at *q* = $1x10^{-3}$ A^{o-1} shown as a function of the initial monomer concentration C_0 for PDMAAm hydrogels (filled symbols). *X* =1/60 (●, ○), 1/66 (▲, △), and 1/100 (▼, ▽).

For comparison, the excess scattering data reported for PAAm gels formed at various concentrations and crosslinker ratios are also shown in Figure 6.53 by the open symbols[88,96]. It is seen that the excess scattering from PDMAAm hydrogels is about tenfold smaller than that from PAAm hydrogels. Since the excess scattering is a measure of the degree of spatial inhomogeneities, the obtained results demonstrate the homogeneity of PDMAAm hydrogels compared to the PAAm gels formed under identical conditions.

ii. PDMAAm and PAAm hydrogels prepared using APS –SPS

The light scattering measurements of PDMAAm and PAAm hydrogels prepared using APS –SPS redox pair were carried out during the gelation reactions as well as after a reaction time of one day.

Figures 6.54A and 6.54B show scattering intensity I_s versus reaction time plots for crosslinking DMAAm polymerizations initiated by APS-TEMED and APS-SPS redox pairs, respectively. The crosslinker ratio X was varied between 1/80 and 1/50 keeping the total monomer concentration at 5.0 w/v %. The data obtained in linear polymerizations ($X = 0$) are also shown in the figure. The triangles illustrate the gel points in terms of the reaction times. The first interesting point shown from the Figures is that the scattering intensity profiles during the formation process of PDMAAm using APS-SPS redox pair differs from that observed using APS-TEMED. It is seen that if SPS is used as an accelerator instead of TEMED, no significant intensity rise was observed during the crosslinking DMAAm polymerization. As pointed out before PDMAAm gels by APS-TEMED exhibits both a maximum and a minimum, corresponding to the overlap threshold and the gel point, respectively (Figure 6.54A). However, the minimum point disappears if SMS is used as the accelerator. A comparison of the gel points also shows that the gel formation is retarded by replacing TEMED with SPS accelerator. The larger is X the stronger is the increase of I_s, which is obviously due to the crosslinking reactions leading to the formation of larger molecules. Moreover, the intensity increase with the crosslinker ratio is also reduced if SMS is used as the accelerator.

Figures 6.54C and 6.54D show I_s versus reaction time plots for crosslinking AAm polymerizations using APS-TEMED and APS-SPS redox pairs, respectively. It is seen that the shape of I_s versus time plots for AAm polymerizations using both of the

redox pairs is the same with and without crosslinker. Similar to the DMAAm system, if SPS is used as an accelerator instead of TEMED, no significant intensity rise was observed during the crosslinking AAm polymerization. Moreover, the larger the *X*, the stronger the scattered intensity I_s along the AAm polymerization using APS-TEMED redox pairs. However, the intensity increase with the crosslinker ratio is also reduced if SMS is used as the accelerator.

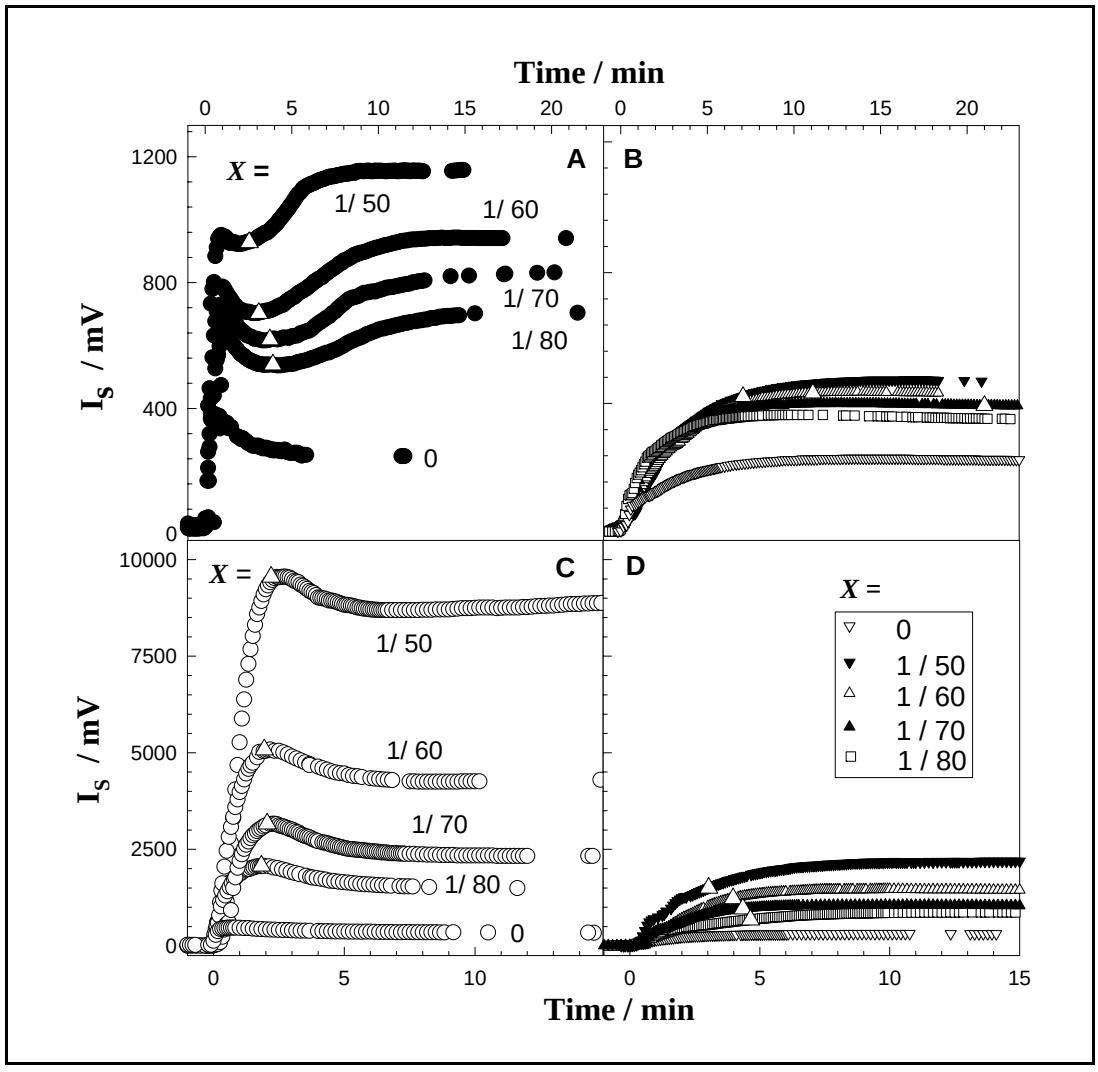

Figure 6.54: The scattered light intensity I_s at $\theta = 90^o$ versus reaction time plots for crosslinking DMAAm (A,B) and AAm polymerizations (C,D). Initiator system: APS-TEMED (A and C), and APS-SPS (B and D). The crosslinker ratios *X* are indicated in the figures. The triangles illustrate the gel points in terms of the reaction times.

The most important result obtained from the scattering intensity profiles of both hydrogels is that during the crosslinking polymerization reactions initiated by APS-SPS system the scattering intensity reduces significantly compared to the APS-

TEMED redox pair. Therefore, replacing TEMED with SPS as the accelerator affects the degree of spatial inhomogeneity in both PDMAAm and PAAm hydrogels. Another distinction between the APS-TEMED and APS-SPS initiated reactions appeared in the growth of the gel molecule. For the APS-SPS system, the gel point was a point at which a soft gel in the lower part of the reactor starts to appear. It required a few hours until the gel occupies the entire polymerization system. However, the formation and growth of gel in APS-TEMED system took place within one minute. This distinction may be attributed to the lower efficiency of crosslinking in APS-SPS initiated reactions[128,129].

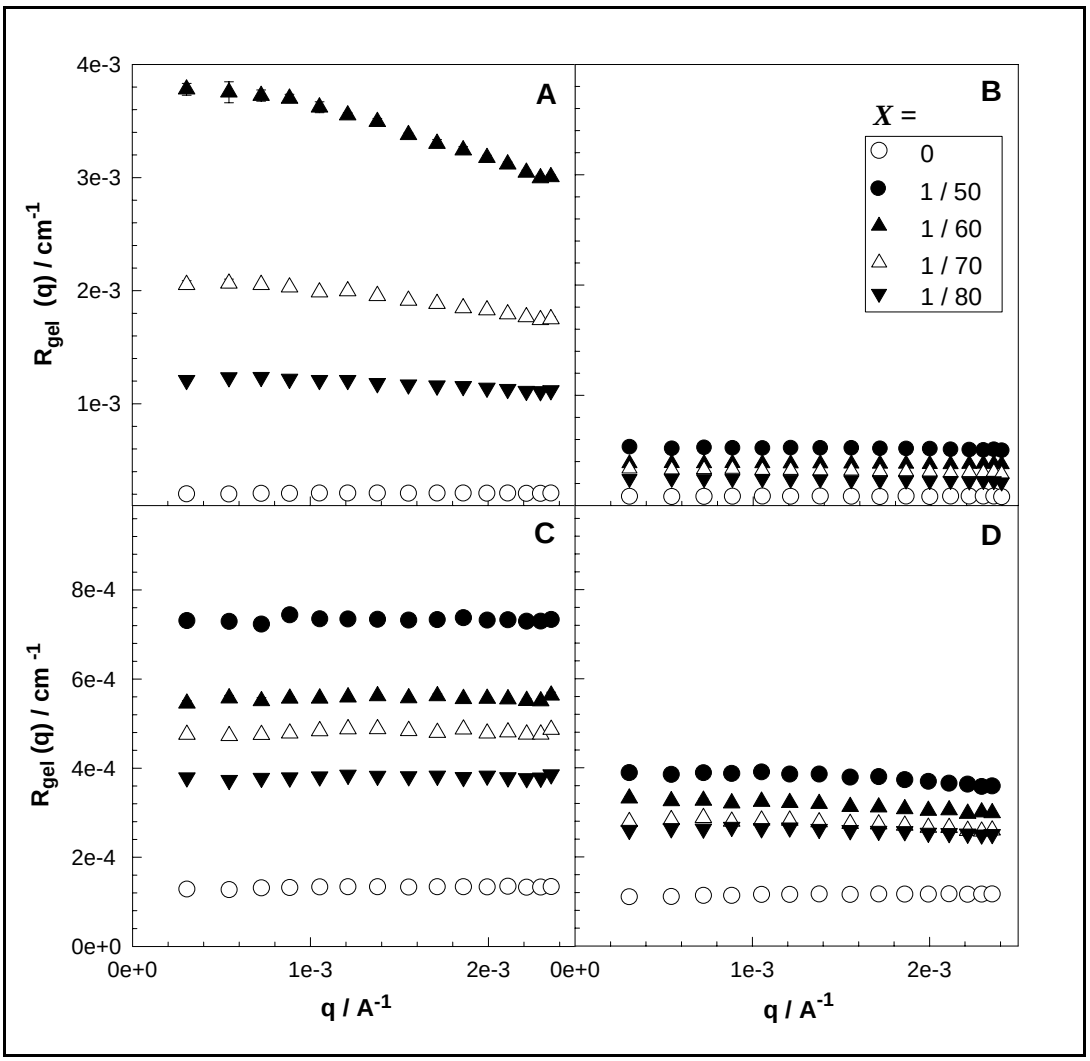

Figure 6.55: Rayleigh ratio $R_{gel}(q)$ versus scattering vector q plots for PAAm (A, B) and PDMAAm hydrogels (C, D). Initiator system: APS-TEMED (A and C), and APS-SPS (B and D). X = 1/50 (●), 1/60 (▲), 1/70 (△), 1/80 (▼), and 0 (❍).

The results in Figure 6.54 show that the scattered light intensity during gelation of both DMAAm and AAm monomers is significantly reduced when APS-SPS initiator

system is used for the radical generation. Therefore, the hydrogels prepared using APS-SPS redox pair becomes more homogeneous. To generalize this finding, the light scattering measurements were carried out on PDMAAm and PAAm hydrogels after one day of polymerization time. Figure 6.55 shows the Rayleigh ratio $R_{gel}(q)$ versus the scattering vector q plots for PDMAAm and PAAm gels formed at various crosslinker ratios. It is seen that the scattering intensity from both PDMAAm and PAAm hydrogels significantly increases with the crosslinker ratio X , when TEMED is used as an accelerator. PAAm gels prepared at X = 1/50 were opaque indicating that these gels have heterogeneities in a spatial scale of submicrometer to micrometer. However, when SPS is used as an accelerator, the intensity rise with the crosslinker ratio is much smaller (Figs. 6.55B and 6.55D). Fig. 6.55 also shows that the light scattering intensity does not change much with the scattering vector q. Therefore, the scattering intensities measured at a fixed scattering angle $\theta = 90^{o}$ will be used in the following.

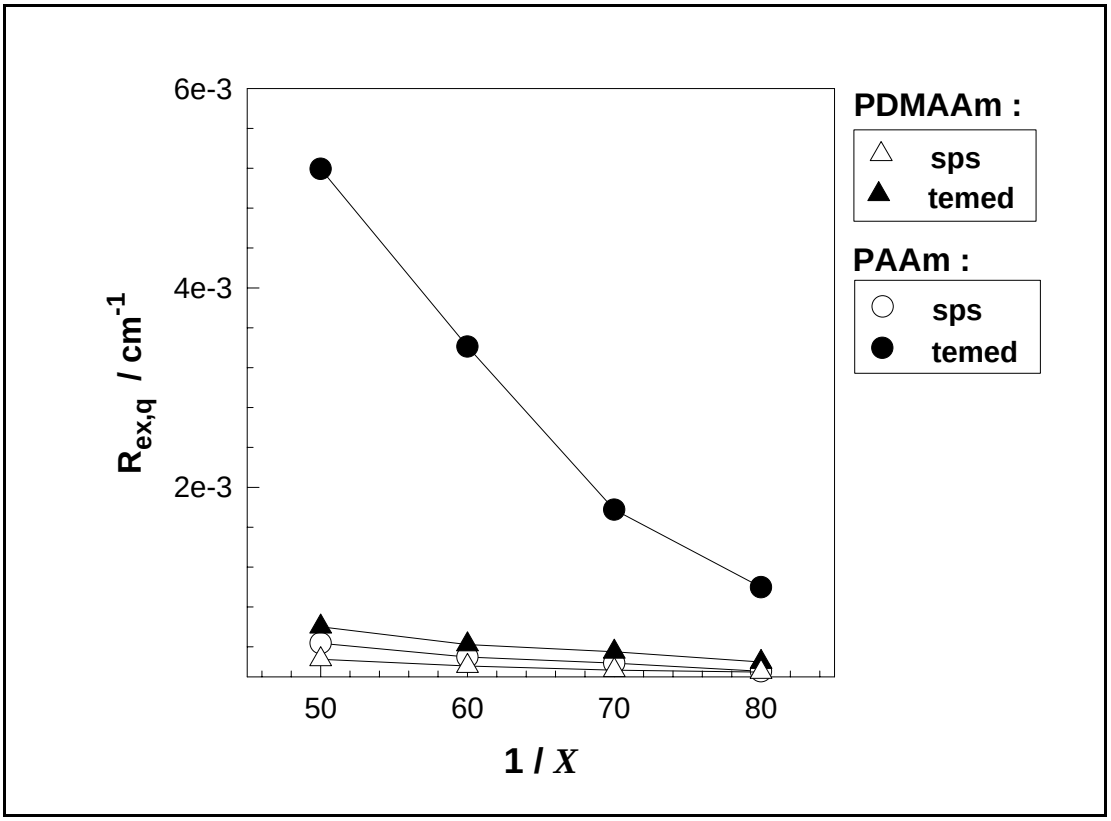

Figure 6.56: The excess scattering $R_{ex,q}$ measured at θ = 90^{o} shown as a function of 1/X for PDMAAm (triangles) and PAAm (circles) hydrogels. Initiator system: APS-TEMED (filled symbols), and APS-SPS (open symbols).

Figure 6.56 shows the excess scattering $R_{ex,q}$ of PDMAAm hydrogels (triangles) and PAAm (circles) plotted as a function of the inverse crosslinker ratio 1/*X* (mole monomer / mole crosslinker). It is seen that the excess scattering intensities from hydrogels formed using SPS are much smaller that those formed using TEMED accelerator. The decrease in $R_{ex,q}$ is particularly significant in PAAm hydrogels. As pointed out before, the excess scattering is a measure of the degree of spatial inhomogeneities. Thus, the results demonstrate that the extent of the inhomogeneities in both PDMAAm and PAAm hydrogels is strongly reduced when APS-SPS redox pair is used in the gel preparation.

The data points shown in Figure 6.55 for PDMAAm and PAAm hydrogels are replotted in the form of Debye-Bueche plots. In Figure 6.57, the calculated values of ξ and $\langle \eta^2 \rangle$ from Debye-Bueche analysis for PDMAAm hydrogels were plotted as a function of 1/ *X*. The correlation length of the scatterers ξ, i.e., the extension of the inhomogeneities in gels is 10^1 nm, while the extent of the concentration fluctuations $\langle \eta^2 \rangle$ is in the range $10^{-6} - 10^{-3}$. Further, ξ increases while $\langle \eta^2 \rangle$ decreases if SPS is used as the accelerator in the gel preparation.

As illustrated schematically in Figure 4.8, an inhomogeneously crosslinked gel contains highly and densely crosslinked regions. The regions, where the multiple crosslinks form, have a higher crosslink density then do others so that they will not swell as much as the other regions. Thus, the inhomogeneous distribution of effective crosslinks and the resulting concentration fluctuations $\langle \eta^2 \rangle$ in gels are a result of multiple crosslinking reactions. As seen in Table 6.3, APS-SPS initiator system produces lower molecular weight polymers compared to the APS-TEMED system. Since decreasing the chain length of polymers necessarily reduces the extent of the multiple crosslinking reactions[91], a more homogeneous distribution of the crosslink points along the gel sample was obtained using the APS-SPS initiator system. Moreover, the shift of the gel point to longer reaction times in APS-SPS initiated crosslinking reactions also contributes to the homogeneity of the resulting gels. This is due to the fact that the late gelation in the crosslinking polymerization using APS-SPS initiator system produces a gel that is much more concentrated than that formed using the APS-TEMED system, so that the former gels exhibit a lesser

degree of inhomogeneity[128]. As the degree of inhomogeneity decreases, the highly crosslinked region of gel absorbs more solvent (water) after the preparation state. As a consequence, their size, represented ξ increases while the extent of the concentration fluctuations $\langle \eta^2 \rangle$ decreases (Figure 6.57).

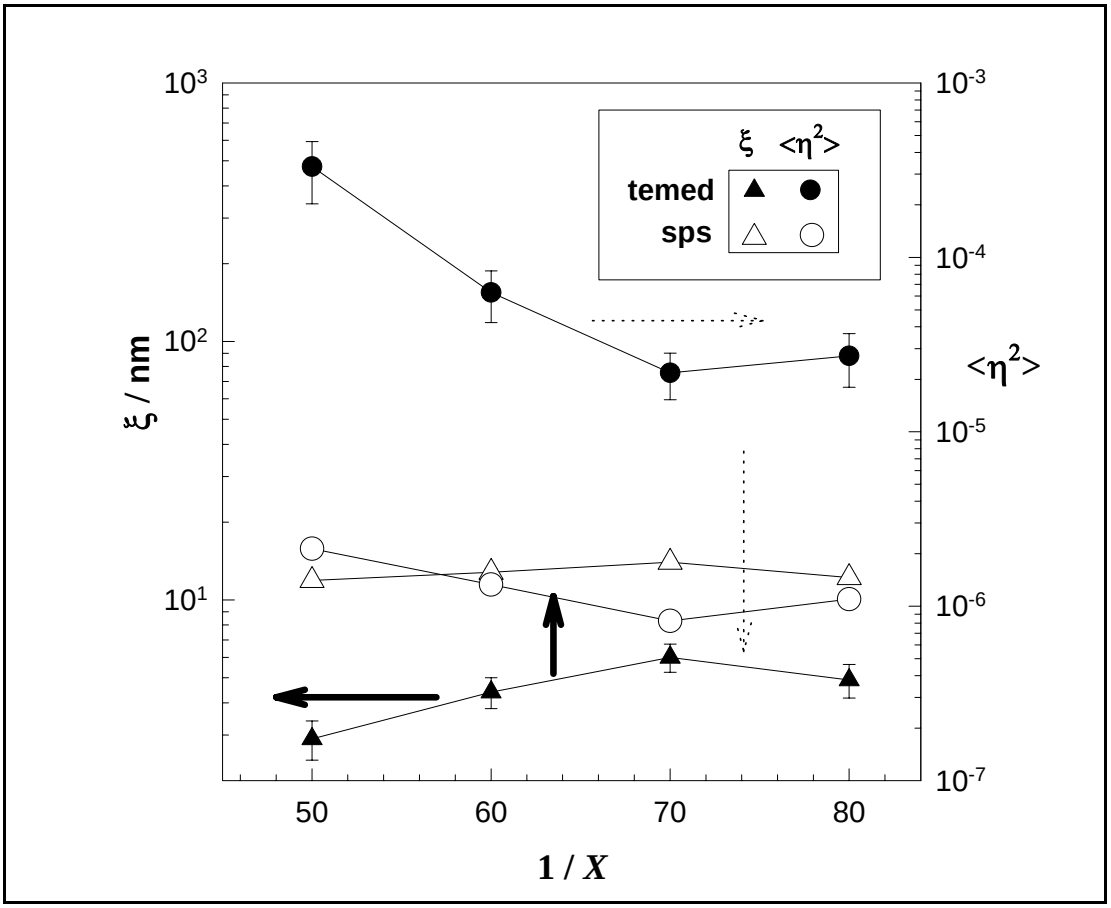

Figure 6.57: The correlation length ξ (triangles) and the mean square fluctuation of the refractive index $\langle \eta^2 \rangle$ (circles) in PDMAAm gels shown as a function of the inverse crosslinker ratio 1/*X*. Initiator system: APS-TEMED (filled symbols), and APS-SPS (open symbols).

6.3.4. Correlation Between The Crosslinking Efficiency and Spatial Inhomogeneity in Hydrogels

The existence of various non-idealities during the gelation result in the formation of polymer gels with inhomogeneous crosslink density distribution, known as the spatial gel inhomogeneity. In this section, the main aim was to obtain a relation between the macroscopic behavior of the hydrogels and their microscopic properties. For this reason, several sets of PAAm gels with varying amounts of the crosslinker

BAAm were prepared at various initial monomer concentrations as described in section 5.4.2. The elasticity and light scattering measurements were made on PAAm gels. The results of these measurements are discussed together to make a correlation between crosslinking efficiency and the extent of the spatial inhomogeneity in the hydrogels.

The uniaxial compression measurements were performed on PAAm hydrogels after preparation. The elastic modulus of hydrogels just after their preparation was used to calculate the effective crosslink densities of the networks ν_e. The results from the elasticity measurements are complied in Table 6.5.

In Fig. 6.58A, the modulus of elasticity G_0 of PAAm hydrogels are plotted against the crosslinker content for three series of hydrogels prepared at C_0 = 3, 5, and 7 %. It is seen that, G_0 increases with the crosslinker concentration. The elastic modulus G_0 also increases when the monomer concentration C_0 is increased at a fixed BAAm content. The initial period of the G_0 versus BAAm mol % plots shown in Figure 6.59B was used to estimate the lower limit of the crosslinker concentration required for the onset of gelation.

Table 6.5: The characteristic data of PAAm hydrogels prepared at various initial monomer concentrations. C_0 = 3, 5 and 7 w/v %. G_0 = the elastic modulus of gels after their preparation.

C_0 (w/v %)	3	5	7
mol % BAAm	G_0 / Pa	G_0 / Pa	G_0 / Pa
0.2	-	51.88	1089.42
0.4	-	415.67	2153.87
0.6	7.92	848.71	3382.51
0.8	35.81	1105.68	3860.14
1.0	61.54	1407.79	4938.81
1.2	89.11	1632.25	5373.62
1.4	148.33	1708.53	5453.98
1.6	173.08	1781.74	5860.48
1.8	219.24	1876.28	6879.78

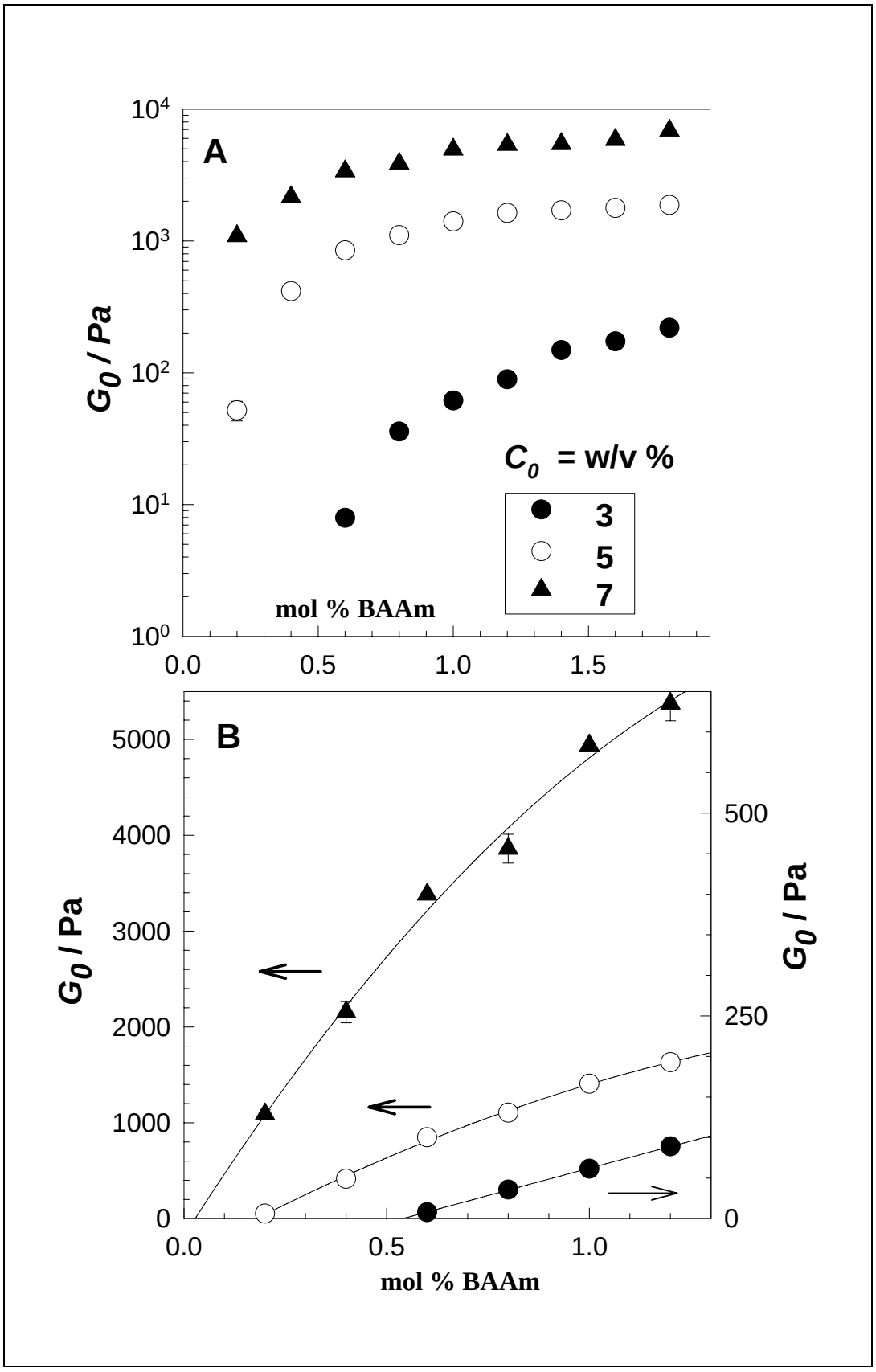

Figure 6.58: (A) The elastic modulus of gels after preparation G_0 shown as a function of BAAm concentration. (B) The initial period of Figure 6.58A. C_0 = 3 (●), 5 (❍), and 7 w/v % (▲).

It was found that the best-fit curves through the G_0 versus BAAm % data intersect with the positive abscissa at 0.03, 0.19, and 0.55 mol % BAAm for C_0 = 7, 5, and 3 %, respectively. Thus, the larger the dilution degree of the reaction system, the higher is the threshold concentration of BAAm for the formation of an infinite network[132]. The upper limit of the crosslinker content for the formation of transparent hydrogels was found to be 1.6 mol % BAAm for $C_0 \geq 5$ %. PAAm hdyrogels prepared at 1.8 mol % BAAm or above became first translucent and then opaque during the gelation reactions. It is clear that these gels have heterogeneities in a spatial scale of submicrometer to micrometer. Therefore, only gel samples with less than or equal to 1.8 % BAAm were subjected to the light scattering measurements. The measurements were conducted after one day of polymerization time. The scattered light intensities both from PAAm hydrogels and solutions were recorded from angles $\theta = 14.5^0$ to 163.3^0 which correspond to the scattering vector q range $3.1 \times 10^{-4} - 2.4 \times 10^{-3}$ A^{o-1}. In Figures 6.59A-6.59F, the Rayleigh ratio $R(q)$ versus scattering vector q plots are shown for PAAm hydrogels. $R(q)$ versus q plots for PAAm solutions are also shown in the Figures by the open circles.

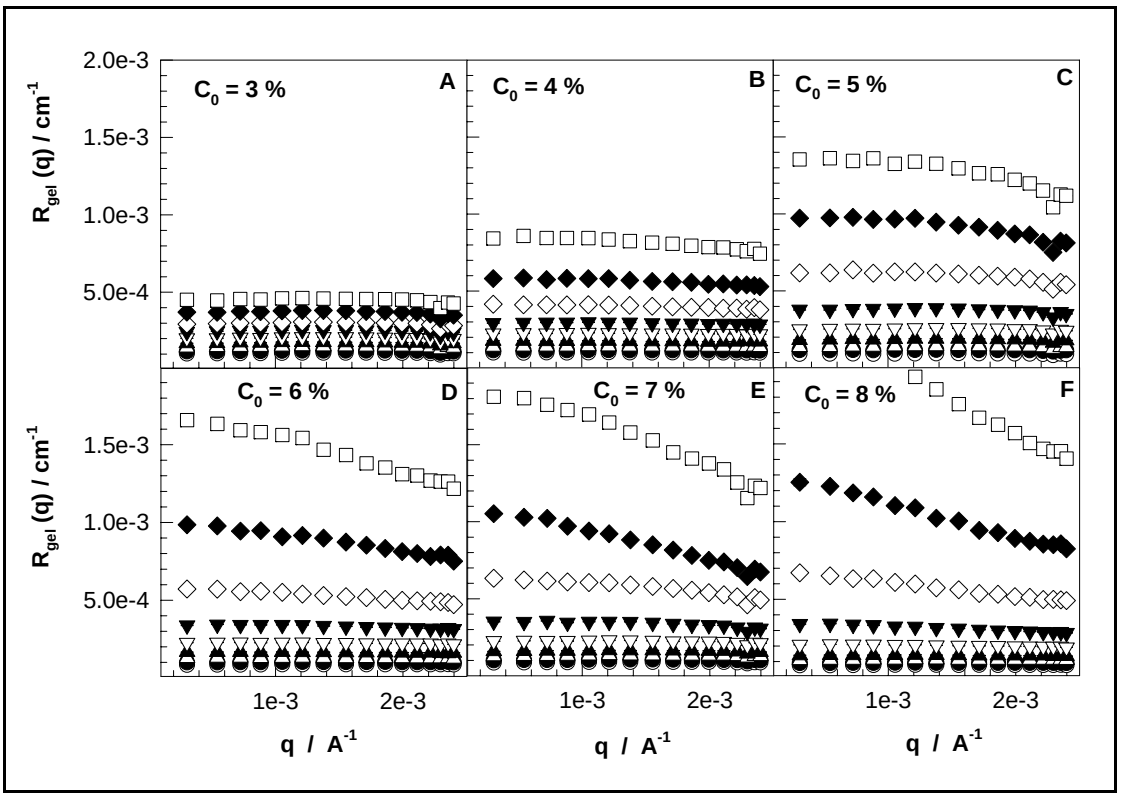

Figure 6.59: Rayleigh ratio $R_{gel}(q)$ versus scattering vector q plots for PAAm hydrogels formed at various initial monomer concentrations. BAAm mol % = 0 (❍), 0.2 (●), 0.4 (△), 0.6 (▲), 0.8 (▽), 1.0 (▼), 1.2 (◇), 1.4 (◆), and 1.6 (□).

It is seen that the hydrogels scatter much more light than the corresponding polymer solution of the same concentration. The addition of a small amount of the crosslinker BAAm results in an increase in the scattered light intensities from the gel samples. It can be seen from the comparison of the Figures 6.59A-6.59F that the scattered light intensity increases with the monomer concentration C_0 for a given crosslinker content. The scattered light intensity is nearly q-independent at low BAAm content, but for higher BAAm content, the scattered light intensity shows a sharp increase.

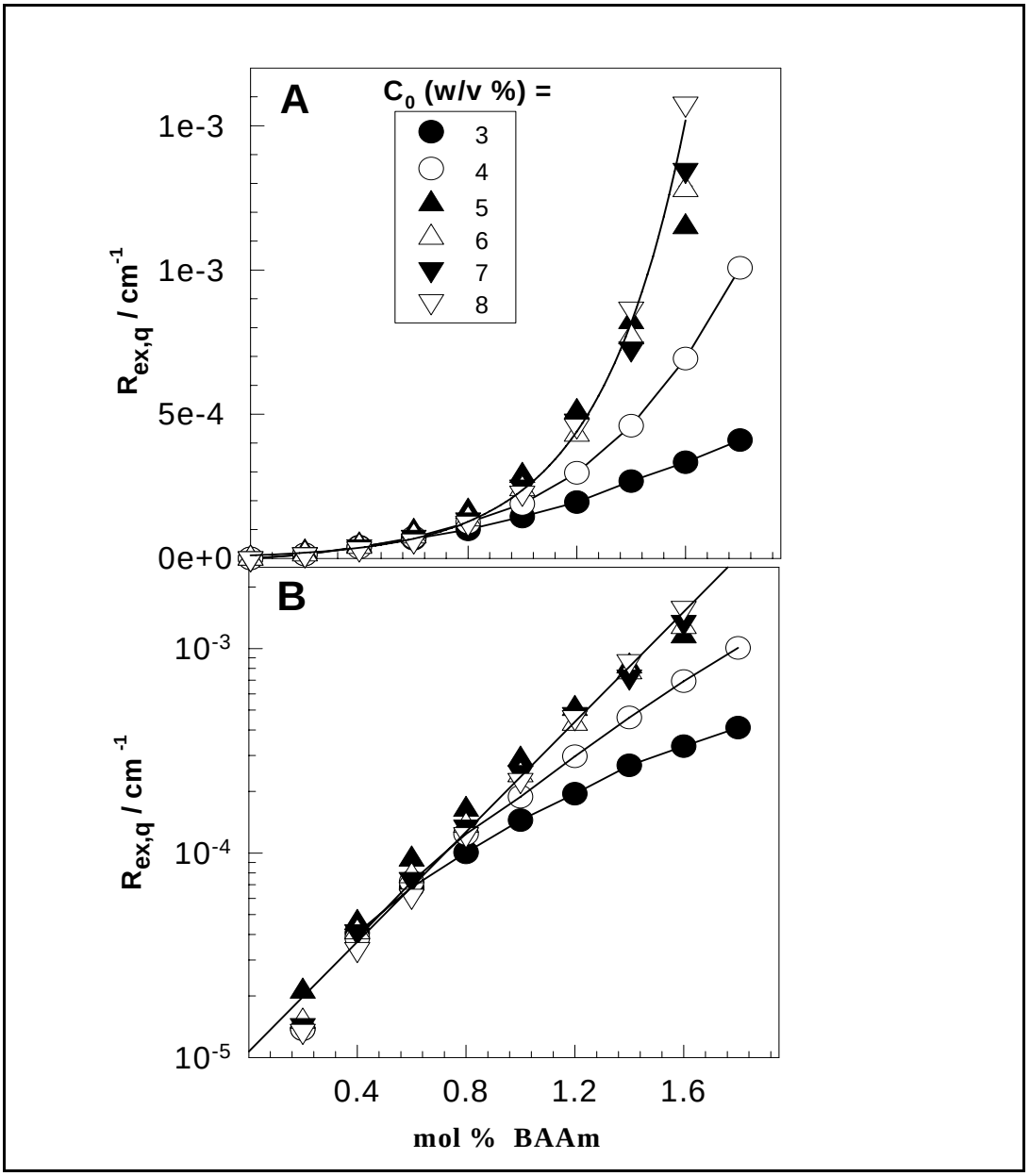

Figure 6.60: (A) The excess scattering $R_{ex,q}$ measured at $\theta = 90^o$ shown as a function of BAAm % for PAAm hydrogels formed at various initial monomer concentrations C_0 indicated in the Figure. (B) The same data is shown in a semi-logarithmic plot .

In Fig. 6.60A the excess scattering $R_{ex,q}$ at $\theta = 90^{o}$ for PAAm hydrogels formed at various initial monomer concentrations C_0 is plotted as a function of BAAm %. It is seen that $R_{ex,q}$ increases first slightly up to about 1 mol% BAAm but then rapidly increases with a further increase in BAAm concentration, suggesting approaching partial phase separation. If the data points for $C_0 \geq 5$ % are redrawn in a semi-logarithmic plot, as seen in Figure 6.60B, a good linear behavior indicating an exponential law between $R_{ex,q}$ and BAAm % was obtained. This suggests the occurrence of a macroscopic phase separation in the gel samples formed at $C_0 \geq 5$ % as the crosslinker content is increased.

From the Debye-Bueche analysis of the data points shown in Figure 6.59, the mean square fluctuation of the refractive index $\langle \eta^2 \rangle$ and the correlation length of the scatterers ξ were calculated using Equation (4.57). In Figure 6.61, the calculated values of ξ and $\langle \eta^2 \rangle$ from DB analysis are shown as a function of BAAm %. The correlation length of the scatterers ξ is about 10^1 nm and slightly increasing function of the BAAm concentration. The mean square fluctuations $\langle \eta^2 \rangle$ are in the range 10^{-7} – 10^{-5} and they increase with the BAAm content. The increase in $\langle \eta^2 \rangle$ with BAAm % is first rapid in the range 0.2 - 1 % but then slight at higher BAAm contents.

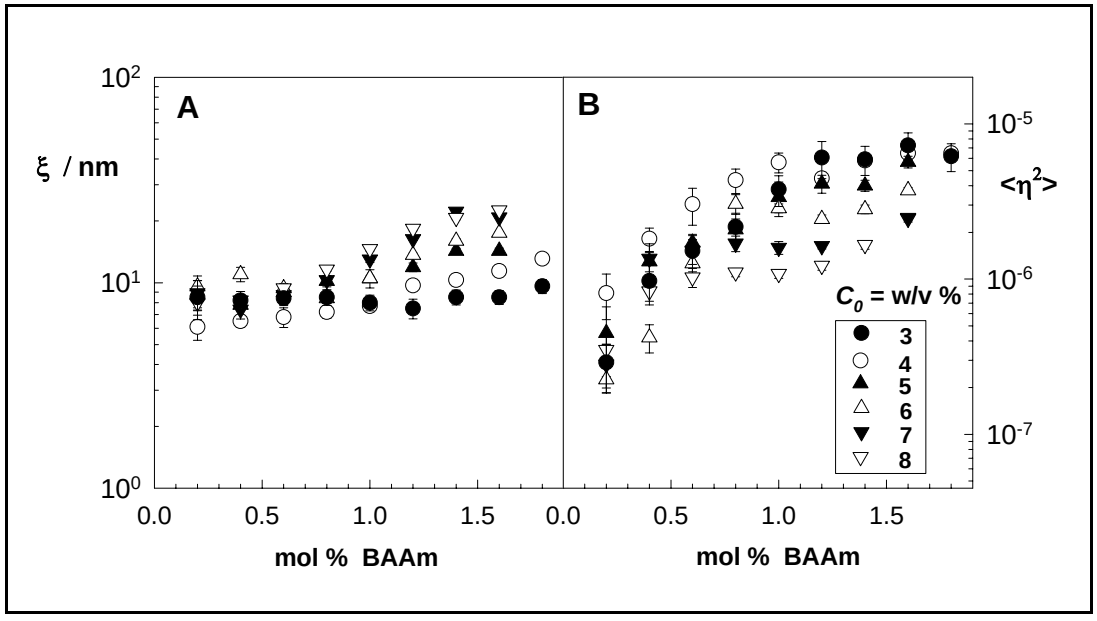

Figure 6.61: The correlation length ξ (A) and the mean square fluctuation of the refractive index $\langle \eta^2 \rangle$ (B) in PAAm hydrogels shown as a function of the BAAm concentration. C_0 = 3 (●), 4 (❍), 5 (▲), 6 (△), 7 (▼), and 8 w/v % (▽).

In order to correlate the elasticity results with the results of the light scattering measurements, not only the chemical crosslink density, that is the BAAm % used in the hydrogel preparation, but also, the effective crosslink density should be taken into account. Thus, the effective crosslink densities ν_e of the hydrogels were calculated from the elastic modulus data of gels shown in Figure 6.58A using Equation (3.61). In the calculations, the phantom network assumption (ϕ = 4) was made and it was also assumed that the gel fraction is unity, i.e., the polymer concentration after the gel preparation ν_2^0 was taken as equal to C_o /(100ρ) where ρ is the polymer density (1.35 g/mL).

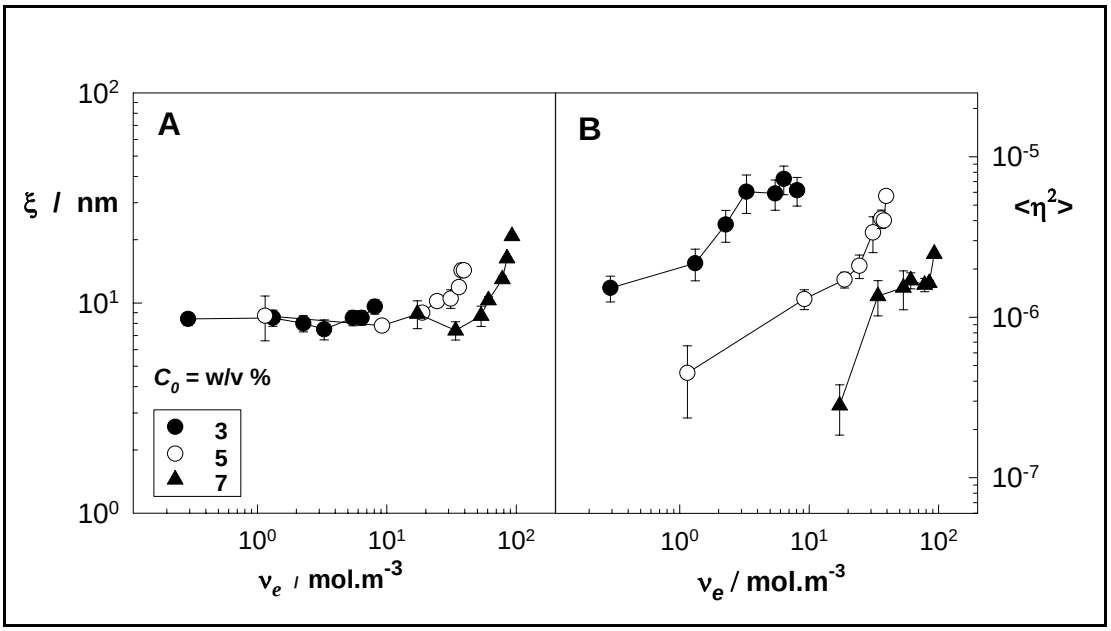

Figure 6.62: ξ (A) and $\langle \eta^2 \rangle$ (B) shown as a function of the effective crosslink density ν_e of PAAm hydrogels formed at C_0 = 3 (●), 5 (❍), and 7 w/v % (▲).

In Fig. 6.62, ξ and $\langle \eta^2 \rangle$ values are replotted against the effective crosslink density ν_e of the hydrogels formed at three different initial monomer concentrations. From the comparison of Figures 6.61 and 6.62, it was concluded that the light scattering data provide a much better correlation with the gel synthesis conditions, if ν_e is taken as the independent experimental parameter instead of BAAm %. Hence ν_e is more sensitive then BAAm % to capture the difference in the network microstructure. The correlation length ξ, i.e., the extension of the inhomogeneities is almost independent of the gel synthesis parameters up to the upper limit of the crosslinker content for

each series of gels. The increase in ξ observed at high BAAm contents for each series of gels is due to the approaching of the reaction system to the phase separation limit. Figure 6.62 also shows that the difference between the gels is due almost entirely to the extent in the concentration fluctuations $\langle \eta^2 \rangle$. The lower the initial monomer concentration C_0, the larger is the concentration fluctuations in gels. This is probably due to the increasing extent of the multiple crosslinking reactions in more diluted reaction systems, leading to the formation of clusters of crosslinks[84,87].

In order to quantify the extent of these non-idealities, the crosslinking efficiency of BAAm ε_{xl}, that is the fraction of BAAm forming effective crosslinks ε_{xl} were calculated using the effective and chemical crosslink densities of the hydrogels according to Equation (6.5). If $\varepsilon_{xl} = 1$, all the crosslinker (BAAm) molecules used in the hydrogel synthesis participate in forming effective crosslinks; as ε_{xl} decreases, more and more BAAm molecules are wasted in the elastically ineffective links.

In Figure 6.63A, the crosslinking efficiency ε_{xl} is plotted against the BAAm % for three series of hydrogels. It is seen that the crosslinking efficiency of BAAm ε_{xl} rapidly decreases with decreasing monomer concentration. At C_o = 3 %, $\varepsilon_{xl} = 10^{-2} - 10^{-3}$, indicating that 99 to 99.9 % of BAAm used in the hydrogel preparation were wasted. As pointed out before, this high fraction of wasted BAAm originates from the characteristics of AAm-BAAm copolymerization[87]. Since, the reactivity ratios of AAm and BAAm monomers are quite different, in copolymerization, the growing chains in the pregel regime are rich in BAAm units. Furthermore, these chains are highly diluted by the solvent and the monomer at low conversion so that a significant fraction of BAAm is consumed by cyclization reactions during the gel formation process.

In Fig. 6.63B, the concentration fluctuations $\langle \eta^2 \rangle$ in hydrogels are plotted against the crosslinking efficiency ε_{xl}. The lines were drawn through the data points of hydrogels having the same BAAm contents. The results demonstrate that the concentration fluctuations $\langle \eta^2 \rangle$ in PAAm hydrogels are reduced as the crosslinking efficiency is increased. Thus, a direct experimental evidence was obtained that the frozen concentration fluctuations in gels originate from the crosslinker molecules forming elastically ineffective links. Moreover, for a given crosslinking efficiency, $\langle \eta^2 \rangle$

decreases further as the BAAm % is decreased. Since multiple crosslinking becomes less probable the smaller the number of pendant vinyl groups in the reaction system, decreasing BAAm concentration also decreases the number of multiple crosslinks so that $\langle \eta^2 \rangle$ decreases. The combination of the light scattering and elasticity data thus shows a direct correlation between the fraction of wasted crosslinker molecules during gelation and the spatial gel inhomogeneity.

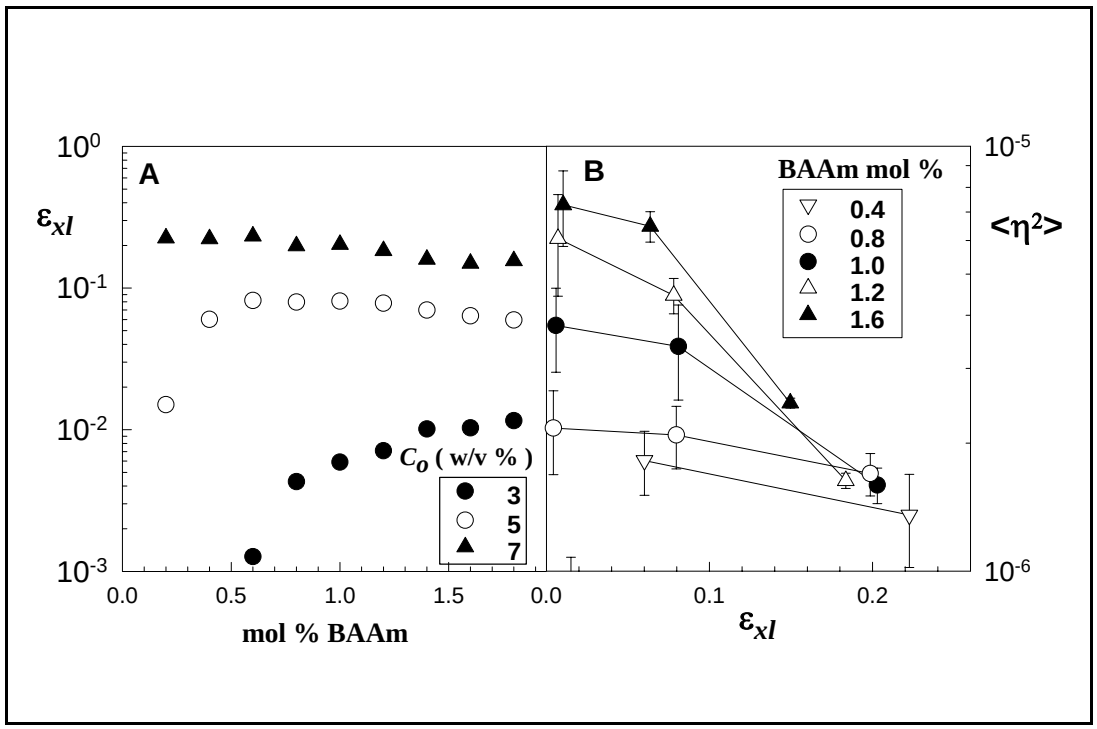

Figure 6.63: (A) The crosslinking efficiency of BAAm ε_{xl} shown as a function of the BAAm content of PAAm hydrogels formed at C_0 = 3 (●), 5 (❍), and 7 w/v % (▲). (B) The mean square fluctuation of the refractive index $\langle \eta^2 \rangle$ in the hydrogels shown as a function of the crosslinking efficiency ε_{xl}. BAAm mol % = 0.4 (▽), 0.8 (❍), 1.0 (●), 1.2 (△), and 1.6 (▲).

7. CONCLUSIONS

The conclusions that can be drawn from the swelling, elasticity and light scattering measurements of the hydrogels can be summarized as follows:

i. The swelling behavior of non-ionic PDMAAm hydrogels was investigated in water as a function of the gel preparation concentration ν_2^0. It was found that the linear swelling ratio of non-ionic PDMAAm hydrogels α (swollen diameter / diameter after synthesis) is not a monotonic function of the initial monomer concentration ν_2^0. As ν_2^0 is increased, α first decreases up to about ν_2^0 = 0.10 and remains constant in a narrow range of ν_2^0, but then it increases continuously up to ν_2^0 = 1. The ν_2^0-dependence of α is due to the variation of the network chain length *N* depending on the gel preparation concentration. In the range of ν_2^0 below 0.1, N follows the scaling relationship $N \approx \left(\nu_2^0\right)^{-2}$, while at higher concentrations, N varies only slightly with ν_2^0. The results were explained with the concentration dependence of the probability of crosslink formation during the free-radical crosslinking reactions.

ii. The swelling behavior of non-ionic PDMAAm hydrogels was investigated in aqueous organic solvent mixtures as functions of solvent species and the concentration of the organic solvent in the solvent mixtures. It was observed that PDMAAm hydrogels exhibit reentrant conformation transition with increasing volume fraction ϕ of acetone, tetrahydrofuran, or 1,4-dioxane in the aqueous solution. During this transition, the hydrogels first deswell in the range of ϕ between 0.4 and 0.9, and then rapidly reswells if the solvent composition is monotonically increased. It was also shown that the reentrant conformation transition in PDMAAm hydrogels requires moderate hydrogen bonding organic solvents, so that the hydrophobic interactions between PDMAAm and the organic solvent dominate the swelling process. The results were interpreted using the theory of equilibrium swelling. The interaction parameters in the gel system as well as the partition parameter of the organic solvent between the gel and the solution phases were

calculated. The calculations show that, due to the less hydrophobic character of PDMAAm compared to PNIPA or TBA/AAm networks, a much higher organic solvent concentration is required for the observation of a reentrant transition in PDMAAm hydrogels.

The ionic PDMAAm hydrogels exhibit reentrant transition at low charge densities in acetone–water mixtures. The reentrant transition gradually disappears and becomes a deswelling transition at high charge densities. Also, the acetone concentration ϕ required for the deswelling transition shifts to smaller values while the reswelling transition becomes weaker as the gel charge density is increased. It was also found that the swelling behavior of ionic PDMAAm hydrogels in water–acetone mixtures is closely related with the ion pair formation. Ionic PDMAAm gels deswell with increasing acetone content in the solution so that the reentrant transition gradually becomes a deswelling transition at high AMPS contents.

iii. The swelling behavior of ionic PDMAAm hydrogels was studied in water. The equilibrium volume swelling ratio q_v of the hydrogels increases with increasing ionic group content. Increasing the ionic group content of the hydrogels increases the number of the fixed charges in the gel ($-SO_3^{2-}$). Moreover, as x_i increases, the mobile counterion concentration (Na^+) inside the gel also increases to maintain the electroneutrality condition. As a result, the difference between the mobile ion concentration inside and out- side the gel increases with increasing x_i, which creates an additional osmotic pressure that expands the gel.

iv. The swelling behaviors of both non-ionic and ionic PDMAAm hydrogels were also investigated in aqueous NaCl solutions ranging in concentration from 10^{-5} to 1 M. It was found that the swelling ratio of the hydrogels decreases with increasing NaCl concentration in the external solution due to a decrease in the concentration difference of counterions inside and outside the hydrogel. The decrease the swelling ratio of the hydrogels is first rapid up to 10^{-2} M NaCl concentration. As the NaCl concentration further increases, this decrease slows down and, between 10^{-1} and 10^{0} M NaCl, the swelling ratio of the hydrogels remains almost constant or slightly decreases with increasing salt concentration.

v. The effective crosslink density of non-ionic PDMAAm hydrogels was investigated as a function of the gel preparation concentration ν_2^0. Depending on the value of ν_2^0,

three different gel regimes were observed: (1) For ν_2^0 < 0.3, increasing ν_2^0 decreases the extent of cyclization during crosslinking so that the effective crosslink density of gels increases with rising ν_2^0. (2) For 0.3< ν_2^0 <0.7, increasing ν_2^0 reduces the accessibility of the pendant vinyl groups during crosslinking due to steric hindrance at high polymer concentrations. As a result, the effective crosslink density of gels decreases with increasing ν_2^0. (3) For ν_2^0 > 0.7, the modulus of elasticity increases sharply with increasing ν_2^0 due to the increasing extent of chain entanglements in this high concentration regime.

The elastic behavior of non-ionic PDMAAm hydrogels swollen to equilibrium in water was also investigated and it was found that the reduced modulus G_r versus V_{eq} plot for hydrogels exhibits a slope of -1/3 and non-ionic PDMAAm hydrogels swollen to equilibrium in water behave as Gaussian.

vi. The mechanical properties of a series of ionic PDMAAm hydrogels containing ionic comonomer AMPS were investigated. The elastic modulus of the hydrogels after their preparation G_0 first increases slightly with ionic comonomer concentration up to about AMPS mole fraction x_i = 0.07 - 0.10, then decreases continuously. The initial increase of the modulus G_0 with x_i is connected with the condensation of counterions to ion pairs. Ion pairs attract each other due to dipole-dipole interactions and form multiplets. After the gel preparation, the concentration of polymer inside the gel is high enough to make formation of multiplets more favorable. Multiplets act as additional crosslinks in the hydrogel and thus increases the elastic modulus by increasing the effective crosslink density of the network. Moreover, the decrease of modulus at higher ionic group content is connected with the electrostatic interactions of the charged groups on the elastic free energy.

The effective and chemical crosslink densities (N and N_{chem}) of ionic PDMAAm hydrogels was calculated by using the elastic modulus of the hydrogels after their preparation G_0 and the crosslinker ratio X used in the gel preparation. It was found that the effective crosslink density N of the hydrogels is much larger than the chemical cross-link density N_{chem}. For ionic PDMAAm hydrogel containing AMPS 10 mol% (x_i = 0.10), N equals 737 or 1961 for phantom or affine network models, respectively, compared to its chemical value of 210. Also, the difference between N and N_{chem} further increases at high charge densities. The difference between the

effective and chemical cross-link densities of PDMAAm hydrogels indicates that a significant fraction of the crosslinker BAAm is wasted during the crosslinking copolymerization, probably due to the cyclization and multiple crosslinking reactions.

vii. The effect of the charge density on the swelling behavior of ionic PDMAAm hydrogels was investigated. The values of the charge density of the network f was calculated and it was found that the calculated value f is much smaller than AMPS mole fraction x_i. Because of the different molar volumes of the monomer units and solvent of the present system, the mole fraction of AMPS units in the network x_i does not correspond to the charge density of the network f.

viii. The elastic behavior of ionic PDMAAm hydrogels in equilibrium swelling was also investigated. The modulus of equilibrium swollen ionic hydrogels *G* increases with increasing x_i up to about 0.30 due to the high stretching of the network chains. For $x_i > 0.30$, the elastic modulus *G* rapidly decreases due to the effect of the electrostatic interaction of charged groups on the elastic free energy.

The dependence of the equilibrium gel volume V_{eq} of ionic PDMAAm hydrogels on the charge density fN was also investigated. From V_{eq} vs. fN plots, the scaling parameter 0.94 ± 0.03 was found for ionic PDMAAm hydrogels. The scaling parameter deviates from the prediction of the Flory-Huggins theory (Equation (6.17)) and indicates non-Gaussian behavior of the network chains in ionic PDMAAm hydrogels.

ix. By using light scattering technique, the extent of the spatial inhomogeneity in non-ionic PDMAAm hydrogels was studied as a function of the initial monomer concentration, i.e., the polymer concentration. A critical polymer network concentration was found where the degree of inhomogeneity in PDMAAm hdyrogels attains a maximum value at $\nu_2^0 = 0.06$. This means that, the PDMAAm hydrogels prepared at a critical polymer network concentration exhibit the highest degree of inhomogeneity. The degree of the spatial inhomogeneity in PDMAAm gels is thus determined by a competition of two opposite effects. At $\nu_2^0 < 0.06$, the crosslink density effect dominates over the concentration effect so that the gel inhomogeneity increases with ν_2^0. At $\nu_2^0 > 0.06$, the concentration effect is more dominant than the

crosslink density effect so that the gel inhomogeneity decreases with ν_2^0. Thus, it can be concluded that the two effects mentioned above determine the spatial inhomogeneity in PDMAAm hydrogels.

x. The effect of charge density on the spatial inhomogeneity in ionic PDMAAm hydrogels was also investigated. The mole fraction of the ionic comonomer AMPS in the monomer mixture x_i was varied between 0 and 0.30. By using time-resolved light scattering technique, it was found that the addition of the ionic comonomer in the DMAAm system reduces the intensity rise after the gel point so that the minima disappear at high ionic comonomer concentrations. Thus, the PDMAAm hydrogels become more homogeneous and the degree of spatial inhomogeneity in the hydrogels decreases as the ionic comonomer concentration increased. From the light scattering measurements after one day of preparation, it was found that the scattering light intensities from PDMAAm hydrogels become equal to the scattering intensities from PDMAAm solutions at $x_i = 0.30$. Thus, the gel with 30 mol% AMPS is homogeneous like a polymer solution. Furthermore, a correlation was found between the macroscopic elastic behavior of PDMAAm hydrogels and the microscopic gel structure. In the range of x_i between 0 and 0.10, the modulus of elasticity G_0 increases with increasing ionic group content of the hydrogels while the excess scattering, that is, the spatial gel inhomogeneity rapidly decreases. Thus, as the mole fraction of the ionic comonomer AMPS x_i is increased, the gel becomes increasingly homogeneous.

By using Debye-Bueche theory, the correlation length ξ of PDMAAm hydrogels was calculated as 10-20 nm, while the mean square fluctuations of the reflactive index were in the range of 10^{-8}-10^{-6} and rapidly decreases with increasing AMPS content. The results suggest that the degree of gel inhomogeneity in PDMAAm gels decreases with increasing AMPS content.

xi. The effect of the initiator system used in the preparation on the spatial inhomogeneity in PDMAAm and PAAm hydrogels was also investigated by light scattering. To initiate the gelation reactions of DMAAm as well as AAm monomers in the presence of BAAm as a crosslinker, two different redox-initiator systems were used: APS-TEMED and APS-SPS.

xii. The linear polymerization reactions of DMAAm and AAm monomers were studied by both dilatometry and the real-time light scattering technique. It was found that the combination of dilatometric and real-time light scattering techniques provides an experimental tool for the determination of the critical overlap concentration in the polymerization systems. The scattering curves display three regimes of the linear polymerization systems; the induction period, the dilute concentration regime and the semi-dilute regime

xiii. The scattered light intensity profile during the formation of PDMAAm hydrogels differs from that observed in PAAm hydrogels. Compared to the PAAm hydrogels, the scattered light intensity from PDMAAm hydrogels is much smaller than that from PAAm gels. This indicates that PDMAAm gels are relatively homogeneous compared to PAAm hydrogels.

During the formation of PAAm hydrogels, the reaction time dependence of the scattered light intensity exhibits a maximum at a critical reaction time or monomer conversion. However, the scattering intensity profile during the formation of PDMAAm gels exhibits both a maximum and a minimum, corresponding to the overlap threshold and the gel point, respectively. This difference in the time-course between the two gel formation systems is due to the late onset of gelation in the DMAAm system with respect to the critical overlap concentration. Moreover, the increase of scattered light intensity becomes visible in DMAAm polymerization due to the gelation occuring much later than the critical overlap concentration.

The late onset of gelation in the DMAAm system with respect to the critical overlap concentration produces a relatively homogeneous distribution of crosslinks so that DMAAm gels exhibit a lesser degree of inhomogeneity. It can be concluded that the spatial inhomogeneity in gels can be controlled by varying the gel point with respect to the critical overlap concentration during the preparation of gels by free-radical crosslinking copolymerization.

xiv. It was found that replacing TEMED with SPS as the accelerator significantly affects the degree of inhomogeneity in both PDMAAm and PAAm hydrogels. Compared to the APS-TEMED redox pair, no significant scattered light intensity rise was observed during the crosslinking polymerization reactions initiated by the APS-SPS system. It was also shown that, both PAAm and PDMAAm gels are much more

homogeneous when APS-SPS redox pair was used as the initiator. The results were explained with the formation of shorter primary chains as well as the delay of the gel point in APS-SPS initiated gel formation reactions.

xv. In order to obtain a relation between the macroscopic elastic behavior of the hydrogels and their microscopic properties, the elasticity and light scattering measurements were carried out on PAAm hydrogels prepared at various initial monomer concentrations. The combination of the light scattering and elasticity data showed a direct correlation between the fraction of wasted crosslinker molecules during gelation and the spatial gel inhomogeneity. Debye-Bueche analysis of the light scattering data indicated that, the correlation length ξ, i.e., the extension of inhomogeneities in the hydrogels is about 10^1 nm. It was also shown that the concentration fluctuations in PAAm hydrogels originate from the BAAm molecules forming elastically ineffective links. The extent of the frozen concentration fluctuations in the hydrogels represented by $\langle \eta^2 \rangle$ decreases with increasing efficiency of the crosslinking reactions, i.e., with increasing monomer concentration during the hydrogel preparation. The concentration fluctuations in PAAm hydrogels strongly reduce as the crosslinker is consumed more effectively during the polymerization reactions, i.e., by suppression the extent of side reactions such as cyclization and multiple crosslinking.

REFERENCES

[1] **Tanaka, T.,** 1992. Phase Transition of Gels, ACS Symposium Series, Vol.480, American Chemical Society, Washington, DC.

[2] **Guenet, J.M.,** 1992. In Thermoreversible Gelation of Polymers and Biopolymers, Academic Press, San Diego.

[3] **Rossi, D., Kajiwara, K., Osada, Y., and Yamauchi, A.,** 1991. Polymer Gels, Plenum, New York.

[4] **Osada, Y. and Kajiwara, K.,** 2001. Gel Hanbook, Academic Press, New York.

[5] **Shibayama, M. and Tanaka, T.**, 1993. Volume phase transition and phenomena of polymer gels, *Adv*. *Polym*. *Sci*., **109**, 1-62.

[6] **Schewe, P.F. and Stein B.,** 1993. Intelligent Gels, *The AIP Bulletin of Physics News*., **130,** 9.

[7] **Fleer, G.J., Stuart, M.A.C., Scheutjens, J.M.H.M., Cosgrove, T. and Vincet, B.,** 1993. Polymers at Interfaces, Chapman & Hall., London.

[8] **Tanaka, T.,** 1978, Collapse of gels and critical endpoint, *Phys*. *Rev*. *Lett*., **40**, 820-828.

[9] **Dusek, K. and Patterson, D.,** 1968. Transition in swollen polymer networks induced by intramolecular condensation, *J*. *Polym*. *Sci*., *A-2*, **6**, 1206-1209.

[10] **Katayama, S., Hirokawa, Y. and Tanaka, T.,** 1984. Reentrant phase-transition in acrylamide-derivative copolymer gels, *Macromolecules*, **17,** 2641-2643.

[11] **Amiya, T., Hirokawa, Y., Hirose, Y., Li, Y. and Tanaka T.,** 1987. Reentrant phase transition of N-isopropylacrylamide gels in mixed solvents, *J*. *Chem*. *Phys*., **86**, Issue 4, 2375-2379

[12] **Melekaslan, D. and Okay, O.,** 2001. Reentrant phase transition of strong polyelectrolyte poly(N-isopropylacrylamide) gels in PEG solutions, *Macromol*. *Chem*. *Phys*., **202**, 304 – 312.

[13] **Melekaslan, D. and Okay, O.,** 2002. Temperature dependent swelling behavior of ionic poly(N-isopropylacrylamide) gels in PEG solutions, *Polymer Bulletin*, **49**, 181-188.

[14] **Gundogan, N. and Okay, O.,** 2002. Reentrant phase transition of poly(N-isopropylacrylamide) gels in polymer solutions: Thermodynamic analysis, *J. Appl. Polym. Sci.*, **85**, 801-813.

[15] **Pagonis, K. and Bokias, G.,** 2004. Upper critical solution temperature - type cononsolvency of poly(N,N-dimethylacrylamide) in water - organic solvent mixtures, *Polymer*, **45**, 2149.

[16] **Liu, X., Tong, Z. and Gao, F.,** 1998. Novel shrinking-swelling hysteresis in DMSO/THF mixtures of copolymer gels containing sulphonate groups, *Polymer Int.*, **47,** Issue 2, 215-220.

[17] **Ozturk, V. and Okay, O.,** 2002. Temperature sensitive poly(N-t-butyl acrylamide-co-acrylamide) hydrogels: synthesis and swelling behavior, *Polymer,* **43**, 5017-5026.

[18] **Ozmen, M.M. and Okay, O.,** 2003. Swelling behavior of strong polyelectrolyte poly(N-t-butyl acrylamide-co-acrylamide) hydrogels, *Eur. Polym. J.*, **39**, 877-886.

[19] **Atherton, E., Clive, D.L.J. and Sheppard, R.C.,** 1975. Polyamide supports for polypeptide synthesis, *J. Am. Chem. Soc.*, **97**, 6584-6585.

[20] **Pacios, I.E., Horta, A. and Renamayor, C.S.,** 2004. Macroporous gels of poly(*N*,*N*-dimethylacrylamide) obtained in the lamellar system AOT/water, *Macromolecules*, **37**, 4643-4650.

[21] **Shibayama, M., Shirotani, Y., Hirose, H. and Namura S.,** 1997. Simple scaling rules on swollen and shrunken polymer gels**,** *Macromolecules*, **30**, 7307-7312.

[22] **Sayil, C. and Okay, O.,** 2001. Macroporous poly(N-isopropyl) acrylamide networks: Formation conditions, *Polymer*, **42,** 7639 – 7652.

[23] **Hirokawa, Y. and Tanaka, T.,** 1984. Volume phase transition in a nonionic gel, *J. Chem. Phys.*, **81**, 6379.

[24] **Tanaka, T.,** 1981. Gels, *Sci. Am.*, **244**, 110-123.

[25] **Tanaka T., Sun, S.T., Nishio, I., Swislow, G. and Shah, A.,** 1980. Phase transition in ionic gels, *Phys. Rev. Lett.*, **45**, 1636-1639.

[26] **Hirotsu, S., Hirokawa, Y., Tanaka, T.,** 1987. Volume-phase transitions of ionized N-isopropylacrylamide gels, *J. Chem. Phys.*, **87**, 2, 1392-1395.

[27] **Shibayama, M., Fujikawa, Y. and Nomura, S.,** 1996. Dynamic light scattering study of poly(*N*-isopropylacrylamide-*co*-acrylic acid) gels, Macromolecules, **29,** 6535-6540.

[28] **Raevsky, O.A.,** 1990. The structure and properties of complexes simulating molecular regognition", *Russ*. *Chem*. *Rev*. *(*Eng. Translation) **59,** 219-233.

[29] **Bae, Y.H., Okano. T. and Kim. S.W.,** 1989. Insulin permeation through thermo-sensitive hydrogels, *J. Controlled Release*, **9**, 271-279.

[30] **Robinson, R.A. and Stokes, R.H.,** 1968. Electrolyte Solutions, Butterworths, London.

[31] **Tanaka, T. and Fillmore, D.J.,** 1979. Kinetics of swelling of gels, *J. Chem Phys*., **70**, 1214-1218.

[32] **Flory, P.J.,** 1953. Principle of Polymer Chemistry, Cornell University Press, Ithaca, New York.

[33] **Flory, P.J. and Rehner, J.,** 1943. Statistical mechanics of cross-linked polymer networks II. swelling, *J*. *Chem*. *Phys*., **11**, 521-526.

[34] **Hildebrant, J.H. and Wood, S.E.,** 1932. The derivation of equations for regular solutions, *J*. *Chem*. *Phys*. **1**, 817-822.

[35] **Flory, P.J.,** 1942. Thermodinamics of high polymer solutions, *J*. *Chem*. *Phys*., **10**, 51-61.

[36] **Huggins, M.L.,** 1942. Some properties of solutions of long chain compounds, *J*. *Chem*. *Phys*., **46**, 151-158.

[37] **Shibiyama, M., Morimoto, M. and Namura, S.,** 1994. Phase separation induced mechanical transition of poly(N-isopropylacrylamide)/ water ısochore gels, *Macromolecules***, 27,** 5060-5066.

[38] **Vasilevskaya, V.V. and Khokhlov, A.R.,** 1992. Swelling and collapse of polymer gel in polymer-solutions and melts, *Macromolecules*, **25**, 384-390.

[39] **Treloar, L.R.G**., 1975. The Physics of Rubber Elasticity, University Press, Oxford.

[40] **Huggins M. L.,** 1941. Solutions of long chain compounds, *J. Chem. Phys*., **9**, 440.

[41] **Grosberg, A.Yu. and Khokhlov, A.R.,** 1994. Statistical Physics of Macromolecules, American Institute of Physics Press, New York.

[42] **Wall F.T.,** 1942. Statistical thermodynamics of rubber. II, *J*. *Chem*. *Phys*. **10**, 485-488.

[43] **James, H.M. and E. Guth.,** 1943. Theory of the elastic properties of rubber, *J*. *Chem*. *Phys*. **11**, 455-481.

[44] **J. P. Queslel and J. E. Mark,** 1987. Encyclopedia of Physical Science and Technology, **12,** 385.

[45] **James, H.M.,** 1947. Statistical properties of networks of flexible chains, *J. Chem. Phys.* **15**, 651-668.

[46] **Flory, P.J.,** 1977. Theory of elasticity of polymer networks. The effect of local constraints on junctions, *J. Chem. Phys.*, **66,** 5720-5729.

[47] **Flory, P.J.,** 1979. The elastic free energy of dilation of a network, *Macromolecules*, **12**(1); 119-122.

[48] **Erman, B. and Flory, P.J.,** 1978. Theory of elasticity of polymer Network. II. The effect of geometric Constraints on Junctions" *J. Chem. Phys.* **68**, 5363-5369.

[49] **Flory, P.J.,** 1979. Molecular theory of rubber elasticity, *Polymer*, **20**, 1317-1320.

[50] **Mooney, M.,** 1948. The thermodynamics of a strained elastomer. I. General analysis, *J. Appl. Phys.,* 19, 434-444.

[51] **Flory, P.J.,** 1950. Statistical mechanics of swelling of network structures, *J. Chem. Phys.*, **18**, 108-111.

[52] **Dusek, K. and Prins, W.,** 1969. Structure and elasticity of non-crystalline polymer networks, *Adv. Polym. Sci.*, **6**, 1-102.

[53] **Gundogan, N., Melekaslan, D. and Okay, O.,** 2004. Swelling and elasticity of poly(N-isopropylacrylamide-co-4-vinylbenzenesulfonic acid sodium salt hydrogels, *J. Appl. Polym. Sci.*, **94**, 135-141.

[54] **Bromberg L**, **Grosberg AY, Matsuo ES, Suzuki, Y. and Tanaka, T.,** 1997. Dependency of swelling on the length of subchain in poly(N,N-dimethylacrylamide)-based gels, *J. Chem. Phys.*, **106**, 2906-2910.

[55] **Okay, O, and Durmaz, S.,** 2002. Charge density dependence of elastic modulus of strong polyelectrolytehydrogels, *Polymer*, **43**, 1215-1221.

[56] **Sedlakova, Z., Bouchal, K., Ilavsky, M.,** 1998. Phase transition in Swollen Gels 24: Effect of the Concentration and Structure of Ionic Comonomers on the Collapse of Poly(acrylamide) Hydrogels, *Polym. Gels. Networks.*, **16**, 163-178.

[57] **Schroeder, U.P. and Oppermann, W.,** 1996. Physical Properties of Polymeric Gels, Cohen Addad, Wiley, New York.

[58] **Durmaz, S. and Okay, O.**, 2001. Inhomogeneities in poly(acrylamide) gels: Position-dependent elastic odulus measurements, *Polymer Bulletin*, **46**, 409 – 418.

[59] **Newton I.,** 1706. Opticks, Latin version, London and in the second English edition of 1718, but not in the original 1704 edition.

[60] **Tyndall, J.,** 1869. On the blue colour of the sky, the polarization of skylight, and the polarization of light by cloudy matter generally, *Phil*, *Mag*. **37**, 384-394.

[61] **Maxwell, J.C.,** 1863. A dynamical theory of the electromagnetic field, *Proc*. *Royal Soc*. **13**, 531-536.

[62] **Rayleigh J.R.,** 1881. On the electromagnetic theory of light, *Phil*. *Mag*. **12**, 81-101.

[63] **Debye, P.,** 1944. Light scattering in solutions, *J*. *Appl*. *Phys*., **15**, 338-342.

[64] **Zimm, B. H.,** 1948. The scattering of light and the radial distribution function of high polymer solutions, *J*. *Chem*. *Phys*., **16,** 1093-1099.

[65] **Poynting J.H.,** 1880. On a simple form of saccharimeter. *Phil*. *Mag*. **10,** 18-21.

[66] **Moore, W.,** 1972. Physical Chemistry, Prentice Hall Inc., New Jersey.

[67] **Einstein, A.,** 1910. Theorie der Opaleszenz von homogenen Flüssigkeiten und Flüssigkeitsgemischen in der Nähe des kritischen Zustands. *Ann. Phys*. **33**, 1275-1298.

[68] **Debye, P.,** 1954. The Collected Papers of P. Debye, Wiley-Interscience, New York.

[69] **Debye, P.,** 1964. Light Scattering from Dilute Polymer Solutions', D. McIntyre and F. Gornick, Gordon and Breach, New York.

[70] **De Gennes, P.G.,** 1979. Scaling Concepts in Polymer Physics, Ithaca, Cornell University Press, New York.

[71] **Brown, W. and Nicolai, T.,** 1993. In Dynamic Light Scattering, The Methods and Application, Brown, W., Clarendon, Oxford.

[72] **Doi, M. and Edwards, S.F.,** 1989. The Theory of Polymer Dynamics, Clarendon Press, Oxford, Chapter 6,7.

[73] **Tanford, C.,** 1961. Physical Chemistry of Macromolecules, Ch. 5, p.298, John Wiley and Sons, New York.

[74] **Flory, P.J.** 1969. Statistical Mechanics of Chain Molecules, Ch. 9, John Wiley and Sons, New York.

[75] **Shibayama, M.,** 1998. Spatial inhomogeneity and dynamic fluctuations of polymer gels, *Macromol*. *Chem*. *Phys*., **199**, 1-30.

[76] **Bastide, J. and Candau, S. J**., 1996. Physical Properties of Polymeric Gels, Cohen Addad, J.P., Wiley. p 143.

[77] **Stein, R.S.,** 1969. The determination of the inhomogeneity of crosslinking of a rubber by light scattering, *Polymer Letters*, **7**, 657-660.

[78] **Bueche, F.,** 1970. Light scattering from swollen gels, *J.Colloid Interface*, **33**, 61-66.

[79] **Jong, L. and Stein, R.S.,** 1991. Synthesis, characterization, and rubber elasticity of end-linked poly(tetrahydrofuran) elastomer, *Macromolecules*, **24**(9), 2323-2329.

[80] **Oppermann, W., Lindemann, B., and Vögerl, B.,** 2000. Network inhomogeneities in polymer gels, *Polym. Preprints*, **41**(1), 700-711.

[81] **Baselga, J., Llorente, M.A., Herenandez-Fuentes, I. and Pierolla, I.F.,** 1989. Network defects in polyacrylamide gels, *Eur. Polym. J*., **25**, 471-475.

[82] **Schröder, U.P. and Oppermann, W.,** 1993. Mechanical and stress-optical properties of strongly swollen hydrogels, *Makromol. Chemie, Macromol. Symp*., **76**, 63.

[83] **Okay, O., Kurz, M., Lutz, K. and Funke, W.,** 1995. Cyclization and reduced pendant vinyl group reactivity during the free-radical crosslinking polymerization of 1,4-divinylbenzene, *Macromolecules*, **28**, 2728-2737.

[84] **Okay, O.,** 2000. Macroporous copolymer networks, *Prog. Polym. Sci*., **25**, 711-779.

[85] **Okay, O., Naghash, H.J. and Capek, I.,** 1995. Free-radical crosslinking copolymerization: Effect of cyclization on diffusion-controlled termination at low conversion, *Polymer*, **36**, 2413-2419.

[86] **Okay, O.,** 1994. Kinetics of gelatin in free radical crosslinking copolymerization, *Polyme*r, **35**, 2613-2618.

[87] **Funke, W., Okay, M. and Joos-Muller,B.,** 1998. Microgels-intramolecularly crosslinked macromolecules with a globular structure, *Adv. Polym. Sci*., **136**, 139-234.

[88] **Okay, O. and Kızılay, M.Y.,** 2003. Effect of initial monomer concentration on spatial inhomogeneity in poly(acrylamide) gels, *Macromolecules*, **36,** 6856-6862.

[89] **Yazici, I. and Okay, O.,** 2005. Spatial inhomogeneity in poly(acrylic acid) hydrogels, *Polymer*, **46,** 2595-2602.

[90] **Kızılay, M.Y. and Okay, O.,** 2003. Effect of hydrolysis on spatial inhomogeneity in poly(acrylamide) gels of various crosslink densities, *Polymer*, 44, 5239-5250.

[91] **Cerid, H. and Okay, O.,** 2004**.** Minimization of spatial inhomogeneity in polystyrene gels formed by free-radical mechanism, *Eur*. *Polym*. *J*. **40,** 579-587.

[92] **Keskinel, M. and Okay, O.,** 1998. Effects of cyclization and electrostatic interactions on the termination rate of macroradicals in free-radical crosslinking copolymerization, *Polymer Bulletin*, **40**, 491- 498.

[93] **Soni, V.K. and Stein, R.S.,** 1990. Light scattering studies of poly(dimethylsiloxane) solutions and swollen networks, *Macromolecules*, **23**, 5257-5265.

[94] **Debye, P.J. and Bueche, A.M.,** 1949. Scattering by an inhomogeneous solid, *Journal Apply*. *Phys*., **20,** 518-525.

[95] **Lovell, G.L. and Bowman, C.N.,** 2003. The effect of kinetic chain length on the mechanical relaxation of crosslinked photopolymers, *Polymer,* **44,** 39-47.

[96] **Okay, O. and Kızılay, M.Y.,** 2004. Effect of swelling on spatial inhomogeneity in poly(acrylamide) gels formed at various monomer concentrations, *Polymer,* **45,** 2567-2574.

[97] **Shibayama, M., Ikkai, F., Shiwa, Y. and Rabin, Y.,** 1997. Effect of degree of crosslinking on spatial inhomogeneity in charged gels. I. Theoretical predictions and light scattering study, *J*. *Chem*. *Phys*., **107**, 5227-5235.

[98] **Mallam, S., Horkay, F., Hecht, A. M. and Geissler, E.,** 1989. Scattering and swelling properties of inhomogeneous polyacrylamide gels, *Macromolecules*, **22**, 3356-3361.

[99] **Shibayama, M., Tanaka, T. and Han, C.C.J.,** 1992. Small angle neutron scattering study on poly(N-isopropylacrylamide) gels near their volume-phase transition temperature, *J*. *Chem. Phys*., **97**, 6829-6841.

[100] **Shibayama, M. and Mallam, S.,** 1998. Spatial inhomogeneity and dynamic fluctuations of polymer gels, *Macromol*. *Chem*. *Phys*., **199,** 1-30.

[101] **Stein, R.S., Soni, V.K., Yang, H. and Erman, B.,** 1988. The Scattering of Light by Swollen Networks, in Biological and Synthetic Networks, O. Kramer, Elsevier, New York, p. 383.

[102] **Feng, X.D., Guo, X.Q. and Kun, Y.Q.,** 1988. Study of the initiation mechanism of the vinyl polymerization with the system persulfate/ N,N,N',N'-tetramethylethylenediamine, *Macromol*. *Chem*. 189, 77-83.

[103] **Ebdon, J.R., Hunckerby, T.N. and Hunter, T.C.,** 1994. Free-radical aqueous slurry polymerizations of acrylonitrile: 1. End-groups and other minor structures in polyacrylonitriles initiated by ammonium persulfate/sodium metabisulfite, *Polymer*, **35**, 250-256.

[104] **Bokias, G., Durand, A. and Hourdet, D.,** 1998. Molar mass control of poly(N-isopropylacrylamide) and poly(acrylic acid) in aqueous polymerizations initiated by redox initiators based on persulfates, *Makromol*. *Chem*. *Phys*., **199**, 1387-1392.

[105] **Gundogan, N., Okay, O. and Oppermann, W.,** 2004. Swelling, elasticity and spatial inhomogeneity of poly(N,N-dimethylacrylamide) hydrogels formed at various polymer concentrations, *Macromol*. *Chem*. *Phys*., **205**, 814-823.

[106] **Orakdogen, N. and Okay, O.,** 2006. Effect of initial monomer concentration on the equilibrium swelling and elasticity of hydrogels, *Eur*. *Polym*. *J*. **42**, 955-960.

[107] **Erman, B. and Flory, P.J.,** 1986. Critical phenomena and transitions in swollen polymer networks and in linear macromolecules, *Macromolecules*, **19**, 2342-2353.

[108] **Orakdogen, N. and Okay, O.,** 2006. Reentrant conformation transition in poly(N,N-dimethylacrylamide) hydrogels in water-organic solvent mixtures, *Polymer* **47**, 561-568.

[109] **Wang, Y. and Morawetz, H.,**1989. Fluorescence study of the complexation of poly(acrylic acid) with poly(N,N-dimethylacrylamide-co-acrylamide), *Macromolecules*, **22**, 164-167.

[110] **Yamamoto, H., Mizusaki, M., Yoda, K. and Morishima, Y.**, 1998. Fluorescence studies of hydrophobic association of random copolymers of sodium 2-(Acrylamido)-2-methylpropanesulfonate and *N*-Dodecylmethacrylamide in water**,** *Macromolecules***,** **31**(11), 3588-3594.

[111] **Peria, E.D., Gorrido, I.Q., Rienda, J.M.B., Schnell, I. and Spiess, H.W.,** 2004. Advanced 1H solid-state NMR spectroscopy on hydrogels, *Macromol*. *Chem*. *and Phys*., **4**, 205, 438-447.

[112] **Maeda, Y., Nakamura, T. and Ikeda, I.,** 2002. Change in solvation of Poly(*N*,*N*-diethylacrylamide) during phase transition in aqueous solutions as observed by IR spectroscopy, *Macromolecules*, **35**(27), 10172-10177.

[113] **Gardon, J.L., Mark, H.F., Gaylord, N.G. and Bikales, N.M.,** 1965. Encyclopedia of Polymer Science and Technology, vol. 3. New York, p. 833.

[114] **Hansen, C.M. and Beerbower, A.** 1971. In: Standen A, Kirk-Othmer encyclopedia of chemical technology, supplement volume. New York, Interscience, p. 889.

[115] **Gundogan, N. and Okay, O.,** 2002. Reentrant phase transition of poly(N-isopropylacrylamide) gels in polymer solutions: Thermodynamic analysis, *J. Appl. Polym. Sci.* **85**, 801-813.

[116] **Kayaman, N., Okay, O. and Baysal, B.M.,** 1998. Swelling of Polyacrylamide Gels in Polyacrylamide Solutions, *J. Polym. Sci*, *Polym. Phys. Ed.*, **36,** 1313-1320.

[117] **Naghash, H.J. And Okay, O,** 1996. Formation and structure of polyacrylamide gels *J. Appl. Polym. Sci.*, **60**, 971-979.

[118] **Okay, O. and Naghash, H.J.,** 1994. Pendant vinyl group reactivity during the free-radical copolymerization of methyl methacrylate and ethylene glycol dimethacrylate, *Polymer Bulletin*, **33**, 665 – 672.

[119] **Zeldovich, K.B. and Khokhlov, A.R.,** 1999. Osmotically active and passive counterions in inhomogeneous polymer gels, *Macromolecules*, **32**, 3488-3494.

[120] **Tong, Z. and Liu, X.,** 1994. Swelling equilibria and volume phase transition in hydrogels with strongly dissociating electrolytes, *Macromolecules*, **27**, 844-848.

[121] **Ilavsky, M., Sedlakova, Z., Bouchal, K. and Plestil, J.,** 1995. Phase transition in swollen gels. 21. Effect of acrylamide quaternary salts with various alkyl lengths on the collapse, mechanical, and SAXS behavior of poly(acrylamide) networks, *Macromolecules,* **28,** 6835-6842.

[122] **Naghash H.J., Okay O, and Yagci Y.,** 1996. Size distribution of polymers during the photoinitiated free-radical copolymerization of methyl methacrylate and ethylene glycol dimethacrylate, *Polymer Bulletin*, **37**, 207-213.

[123] **Okay, O., Balimtas, N.K. and Naghash, H.J.,** 1997. Effects of cyclization and pendant vinyl group reactivity on the swelling behavior of polyacrylamide gels, *Polymer Bulletin*, **39**, 233-239.

[124] **Haward, RN.,** 1999. The application of non-Gaussian chain statistics to ultralow density polyethylenes and other thermoplastic elastomers, *Polymer*, **40**, 5821-5832.

[125] **Gundogan, N., Melekaslan, D. and Okay, O.,** 2002. Rubber elasticity of poly(N-isopropylacrylamide) gels at various charge densities *Macromolecules*, **35**, 5616-5622.

[126] **Gundogan, N., Melekaslan, D. and Okay, O.,** 2003. Non-Gaussian elasticity of swollen poly(N-isopropylacrylamide) gels at high charge densities, *Eur. Polym. J.*, **39**, 2209-2216.

[127] **Huglin, M.B.,** 1972. Light Scattering From Polymer Solutions, Academic Press, London.

[128] **Orakdogen, N., Kizilay, M.Y. and Okay, O.,** 2005. Suppression of inhomogeneities in hydrogels formed by free-radical crosslinking copolymerization, *Polymer*, **46**, 11407-11415.

[129] **Orakdogen, N. and Okay, O.,** Influence of the initiator system on the spatial inhomogeneity in acrylamide-based hydrogels (submitted, *J. Appl. Polym. Sci.*).

[130] **Okay, O. and Sariisik, S.B.,** 2000. Swelling behavior of poly(acrylamide-co-sodium acrylate) hydrogels in aqueous salt solutions: Theory versus experiments, *Eur. Polymer J.*, **36**, 393-399.

[131] **Hocking, M.B., Klimchuk, K.A. and Lowen, S.,** 2000. Water-soluble acrylamide copolymers. VI. Preparation and characterization of poly[N,N-dimethylacrylamide-co-acrylamide] and control polyacrylamides, *J. Polym. Sci., Part A, Polym.Chem.*, **38**, 3128-3145.

[132] **Orakdogen, N. and Okay, O.,** 2006. Correlation between crosslinking efficiency and spatial inhomogeneity in poly(acrylamide) hydrogels, *Polymer Bulletin*, ***57***, 631-641.

APPENDICES

APPENDIX A

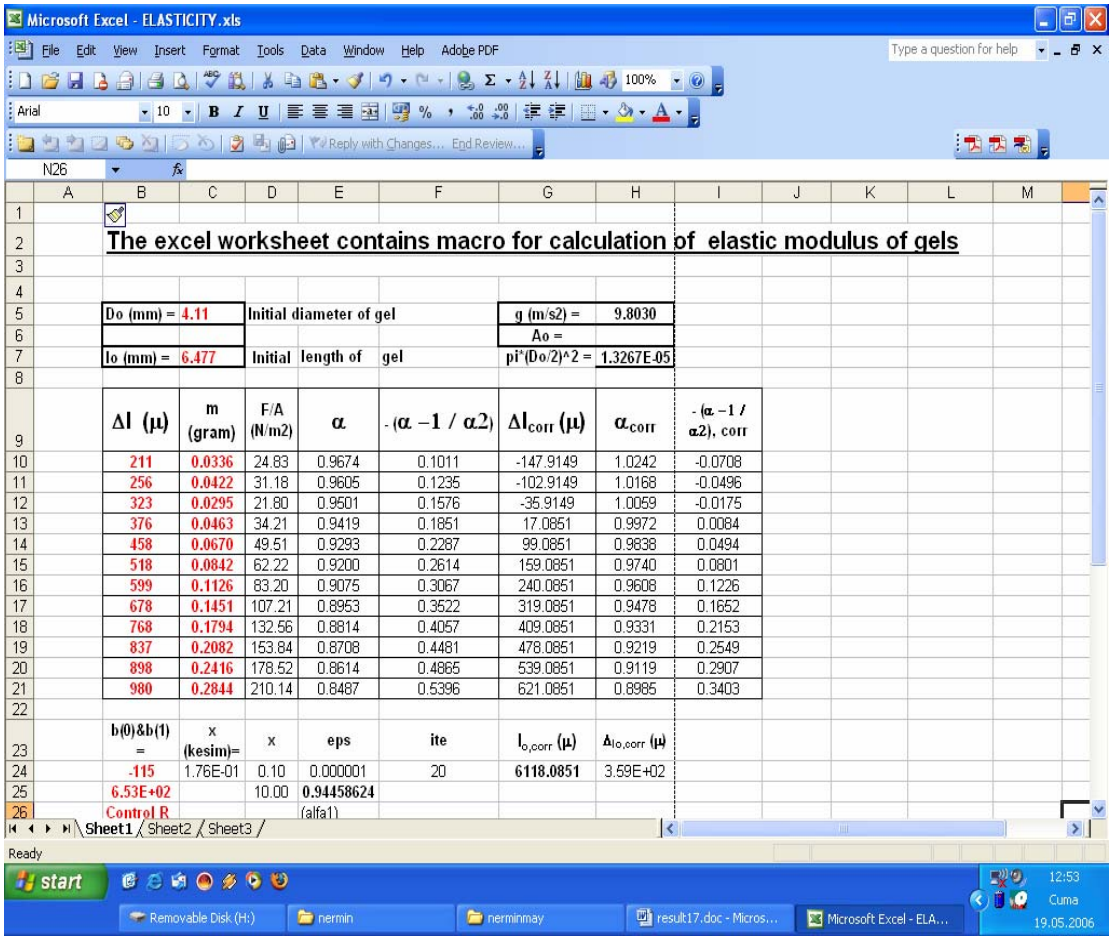

Figure A.1: The excel worksheet contains macro to calculate the elastic modulus of hydrogels from mechanical measurements.

APPENDIX B

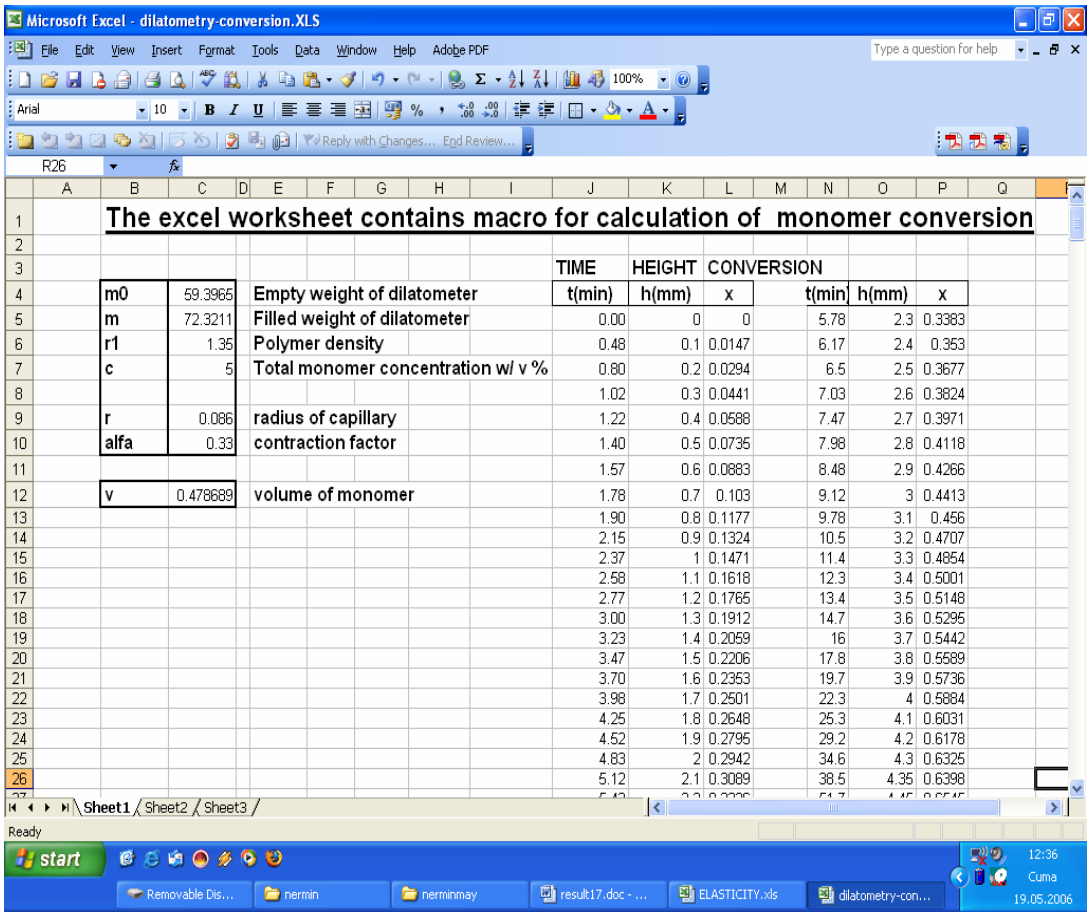

				TIME	HEIGHT	CONVERSION			
				t(min)	h(mm)	x	t(min)	h(mm)	x
m0	59.3965	Empty weight of dilatometer		0.00	0	0	5.78	2.3	0.3383
m	72.3211	Filled weight of dilatometer		0.48	0.1	0.0147	6.17	2.4	0.353
r1	1.35	Polymer density		0.80	0.2	0.0294	6.5	2.5	0.3677
c	5	Total monomer concentration w/ v %		1.02	0.3	0.0441	7.03	2.6	0.3824
r	0.086	radius of capillary		1.22	0.4	0.0588	7.47	2.7	0.3971
alfa	0.33	contraction factor		1.40	0.5	0.0735	7.98	2.8	0.4118
				1.57	0.6	0.0883	8.48	2.9	0.4266
v	0.478689	volume of monomer		1.78	0.7	0.103	9.12	3	0.4413
				1.90	0.8	0.1177	9.78	3.1	0.456
				2.15	0.9	0.1324	10.5	3.2	0.4707
				2.37	1	0.1471	11.4	3.3	0.4854
				2.58	1.1	0.1618	12.3	3.4	0.5001
				2.77	1.2	0.1765	13.4	3.5	0.5148
				3.00	1.3	0.1912	14.7	3.6	0.5295
				3.23	1.4	0.2059	16	3.7	0.5442
				3.47	1.5	0.2206	17.8	3.8	0.5589
				3.70	1.6	0.2353	19.7	3.9	0.5736
				3.98	1.7	0.2501	22.3	4	0.5884
				4.25	1.8	0.2648	25.3	4.1	0.6031
				4.52	1.9	0.2795	29.2	4.2	0.6178
				4.83	2	0.2942	34.6	4.3	0.6325
				5.12	2.1	0.3089	38.5	4.35	0.6398

Figure B.1: The excel worksheet contains macro to calculate the monomer conversion from dilatometric measurements.

APPENDIX C

i. The calculations of the characteristic data of hydrogels from swelling measurements (q_w , q_F , q_v , ν_2^0, V_{eq}, and ν_2)

Calculation of q_w :

For a PDMAAm hydrogel sample, swelling data from the gravimetric analysis was the following:

Weight of the sample after preparation, m_0	0.0542 gr.
Dry weight of the sample, m_{dry}	0.0038 gr.
Swollen weight of the sample in water, m_{sw}	0.0921 gr.

The equilibrium weight swelling ratio q_w was calculated by using Equation (2.2) as follows:

$$q_w = \frac{m_{sw}}{m_{dry}} = \frac{0.0921}{0.0038} = 24.2368 \qquad \text{(C.1)}$$

Calculation of q_F :

The dilution degree after the gel preparation was calculated by using Equation (2.15) as follows:

$$q_F = \frac{m_o}{m_{dry}} = \frac{0.0542}{0.0038} = 14.2631 \qquad \text{(C.2)}$$

Calculation of ν_2^0 :

ν_2^0, the volume fraction of the crosslinked polymer after the gel preparation was calculated by using the Equation (2.14) as follows:

$$\nu_2^0 = \left[1 + \frac{(q_F - 1)\rho}{d_1}\right]^{-1} = \left[1 + \frac{(14.2631 - 1)1.213}{1}\right]^{-1} = 0.0586 \qquad \text{(C.3)}$$

where q_F is the dilution degree after the gel preparation, ρ is the PDMAAm density (1.213 g/ml) and d_1 is the solvent density (1.00 g/ml).

Calculation of V_{eq} :

The data for a PDMAAm hydrogel sample taken from the calibrated digital compass as follows:

The initial diameter of the gel after synthesis, D_0	4.03 mm
Swollen weight of the sample in water, D	4.91 mm

The normalized volume of the equilibrium swollen gel V_{eq} (volume of equilibrium swollen gel/volume of the gel just after preparation) was calculated by using the Equation (5.6).

$$V_{eq} = \frac{V}{V_o} = \left(\frac{D}{D_o}\right)^3 = \left(\frac{4.91}{4.03}\right)^3 = 1.8085 \tag{C.4}$$

Calculation of ν_2 :

The volume fraction of crosslinked polymer in the equilibrium swollen gel ν_2 was calculated as:

$$\nu_2 = \frac{\nu_2^0}{V/V_0} = \frac{0.0586}{1.8085} = 0.0324 \tag{C.5}$$

Calculation of q_v :

Equilibrium volume swelling ratio q_v (volume of swollen gel/volume of dry gel) was calculated as:

$$q_v = \frac{1}{\nu_2} = \frac{1}{0.0324} = 30.8642 \tag{C.6}$$

ii. The calculations of the characteristic data of hydrogels from mechanical measurements (ν_e , ν_{chem} , G_{theo}, and ε_{xl})

Calculation of ν_e :

The effective crosslink density ν_e of the hydrogels was calculated using the elastic modulus of gels after preparation; $G_0 = A\nu_e RT\nu_2^0$. Since for a PDMAAm gel, G_0 = 3699 Pa and ν_2^0 = 0.0586, ν_e can be calculated by assuming phantom network behavior ($\phi = 4$) as:

$$\nu_e = \frac{2G_0}{RT\nu_2^0} = \frac{2(3699)}{(8.314)(297)(0.0586)} = 51.1269 \tag{C.7}$$

Calculation of ν_{chem} :

ν_{chem} is the chemical crosslink density of the hydrogels can be calculated from the Equation (6.2). Since for a PDMAAm gel, X = 1/82, and M_r = 99 gr/mol, ν_{chem} can be calculated as:

$$\nu_{chem} = \rho \frac{2X}{M_r} = 1213\left(\frac{2(1/82)}{99.10^{-3}}\right) = 298 \text{ mol.m}^{-3} \quad \text{(C.8)}$$

Calculation of G_{theo} :

Assuming phantom network behavior (ϕ = 4), the theoretical elastic modulus G_{theo} of PDMAAm gels which were prepared at X= 1/50 can be calculated using Equation (6.18) as follows:

$\rho = 1.213$ gr/ml

$M_c = 99$ gr/mol

$\nu_2^0 = 0.04$

$T = 21^{\circ}\text{C}$

$R = 8.314$ J.mol^{-1}.K^{-1}

$X = 1/50$

$$G_{theo} = A\frac{2\rho X}{M_r} RT\nu_2^0 = \frac{1213\times 8.314\times 294\times 0.04\times 1/50}{99\times 10^{-3}} = 23899.97 \text{ Pa} \quad \text{(C.9)}$$

where the front factor A equals to 1 for an affine network.

Calculation of ε_{xl} :

For the PDMAAm which were prepared at X= 1/50, having elastic modulus after synthesis G_0 =238.52 Pa and the theoretical elastic modulus G_{theo} = 23899 Pa, the crosslinking efficiency ε_{xl} can be calculated as follows:

$$\varepsilon_{xl} = \frac{G_0}{G_{theo}} = \frac{238.52}{23899.97} = 0.0099 \quad \text{(C.10)}$$

APPENDIX D

Computer program to calculate the critical parameters for the reentrant phase transition of non-ionic PDMAAm networks in organic solvent mixtures.

```
DIM SS(15000), NNN(15000), E9(15000)
   CLS
   GOSUB baslik
   Y = 4.1: '******RATIO OF THE MOLAR VOLUMES OF LIQUID COMPONENTS
   V20 = .056:         'VOLUME FRACTION OF NETWORK AFTER SYNTHESIS
   NNN = 1.6*10^3 ' NUMBER OF SEGMENTS
   ALFA =V20/X      'LINEAR SWELLING RATIO
   KAI12 = 0.48 + 0.33*X        ' INTERACTION PARAMETERS
   KAI23 =(-LN(1-X) - X –Y(1/NNN)X(V20/X^2-0.5))(1/Y*X^2)
   KAI13 = .44 - 6.96 * PSI + 15.94 * PSI ^ 2 - 9.27 * PSI ^ 3: '.777 + .197 / (1 - .704 * PSI)'

   PSI = .142:                    ' VOL. FRACTION OF ORGANIC SOLVENT
   V3# = .01394
20   V3# = V3# + .0001#
   FI=V3# / (PSI*(1-X))    ' ORGANIC SOLVENT PARTITION PARAMETER
   DEF FNF1 (X) = LN((1 - X - V3#) / (1 - PSI)) + (1 / Y) * LN(V3# / PSI) - 2 * KAI13 * (V3# - PSI) - (0.48 + 0.33*X + KAI13 – KAI23) * X

   DEF FNF2 (X) = LN((1 - X - V3#) / (1 - PSI)) + (X + V3# - PSI) - (V3# - PSI) / Y + (0.48 + 0.33*X) * X ^ 2 + KAI13 * (V3# ^ 2 - PSI ^ 2) + (0.48 + 0.33*X + KAI13 - KAI23) * X * V3# - (1/NNN)*X * (V20/X^2-0.5)
    '
     BAS# = .000001#: BITT# = .52: HASSAS = .0000001#
50   BASY1 = FNF1(BAS#): BITTY2 = FNF1(BITT#)
   IF SGN(BASY1) = -SGN(BITTY2) THEN 200
   UZUN = (BITT# - BAS#) / 10
   FOR BASAMAK = 1 TO 9: BASY9 = FNF1(BAS# + BASAMAK * UZUN)
   IF SGN(BASY9) = SGN(BASY1) THEN 100
   BITT# = BAS# + BASAMAK * UZUN: GOTO 200
100  NEXT BASAMAK
   BITT# = BITT# + .01: GOTO 50
200  BASY1 = FNF1(BAS#)
   BITTY2 = FNF1(BITT#)
   IF ABS(BITT# - BAS#) < ABS(HASSAS) THEN v21 = .5 * (BAS# + BITT#): GOTO 300
   ORTA = .5 * (BAS# + BITT#)
   ORTAY3 = FNF1(ORTA)
   IF SGN(ORTAY3) = SGN(BASY1) THEN BAS# = ORTA: GOTO 200
   BITT# = ORTA: GOTO 200
300
   BAS# = .000001#: BITT# = .2136
350  BASY1 = FNF2(BAS#): BITTY2 = FNF2(BITT#)
   IF SGN(BASY1) = -SGN(BITTY2) THEN 500
```

```
    UZUN = (BITT# - BAS#) / 2
    FOR BASAMAK = 1 TO 9: BASY9 = FNF2(BAS# + BASAMAK * UZUN)
    IF SGN(BASY9) = SGN(BASY1) THEN 400
    BITT# = BAS# + BASAMAK * UZUN: GOTO 500
400  NEXT BASAMAK
    BITT# = BITT# + .01: GOTO 350
500  BASY1 = FNF2(BAS#)
    BITTY2 = FNF2(BITT#)
    IF ABS(BITT# - BAS#) < ABS(HASSAS) THEN v22 = .5 * (BAS# + BITT#):
GOTO 600
    ORTA = .5 * (BAS# + BITT#)
    ORTAY3 = FNF2(ORTA)
    IF SGN(ORTAY3) = SGN(BASY1) THEN BAS# = ORTA: GOTO 500
    BITT# = ORTA: GOTO 500
600  JJJ = JJJ + 1
    IF JJJ < 30 THEN GOTO 601
    JJJ = 0
 ***************************************************************
    ZZZ = ZZZ + 1
    IF ZZZ > 21 THEN GOSUB baslik:
    PRINT USING "##.#####^^^^   "; v21, v22, ABS(v21 - v22), V3#, V20 / ((v21 +
v22) / 2)
601
    IF ABS(v21 - v22) > HASSAS THEN GOTO 20
    PRINT "V3#="; V3#, "V21="; v21, "V22="; v22, V20 / ((v21 + v22) / 2)
    REM  ***********************************************************
    REM            7 = FREE ENERGY PER LATTICE SITE per RT
    REM  ***********************************************************
    DEF FNF7 (X) = (1 - X - V3#) * LOG(1 - X - V3#) + (V3# / Y) * LOG(V3#) +
KAI12 * (1 - X - V3#) * X + KAI13 * (1 - X - V3#) * V3# + KAI23 * X * V3# + (3
/ 2) * (1 / NNN) * X * ((V20 / X) ^ (2 / 3) - 1 - LOG((V20 / X) ^ (1 / 3))) + MMN *
X * LOG( _MMN * X)
 ************************************************************
    REM             8 = 2g CHEM POT OF NETWORK SEGMENTS
    REM
************************************************************
    DEF FNF8 (X) = (3 / 2) * (1 / NNN) * ((V20 / X) ^ (2 / 3) - 1 - LOG((V20 / X) ^
(1 / 3))) - (1 / NNN) * (V20 ^ (2 / 3) * X ^ (1 / 3) - X / 2) * (1 - X) / X - (1 - X - V3#)
- V3# / Y + KAI12 * (1 - X - V3#) * (1 - X) + KAI23 * V3# * (1 - X) -  _
KAI13 * V3# * (1 - X - V3#) + MMN * (1 - X + LOG(MMN * X))
   VOR = .5 * (v21 + v22)
    PRINT
    PRINT " chem. potential of network segments:"; FNF8(VOR)
    PRINT " Gibbs free enrgy per site          :"; FNF7(VOR)
    END

baslik: CLS : ZZZ = 0
     PRINT " V2 (1.eq)     V2 (2.eq)      DELTA(V2)       V3#         PSI         FI "
     RETURN
```

BIOGRAPHY

Nermin Orakdöğen was born in May 18, 1975 in Istanbul. She enrolled in the preparation class Istanbul Technical University in 1994. She completed her Bachelor of Science degree in Mathematical Engineering in May 1998, then she graduated from Department of Chemistry in 1999 with second honor. She entered the Master of Science program of Polymer Science and Technology at the Istanbul Technical University in 1999 and she completed her M.Sc. degree, authoring a thesis titled "Thermodynamic Analysis of Poly(N-isopropylacrylamide) Network-Linear polymer and Solvent Systems" under the direction of Prof. Dr. Oğuz OKAY. In October 2001, she was registered Ph.D. program of Polymer Science and Technology at the Istanbul Technical University. Her doctoral research was also completed under the guidance of Prof. Dr. Oğuz OKAY.

She has been working as a research assistant in Physical Chemistry Department since July 2000. A number of published and submitted papers to peer reviewed journals have been completed during her graduate research including:

1. Okay O, and Gundogan N, Volume phase transition of polymer networks in polymericsolvents, *Macromol. Theory and Simul.* 11, 287-292 (2002).

2. Gundogan N, and Okay O, Reentrant phase transition of poly(N-isopropylacrylamide) gels in polymer solutions: Thermodynamic analysis, *J. Appl. Polym. Sci.* 85, 801-813 (2002).

3. Gundogan N, Melekaslan D, and Okay O, Rubber elasticity of poly(N-isopropylacrylamide) gels at various charge densities, *Macromolecules* 35, 5616-5622 (2002).

4. Melekaslan D, Gundogan N, and Okay O, Swelling and elasticity of poly(N-isopropylacrylamide) gels immersed in the melt of poly(ethylene glycol) chains *Polymer* 44, 2281-2288 (2003).

5. Melekaslan D, Gundogan N, and Okay O, Elasticity of poly(acrylamide) gel beads, *Polymer Bulletin*, 50, 287-294 (2003).

6. Gundogan N, Melekaslan D, and Okay O, Non-Gaussian elasticity of swollen poly(N-isopropylacrylamide) gels at high charge densities, *Eur. Polym. J.* 39, 2209-2216 (2003).

7. Gundogan N, Melekaslan D, and Okay O, Swelling and elasticity of poly(N-isopropylacrylamide-co-4-vinylbenzenesulfonic acid sodium salt) hydrogels *J. Appl. Polym. Sci.* 94, 135-141 (2004).

8. Gundogan N, Okay O, and Oppermann W, Swelling, elasticity and spatial inhomogeneity of poly(N,N-dimethylacrylamide) hydrogels formed at various polymer concentrations. *Macromol. Chem. Phys.* 205, 814-823 (2004).

9. Orakdogen N, Kizilay MY, and Okay O, Suppression of inhomogeneities in hydrogels formed by free-radical crosslinking copolymerization. *Polymer* 46, 11407-11415 (2005).

10. Orakdogen N, and Okay O, Reentrant conformation transition in poly(N,N-dimethylacrylamide) hydrogels in water-organic solvent mixtures, *Polymer* 47, 561-568 (2006).

11. Orakdogen N, and Okay O, Effect of initial monomer concentration on the equilibrium swelling and elasticity of hydrogels, *Eur. Polym. J. 42,* 955-960(2006).

12. Orakdogen N, and Okay O, Correlation between crosslinking efficiency and spatial inhomogeneity in poly(acrylamide)hydrogels, *Polymer Bulletin 57,* 631-641 (2006).

13. Orakdogen N, and Okay O, Influence of the initiator system on the spatial inhomogeneity in acrylamide-based hydrogels (submitted, *J. Appl. Polym. Sci.*).